

# 輔仁學誌—理工類

中華民國九十六年十二月

第四十一期

## 目 錄

頁次

實現高品質提升和降低整備成本的三階整合模型 .....	耿伯文 陳放子 .....	1
$R^N$ 空間上能量泛函的最小值之存在性 .....	李樹政 張茂盛 嚴健彰 .....	17
影響因子對錐形彈簧中自然頻率行為最佳化之探討 .....	蔡 龍 劉宏毅 .....	27
使用四端主動電流傳輸器合成浮接電感電路 .....	鄧永昌 鄧永傳 .....	47
直流對直流降壓轉換所用之序向回授數位脈波寬度調整控制器 ....	杜弘隆 黃政偉 .....	57
拿破崙紙燈籠與虧格數 .....	呂克明 曹子殷 .....	71
使用 BSCR 方法計算 Ca 原子在 4p-5s 間的共振態能量和寬度 .....	陳昭宏 .....	105
利用聲部結構於多音音樂之比對與排序 .....	袁欣華 徐嘉連 .....	119
有效率及擴充性的連結分散式雜湊表為基礎之點對點網路 .....	呂俊賢 郭正夫 .....	149
指數韋伯分佈在型 I 設限資料之估計 .....	陳思勉 李欣馨 .....	167
半導體雷射泵浦之 Nd:GdVO <sub>4</sub> 雷射其熱負載對光束品質之影響 .....	張連璧 黃承平 陳譽云 .....	191
96 年度理工學院專任教師對外發表之論文摘要 .....		203

# FU JEN STUDIES

## SCIENCE AND ENGINEERING

NO. 41, dec. 2007

### CONTENTS

	Page
Implementing a three-echelon integrated model for quality promotion and setup cost reduction.....by Victor B. Kreng and Fang-Tzu Chen*	1
Minimizers of Energy Functional over $IR^N$ Space .....	
.....by Mao-Sheng Chang and Shu-Cheng Lee and Chien-Chang Yen*	17
Study on Optimization of the Influential Factors on Natural Frequencies of Tapered Helical Springs .....	27
.....by Lung Tsai and Horng-Yith Liou*	
Floating Inductance using Four-terminal Active Current Conveyors .....by Yung-Chang Yin and Yung-Chwan Yin	47
A Serial Feedback Digital PWM Regulator for DC-DC Buck Conversion.....	
.....by Steve Hung-Lung Tu and Philip Jung-Wei Huang	57
Napoleon Origamic Lanterns and Genus.....by Keh-Ming Lu and Alan S Tsaur	71
Calculating Resonance Energies and widths of Ca between 4p and 5s by BSCR method.....by J. H. Chen	105
Pattern Matching and Ranking with Voice Structure in Polyphonic Music Databases .....	119
.....by Hsin-Hua Yuan and Jia-Lien Hsu	
Scalable and Efficient Interconnection of DHT-Based Peer-to-Peer Systems .....by Chun-Hsien Lu and Cheng-Fu Kuo	149
Estimation for Exponentiated Weibull under Type-I Censoring .....by Sy-Mien Chen and Hsin-Hsin Lee	167
The influence of thermal loading in a diode-pumped Nd:GdVO <sub>4</sub> laser on its beam propagation ratio( $M^2$ ).....by Lien-Bee Chang* and Cheng-Ping Huang and Yu-Yun Chen	191
Abstracts of Papers by Faculty Members of the College of Science and Engineering that Appeared in the 2006~2007 Academic Year .....	203

# Implementing a three-echelon integrated model for quality promotion and setup cost reduction

Victor B. Kreng

*Institute of Industrial and Information Management, National Cheng Kung University*

Fang-Tzu Chen

*Department of International Business Management, Tainan University of Technology*

## Abstract

For the JIT buyer, to reduce inventory cost is an important purpose in the supply chain logistic system. Overall system optimal benefits are considered, for the purpose of maximization of supply chain surplus. Traditionally, most of the literatures deal with vendor-buyer two-echelon integrated inventory model. In practice, distribution center (DC) widespread exists. Coordination of three parties or more than three parties will have more managerial implications than relatively two parties. We first recall the three-echelon distribution system which includes the manufacturer, the DC and the retailer. In order to motivate the buyer to cooperate, we follow the literature paper to consider a cooperative strategy. These include the analysis of the impact of (1) quality improvement investment (2) reducing setup cost investment. The numerical results reveal the overall system cost is reduced significantly under the three-echelon integrated model with optimal setup and quality.

**Keywords:** supply chain management 、 integration 、 three echelons

---

\* Correspondence: Fang-Tzu Chen, Department of International Business Management, Tainan University of Technology  
529 Chung Cheng Rd., Yung Kang, Tainan, Taiwan, R.O.C.  
Tel: (886)-6-2422609,  
Fax: (886)-6-2530313, E-mail: t20012@mail.tut.edu.tw

## 1. Introduction and literature review

To reduce inventory cost is an important purpose in the supply chain logistic system. Therefore, the JIT system plays an important role in supply chain management. Not only consider each party's optimal policy but also consider total system's optimal benefits. Traditionally, most of the literatures deal with two-echelon integrated inventory model. The two parties must to negotiate to determine how to divide the substantial saving benefits (Thomas and Griffin 1996). Sharafali and Co (2000) show only the supplier benefits from full cooperation. The supplier has to motivate the buyer to order larger quantities. The buyer would cooperate with manufacturer only if compensated and motivated. The supplier offers the following options:

- (1) To share the savings with the buyer.
- (2) To offer a discount in unit price.
- (3) The buyer may agree to order more but may request the order to be sent in partial deliveries.

Due to the changing customer requirements and increasing introduction of new products, the retailer's inventory has to be reduced drastically. Goyal (1988), Lu (1995) and Aderohunmu et al. (1995) assumed that items are sent to the buyer in equal sized shipments. Goyal (2000) assumed that each quantity will be received by the buyer in  $n$  shipments. The first shipment will be of small size followed by  $(n-1)$  equal-sized shipments. These models consider multiple deliveries of an order, but they don't emphasize the optimal number of shipments. Kelle et al. (2003) studies quantitative models of establishing and negotiating buyer-supplier partnerships, and explored two typical cases: supplier's dominance with large production lot sizes and shipment sizes, and buyer's dominance with small, frequent shipments, and compared the optimal shipment policy of the dominant party to a joint optimal policy. The joint model can contribute to improve the vendor-buyer relation (Pan and Yang, 2004), and reduce total system cost.

Furthermore, the retailers often sell many kinds of goods which come from a lot of different suppliers. If they lack the efficient delivery planning of distribution center, not only the inventory cost will increase, but also will make the personal cost raise and have seriously influences on the operation because of the delivery and unloading of numerous suppliers. In addi-

tion, the supplier is facing the problem of more frequent delivery with small batch. All the above give rise to the demand for Distribution center (DC). The existence of distribution center is for a long time; its contributions and importance on supplier-buyer relationship were less likely to study at the same time.

Because of the above reason, we borrow Kreng and Chen's (2007) three-echelon integrated model with distribution center (DC) as an intermediary. This literature model focused on partial deliveries of an order. In addition, the manufacturer would share the savings with the buyers.

Porteus (1986) introduced the notion of a simultaneous investment in process quality improvement and setup cost reduction. Using logarithmic functions to model quality and setup cost, he found that the joint optimal cost with simultaneous investment (45%, saving percentage) was below that of the classical EOQ. Following Porteus, there is abundant quality improvement related literature; for example, see Hong and Hayya (1995), Ouyang et al. (2002) and Pan and Yang (2004). In this study, the manufacturer adopts the investment functions of Porteus (1986) quality improvement and setup cost reduction to motivate the buyer into cooperation.

This paper is organized as follows: first, a quantitative model is recalled. In section 3, a cooperative strategy is considered. These include the analysis of the impact of (1) quality improvement investment (2) reducing setup cost investment. In section 4, we illustrate with a numerical example and the cost savings of the three-echelon is compared with the two-echelon. Finally, the paper ends with a summary.

## **2. Model review**

### **2.1 Model assumptions and notations**

1. Demand for the item is constant over time
2. Shortages are not allowed
3. Time horizon is infinite
4. Ordering cost/setup cost, unit inventory cost and the cost of a shipment are known

5. Annual production rate is larger than demand rate
6. Lead time is constant
7. The out-of-control probability  $\tau$  and setup cost  $A_M$  are continuous decision variable and follow Parteus (1986) are described by logarithmic investment functions  $F$  and  $S$  as follows:

$$F = a_1 - b_1 \ln(\tau), \text{ for } 0 \leq \tau \leq \tau_0$$

$$S = a_2 - b_2 \ln(A_M), \text{ for } A_M \in [0, A_{M_0}]$$

8. Replenishment of the retailer's inventory is instantaneous, and the retailer follows the  $(s, q_1)$  policy. Whenever the inventory position falls to  $s$ , the retailer places an order for  $q_1$  units.
9. The distribution center's order quantity is an integer multiple of the retailer's order quantity, and the distribution center (DC) follows the  $(-q_1, (n-1) q_1)$  policy.

The retailer's demand and cost parameters are

D	annual demand quantity of the retailer
d	annual demand rate of the retailer
$A_R$	the retailer's ordering cost per contract
$h_R$	stock holding cost per unit per year for the retailer
$Z_R$	the fixed cost of receiving a shipment from the DC
$\theta_R$	cost of losing flexibility per unit per year

The distribution center's cost parameters are

$A_D$	the DC's ordering cost per contract
$h_D$	stock holding cost per unit per year for the DC
$Z_{1D}$	the fixed cost of receiving a shipment from the manufacturer
$Z_{2D}$	cost of a shipment from the DC to the retailer
$\theta_D$	cost of losing flexibility per unit per year

The manufacturer's production and cost parameters are

p	Annual production rate of the manufacturer
$A_M$	Production setup cost per lot

$Z_M$	cost of a shipment from the manufacturer to the DC
$h_M$	stock holding cost per unit per year for the manufacturer
$\tau$	Probability of producing defective products
$C_M$	Cost of replacing a defective unit
$i$	The fractional per unit time opportunity cost of capital

#### Relevant variables

$m_1$	number of shipments per order of retailer
$m_2$	number of shipments per lot of manufacturer
$q_1$	shipment quantity from the DC to the retailer
$q_2$	shipment size from the manufacturer to the DC
$q_{JR}$	shipment quantity due to the joint model of DC and retailer
$q_{JM}$	shipment quantity due to the joint model of DC and manufacturer
$Q^*$	economics order quantity

## 2.2 A quantitative model review

Kreng and Chen (2007) consider a three echelon model - one manufacturer, one distribution center and one retailer. This model focused on partial deliveries of an order. The authors develop a two-integrated model (TIM), accordingly. We briefly review their models and we will modify them latter.

### 2.2.1 Retailer's total cost

Based on the above assumptions and notations, the annual total relevant cost for the retailer is described as follows:

$$TRC_R = \frac{DA_R}{m_1 q_1} + \frac{DZ_R}{q_1} + \frac{h_R q_1}{2} + \frac{\theta_R m_1 q_1}{2} \quad (1)$$

First term is ordering cost.

Second term considers transportation cost of receiving products.

Third term is stock holding cost.

The last term, Kelle (2003) introduced cost of losing flexibility. Since the products are delivered by partial, concerns of products change and long commitments can result in a severe risk that may outweigh the annual saving in ordering cost.

### 2.2.2 DC's total cost

The annual total relevant cost for the DC includes ordering cost, receiving shipments cost (from the manufacturer), and the shipments cost (to the retailer), holding cost and the cost of lost flexibility can be expressed as

$$TRC_D = \frac{DA_D}{m_2 q_2} + \frac{DZ_{1D}}{q_2} + \frac{m_1 DZ_{2D}}{q_2} + \left( \frac{(m_1 - 1)q_2}{2m_1} \right) h_D + \theta_D m_2 q_2 / 2 \quad (2)$$

### 2.2.3 Manufacturer's total cost

The manufacturer delivers the entire batch quantity,  $m_2 q_2$ , in  $m_2$  shipments, each equal to  $q_2$ . The annual total relevant cost which includes setup cost, the shipments cost (to DC), and holding cost (Joglekar, 1988), can be expressed as the followings:

$$TRC_M = (A_M + m_2 Z_M) \frac{D}{m_2 q_2} + h_M \frac{m_2 q_2}{2} \left( 1 - \frac{d}{p} - \frac{1}{m_2} + \frac{2d}{pm_2} \right) \quad (3)$$

### 2.2.4 The first integrated model

Kreng and Chen (2007) develop a two-integrated model (TIM), accordingly. The first integrated annual total cost of the retailer and distribution center,  $TRC_{RD}$  can be represented by

$$TRC_{RD} = TRC_R \text{ (Eq.1)} + TRC_D \text{ (Eq.2)}.$$

The annual total cost function can, then, be rearranged to be:

$$\begin{aligned} & TRC_{RD} (m_1, q_{JR}) \\ &= \frac{D}{q_{JR}} \left( \frac{1}{m_1} (A_R + A_D + m_2 Z_{1D}) + Z_R + Z_{2D} \right) + \frac{q_{JR}}{2} (h_R + \theta_R m_1 + h_D (m_1 - m_2) / m_2 + \theta_D m_1) \end{aligned} \quad (4)$$

In the above expression,  $m_1$  is an integer representing the number of shipments delivered to the retailer from the DC with the shipment size of  $q_{JR}$ . In addition,  $m_2$  is an integer represent-

ing the number of shipments delivered to the DC. With the fixed  $m_1$  and  $m_2$ , the integrated optimal shipment size,  $q_{JR}$ , can be obtained as follows:

$$q_{JR}^* = \left( \frac{2D((A_R + A_D + m_2 Z_{1D}) / m_1 + Z_R + Z_{2D})}{h_R + \theta_R m_1 + h_D \left( \frac{m_1}{m_2} - 1 \right) + m_1 \theta_D} \right)^{1/2} \quad (5)$$

By substituting  $q_{JR}^*$  in the cost function of  $TRC_{RD}$ , and differentiate the function with respect to  $m_1$ , the one of two nearest integers of the optimal  $m_1$  can be found in the followings:

$$m_1^* = \left( \frac{(A_R + A_D + m_2 Z_{1D})(h_R - h_D)}{(Z_R + Z_{2D})(\theta_R + \theta_D + h_D / m_2)} \right)^{1/2} \quad (6)$$

### 2.2.5 The second integrated model

$TRC_{DM}$  is the sum of the manufacturer and the DC's annual total cost which can be represented by

$$TRC_{DM} = TRC_D \text{ (Eq.2)} + TRC_M \text{ (Eq.3)},$$

The integrated annual total cost function can, therefore, be rearranged to be:

$$\begin{aligned} TRC_{DM}(m_2, q_{JM}) &= \frac{D}{q_{JM}} ((A_D + A_M + m_1 Z_{2D}) / m_2 + Z_{1D} + Z_M) \\ &+ \frac{q_{JM}}{2} (h_D (1 - m_2 / m_1) + \theta_D m_2 + h_M m_2 (1 - D / P) - h_M (1 - 2D / P)) \end{aligned} \quad (7)$$

In the above,  $m_2$  is an integer representing the number of shipments delivered to the DC from the manufacturer with the volume of  $q_{JM}$ .

Once again, by minimizing  $TRC_{DM}$ , the integrated optimal shipment size and, the number of delivery for the manufacturer and DC can be obtained as follows:

$$q_{JM}^* = \left( \frac{2D((A_D + A_M + m_1 Z_{2D}) / m_2 + Z_{1D} + Z_M)}{h_D (1 - m_2 / m_1) + \theta_D m_2 + h_M m_2 (1 - D / P) - h_M (1 - 2D / P)} \right)^{1/2} \quad (8)$$

$$m_2^* = \left( \frac{(A_D + m_1 Z_{2D} + A_M)(h_D - h_M(1 - 2D/P))}{(Z_{1D} + Z_M)(\theta_D - h_D/m_1 + h_M(1 - D/P))} \right)^{1/2} \quad (9)$$

Using the expressions from (5), (6), (8), (9), the integrated optimal integer of  $m_1$ , and  $m_2$  can be obtained by iteration. Accordingly, the decision variables of  $m_1$ ,  $m_2$ ,  $q_{JM}$ , and  $q_{JR}$  can be optimized simultaneously.

Kreng and Chen (2007) link the two integrated models. That is, the manufacturer's actual production lot size,  $m_2 q_{JM}$ , is the same as the DC's order quantity, which deliver in  $m_2$  equal-sized shipment with quantity of  $q_{JM}$ . The retailer's contract order quantity,  $m_1 q_{JR}^*$ , is the same of  $m_2 q_{JM}$  and deliver in  $m_1$  equal-sized shipment of volume,  $q_{JR}^*$ .

### 2.3 The modified second integrated model

The manufacturer enhances the quality and reduces the cost to motivate the buyer to cooperate. In order to include an imperfect production process, consider the assumption made by Porteus (1986), the expected defective cost per unit time is given by  $m_2 q_2 C_M D\tau/2$ . Additionally, we consider the invest rate per unit time is  $i$ , and base on assumption 7., the costs of the options of investing in improved process quality and setup costs reduction is  $i(F+S)$  (Porteus 1985, 1986). Thus, the annual total cost of the manufacturer is modified as follows:

$$\begin{aligned} TC_M(q_2, m_2, A_M, \tau) &= TRC_M + m_2 q_2 C_M D\tau/2 + i(F + S) \\ &= (A_M + m_2 Z_M) \frac{D}{m_2 q_2} + h_M \frac{m_2 q_2}{2} \left(1 - \frac{d}{p} - \frac{1}{m_2} + \frac{2d}{m_2 p}\right) \\ &\quad + m_2 q_2 C_M D\tau/2 + i(F + S) \end{aligned} \quad (10)$$

Where,  $F(\tau) = a_1 - b_1 \ln(\tau)$  and  $S(A_M) = a_2 - b_2 \ln(A_M)$

Subject to  $0 \leq \tau \leq \tau_0$  and  $A_M \in [0, A_{M_0}]$

Porteus assumes the logarithmic form  $F = a_1 - b_1 \ln(\tau)$  is investment cost of changing the probability of imperfect product to the level  $\tau$  from original level  $\tau_0$ . Also, investment cost  $S = a_2 - b_2 \ln(A_M)$  is required to change the setup cost to  $A_M$  from original level  $A_{M_0}$ , where  $a_1$ ,  $b_1$ ,  $a_2$ , and  $b_2$  are given positive constants. The logarithmic case is convex and strictly de-

creasing in its domain of the interval of  $\tau$  or  $A_{M_0}$ .

$TRC_{DM}$  is the sum of the manufacturer and the DC's annual total cost which can be represented by

$$TRC_{DM} = TRC_D \text{ (Eq.2)} + TRC_M \text{ (Eq.10)},$$

The integrated annual total cost function can, therefore, be rearranged to be:

$$\begin{aligned} & TRC_{DM}(m_2, q_{JM}) \\ &= \frac{D}{q_{JM}}((A_D + A_M + m_1 Z_{2D})/m_2 + Z_{1D} + Z_M) \\ &+ \frac{q_{JM}}{2}(h_D(1 - m_2/m_1) + \theta_D m_2 + h_M m_2(1 - D/P) - h_M(1 - 2D/P) + m_2 C_M D \tau) \\ &+ i(F + S) \end{aligned} \quad (11)$$

In the above,  $m_2$  is an integer representing the number of shipments delivered to the DC from the manufacturer with the volume of  $q_{JM}$ .

The integrated optimal shipment size,  $q_{JM}$ ; deliver number,  $m_2$ ; setup cost,  $A_M$ ; and the Probability of producing defective products,  $\tau$ , for the manufacturer can be obtained simultaneously as follows:

$$q_{JM}^* = \left( \frac{2D((A_D + A_M + m_1 Z_{2D})/m_2 + Z_{1D} + Z_M)}{h_D(1 - m_2/m_1) + \theta_D m_2 + h_M m_2(1 - D/P) - h_M(1 - 2D/P) + m_2 C_M D \tau} \right)^{1/2} \quad (12)$$

$$m_2^* = \left( \frac{(A_D + m_1 Z_{2D} + A_M)(h_D - h_M(1 - 2D/P))}{(Z_{1D} + Z_M)(\theta_D - h_D/m_1 + h_M(1 - D/P) + C_M D \tau)} \right)^{1/2} \quad (13)$$

$$A_M = \frac{ib_2 m_2 q_{JM}}{D} \quad (14)$$

$$\tau = \frac{2ib_1}{m_2 q_{JM} C_M D} \quad (15)$$

The decision variables of  $m_1$ ,  $m_2$ ,  $q_{JM}$ ,  $q_{JR}$ ,  $A_M$ , and  $\tau$  can be optimized simultaneously. Link the two integrated models by  $m_1 q_{JR}^* = m_2 q_{JM}^*$ . The linkage methods used, like Kreng and Chen (2007).

### 3. Cooperative integrated models

#### 3.1 The delivery policy I-A two-echelon integrated model

As the DC is integrated backward and established by the retailer, naturally, the DC cooperates with the retailer to determine order quantity, and shipment lot-size, in order to reduce the inventory cost. By substituting  $q_{JR}^*$  (Eq. 5) in the cost function,  $TRC_{RD}$  (Eq.4), and differentiating with respect to  $m_1$ , and  $m_2$ , separately, the optimal  $m_1$  can be reached as the one of two nearest integer to

$$m_1^* = \left( \frac{A_R + A_D + m_2 Z_{1D}}{(Z_R + Z_{2D})(\theta_R + \theta_D + h_D / m_2)} (h_R - h_D) \right)^{1/2} \quad (16)$$

And the optimal  $m_2$  can be reached as the one of two nearest integer to

$$m_2^* = \left( \frac{h_D (A_R + A_D + m_1 Z_R + m_1 Z_{2D})}{Z_{1D} \left( \frac{h_R}{m_1} + \theta_R - \frac{h_D}{m_1} + \theta_D \right)} \right)^{1/2} \quad (17)$$

The manufacturer schedules production in anticipation of the order; this is two-echelon delivery policy.

#### 3.2 The delivery policy II-A three-echelon integrated model

A lot of approaches discuss different topics with integrated model. Buying and selling relationship often involve more than three parties in supply chain. It will be difficult to reach the real minimum cost if we don't adopt system coordination strategy. Coordination of three parties or more than three parties will have more managerial implications than relatively two parties. Base on the results of the previous sections formula (5), formula (6), and formula (12) to formula (15), the shipment lot size, the number of delivery, the optimal setup cost, and probability of producing defective products can be obtained. We link the first integrated model and the modified second integrated model. That is, the manufacturer's shipment size,  $q_{JM}$ , is arran-

ged just enough to cover multiplication of  $q_{JR}^*$ , and  $m_1 = nm_2$ . The delivery quantity and number of delivery are jointly determined within common inventory cycle. So that total of production quantity is equal to total of shipment quantity, i.e.  $m_2 q_{JM} = m_1 q_{JR}$ .

In order to motivate the buyer to cooperate, manufacturer invests in reducing the setup cost and improving quality. Reducing the system total cost what can be expected. Thus, the manufacturer enhances the quality and shares the cost savings with the buyer. This model can be used when both the vendor and the buyer belong to the same or different organization.

#### 4. Numerical Example

As an illustration to the proposed model, an example is considered which is taken from the work of Kreng and Chen (2007). The cost parameters and production quantity are illustrated in table 1, and the numerical results for the example are shown on table 2. The probability of imperfect product,  $\tau$ , is 0.0004.

- (a) When the two-echelon model is adopted, all parties' optimal quantity can be obtained as  $q_{JM} = 144$ , and  $q_{JR} = 144$ , then, to ascertain the numbers of delivery ( $m_1 = 2$ ,  $m_2 = 2$ ,  $n = 1$ ) through coordination. The numerical results (the first column of table 2) reveal that the annual total cost of system is \$48,876.
- (b) Through the expressions of (5), (6), (12)–(15), the integrated optimal integer,  $m_1 = 4$ ,  $m_2 = 2$ , and, shipment quantity,  $q_{JM}^* = 288$  units,  $q_{JR}^* = 144$  units can be obtained by iteration. The integrated optimal quantity addresses the effect of collaboration. The savings can then be analyzed compared to the two-echelon model. The annual total relevant cost, \$39,258, of the integrated system is significantly less than the annual total cost of the typical delivery policy.

As to operate in coordination with the retailer's JIT purchasing plan which one contract and multiple deliveries, the manufacturer considers quality improvement and setup cost reduction simultaneously (the last column of table 2), the retailer's total cost, \$15,460 increases, but gains superior quality ( $\tau = 0.000005$ ). And, the manufacturer's annual total cost decreases. Obviously, the manufacturer acts as an intermediary, all the parties benefit from the three-echelon joint model with optimal setup and quality, and the overall system cost decrease significantly. We showed that significant savings could be achieved.

We note that the integrated analysis the retailer's loss and DC's loss are less than the manufacturer's gain. Hence, the manufacturer can share the gain with the buyers. The manufacturer compensates the retailer's loss,  $\$1,342(=\$15,460-\$14,118)$ , and compensates the DC's loss,  $\$122(=\$11,488-\$11,366)$ .

## 5. Conclusions

Many researches focus on the two-echelon model. The manufacturer tends to lot-for-lot production and shipment. However, consideration of the retailer's JIT purchasing plans, cooperation is increasingly important.

A three-echelon model which includes the manufacturer, the DC, and the retailer is practice. This study modifies a two- joint model, the manufacturer considers quality improvement and setup cost reduction simultaneously, this is delivery policy II. The impact of quality improvement investment and reducing setup cost investment are analyzed. We showed that significant savings could be achieved. In order to have a better cooperation with the buyer, the manufacturer will pass part of his savings to the buyer even if he perfectly dominates the buyer (Lu., L., 1995). A saving-sharing mechanism is proposed so that Pareto improvements (i.e., one party is better off and the other is no worse off)(Chen & Chen, 2005) can be achieved among channel participants. As compare with Kreng and Chen (2007), there is very large saving in the total cost of distribution center. All the parties benefit from the policy II, the relevant total cost is low and quality is promotion. This is the main reason persuading other party to adopt the policy.

If distribution center is established backward by the retailer which is the focal company in the supply chain, the retailer enforces others to adopt its own optimal policy. The manufacturer has quite high total relevant cost (\$23,392). The manufacturer would like to consult and cooperate with retailer. The manufacturer's annual total relevant cost, \$12,310, of the integrated system is significantly less than the annual total cost of the delivery policy I. The buyer would cooperate with manufacturer only if compensated and motivated. The manufacturer offers the following options:

- (1) To share the savings with the buyer.
- (2) To offer a discount in unit price.
- (3) To enhance the quality.

The DC plans an important role in the logistic distribution system, and lowers the conflict between the two parties. Once again, for the purpose of global minimization of the total cost, coordination between all parties has to be implemented. However, there are several limitations in this study, which suggests that further research is needed. The assumptions of the fixed demand and shortage consideration should be relaxed. In addition, a model of multiple items products and multiple manufacturers should be undertaken, which implies the need for a further research into a more general model of the optimal setup and quality.

## References

- Aderohunmu, R., Mobolurin, A., Bryson, N., 1995. Joint vendor-buyer policy in JIT manufacturing. *Journal of Operational Research Society* 46(2), 375-383
- Chen, T. H., Chen, J. M., 2005. Optimizing supply chain collaboration based on joint replenishment and channel coordination. *Transportation Research Part E* 41, 261-285
- Goyal, S. K., 1988. A joint economics lot size model for purchaser and vendor. *Decision Sciences*, 236-241
- Goyal, S. K., Nebebe, F., 2000. Determination of economic production-shipment policy for a single-vendor-single-buyer system. *European Journal of Operational Research* 121, 175-178
- Hong, J. D. , Hayya, J.C., 1995. Joint investment in quality improvement and setup reduction. *Computer & Operations Research* 22,567-574
- Joglekar, P. N., 1988. Comments on a quantity discount pricing model to increase vendor profits. *Management science* 34 (11), 1391-1398
- Kelle, P., Al-khateeb, F., Miller, P. A., 2003. Partnership and negotiation support by joint optimal ordering/setup policies for JIT. *International Journal Production Economics* 81-82, 431-441
- Kreng, V. B., Chen, F. T., 2007. Three echelon buyer-supplier delivery policy--a supply chain collaboration approach. *Production Planning and Control* 18(4), 338-349.
- Lu., L., 1995, A one-vendor multi-buyer integrated inventory model, *European Journal of Operation Research* 81,312-323
- Ouyang, L. Y., Chen, C. K., Chang, H. C., 2002. Quality improvement, setup cost and lead-

- time reduction in lot size reorder point models with an imperfect production process. *Computer & Operations Research* 29, 1701-1717
- Porteus, E. L., 1986. Optimal lot sizing, process quality improvement and setup cost reduction. *Operations research* 34, 137-144.
- Sharafali, M., CO, H. C., 2000. Some models for understanding the cooperation between the supplier and the buyer. *International Journal of Production Research* 38,(15),3425-3449
- Thomas, D. J., Griffin, P. M., 1996. Coordinated supply chain management. *European Journal of Operational Research* 94, 1-15.
- Yang, J. S., Pan, J. C. H., 2004. Just-in-time purchasing: an integrated inventory model involving deterministic variable lead time and quality improvement investment. *International Journal of Production Research* 42(5), 853-863

**Table 1 Costs parameter for the case (P=2,000unit/year, D=1,800unit/year)**

	Manufacturer	Distribution Center	Retailer
Ordering cost /setup cost	$A_M = \$1600/\text{order}$	$A_D = \$400/\text{order}$	$A_R = \$400/\text{order}$
Shipment cost/receive cost	$Z_M = \$864/\text{shipment}$	$Z_{1D} = \$216/\text{shipment}$ $Z_{2D} = \$400/\text{shipment}$	$Z_R = \$100/\text{shipment}$
Stock holding cost	$h_M = \$21.6/\text{unit/year}$ $(C_M * r_M)$	$h_D = \$21.6/\text{unit/year}$ $(= C_{DC} * r_{DC})$	$h_R = \$108/\text{unit/year}$ $(= C_R * r_R)$
losing flexibility cost		$\theta_D = \$8.1/\text{unit/year}$ $(= C_{DC} * r_1)$	$h_R = \$18/\text{unit/year}$ $(= C_R * r_R)$
Production cost/selling cost	$C_M = 270$	$C_{DC} = 270$	$C_R = 600$
Annual inventory carrying cost rate	$r_M = 0.08$	$r_{DC} = 0.08$	$r_R = 0.18$
Cost rate of losing flexibility		$r_1 = 0.03$	$r_2 = 0.03$

**Table 2 Summary of the comparison of delivery policies I and II**

	Delivery policy I (Joint DC and retailer)	Delivery policy II (Two-Joint model)
Retailer's annual Cost (Allocated cost)	14118	15460(14118)
Manufacturer's annual cost(Allocated cost)	23392	12310(13774*)
DC's annual cost(Allocated cost)	11366	11488(11366)
Joint total annual cost	48876	39258
number of shipments per order from manufacturer to the DC : $m_2$	2	2
number of shipments per order from DC to the retailer: $n$	1	2
number of shipments per order of retailer: $m_1$	2	4
shipment quantity from manufacturer to DC: $q_{JM}$	144	288
optimal shipment quantity from DC to retailer: $q_{JR}^*$	144	144

\*\$13,774=\$12,310 + (\$15,460-\$14,118) + (\$11,488-\$11,366)

*Received September 3, 2007*

*Revised December 4, 2007*

*Accepted December 11, 2007*

## 實現高品質提升和降低整備成本的三階整合模型

耿伯文

成功大學工業與資訊管理研究所

陳放子

台南科技大學國際企業經營系

### 摘 要

對及時系統之買方而言，降低存貨成本在供應鏈物流系統中是很重要的目的。爲了供應鏈盈餘的最大化，考慮整體系統之最適利益。傳統上，大部分文獻討論二階存貨整合模型，實際上，物流中心普遍存在，三階或三階以上之整合相對於二階有更大的管理意涵。首先，作者回顧有製造商，物流中心及零售商之三階整合模型，爲了吸引買方之合作，作者考慮一合作策略，包括品質改善投資及降低整備成本投資之影響分析，數據結果顯示最適整備及品質改善之三階整合模型顯著降低系統總成本。

**關鍵詞：**供應鏈管理，整合，三階

# Minimizers of Energy Functional over $\mathbb{R}^N$ Space

Mao-Sheng Chang<sup>1</sup> Shu-Cheng Lee<sup>2</sup> Chien-Chang Yen<sup>3</sup>

<sup>1,2,3</sup> Department of Mathematics, Fu Jen Catholic University, Hsinchuang, Taipei, Taiwan

## Abstract

This paper considers the energy functionals over the whole space  $\mathbb{R}^N$ . Under certain constraint, we show the existence of minimizers for this problem via the direct method in the calculus of variations.

**Keywords.** energy functionals, minimizer, direct method

## 1. Introduction and Statement of Results

In the Van der Waals-Cahn-Hilliard theory of phase transitions, the total energy functional is

$$E_\varepsilon(u) = \int_{\Omega} [W(u(x)) + \varepsilon |\nabla u(x)|^2] dx$$

with the constraint

$$\int_{\Omega} u(x) dx = m |\Omega|, \quad (1)$$

in which the density distribution of a two-phase fluid is based on a free energy that depends on both the density  $u$  and its gradient  $\nabla u$ . In general, people assume that the fluid is contained in a bounded domain  $\Omega \subset \mathbb{R}^N$  and characterize the stable distributions of fluid in  $\Omega$ , that is, to find a minimizer of  $E_\varepsilon$  subject to the constraint (1) (cf: [4]).

---

\*Corresponding author. Tel: +886-2-29053547

E-mail: yen@math.fju.edu.tw

In this paper, we try to consider an extremal case,  $\Omega$  is large enough and the quantity of one phase is relatively far more than the other phase. More precisely, the problem is described as the following. A family of energy functionals is

$$E_\varepsilon(u) = \int_{\mathbb{R}^N} [W(u(x)) + \varepsilon |\nabla u(x)|^2] dx, \quad \varepsilon > 0, \quad (2)$$

where  $W(u) = \frac{1}{4}u^2(1-u)^2$ , with the constraint

$$\int_{\mathbb{R}^N} e^{-|x|} u(x) dx = m\sigma_N, \quad 0 < m < 1. \quad (3)$$

The notation of  $\sigma_N$  denotes the volume of the unit ball in  $\mathbb{R}^N$ . Let us define a subset of the function space  $H^1(\mathbb{R}^N)$

$$\Sigma_m = \left\{ u \in H^1(\mathbb{R}^N) : \int_{\mathbb{R}^N} e^{-|x|} u(x) dx = m\sigma_N \right\} \quad (4)$$

The main result of this paper is the following theorem.

**Theorem 1.1** *The functional  $E_\varepsilon$  defined in Equation (2) has a minimizer on  $\Sigma_m$  defined in Equation (4) for  $N \geq 3$ .*

## 2. Preliminaries

We give an brief introduction the direct method in the calculus of variations. Let us define  $\Omega$  be a subset of  $\mathbb{R}^N$ . It is known that a bounded continuous  $f$  on a compact set (bounded and closed)  $\Omega$  attains its minimum value. Since  $f$  is bounded, the infimum exists

$$m = \inf_{x \in \Omega} f(x).$$

Furthermore, there is a sequence  $\{x_n\}$  such that

$$\lim_{n \rightarrow \infty} f(x_n) = m.$$

The set  $\Omega$  is compact, it follows that there exists a subsequence  $\{x_{n_j}\}$  and a point  $x \in \Omega$  such that  $x_{n_j} \rightarrow x$  as  $j \rightarrow \infty$ . By the continuity of  $f$  at  $(x)$ , it implies

$$m = \lim_{j \rightarrow \infty} f(x_{n_j}) = f(x).$$

This shows the existence of the minimum value.

The space  $R^N$  is replaced by  $L^2(\Omega, d\mu)$  and let  $F(u)$  be some functional defined on the space. Let the subset  $\Sigma = \{u \in L^2(\Omega, d\mu) : \|u\|_2 \leq 1\}$  of  $L^2(\Omega, d\mu)$ . We wish to show that the infimum of  $F$  is attained on the closed and bounded set  $\Sigma$ . If the functional  $F$  is strongly continuous, that is,  $F(u_n) \rightarrow F(u)$  as  $n \rightarrow \infty$  whenever  $\|u_n - u\|_2 \rightarrow 0$  as  $n \rightarrow \infty$ . It is a fact that for a bounded sequence  $\{u_n\} \subset \Sigma$ , there need not be a strongly convergent subsequence. Furthermore, the strength of convergence is relax to be weak convergence, every sequence in  $\Sigma$  has a weakly convergent subsequence. Indeed, the set of convergent sequences has been enlarged-but the functional  $F$  need not be weakly continuous- and it rarely is. Let us summarize that the more sequences exist that have convergent subsequences the less likely it is that  $F$  is continuous on these sequences.

**Definition 2.1** A functional is weakly lower semicontinuous if

$$\liminf_{n \rightarrow \infty} F(u_n) \geq F(u) \text{ whenever } u_n \rightarrow u \text{ weakly.}$$

**Definition 2.2**  $\{u_n\}$  is a minimizing sequence of  $F$  if

$$F(u_n) \rightarrow \inf \{F(u) : u \in \Omega\} = \lambda.$$

**Definition 2.3** A sequence  $\{u_n\}$  in  $L^p(\Omega)$  converges weakly to  $u \in L^p(\Omega)$ , denoted it by

$$u_n \xrightarrow{\text{weakly}} u \text{ in } L^p(\Omega)$$

provided that

$$\lim_{n \rightarrow \infty} \int_{\Omega} u_n(x) v(x) dx = \int_{\Omega} u(x) v(x) dx,$$

for each  $v \in L^q(\Omega)$ , where  $\frac{1}{p} + \frac{1}{q} = 1$  and  $1 < q \leq \infty$ .

The space  $L^p(\Omega)$  has the property of weak compactness.

**Theorem 2.4** ([2], p.57) Suppose  $1 < p < \infty$ . Let  $\{u_n\}_{n=1}^{\infty}$  be a sequence of functions in  $L^p(\Omega)$  satisfying

$$\sup_n \|u_n\|_{L^p(\Omega)} < \infty.$$

Then there is a subsequence  $\{u_{n_j}\}_{j=1}^{\infty}$  and a function  $u \in L^p(\Omega)$  such that

$$u_{n_j} \xrightarrow{\text{weakly}} u \quad \text{in} \quad L^p(\Omega).$$

Assume that  $\{u_n\}_{n=1}^{\infty}$  is a minimizing sequence, then there is a subsequence  $\{u_{n_j}\}_{j=1}^{\infty}$  such that  $u_{n_j} \xrightarrow{\text{weakly}} u$ , and hence

$$\lambda = \lim_{j \rightarrow \infty} F(u_{n_j}) \geq F(u) \geq \lambda.$$

Therefore,  $F(u) = \lambda$  is attained and our goal is achieved.

We further introduce the concept of weak partial derivative of a function  $u$ .

**Definition 2.5** Let  $\Omega$  be a subset of  $\mathbb{R}^N$  and  $u \in L^1_{loc}(\Omega)$ . A function  $v_i \in L^1_{loc}(\Omega)$  is the weak partial derivative of  $u$  with respect to  $x_i$ , where  $1 \leq i \leq N$ , in  $\Omega$  if and only if

$$\int_{\Omega} u(x) \frac{\partial \varphi}{\partial x_i}(x) dx = - \int_{\Omega} v_i(x) \varphi(x) dx,$$

for all  $\varphi \in C_c^1(\Omega)$ .

A Sobolev space  $W^{1,p}(\Omega)$  means that the collection of all functions  $u$  which satisfies  $u \in L^p(\Omega)$  and the weak partial derivatives  $\partial u / \partial x_i$  exist and also in  $L^p(\Omega)$ . A norm is introduced for  $W^{1,p}(\Omega)$ ,

$$\|u\|_{W^{1,p}(\Omega)} \equiv \left( \int_{\Omega} |u(x)|^p + \sum_{i=1}^N \left| \frac{\partial u}{\partial x_i}(x) \right|^p dx \right)^{1/p}$$

for  $1 \leq p < \infty$ . We denote

$$u_n \rightarrow u \quad \text{in} \quad W^{1,p}(\Omega)$$

provided

$$\|u_n - u\|_{W^{1,p}(\Omega)} \rightarrow 0$$

and

$$u_n \rightarrow u \quad \text{in} \quad W_{loc}^{1,p}(\Omega)$$

which is equivalent to

$$\|u_n - u\|_{W^{1,p}(U)} \rightarrow 0 \quad \text{for each} \quad U \subset\subset \Omega.$$

Let us recall some lemma and theorem which will be used in the proof.

**Theorem 2.6** (*Rellich-Kondrachov Compactness Theorem*). Assume  $\Omega$  is a bounded open subset of  $R^N$  and  $\partial\Omega$  is  $C^1$ . Suppose  $1 \leq p < n$ . Then

$$W^{1,p}(\Omega) \subset\subset L^q(\Omega)$$

for each  $1 \leq q < p^* = \frac{Np}{N-p}$ , means that

(i)  $\|u\|_{L^q(\Omega)} \leq C\|u\|_{W^{1,p}(\Omega)}$  for all  $u \in W^{1,p}(\Omega)$  and for some constant  $C$ .

(ii) Each bounded sequence in  $W^{1,p}(\Omega)$  is precompact in  $L^q(\Omega)$ .

**Theorem 2.7** (*L.C. Evans, PDE. 1998, p.263*) Gagliardo-Nirenberg-Sobolev inequality: Assume  $1 \leq p < N$ . There exists a constant  $C$ , depending only on  $p$  and  $N$ , such that

$$\|u\|_{L^{p^*}(R^N)} \leq C\|Du\|_{L^p(R^N)}$$

for all  $u \in C_c^1(R^N)$ , where  $p^* = \frac{Np}{N-p}$ .

### 3. The proof of the Theorem 1.1

We first show the lemma below.

**Lemma 3.1** Let  $u_n \in \Sigma_m$  and  $E_\varepsilon(u_n) \rightarrow \alpha$  as  $n \rightarrow \infty$ , then  $\{u_n\}_{n=1}^\infty$  is bounded in  $H^1(R^N)$ .

**Proof.** Since  $E_\varepsilon(u_n) \rightarrow \alpha$  as  $n \rightarrow \infty$ , the sequence  $\{E_\varepsilon(u_n)\}_{n=1}^\infty$  is bounded, denoted by  $M$ . For such  $u_n$ , let

$$A_n = \left\{ x \in \mathbb{R}^N \mid |u_n(x) - 1| \leq \frac{1}{2} \right\}.$$

Since  $1 < 2u_n < 3$  on  $A_n$  and  $2 < 2^*$ , we have

$$\int_{A_n} (2u_n(x))^2 dx \leq \int_{A_n} (2u_n(x))^{2^*} dx. \quad (6)$$

By  $H_0^1(\mathbb{R}^N) = H^1(\mathbb{R}^N)$  and Gagliardo-Nirenberg-Sobolev inequality [1] (p.263), there is a positive constant  $C$  depending on  $N$  such that

$$\int_{A_n} (2u_n(x))^{2^*} dx \leq C \left( \int_{\mathbb{R}^N} |\nabla(2u_n(x))|^2 dx \right)^{2^*/2}. \quad (7)$$

Since  $\{E_\varepsilon(u_n)\}_{n=1}^\infty$  is bounded above by  $M$  and by (6) and (7), an upper bound of the integral of the function  $u_n^2$  over the set  $A_n$  is

$$\int_{A_n} u_n^2(x) dx \leq C 2^{4/(N-2)} \left( \frac{1}{\varepsilon} M \right)^{2^*/2}.$$

Furthermore,

$$\int_{\mathbb{R}^N \setminus A_n} u_n^2(x) dx \leq 4 \int_{\mathbb{R}^N \setminus A_n} u_n^2(x) (1 - u_n(x))^2 dx \leq 16 \int_{\mathbb{R}^N \setminus A_n} W(u_n(x)) dx \leq 16M.$$

Therefore,  $u_n \in L^2(\mathbb{R}^N)$  is obtained. Note that  $E_\varepsilon(u_n) \leq M$  implies that each first order weak derivative  $\frac{\partial}{\partial x_i} u_n \in L^2(\mathbb{R}^N)$ ,  $i=1, \dots, N$ . So,  $\{u_n\}_{n=1}^\infty$  is bounded in  $H^1(\mathbb{R}^N)$ . This lemma is proved.

**Proof of Theorem 1.1.** We divide the proof into two steps.

*Step 1.* Let  $\{u_n\}_{n=1}^\infty \subset \Sigma_m$  and  $E_\varepsilon(u_n) \rightarrow \alpha$  as  $n \rightarrow \infty$ . By Lemma 3.1,  $\{u_n\}_{n=1}^\infty$  is bounded in  $H^1(\mathbb{R}^N)$ . By Rellich-Kondrashov theorem [3] (p.198), there is a subsequence, still named  $\{u_n\}_{n=1}^\infty$ , and a function  $\tilde{u}$  in  $H^1(\mathbb{R}^N)$  such that

$$\begin{array}{ll} u_n \rightarrow \tilde{u} & \text{strongly in } L^2_{loc}(R^N) \\ \nabla u_n \xrightarrow{\text{weakly}} \nabla \tilde{u} & \text{weakly in } L^2(R^N; R^N) \\ u_n \rightarrow \tilde{u} & \text{a.e. in } R^N. \end{array}$$

Then

$$\int_{R^N} |\nabla \tilde{u}(x)|^2 dx \leq \liminf_{n \rightarrow \infty} \int_{R^N} |\nabla u_n(x)|^2 dx$$

and

$$\int_{R^N} \tilde{u}(x)^2 (1 - \tilde{u}(x))^2 dx \leq \liminf_{n \rightarrow \infty} \int_{R^N} u_n^2(x) (1 - u_n(x))^2 dx.$$

These imply

$$E_\varepsilon(\tilde{u}) \leq \liminf_{n \rightarrow \infty} E_\varepsilon(u_n) = \alpha.$$

Step 2. We show that  $\tilde{u} \in \Sigma_m$ . We also assume  $\|u_n\|_{L^2(R^N)} \leq K$  and denote

$$B_\delta = \{x \in R^N \mid \|x\| < \delta\}.$$

Fix  $\tilde{\varepsilon} > 0$ , choose  $r > 0$  and an increasing sequence of positive numbers  $\{R_n\}_{n=1}^\infty$  such that  $R_n \rightarrow \infty$  as  $n \rightarrow \infty$ ,

$$\left( \int_{R^N \setminus B_r} e^{-2|x|} dx \right)^{1/2} < \frac{\tilde{\varepsilon}}{4K}, \quad \int_{R^N \setminus B_r} e^{-|x|} \tilde{u}(x) dx < \frac{\tilde{\varepsilon}}{4},$$

and

$$\left| \int_{B_{R_n}} e^{-|x|} u_n(x) dx - m\sigma_N \right| < \frac{\tilde{\varepsilon}}{4}, \quad \text{for each } n.$$

Pick  $m$  such that  $R_m > r$ . Since  $u_n \rightarrow \tilde{u}$  strongly in  $L^2(B_{R_n})$ , there exists  $M > m$  such that

$$\|u_M - \tilde{u}\|_{L^2(B_{R_m})} < \frac{2^N \tilde{\varepsilon}}{4\sigma_N(N!)}.$$

We calculate

$$\begin{aligned} \left| \int_{\mathbb{R}^N} e^{-|x|} \tilde{u}(x) dx - m\sigma_N \right| &\leq \left| \int_{\mathbb{R}^N \setminus B_{R_m}} e^{-|x|} \tilde{u}(x) dx \right| + \left| \int_{B_{R_m}} e^{-|x|} (\tilde{u}(x) - u_M(x)) dx \right| \\ &\quad + \left| \int_{B_{R_m}} e^{-|x|} u_M(x) dx - \int_{B_{R_M}} e^{-|x|} u_M(x) dx \right| \\ &\quad + \left| \int_{B_{R_M}} e^{-|x|} u_M(x) dx - m\sigma_N \right| < \tilde{\varepsilon}. \end{aligned}$$

So, Equation (3) is holds for  $\tilde{u}$ . It follows that  $\tilde{u} \in \Sigma_m$  and Theorem 1.1 is achieved.

## References

- [1] L. C. Evans, *Partial Differential Equations*, American Mathematical Society, Providence, Rhode Island, (1998).
- [2] L. C. Evans and R. F. Gariepy, *Measure Theory and Fine Properties of Functions*, CRC Press, (1992).
- [3] E.H. Lieb and M. Loss, *Analysis*, American Mathematical Society, Providence, Rhode Island, (1997).
- [4] L. Modica, The *Gradient Theory of Phase Transitions and the Minimal Interface Criterion*, Arch. Rational Mech. Anal., 98, (1987), 123-142.

*Received September 5, 2007*

*Revised December 5, 2007*

*Accepted December 11, 2007*

# $\mathbf{R}^N$ 空間上能量泛函的最小值之存在性

李樹政 張茂盛 嚴健彰

輔仁大學數學系

## 摘 要

本文是討論在  $\mathbf{R}^N$  空間上的能量泛函。在某些條件的限制下，我們利用變分學中的直接法，證明最小值之存在性。

**關鍵詞：**能量泛函，最小值，直接法。



# Study on Optimization of the Influential Factors on Natural Frequencies of Tapered Helical Springs

Lung Tsai and Horng-Yith Liou\*

*Dept. of Mechanical Engineering, Ching-Yun University, Zhong-Li, Taiwan.*

## Abstract

The development of grey relational analysis model to survey the influential factors, i.e., the helical angle, coil diameter, wire diameter, the number of active coils, and the angle of inclination on the dynamic properties of a tapered helical spring is presented in this paper. As to those properties, the natural frequencies of free vibration are quite often the main concern for engineers; consequently, they are selected as the quality targets in the present research. In order to bypass the tedious laboratory tasks in measuring the natural frequencies related to these  $3^5$  combinations of the influential factors, a finite-element model with the aid of ANSYS package is established for the computer simulation instead. The degree of influence on the natural frequencies that the controllable factors exert on is surveyed by the correlation among them, and based on the grey relational grade matrix, the parameter which primarily dominates the quality targets reveals in the research. Among these five significantly geometric variables under investigation, the helical angle is found to be the most influential one for the first four natural frequencies, two for longitudinal modes, and two for bending modes, respectively. The method proposed in this paper may serve the purpose of furnishing the researchers with an alternative approach to some other relevant applications.

---

\* Corresponding author: Fax: +886-3-468-3301.

E-mail address: johntsai @cyu.edu.tw

**Keywords:** *Grey Relational Analysis, Tapered Helical Spring, Natural Frequency, Finite Element, ANSYS.*

## 1. Introduction

The applications of helical springs have been greatly enhanced to industries through their unique dynamic properties, and they have played the major role in many engineering designs, such as the components of shock- absorbing and shock-isolation systems, automobile suspensions, fuel supply and valve mechanisms in the vehicle manufacturing world. With an eye to getting a clear understanding of the dynamic characteristics of helical springs, numerous reports have been published for over one century using both an analytical approach and a numerical approach.

In the analytical approach, mainly in the establishment of the governing equations, Michell derived equations of the helical spring motions with four degrees of freedom, i.e., three independent axial and one rotational variable, which was probably the earliest governing equations to describe the behaviors of the helical spring (Michell, 1890). Following the assumptions made by Michell, Love (Love, 1899), developed six equations of motion, which included the other two independent rotational variables lacking in Michell's paper. With the inclusion of mechanical properties, two researchers (Yoshimura, 1952 and Wittrick, 1966) respectively plugged the torsional inertia and Timoshenko shear effect into the governing equations of motion, and then under the assumption of small deformation, Jiang et al. tried and presented successfully an analytical solution to those of the helical spring, in which the mechanical properties were more involved by taking into account the extensional and torsional dynamic properties to describe the behaviors of the helical spring (Jiang et al., 1989). The analytical approach, which incorporates the geometric as well as the mechanical properties, herein is well established and has achieved a high degree of sophistication and success in recent years. However, in evolving the governing equations to simulate the real-world dynamic behaviors, the difficulty arises to such a limit that the exact analytical solution can hardly exist. Even though lots of work has been done in this respect during the past time, it merely leads to a tedious and time-consuming approach. As a consequence, a variety of numerical methods have been proposed to deal with

such problems.

In the numerical approach, finite element method has become one of the most popular tools owing to its efficiency of transformation from governing equations into a finite-element model, the convenience of picking up the shape function for elements suitable to elucidate the physical meaning of the model, and the success of the numerical solution compared with the partial success from the analytical approach. Busse chose a helical beam element to set up the discretized governing equations with the global stiffness and lumped mass matrix (Busse, 1974). Go, however, applied the inverse iteration technique for the solutions of eigenvalues and corresponding eigenvectors by using the so-called straight beam element (Go, 1982). Later, Chen utilized a three-node element with Hermitian shape functions to interpolate the primary variables for simulating the large-deflection dynamic behaviors of a helical spring (Chen, 1983). In the same year, through a finite-element model, Sawanobori introduced the governing equations of motion which includes the effects of the helical angle as well as the number of active coils, and a deep discussion on the dynamic behaviors was propounded therein as to both effects (Sawanobori 1983). Later, the same author also surveyed the influence of helical angle on the stress and the life of a helical spring using a finite-element model (Sawanobori, 1985).

From the above review, it reveals the fact that while lots of efforts were made to deliberate the governing equations by taking into account more and more influential factors and whatever approaches were undertaken to reveal the dynamic behaviors of a helical spring, the interesting couple effects among the helical angle, wire diameter, coil diameter and the number of active coils were less involved and the preferential ranking of them was far less concerned in the literatures. Tsai et al. presented the grey relational analysis as a tool to investigate the influential factors on the dynamical behaviors of a helical spring and found that the helical angle plays the most important role controlling the behavior (Tsai et al., 2005). With the goal of providing a deep insight into such problems, the authors of this paper will continue on the study with the "grey relational analysis". Emphasis in this paper is specially placed on the influential factors stated above together with the angle of inclination on the dynamic behaviors of a helical spring, the so-called tapered helical spring in order to get a wider vision of the helical-spring world. Since the natural frequencies are always the major concern for engineers, they are thus chosen as the targets in this article, and grey relational analysis is adopted to assess the preferential ranking from the grey relational grade matrix. In saving the expenses on the manufacturing of heli-

cal springs as the tested samples and the tedious tasks for the measurement of the natural frequencies in the laboratory, the finite-element method with the aid of ANSYS package is used to set up  $3^5$  samples from three randomly picked values for each of these five influential factors.

## 2. Grey Relational Analysis

### 2.1 Data Processing

The essence of grey relational analysis lies in the survey of the correlative degrees of some comparable sequences of data on the preferred reference sequence by means of a straightforward and simple model, from which the preferential ranking influencing the target, i.e., reference sequence, can then be made. However, the raw data sequence may every so often differ from the others in terms of the range and unit; as a result, it brings about the incomparable condition during grey relational analysis. Based on the above reason, ahead of implementing the present analysis, data pre-processing of transferring the original sequence to a comparable one is required.

Usually, there are four criteria of data pre-processing (Tsai, 2002; Fung, 2003) available in grey relational analysis. Suppose the target and comparable sequences are respectively denoted as  $x_0^{(o)}(k)$ , and  $x_i^{(o)}(k)$ , where  $i = 1, 2, 3, \dots, m$ , and  $k = 1, 2, 3, \dots, n$ . If one of the values in the original sequences is infinitely large, then there is a characteristic of "the larger the better". The original sequence can be normalized as

$$x_i^*(k) = \frac{x_i^{(o)}(k) - \min x_i^{(o)}(k)}{\max x_i^{(o)}(k) - \min x_i^{(o)}(k)}, \quad (1)$$

where  $x_i^*(k)$  is the sequence after data pre-processing,  $\max x_i^{(o)}(k)$  the largest value of  $x_i^{(o)}(k)$  and  $\min x_i^{(o)}(k)$  the smallest value of  $x_i^{(o)}(k)$ . Conversely, if the original sequence bears a characteristic of "the smaller the better", it ought to be normalized as

$$x_i^*(k) = \frac{\max x_i^{(o)}(k) - x_i^{(o)}(k)}{\max x_i^{(o)}(k) - \min x_i^{(o)}(k)}. \quad (2)$$

If there is a specific value needed to be achieved, then the original sequence will be normalized as follows

$$x_i^*(k) = 1 - \frac{|x_i^{(o)}(k) - OB|}{\max\{\max x_i^{(o)}(k) - OB, OB - \min x_i^{(o)}(k)\}}, \quad (3)$$

where  $OB$  represents some specific value. Alternatively, the original sequences can be normalized in such a way that the original sequence is divided by the first value of the respective sequence, i.e.,

$$x_i^*(k) = \frac{x_i^{(o)}(k)}{x_i^{(o)}(1)}. \quad (4)$$

## 2.2 Grey Relational Coefficient and Grey Relational Grade

After the establishment of data pre-processing as stated in the last subsection, the grey relational coefficient can then be calculated, which is defined as

$$\gamma(x_0^*(k), x_i^*(k)) = \frac{\Delta_{\min} + \xi \Delta_{\max}}{\Delta_{oi}(k) + \xi \Delta_{\max}} \quad (5)$$

where  $\Delta_{oi}(k) = |x_0^*(k) - x_i^*(k)|$ , the deviation sequences

$$\Delta_{\max} = \max_{\forall j \in I} \max_{\forall k} |x_0^*(k) - x_j^*(k)|$$

$$\Delta_{\min} = \min_{\forall j \in I} \min_{\forall k} |x_0^*(k) - x_j^*(k)|$$

$\xi$  = distinguishing coefficient,  $\in [0, 1]$ .

The grey relational grade is actually a weighting sum of grey relational coefficient and can be derived from

$$\Gamma(x_0^*, x_i^*) = \sum_1^n \beta_k \gamma(x_0^*(k), x_i^*(k)) \quad (6)$$

The weighting factor,  $\beta_k$ , must satisfy  $\sum_1^n \beta_k = 1$ . In general, the grey relational grade is performed in equal weighting fashion, i.e.,

$$\beta_k = \frac{1}{n}, \quad k = 1, 2, 3, \dots, n. \quad (7)$$

The grey relational grade,  $\Gamma(x_0^*, x_i^*)$ , stands for the level of correlation between the target sequence and the comparable sequence. It also indicates the degree of influence on the target sequence exerted by the comparable sequence. Therefore, if one of the comparable sequences influences more on the target sequence than the others, the corresponding value of grey relational grade is larger than those values of the other grades.

### 3. Numerical Experiment and Results

In this paper, in order to assure the validity of the numerical experimental model, a finite-element technique with the aid of ANSYS package is adopted, and the pipe- element (Kohnke, 1999) is chosen as the shape function for interpolating the primary variables of six degrees of freedom, three for axial and three for rotational directions. The comparisons of the data out of the present model can then be made with those from other papers. The geometric and material properties of the spring in this study are tabulated as follows (Ünlüsoy, 1988)

Helical angle =  $59.75^\circ$

Mean coil diameter = 10 mm

Wire diameter = 1 mm

Number of active coils = 7.6

Material density =  $7900 \text{ kg/m}^3$

Modulus of elasticity = 200 GPa

Shear modulus = 77 GPa.

Angle of inclination =  $0^\circ$

In general, the dynamic behaviors of structure for undamped natural frequencies can be expressed in the following mathematical equation,

$$m\ddot{u} + ku = 0. \quad (8)$$

For transferring the above equation into the global finite element system, it can be reformulated as,

$$[M]\{\ddot{u}\} + [k]\{u\} = 0 \quad (9)$$

where

$$[M] = \sum_{i=1}^n [M_i]$$

$$[k] = \sum_{i=1}^n [k_i]$$

$\{u\}$  = nodal displacement vector

$\{\ddot{u}\}$  = nodal acceleration vector

$n$  = number of elements.

Based on the above properties and the chosen element, the finite-element model with 345 elements and 1031 nodes is built and shown in Fig. 1 with fixed ends on both sides as the boundary condition, which is exactly the same as that from Ünlüsoy's paper for comparisons.

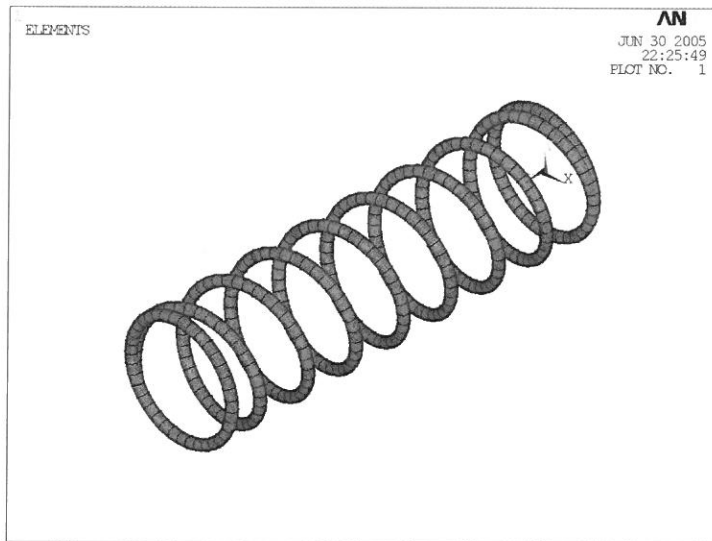


**Fig. 1 The finite element model of helical spring**

Listed in table 1 are the first ten natural frequencies together with the results obtained by Mottershead, Pearson and Ünlüsoy (Mottershead, Pearson and Ünlüsoy, 1988). The survey indicates a remarkable agreement between the theoretical and experimental results; accordingly, the

conclusion can be made that the model performed in the present analysis is adequate for the purpose of this study. Again, by following up the procedures in Tsai's paper, the current experiment is conducted with five influential factors to deal with four response variables, i.e., the four quality targets.

**Table 1 Comparison of present work with other results**

	Mottershead			Person		Unlusoy		Present Work	
	Exp	FEM	Error	TMM	Error	SRFEM	Error	ANSYS	Error
1	391	396	1.2 %	395	1 %	389	0.5 %	391	0 %
2	391	397	1.5 %	398	1.8 %	392	0.2 %	394	0.8 %
3	459	469	2.1 %	456	0.6 %	461	0.4 %	457	0.4 %
4	528	532	0.7 %	518	1.8 %	523	0.9 %	522	1.1 %
5	878	887	1 %	860	2 %	856	2.5 %	858	2.2 %
6	878	900	2.5 %	875	0.3 %	869	1 %	872	0.6 %
7	906	937	3.4 %	902	0.4 %	910	0.4 %	900	0.7 %
8	—	1067	—	1024	—	1032	—	1029	—
9	1282	1348	5.1 %	1293	0.9 %	1305	1.8 %	1300	1.4 %
10	1386	1409	1.6 %	1352	2.4 %	1352	2.4 %	1346	2.8 %

Three different levels on each of the five influential factors, which include helical angle, coil diameter, wire diameter, the number of active coils, as well as the angle of inclination, are shown in table 2, and the finite element model is set up in Fig. 2.

**Table 2. Levels of influential factors**

Levels of influential factors	Influential factors				
	Helical angle	Coil diameter (mm)	Wire diameter (mm)	Numbers of active coils	Angle of inclination
1	59.75°	9	1	7.6	5°
2	54.75°	12	3	10.6	10°
3	49.75°	16	6	12.6	15°

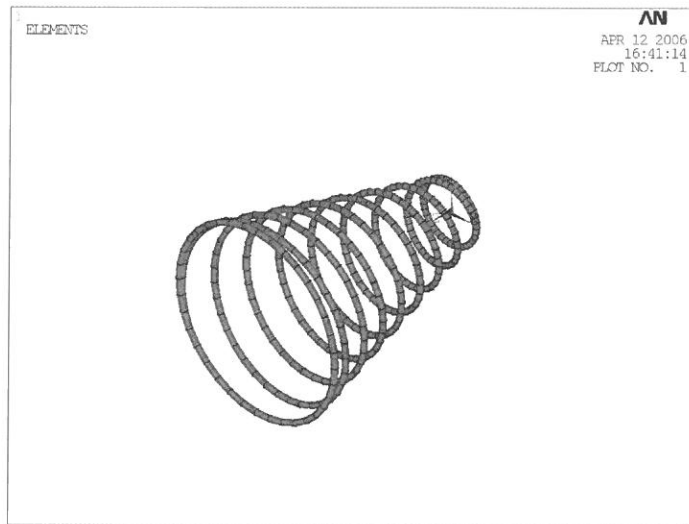


**Fig. 2 The finite element model of the tapered helical spring**

Four response variables consist of two natural frequencies for longitudinal modes and two for bending modes. By virtue of the fact that the traditional experimental runs in the laboratory for the current  $3^5$  combinations will result in the tremendous expenses on spring manufacturing as well as time consumption, the numerical experiment is introduced instead as part of the main idea of the present research. The results obtained after normalization by the present method are plotted in Fig. 3, 4, 5, and 6 with four different modes, respectively, in which quite different natural frequencies associated with some combinations of the influential factors can be perceived. This hence demonstrates the urgency of surveying the influence of those factors on the natural frequencies.

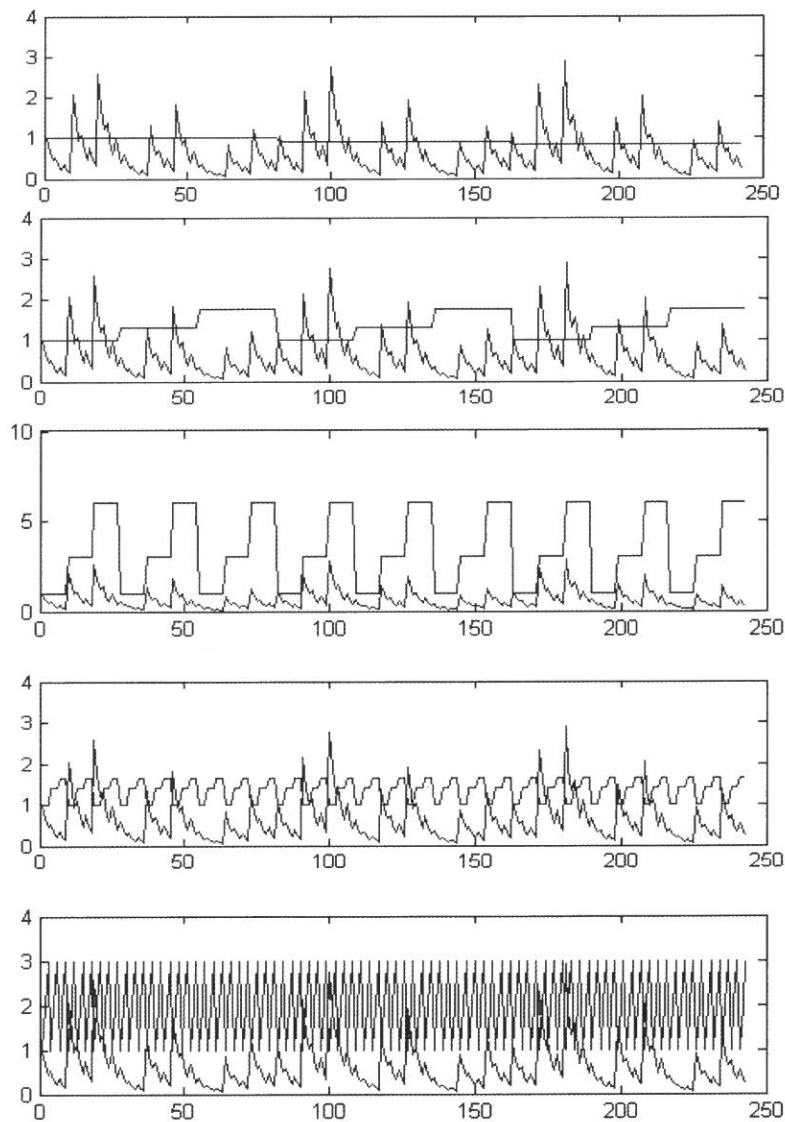


**Fig.3** Comparisons of the frequencies of mode 1 (straight or zigzag lines) with the helical angle, coil diameter, wire diameter, the number of active coils, and the angle of inclination (fluctuating lines), respectively, after normalization.

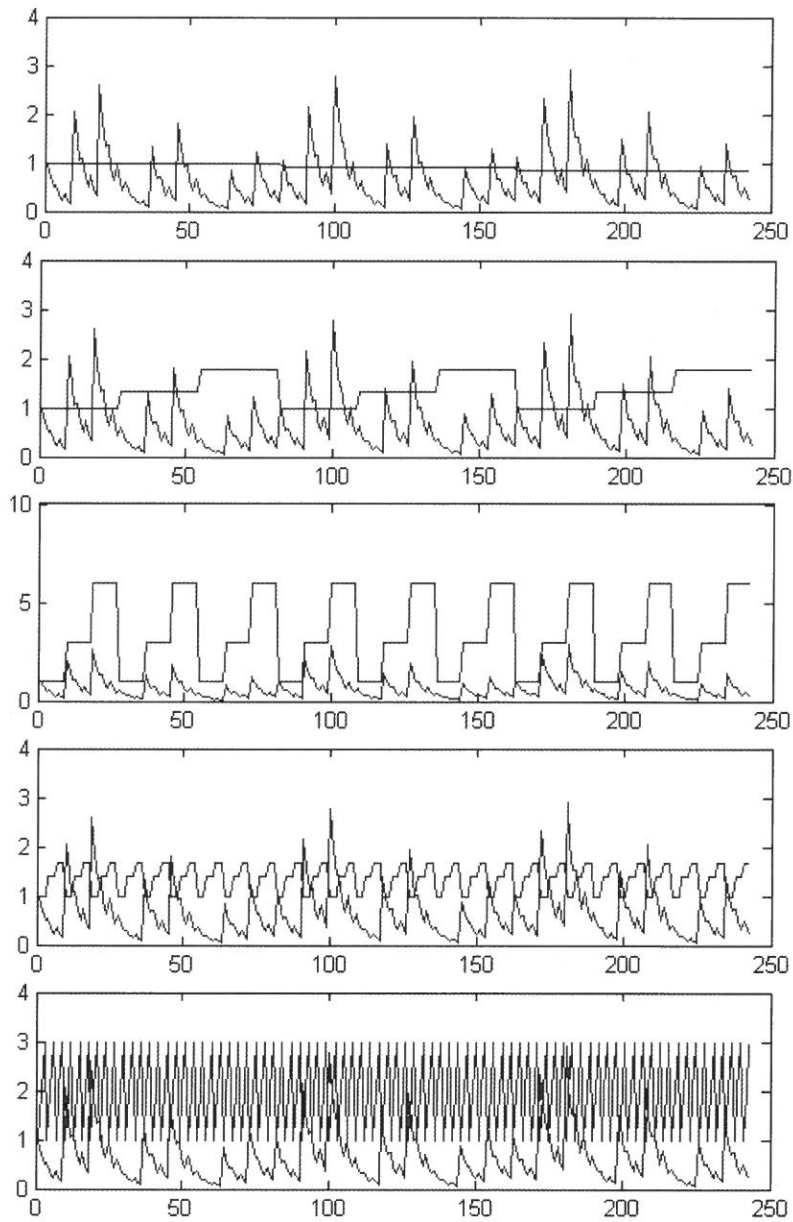


**Fig.4 Comparisons of the frequencies of mode 2 (straight or zigzag lines) with the helical angle, coil diameter, wire diameter, the number of active coils, and the angle of inclination (fluctuating lines), respectively, after normalization.**

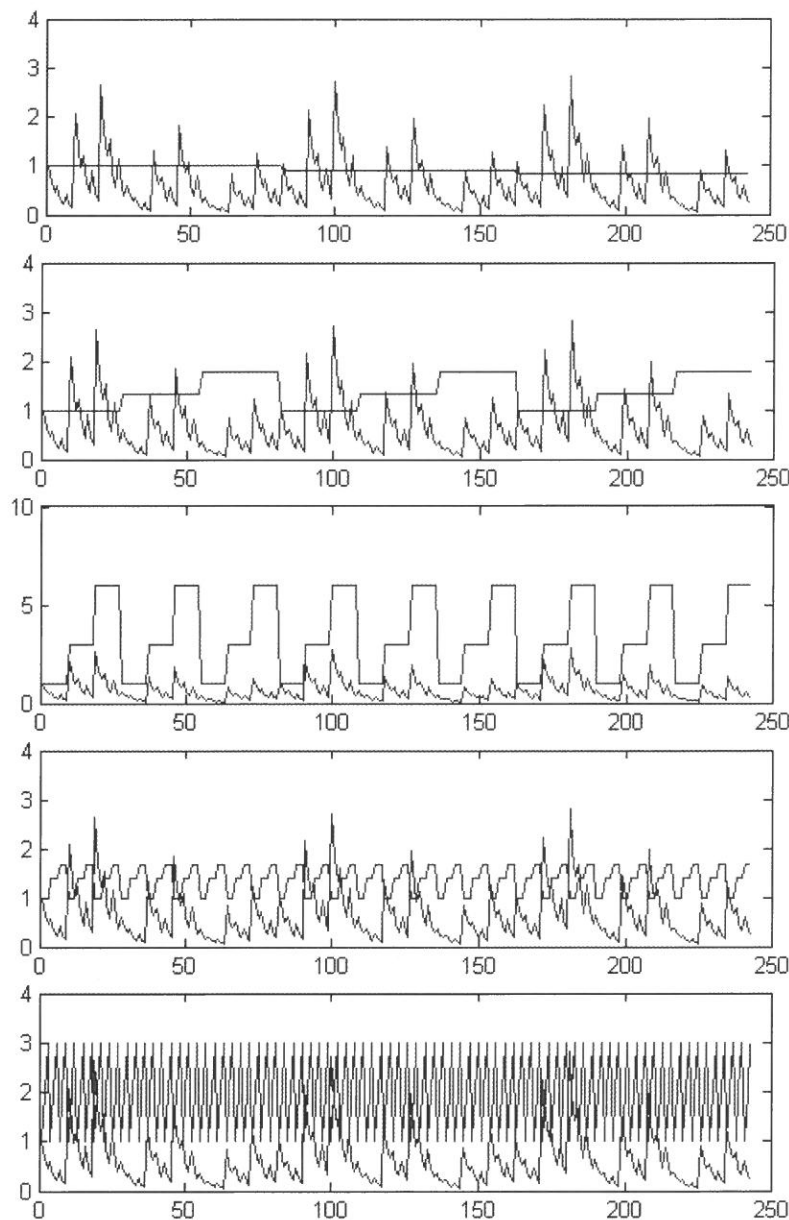


**Fig.5** Comparisons of the frequencies of mode 3 (straight or zigzag lines) with the helical angle, coil diameter, wire diameter, the number of active coils, and the angle of inclination (fluctuating lines), respectively, after normalization.

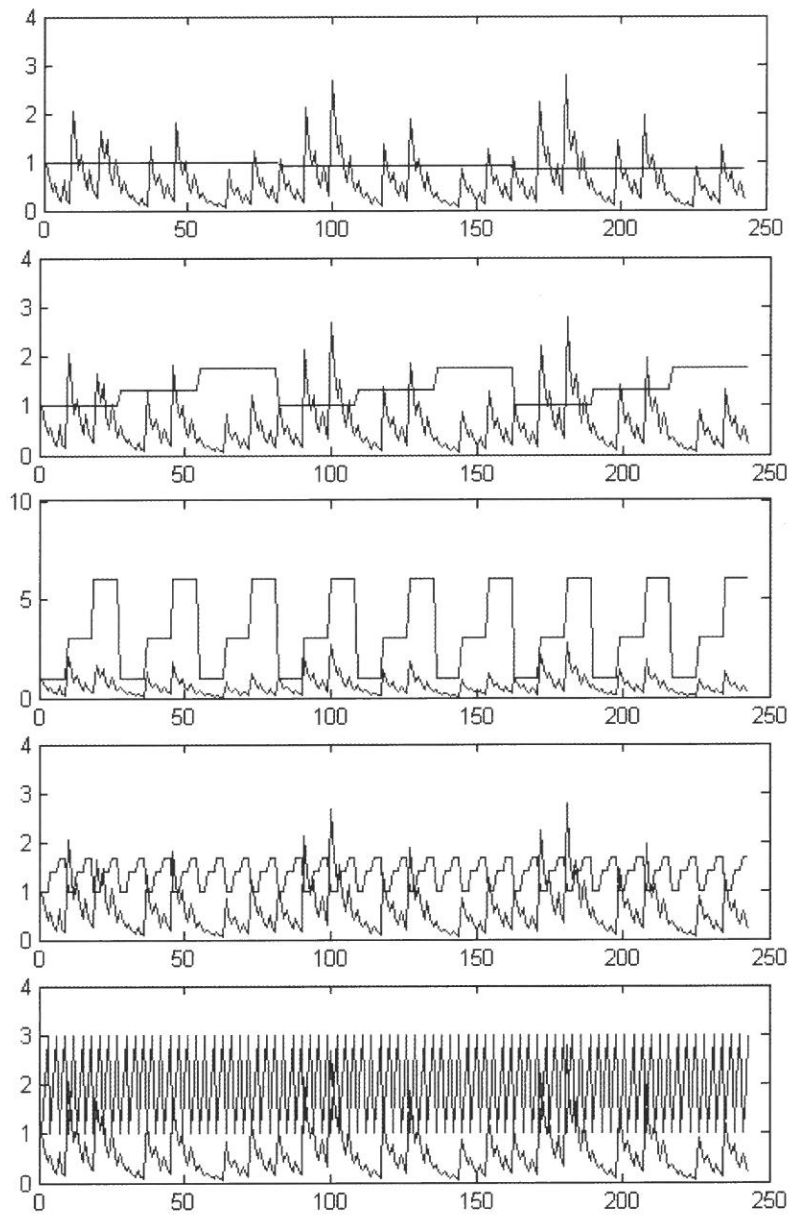


**Fig.6 Comparisons of the frequencies of mode 4 (straight or zigzag lines) with the helical angle, coil diameter, wire diameter, the number of active coils, and the angle of inclination (fluctuating lines), respectively, after normalization.**

## 4. Analysis and Discussion

With the results computed by the formula in the preceding section, that the influential factors affect the natural frequencies of helical spring can be investigated according to the grey relational analysis in section 2. In this study, let the original natural frequencies out of the  $3^5$  runs be denoted as  $x_{n1}^{(0)}(k)$ ,  $x_{n2}^{(0)}(k)$ ,  $x_{n3}^{(0)}(k)$  and  $x_{n4}^{(0)}(k)$ , where the subscripts  $n1$ ,  $n2$ ,  $n3$  and  $n4$  represent the natural frequencies from 1 to 4, respectively, and the influential factors, i.e., the helical angle, coil diameter, wire diameter, the number of active coils, and the angle of inclination are respectively denoted as  $x_A^{(0)}(k)$ ,  $x_B^{(0)}(k)$ ,  $x_C^{(0)}(k)$ ,  $x_D^{(0)}(k)$  and  $x_E^{(0)}(k)$ , where  $k = 1, 2, 3, \dots, 243$ .

The data pre-processing is followed in accordance with eq.(4), i.e., the individual sequence is divided by its first value, which thus leads to the normalized procedure to the data pre-processing. The deviation sequences are calculated and the distinguishing coefficient  $\zeta$  is chosen for substituting into eq.(5) to obtain the grey relational coefficient. Normally, if all the process parameters are of equal weighting,  $\zeta$  is 0.5, which is the value selected in the present study. In the last step, the grey relational coefficients are averaged in equal weighting in eq.(6) so as to attain the grey relational grade in Table 3.

**Table 3 Grey relational grades for frequencies 1, 2, 3 and 4**

	Grey relational grade				
Mode 1	0.8562	0.7773	0.5774	0.7764	0.6892
Mode 2	0.8563	0.7780	0.5792	0.7766	0.6915
Mode 3	0.8563	0.7778	0.5788	0.7785	0.6900
Mode 4	0.8563	0.7770	0.5763	0.7770	0.6886

The grey relational grades can then be rearranged in the matrix form similar to Fung as follows (Fung, 2003):

$$\begin{aligned}
& \Gamma(x_0^*, x_i^*) \\
&= \begin{bmatrix} \Gamma(x_A^*, x_{n1}^*) & \Gamma(x_B^*, x_{n1}^*) & \Gamma(x_C^*, x_{n1}^*) & \Gamma(x_D^*, x_{n1}^*) & \Gamma(x_E^*, x_{n1}^*) \\ \Gamma(x_A^*, x_{n2}^*) & \Gamma(x_B^*, x_{n2}^*) & \Gamma(x_C^*, x_{n2}^*) & \Gamma(x_D^*, x_{n2}^*) & \Gamma(x_E^*, x_{n2}^*) \\ \Gamma(x_A^*, x_{n3}^*) & \Gamma(x_B^*, x_{n3}^*) & \Gamma(x_C^*, x_{n3}^*) & \Gamma(x_D^*, x_{n3}^*) & \Gamma(x_E^*, x_{n3}^*) \\ \Gamma(x_A^*, x_{n4}^*) & \Gamma(x_B^*, x_{n4}^*) & \Gamma(x_C^*, x_{n4}^*) & \Gamma(x_D^*, x_{n4}^*) & \Gamma(x_E^*, x_{n4}^*) \end{bmatrix} \\
&= \begin{bmatrix} 0.8562 & 0.7773 & 0.5774 & 0.7764 & 0.6892 \\ 0.8563 & 0.7780 & 0.5792 & 0.7766 & 0.6915 \\ 0.8563 & 0.7778 & 0.5788 & 0.7785 & 0.6900 \\ 0.8563 & 0.7770 & 0.5763 & 0.7770 & 0.6886 \end{bmatrix}
\end{aligned} \tag{10}$$

where

row 1= [0.8562, 0.7773, 0.5774, 0.7764, 0.6892] ,

row 2= [0.8563, 0.7780, 0.5792, 0.7766, 0.6915] ,

row 3= [0.8563, 0.7778, 0.5788, 0.7785, 0.6900] ,

row 4= [0.8563, 0.7770, 0.5763, 0.7770, 0.6886] ,

and

column 1= [0.8562, 0.8563, 0.8563, 0.8563]<sup>T</sup>,

column 2= [0.7773, 0.7780, 0.7778, 0.7770]<sup>T</sup>,

column 3= [0.5774, 0.5792, 0.5788, 0.5763]<sup>T</sup>,

column 4= [0.7764, 0.7766, 0.7785, 0.7770]<sup>T</sup>,

column 5= [0.6892, 0.6915, 0.6900, 0.6886]<sup>T</sup>

In the above matrix, the values displayed in rows 1 and 2 represent the grey relational grades for the influential factors on the natural frequencies of the longitudinal modes in y and z directions, respectively, while the values in rows 3 and 4 represent those of the bending modes in y and z directions, respectively. From rows 1, 2, 3, and 4, hardly can it be perceived that there is any difference between them, and it reveals that the natural frequencies associated with the longitudinal and bending modes have equal correlation to the five influential factors. On the other hand, the grey relational grades for any corresponding influential factors are shown in the

columns 1, 2, 3 and 4, respectively indicating the influences on the behaviors of natural frequencies controlled by the helical angle, coil diameter, wire diameter, the number of active coils, and the angle of inclination. The degree of factors influencing on the natural frequencies can therefore be observed from these columns, where column 1 exhibits the maximum values and column 3 the minimum. It means that the helical angle plays the role dominating the behaviors of natural frequencies for both the longitudinal and bending modes, while the wire diameter is of the least importance among five factors. In this paper, with the angle of inclination included, though the most and the least preferential ranking are the same as those revealed in Tsai's paper (Tsai et. al., 2005), it indeed plays some important roles controlling the behaviors of the frequencies as shown in column five. Furthermore, of these four items in column 1, it clearly shows that the first one is less than the rest of the items, which means, although the helical angle plays the most important role for the modes of helical spring, the longitudinal mode in y direction is harder to be affected by the helical angle than the other modes.

## 5. Conclusions

This paper provides a simple and an efficient tool for assessing the degree of influence of five geometric parameters on the natural frequencies of a tapered helical spring. The finite element model with the aid of ANSYS package is performed first to set up natural frequencies out of the  $3^5$  combinations of the five influential factors, and then the grey relational analysis model to establish the grey relational coefficients and grey relational grade matrix as a profile for the preferential ranking. The results are summarized as follows:

1. The longitudinal and the bending modes of the natural frequencies in y and z directions demonstrate the equal strong reference sequences, which mean that they have an equal correlation to the five influential factors.
2. Of the five influential factors, the helical angle reveals the most important to control the behaviors of helical spring, while the wire diameter the least among them. In addition, with further insight into those grey relational grades related to the influential factor of the tapered helical angle, the variable of the angle of inclination plays to some extent the controlling role on the behaviors of the helical spring.
3. The results shown above may offer an alternative approach to the research associated with

the behaviors of helical spring and the controlling of the natural frequencies in the spring manufacturing industry. However, for some other types of springs with different geometric and mechanical properties, such as the torsion spring, blade spring, etc., the influential factors on the dynamic behaviors of them are still an unexplored field in the research. This topic should be further investigated in order to make the grey relational analysis applicable to large sets of practical problems encountered in the spring manufacturing industry.

## References

- (1) Busse, L., "Vibrations of Cylindrical Springs" (in German), *Konstruktion*, Vol. 26, pp. 171-176 (1974).
- (2) Chang, S. H., Wu, J. H., and Zhu, L., "Optimizing ACURAD DIE CASTING Process Via the Grey Relational Analysis," *J. Grey System*, Vol. 3, pp. 269-282 (1997).
- (3) Chen, W. H., and Tsai, P., "On Static and Dynamic Finite Element Analysis of Helical Springs and Experimental Verifications" (in Chinese), *J. Chinese Inst. Eng.*, Vol.6, No. 1, pp.9-20 (1983).
- (4) Deng, T. L., "Introduction to Grey System Theory," *J. Grey System*, Vol. 1, pp. 1-24 (1989).
- (5) Fung, C., "Manufacturing Process Optimization for Wear Property of Fiber-Reinforced Polybutylene Terephthalate Composites with Grey Relational Analysis," *WEAR*, pp. 1-9 (2003).
- (6) Go, G. D., "On the Vibrational Characteristics of Helical Compression Spring" (in German), *ATZ*, Vol. 84, No.5, pp. 223-226 (1982).
- (7) Jiang, W., Jones, W. K., Wu, K. H., and Wang, T. L., "Nonlinear and Linear, Static and Dynamic Analyses of Helical Springs," *Proc. of the 30th AIAA/ASME/ASCE/AHS/ ASC Structures, Structural Dynamic and Materials Conference*, Mobile, Ala., Apr., pp. 386-395 (1989).
- (8) Kohnke, P., *ANSYS Theory Reference*, 001242, 11th Edition, SASIP, Inc., pp. 14-71 (14-76 (1999).
- (9) Love, A. E. H., "The propagation of Waves of Elastic Displacement Along a Helix Wire," *Trans. Camb. Phil. Soc.*, Vol. 18, pp. 364-374 (1899).

- (10) Meng, K., "Grey Relational Analysis of Lead Pollution in Urban Environment in China," J. Grey System, Vol. 1, pp. 75-80 (1995).
- (11) Michell, J. H., "The Small Deformation of Curves and Surfaces with Application to the Vibrations of a Helix and a Circular Ring," Mess, Math, Vol. 19, pp.68-82 (1890).
- (12) Sawanobori, T. and Fukushima, Y., "A Finite Element Approach to Dynamic Characteristics of Helical Spring," Bulletin of JSME, Vol. 26, No. 221, pp. 2002-2009 (1983).
- (13) Sawanobori, T., Akigama, Y., Tsukahara, Y., and Fukushima, Y., "Analysis of Static and Dynamic Stresses in Helical Spring," Bulletin of JSME, Vol. 28, No. 238, pp. 726-734 (1985).
- (14) Tsai, L., Chiu, S., and Wu, H., "A Study of GRA for Synthetic Evaluation of Eutrophic Fetsui Reservoir," J. Grey System, Vol. 3, pp. 251-258 (2002).
- (15) Ünlüsoy, Y. S., "Mobility Analysis of Helical Coil Springs," J. Modal Analysis, pp. 96-100 (1988).
- (16) Wittrick, W. H., "On Elastic Wave Propagation in Helical Springs," International J. Mechanical Science, Vol. 8, No. 25, pp. 25-47 (1966).
- (17) Yoshimura, Y. and Murata, Y., "On Elastic Waves Propagated Along Coil Springs," Rep. Inst. Sci. and Tech. Tokyo University, Vol. 6, No.1, pp. 27-35 (1952).

*Received October 9, 2007*

*Accepted December 14, 2007*

# 影響因子對錐形彈簧中自然頻率行為最佳化之探討

蔡龍 劉宏毅

私立清雲科技大學  
機械工程學系  
桃園縣中壢市健行路 229 號

## 摘 要

本篇文章旨在運用灰關聯分析就錐形彈簧中之螺旋角、彈簧直徑、彈簧線徑、作用圈數及傾斜角等五影響因子對該彈簧動態特性之影響作一探討與分析。鑑於動態特性中之自然頻率行為往往為研究人員所專注與感興趣，本文即以其為影響目標。分析過程中由於五影響因子組合下須次數方可滿足，因此在本文裡採用 ANSYS 有限元素軟體以取代繁瑣的實驗室工作以求得影響目標之數據，再以灰關聯分析探討五因子對其影響之程度作一排列，結果可發現螺旋角無論對縱向模態與彎曲模態之影響皆為最顯著。由本文所提出之方法與思考途徑可作為研究人員對相關議題之推廣與延伸。

**關鍵詞：**灰關聯分析；錐形彈簧；自然頻率；有限元素；ANSYS。



# Floating Inductance using Four-terminal Active Current Conveyors

Yung-Chang Yin

*Department of Electronic Engineering, Fu Jen Catholic University Taipei 242, Taiwan, R.O.C.*

Yung-Chwan Yin

*Department of Animation Design and Game Programming, TOKO University,  
Chia-Yi 613, Taiwan, R.O.C*

## ABSTRACT

An active resistor-capacitor (RC) network, employing three four-terminal active current conveyors (CFCCIs) as active elements, is proposed for the realization of floating inductance. The unique features of this circuit offer the following advantages: (i) No requirement on component matching for the desired schema; (ii) Independent control of inductance value facilitated through two resistors. The inductor in the LCR passive filter circuits can be replaced by the proposed simulation floating-inductor. Thus, the advantages of these new active RC filters without an inductor can include low component sensitivities and utilize the extensive capability of the primary LCR filter design. The experimental results of a series RLC passive bandpass filter confirming the theory described below.

**Key words:** four-terminal active current conveyor

---

\*Corresponding author.

E-mail:yin@ee.fju.edu.tw

## I. INTRODUCTION

Current conveyors (CCII), first introduced by noted experts, B.Smith and A. S.Sedra in 1970, have attracted considerable attention, and their various circuit applications have been explored [1][2]. Many circuits for filters [3]~[9] and a few circuits for floating inductance simulation [10]~[12] have been presented earlier employing CCII as active elements. R. Senani and V. K. Singh, circuit experts, conducted three experiments on circuit simulation:

1. Senani employed only a single CCII along with a single capacitor and two resistors to realize a circuit for the simulation of a parallel floating- inductor and resistor (parallel RL). This circuit does not require matching components. [10].
2. Singh used a single CCII, a single capacitor and two resistors to simulate a lossy floating inductance series resistor (series RL), with no component-matching requirement [11].
3. Senani proposed two new active RC networks, employing two CCII, a single capacitor and four resistors, to realize series/parallel RL impedance, with no element matching conditions [12].

Four-terminal active current conveyor (CFCCII) is a versatile active-circuit building block. It can also be used to synthesize multifunction filters and simulation inductance. Several experiments have been conducted in pursuit of this theory:

1. Gunes and Andy employed three CFCCII, two capacitors and two resistors to synthesize current-mode universal filters [13]. This proposed circuit can simultaneously realize low-pass, highpass, and bandpass filters.
2. Chang and Tu also constructed universal current-mode filters using four CFCCII and some passive elements [14].
3. Yin realized a current-mode biquad using two CFCCII and three/six passive elements [15]
4. Yin employed only one CFCCII and some resistors and capacitors to realize highpass, low-pass, and bandpass filters. The functions of notch and allpass were not constructed [16].
5. Yin realized notch and allpass filters using only one CFCCII and five/four passive elements [17].

In 2006, the first grounded inductance simulation circuit with two CFCCII, a capacitor and two resistors was constructed by Yin [18]. However, the floating inductance simulation cir-

cuit using CFCCII as active element has never been synthesized. Therefore, the purpose of this paper is to propose a circuit configuration for the simulation of floating inductance. The proposed circuit is composed of three CFCCIIs, two resistors, and one capacitor with no component matching condition imposed.

LCR passive filters with simulated immittance have also received considerable interest, because designing active filters by simulating the inductor of a passive LCR realization of the filter includes low component sensitivities and the ability to utilize the inherent advantage of LCR filter design. If the inductor of the LCR passive filters was replaced by the proposed simulation floating inductance, the new RC active filters will benefit from the LCR passive filters.

Therefore, the proposed simulation-inductor circuit using three CFCCIIs and three passive elements was used to replace the inductor of the passive LCR filters. In addition, the CFCCII can also circumvent the finite gain-bandwidth limitation of the conventional operational amplifier. It can also offer both a constant bandwidth and a high slew rate (i.e. 2000 V/us) [19] [20]. Finally, the series LCR passive bandpass filter using the proposed simulated inductor is experimentally validated.

## II. CIRCUIT DESCRIPTION

The circuit symbol for a CFCCII is shown in Fig.1. The port relations of a CFCCII can be characterized as  $i_z = \pm i_x$ ,  $v_x = v_y$ ,  $i_y = 0$  and  $i_0 = i_x$ . The '+' and '-' signs of the current  $i_z$  denote the non-inverting and inverting, respectively. The proposed simulation of floating inductor circuit is shown in Fig. 2. Using the standard notations of ideal CFCCII, the input impedance of the circuit in Fig. 2 can be expressed as

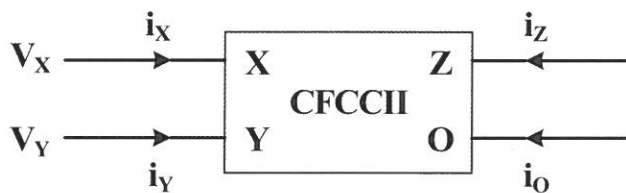
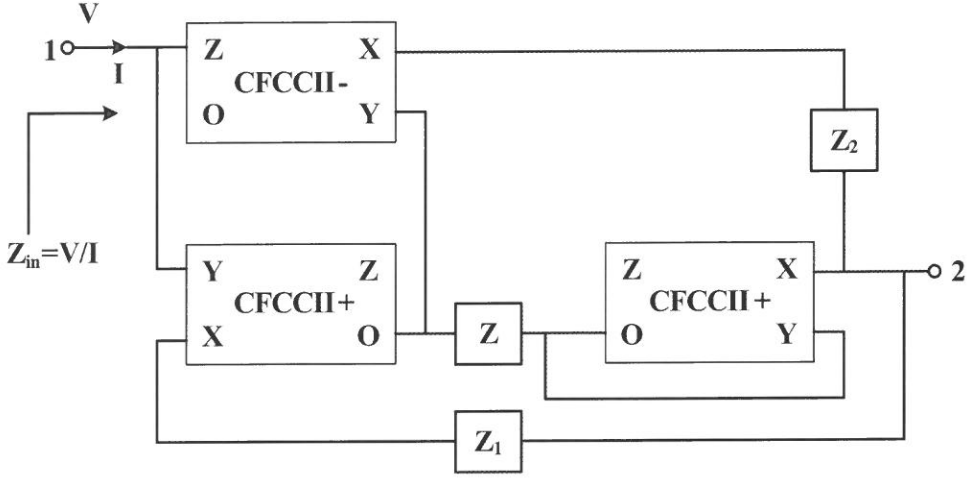


Fig.1. A CFCCII symbol



**Fig.2 The proposed floating impedance simulator.**

$$Z_{in} = \frac{Z_1 Z_2}{Z} \quad (1)$$

where  $Z - Z_2$  are the impedances. If the impedances are chosen as  $Z_1 = R_1$ ,  $Z_2 = R_2$ , and  $Z = (1/sC_1)$  shown in Fig.3. This is equivalent to an inductor with inductance  $L_{eq}$  given by

$$L_{eq} = R_1 R_2 C_1 \quad (2)$$

From the above equation, and properly selecting values of the resistors  $R_1$ ,  $R_2$  and the capacitor  $C_1$ , both large and small values of inductance can be obtained. Thus, the floating inductance simulator is constructed and its value is independently tunable through the three elements  $R_1$ ,  $R_2$ , and  $C_1$  in the circuit of Fig. 3.

### III. EXPERIMENTAL RESULTS

The AD844, as integrated circuit is now commercially available. The AD844 can be used when constructing a CFCCII. If the proposed simulation floating-inductor was experimentally tested using  $R_1 = R_2 = 1K\Omega$ ,  $C_1 = 1\mu F$  and IC AD844s, the proposed circuit can be equivalent

to an inductor with  $L_{eq} = 1H$ . Then, this simulation floating-inductor can be used in the realization of the series RLC passive bandpass filter as shown in Fig.4 and the transfer function has a biquadratic bandpass characteristic with

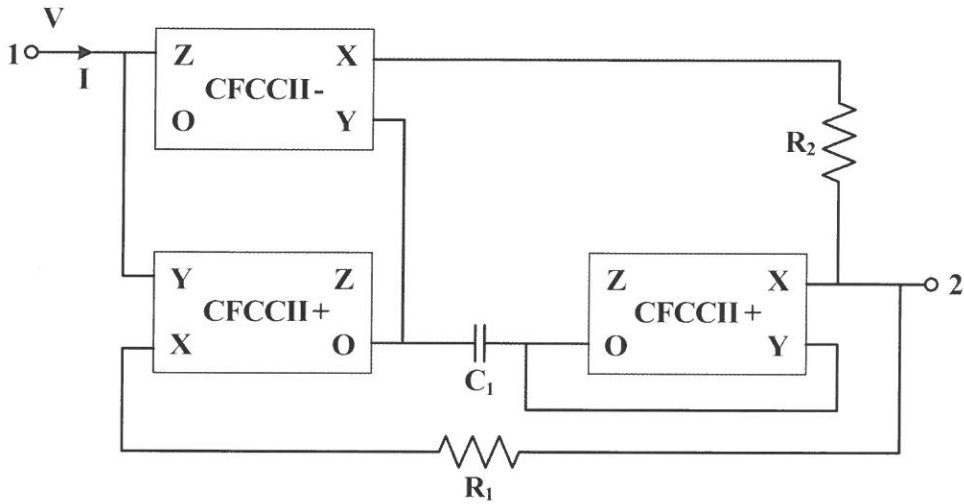


Fig.3 The proposed floating inductance simulator.

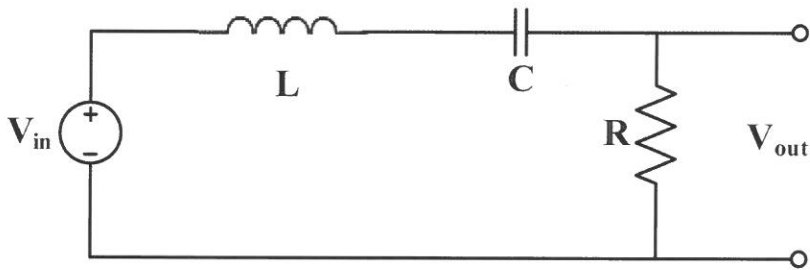


Fig.4 The prototype passive series RLC bandpass filter

$$\frac{V_{out}}{V_{in}} = \frac{\left(\frac{R}{L_{eq}}\right)s}{s^2 + s\left(\frac{R}{L_{eq}}\right) + \frac{1}{L_{eq}C}} \quad (3)$$

the central frequency:  $\omega_0 = \left(\frac{1}{L_{eq}C}\right)^{1/2}$  (4)

the quality factor:  $Q = R \left(\frac{L_{eq}}{C}\right)^{1/2}$  (5)

The sensitivity of  $\omega_0$  and  $Q$  according to passive components are:

$$s_{C_1}^{\omega_0} = s_{R_1}^{\omega_0} = s_{R_2}^{\omega_0} = s_C^{\omega_0} = s_C^Q = -\frac{1}{2}, s_{R_1}^Q = s_{R_2}^Q = s_{C_1}^Q = \frac{1}{2}, s_R^Q = 1$$

all of which are small.

In Fig.5, a second-order bandpass filter was constructed with  $R = 1K\Omega$ ,  $C = 1\mu F$  and  $L_{eq} = 1H$ . The Matlab has simulated the ideal curves of the bandpass filter. The measured values were found using a Hewlett Packard network/spectrum analyzer 4195A. The resonance frequency was monitored and measured and the corresponding inductance value was calculated and compared with the theoretical value calculated using equation (2). The experimental results for the gain and phase responses shown in Fig.6 (a) (b) demonstrate similarity between theoretical calculation and actual measurement. There is a high correlation between the theoretical analyses and the measured results with only minor errors due to the use of passive elements.

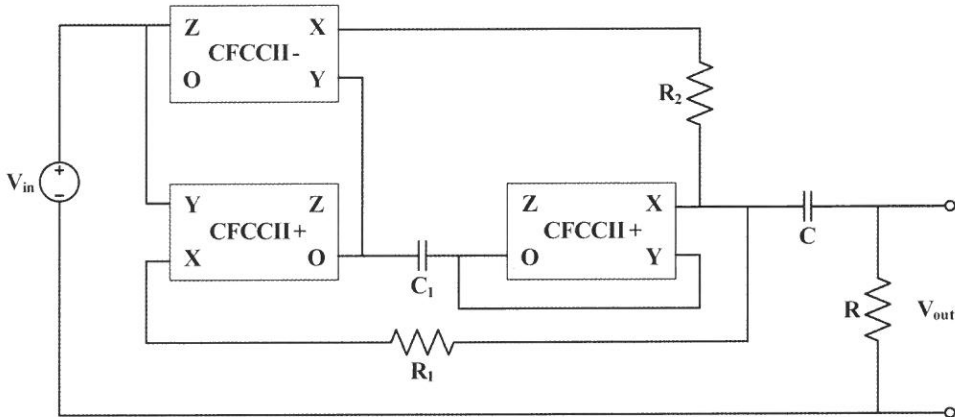
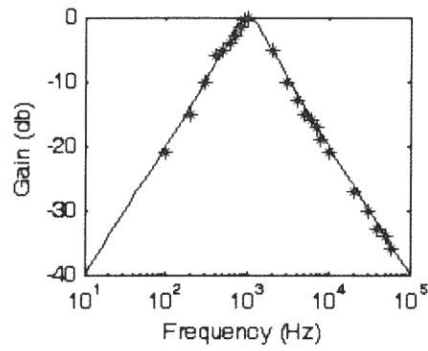
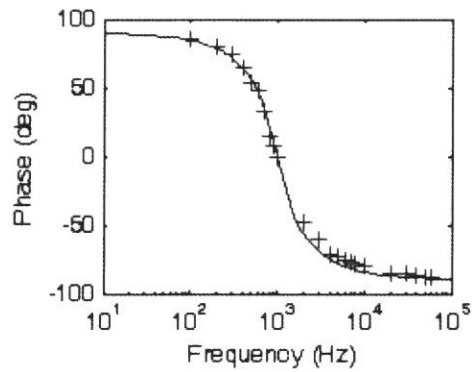


**Fig.5** Bandpass filter circuit used to test the inductor realized using circuit of Fig. 3



(a) The gain response curve of the bandpass filter using simulated inductor.



(b) The phase response curve of the bandpass filter using simulated inductor.

Fig.6 (a) The gain response curve of the bandpass filter using simulated inductor.

(b) The phase response curve of the bandpass filter using simulated inductor.

\* : Experimental result for bandpass gain

+ : Experimental result for bandpass phase

—: Ideal curve

## IV.CONCLUSION

The concept of a floating inductor using three four-terminal active current CFCCII's and three passive elements is proposed. The inductance value of the proposed circuit can be independently tunable through the three elements —  $R_1$ ,  $R_2$ , and  $C_1$ , and it does not require matching of any passive component. The advantages of RC active when constructing filter transferred by the proposed circuit includes low component sensitivities and the ability to utilize the extensive capability of LCR filter design. Therefore, the experimental results on floating inductor utilizing a LCR bandpass passive filter confirmed the theoretical analysis.

## REFERENCES

- [1] B.Wilson, "Recent Developments in Current Conveyors and Current-Mode Circuits", *IEE Proc-G*, vol. 137, no. 2, pp.63-77, 1990.
- [2] G.W.Rober and A.S.Sedra, "All Current-Mode Frequency Selective Circuits", *Electron. Lett.*, Vol.25, pp.759-761, 1989.
- [3] C.Toumazou and E.J.Lidgey, "Universal active filter using current conveyors", *Electron. Lett.*, vol. 22, pp.662-664, 1986.
- [4] Y.Sun and J.K.Fidler, "Versatile active biquad based on second-generation current conveyors", *Int. J Electron.*, vol. 76, pp91-98, 1994.
- [5] V.K.Singh and R.Senani, "New multifunction active configuration employing current conveyors", *Electron. Lett.*, vol. 26, pp.1814-1816, 1990.
- [6] G.W.Robert and A.S.Sedra, "A general class of current amplifier-based biquadratic filter circuits", *IEEE Transactions on Circuits and Systems.*, vol. 39, pp.257-263, 1992.
- [7] C.M.Chang, "Universal active current filters using single second-generation current conveyors", *Electron. Lett.*, vol. 27, no.18, pp.1614-1617, 1991
- [8] C.M.Chang and P.C.Chen, "Universal active current filter with three inputs and one output using current conveyors", *Int. J Electron.*, vol. 71, no.5, pp.817-819, 1991.
- [9] R. Senani, "New current-mode biquad filter", *Int. J Electron.*, vol. 73, no. 4, pp.735-742, 1992.

- [10] R.Senani, "Novel active RC circuit for floating inductor simulation", *Electron. Lett.*, Vol. 15, pp.679-680, 1979.
- [11] V.Singh, "A new active RC circuit realization of floating inductance", *Proceeding IEEE*, Vol.67, pp.1659-1660, 1979.
- [12] R. Senani, "Novel active RC realizations of tunable floating inductors", *Electron. Lett.*, Vol.16, pp.154-155, 1980.
- [13] E.O.Gues and F. Anday, "Realization of current-mode universal filter using CFCCII<sub>ps</sub>", *Electron. Lett.*, vol. 32, pp.1081-1082, 1996.
- [14] C.M. Chang and S.H. Tu, "Universal current-mode filters employing CFCCII<sub>ps</sub>", *Int. J Electron.*, vol. 85, no.6, pp.749-754, 1998.
- [15] Y.C.Yin, "Current-Mode Biquad Using Two CFCCII<sub>ps</sub>", *Fu Jen Studies*, No.37, pp.64-74, 2003.
- [16] Y.C.Yin, Y.C. Liou "Realization of Current-Mode Highpass Lowpass and Bandpass Biquad Filters using Single CFCCII<sub>p</sub>", *Fu Jen Studies*, No.38, pp.89-99, 2004.
- [17] Y.C.Yin, "Realization of Current-Mode Notch and Allpass Filters using Single CFCCII", *Fu Jen Studies*, No.39, pp.11-22, 2005.
- [18] Y.C.Yin, "Active simulation of grounded inductor using CFCCII<sub>s</sub>", *Fu Jen Studies*, No.40, pp.71-79, 2006.
- [19] C.Toumazou and E.J.Lidgey, "Universal active filter using current conveyors", *Electron. Lett.*, vol. 22, pp.662-664, 1986.
- [20] Y.Sun and J.K.Fidler, "Versatile active biquad based on second-generation current conveyors", *Int. J Electron.*, vol. 76, pp91-98, 1994.

*Received October 9, 2007*

*Revised December 10, 2007*

*Accepted December 17, 2007*

## 使用四端主動電流傳輸器合成浮接電感電路

鄧 永 昌

輔仁大學大學電子工程學系

鄧 永 傳

稻江科技暨管理學院動畫與遊戲軟體設計學系

### 摘 要

本文提出使用四端主動電流傳輸器當主動元件合成浮接式電感模擬電路。此合成浮接式電感模擬電路，有兩點利益。其一是：沒有任何元件匹配要求；其二是：模擬浮接式電感值可以經由兩個電阻分別獨立調整。電感模擬電路的好處是，可以用來取代現有被動濾波器的電感值，使其可以被製作成積體電路，同時被動濾波器既有的好處，在被轉換成主動濾波器後，這些好處仍可繼續存在。最後，本文以既有的串接式二階被動帶通濾波器，應用本文所提出的電感模擬電路取代其電感值，以驗證本文之理論預測。

**關鍵詞：**四端主動電流傳輸器

# A Serial Feedback Digital PWM Regulator for DC-DC Buck Conversion

Steve Hung-Lung Tu and Philip Jung-Wei Huang

## Abstract

This paper describes a newly proposed digital pulse-width modulation (DPWM) power regulator using the system serial-error feedback voltage to adjust the input voltage for high frequency switching dc-dc buck conversion. The proposed digital controller comprises an error process unit (EPU), a table look-up based PID compensator and a digital PWM. Compared with the conventional architecture with an analog-to-digital converter, the employment of a serial comparator and an EPU can greatly reduce the system complexity. A prototype is realized to validate the correctness of the proposed regulator.

*Index Terms*-Pulse-width modulation, buck conversion, PID compensator.

## I. INTRODUCTION

Recent efforts in digital technologies have seen a breakthrough in both performance and size through the employment of device scaling, which makes digital controllers offer a number of advantages such as flexibility, lower sensitivity and programmability over their analog

---

\* Corresponding author. Tel.: +886-2-29052427; fax: +886-2-29042638

E-mail address : s.tu@ieee.org

counterparts in dc-dc power conversion. Moreover, the power management function has been increasingly desirable with the proliferation of systems-on-a-chip (SOC) applications. On the other hand, the common control rules can also be applied in different parameters of dc-dc power converters. Fig.1 shows a general regulator based on a table look-up approach [1]-[3]. The system includes a buck converter, a PID compensator, a DPWM and an A/D converter. A digitized reference voltage is generated by firstly changing the  $V_{ref}$  into digital format  $V_{ref}[n]$ . Then digitized output voltage  $V_{out}[n]$  is compared with  $V_{ref}[n]$  and the resultant error signal is sent to a PID compensator. According to the output signal, the DPWM develops different duty cycle signal duty,  $d(t)$  which controls the switching buck converter and hence, develops  $V_{out}$  on the load.

In this paper, we propose a digital PWM regulator based on the system serial-error feedback correcting mechanism. Moreover, the proposed architecture employs a 1-bit comparator and an EPU, which not only makes the implementation much more easily but also does not necessitate the conventional non-linear delay-line A/D converter [2].

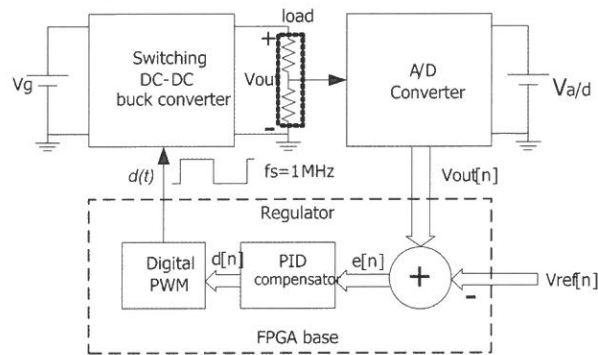


Fig.1. General regulator controls a switching converter.

## II. THE PROPOSED SERIAL FEEDBACK ARCHITECTURE

Fig.2 shows the proposed regulator, which employs a comparator to control a switching dc-dc buck converter. The regulator comprises an error process unit, a PID compensator and a

digital PWM, where  $V_g$  and  $V_{out}$  are the line input voltage and output voltage on the load of the switching converter, respectively.  $V_{ref}$  is the reference voltage employed to compare with  $V_{out}$  and yields a serial error (1 or 0) from the comparator. The serial\_error is developed with the difference of buck converter output voltage  $V_{out}$  and the reference voltage  $V_{ref}$  as shown in Fig. 3.

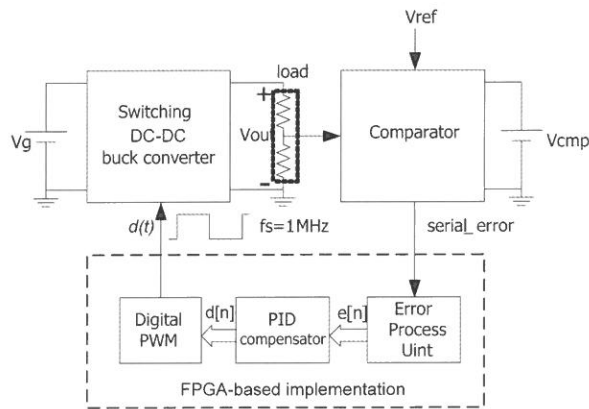


Fig.2. Proposed regulator controls a switching converter.

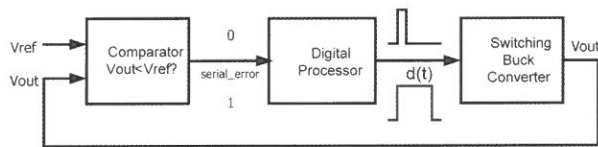


Fig.3. Relationship of the comparator with the system.

When  $V_{out}$  is greater than  $V_{ref}$ ,  $serial\_error = 0$ , which decreases the duty cycle of  $d(t)$  signal. By contrast,  $serial\_error = 1$  when  $V_{out}$  is less than  $V_{ref}$ , and then increases the duty cycle of  $d(t)$  signal. The output of the  $serial\_error$  signal is sent to the EPU which generates  $e[n]$  ranging from -4 to +4 [2]. Since the requirement for a high-resolution digital PWM is one of the important considerations in digitally controlled high-frequency power regulators [2], the compensated signal  $d[n]$  is ranging from 1 to 255. Therefore, the digital PWM generates a

1MHz switching frequency  $d(t)$  signal with a duty cycle  $d[n]/256$ . According to  $d(t)$  and all internal parameters, the converter develops output voltage  $V_{out}$  on the load and the operation iterates until  $V_{out}$  is approaching to  $V_{ref}$ .

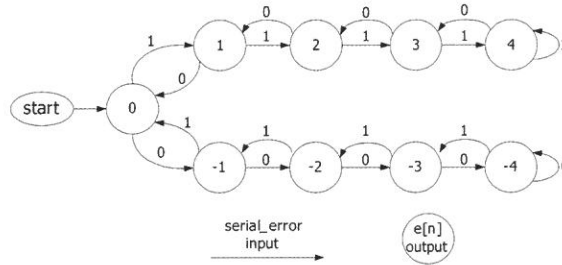


Fig.4. State diagram of the EPU.

#### A. EPU (Error Process Unit)

The EPU is a state machine developing error signal  $e[n]$  according to  $serial\_error$  signal. Fig.4 shows the EPU state diagram. If input  $serial\_error$  is 1, then  $e[n]$  is not greater than +4. On the contrary, if  $serial\_error$  is 0, then  $e[n]$  is not less than -4. Obviously, it can be implemented with a 4-bit register to cover the range from -4 to +4. Table 1 shows the truth table.

TABLE I TRUTH TABLE OF THE EPU

present state					Next state									
					serial error=0					serial error=1				
Q3	Q2	Q1	Q0		D3	D2	D1	D0		D3	D2	D1	D0	
0	0	0	0	(0)	1	1	1	1	(-1)	0	0	0	1	(1)
0	0	0	1	(1)	0	0	0	0	(0)	0	0	1	0	(2)
0	0	1	0	(2)	0	0	0	1	(1)	0	0	1	1	(3)
0	0	1	1	(3)	0	0	1	0	(2)	0	1	0	0	(4)
0	1	0	0	(4)	0	0	1	1	(3)	0	1	0	0	(4)
1	1	0	0	(-4)	1	1	0	0	(-4)	1	1	0	1	(-3)
1	1	0	1	(-3)	1	1	0	0	(-4)	1	1	1	0	(-2)
1	1	1	0	(-2)	1	1	0	1	(-3)	1	1	1	1	(-1)
1	1	1	1	(-1)	1	1	1	0	(-2)	0	0	0	0	(0)

The logic equations for the truth table are given by

$$D_3 = Q_3 \cdot (s\_e \cdot Q_1 \cdot Q_0) + (s\_e + Q_2 + Q_1 + Q_0) \quad (1)$$

$$D_2 = D_3 + s\_e \cdot \overline{Q_3} \cdot (Q_2 + Q_1 \cdot Q_0) \quad (2)$$

$$D_1 = s\_e \oplus (Q_1 \oplus Q_2) + Q_3 \cdot \overline{Q_2} \quad (3)$$

$$D_0 = \overline{Q_0} \cdot (Q_1 + s\_e \oplus Q_3 + s\_e \cdot \overline{Q_2}) \quad (4)$$

where  $s\_e$  represents serial\_error.

## B. PID Compensator

The PID compensator can be described with the following general form [1],

$$U(s) = \frac{d(s)}{e(s)} = K \cdot (1 + \frac{1}{T_I s} + T_D s) \quad (5)$$

in which  $K$  is the proportional gain,  $T_I$  the integral time,  $T_D$  the derivative time and the differential equation relating  $d(t)$  and  $e(t)$  is

$$\dot{d} = K(\dot{e} + \frac{1}{T_I} e + T_D \ddot{e}) \quad (6)$$

With the Euler's method [6], equation (6) can be expressed as

$$\frac{d(n) - d(n-1)}{T_s} = K[\frac{e(n) - e(n-1)}{T_s} + \frac{e(n)}{T_I} + T_D \frac{\partial}{\partial n}(\dot{e})] \quad (7)$$

where the last term is given by

$$T_D \frac{\partial}{\partial n}(\dot{e}) = T_D \frac{\partial}{\partial n}[\frac{e(n) - e(n-1)}{T_s}] = \frac{T_D}{T_s^2} [e(n) - 2e(n-1) + e(n-2)] \quad (8)$$

Therefore, equation (7) can be described as

$$d(n) = d(n-1) + K[(1 + \frac{T_s}{T_I} + \frac{T_D}{T_s})e(n) - (1 + 2\frac{T_D}{T_s})e(n-1) + \frac{T_D}{T_s}e(n-2)] \quad (9)$$

The PID control law supported by the configuration shown in Fig.2 is therefore given by

$$d(n) = d(n-1) + a \cdot e(n) + b \cdot e(n-1) + c \cdot e(n-2) \quad (10)$$

where  $d(n)$  and  $d(n-1)$  are the current and last-iteration outputs of the compensator, respectively.

ely.  $e(n)$ ,  $e(n-1)$ , and  $e(n-2)$  are the current, one-iteration before and two-iteration before error outputs, respectively. Comparing (9) with (10) yields

$$a = K(1 + T_s/T_I + T_D/T_s) \quad (11)$$

$$b = -K(1 + 2T_D/T_s) \quad (12)$$

$$c = K(T_D/T_s) \quad (13)$$

where  $T_s = 1/f_s$  and  $f_s$  is the switching frequency.  $K$ ,  $T_I$ , and  $T_D$  are the constants of a PID compensator. Note that as shown in Fig. 5, the products of  $(a \cdot e)$ ,  $(b \cdot e)$ , and  $(c \cdot e)$  can be implemented with look-up table  $a$ , table  $b$ , and table  $c$ , respectively, in which  $a$ ,  $b$ , and  $c$  are the gains.

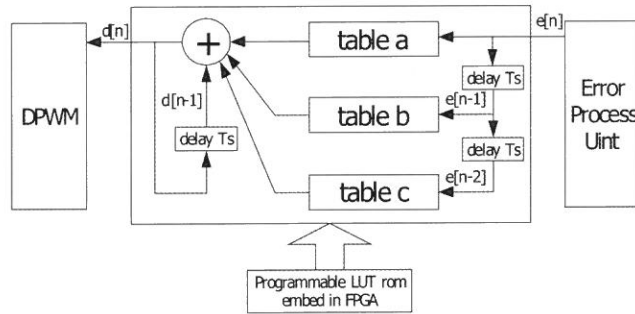
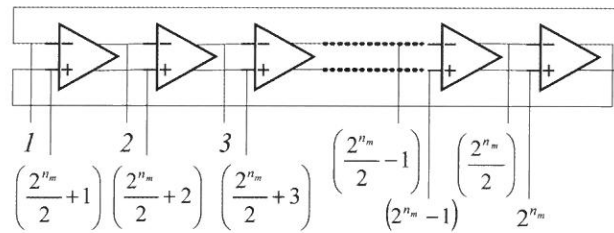


**Fig.5. Block diagram of the PID compensator.**

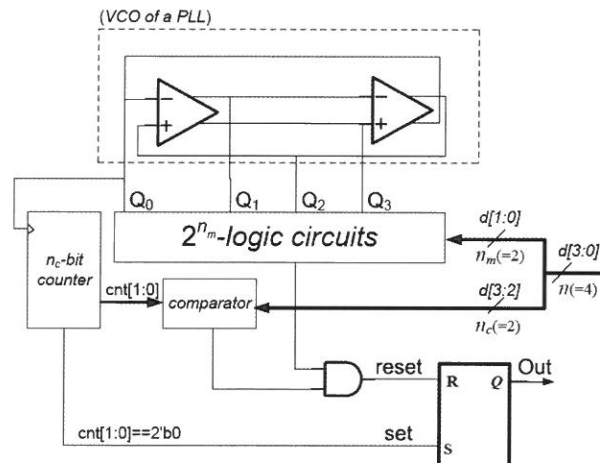
### C. Digital Pulse Width Modulation

In Fig.2, the DPWM generates switching signals with a frequency  $f_s$  and variable duty cycles according to the input values of  $d[n]$ . The DPWM is based on a multi-phase/counter approach. The multi-phase clock source is generated from the VCO of a PLL instead of a ring oscillator, which the former one can provide even more accurate timing leading to accurate duty ratio and lower ripple of the output regulated voltage. Notice that due to the effects of process and/or temperature variations, the output clock signals of the ring oscillator constructed with flip-flops may suffer serious jitter problems.

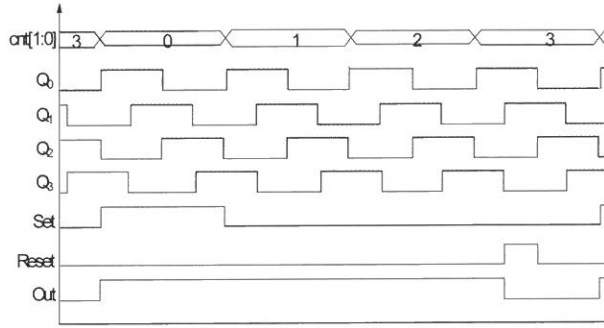
The  $n$ -bit resolution can be achieved using  $n_m$ -phase clock signals [4] and the remaining  $n_c$ -bit resolution is obtained from an  $n_c$ -bit counter. Note that here  $n = n_m + n_c$ . The multi-phase signals 1, 2, 3, ...  $2^{n_m}$  are generated from a PLL, in which the VCO is constructed with a differential ring-oscillator as shown in Fig. 6(a).



(a) Differential ring-oscillator VCO of a PLL to generate multi-phase clock signals.



(b) Simplified block diagram of a 4-bit DPWM.



(c) Operating waveforms of the DPWM.

Fig. 6. The DPWM details

The PLL can therefore operate at much lower frequency  $(2^n / 2^{n_m})f_s$  instead of  $2^n f_s$ , where  $f_s$  is the switching frequency of the DPWM. Figs. 6(b) and 6(c) show the block diagram and operating waveforms of the proposed DPWM, respectively. An example of 4-bit resolution ( $n=4$ ) can be used to describe the operation with 2-bit counter ( $n_c=2$ ) and 4-phase clock timing ( $n_m=2$ ). Initially, the SR flip-flop is set ("Out" = 1). When the counter output matches  $n_c$  and the logic circuits of the multi-phase clock timing matches  $n_m$ , "reset" signal is high to reset output signal ("Out" = 0). Since the digital input vector  $\mathbf{d}$  is preset ( $\mathbf{d}=4'$  b1101 in this example) and total resolution is  $2^n$ , the duty cycle of "Out" is therefore  $|\mathbf{d}|/2^n$  (duty cycle of Out is 13/16 in this example).

### III. SIMULATED AND EXPERIMENTAL RESULTS

The complete discrete-time model for the proposed closed loop system is shown in Fig.7, in which the parameters for the buck converter are: the input voltage  $V_g$  is between 3~4 V, the output voltage is regulated at  $V_{out} = 1.8$  V,  $R = 3.6 \sim 18 \Omega$ ,  $L = 47 \mu\text{H}$ ,  $C = 100 \mu\text{H}$ . The parameters of the PID compensator  $a = 25$ ,  $b = -47$ , and  $c = 23$  are computed with the Euler's method using  $K = 2.25$  and  $T_s = 1 \mu\text{s}$ .

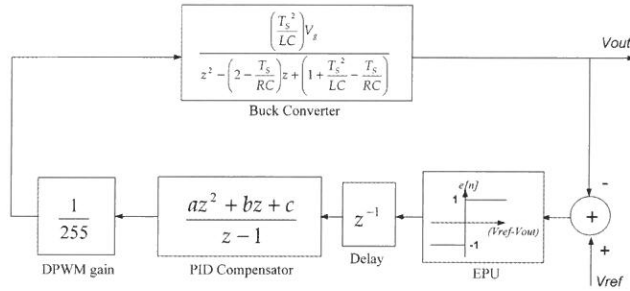


Fig.7. Discrete-time closed loop model for the system.

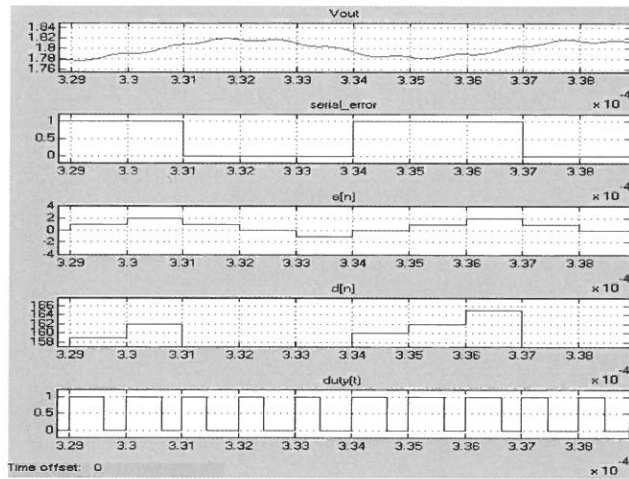


Fig.8. Steady state operating waveforms.

When  $V_{out}$  is less than  $V_{ref}$ , `serial_error` is in high level and vice versa. The EPU performs addition/subtraction operation when it receives `serial_error` and sends  $e[n]$  to PID compensator every  $T_s$  period. Initially,  $V_{out}$  is 0, which is less than  $V_{ref}$ . The pulse of duty will more and more extend to follow  $T_s$  period. When  $V_{out}$  is greater than  $V_{ref}$ , the pulse-width of  $d(t)$  will be reduced until  $V_{out}$  is equal to  $V_{ref}$ . Fig.8 shows the steady state waveforms. Obviously, different  $d[n]$  value is corresponding to different pulse-width  $d(t)$ . Fig.9 shows the implemented circuit with FPGA, in which the PMOS  $Q_p$  and NMOS  $Q_n$  act as the switches in the converter. The input

dc voltage  $V_g$  responds to the load of the buck converter. The comparator takes  $V_{out}$  to compare with the reference voltage. Since  $V_{out}$  may cause overshoot and large current will pass directly through the comparator leading to breakdown at the start-up, we divide  $R_{load}$  into two parts:  $R_{load1}$  and  $R_{load2}$ .

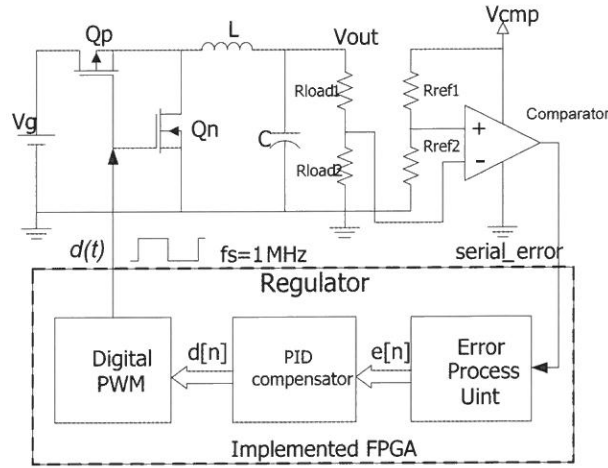


Fig.9. Test circuit configuration.

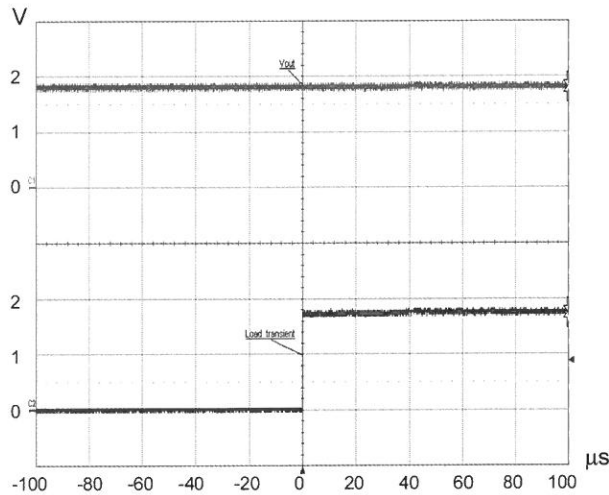


Fig.10. Measured waveforms of  $V_{out}$  for load transient response.

Fig.10 shows the load transient response for the load current from 500mA to 100mA (*i.e.* the load is from  $18\Omega$  to  $3.6\Omega$ ). Fig. 11 indicates the line transient response for the case of  $V_g$  from 3V to 4V. The supply voltage of the system including FPGA voltage is 3.3V,  $V_{cmp}$  is 3V and the output voltage is regulated at  $V_{out} = 1.8V$ . The power-up transient time is about  $150\mu s$  as shown in Fig.12.

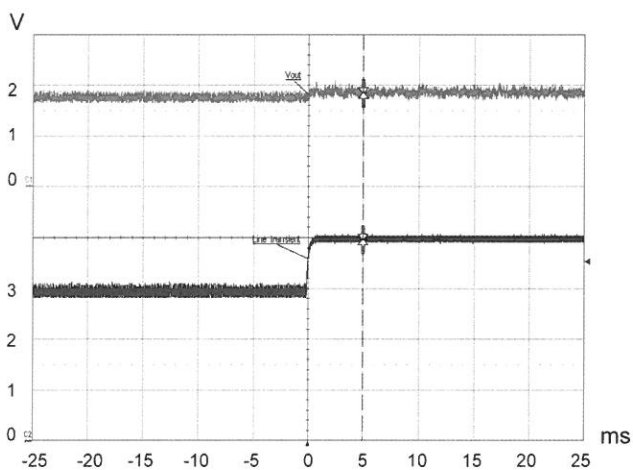


Fig.11. Measured waveforms of  $V_{out}$  for line transient response.

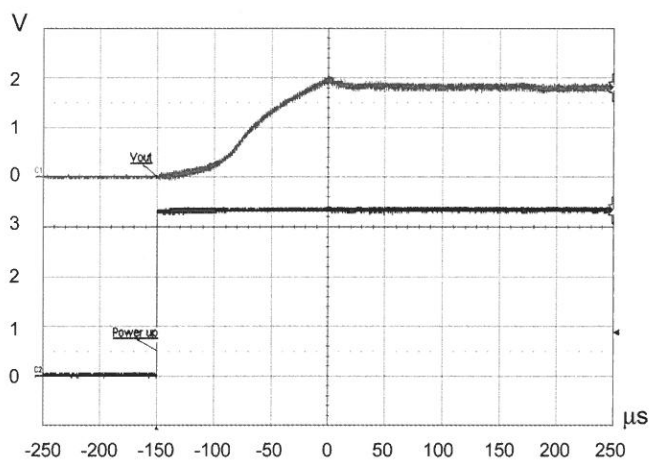


Fig.12. Waveforms of  $V_{out}$  at the power-up transient.

## IV. CONCLUSION

This paper describes a serial DPWM regulator. The employment of the proposed comparator and EPU makes the implementation much more efficiently. Furthermore, the EPU, table look-up based PID compensator and DPWM can be implemented with hardware description language (HDL) and embedded ROMs. The proposed architecture is suitable for the integration of the power management function in SOC implementations.

## REFERENCES

- [1] A. Prodic, D. Maksimovic, and R. Erickson, "Design and implementation of a digital PWM controller for a high-frequency switching DC-DC power converter," in *Proc. IEEE IECON Conf.*, pp. 893-898, 2001.
- [2] B. J. Patella, A. Prodic, A. Zirger, D. Maksimovic, "High-frequency digital PWM controller IC for DC-DC converters," *IEEE Transactions on Power Electronics*, vol. 18, no. 1, pp. 438 - 446, 2003.
- [3] P. J. W. Huang and S. H.-L. Tu, "A Digital PWM Regulator Based on Serial-Error Correcting Mechanism for DC-DC Buck Conversion," *IEEE Conference on Electron Devices and Solid-State Circuits*, Hong Kong, China, pp.289-292, Dec. 2005
- [4] M. M.-H. Chiu and S. H.-L. Tu, "A Novel DPWM Based on Fully Table Look-up for High-frequency Power Conversion," *IEEE Asia Pacific Conference on Circuits and Systems, Singapore*, pp. 679-682, Dec. 2006.
- [5] R. W. Erickson and D. Maksimovic, *Fundamentals of Power Electronics*, 2nd ed. Boston, MA: Kluwer, pp. 266-362, 2002.
- [6] G. F. Franklin and J. D. Powell, *Digital Control of Dynamic Systems*. Reading, MA: Addison-Wesley, 1998.
- [7] A. Prodic, D. Maksimovic, "Mixed-signal simulation of digitally controlled switching converters," *IEEE Workshop on Computers in Power Electronics*, pp. 100-105, June 2002.

*Received October 11, 2007*

*Revised December 11, 2007*

*Accepted December 18, 2007*

## 直流對直流降壓轉換所用之序向回授 數位脈波寬度調整控制器

杜弘隆 黃政偉

輔仁大學電子工程學系

### 摘 要

本論文描述一新提出的給高頻直流對直流切換式降壓轉換所用之數位脈波寬度調整控制器，此調整器運用系統串列誤差回授電壓來調整輸入電壓。所提出的數位控制器包含了誤差處理單元（EPU）、查表方式的比例－積分－微分（PID）補償控制器及數位式脈波寬度調整控制器。和傳統類比－數位轉換器架構相比較，由於採用了一個序向的比較器及一個誤差處理單元故可大幅降低系統的複雜度。藉由實現初步系統雛型，吾人可驗證所提調整控制器的正確性。

**關鍵詞：**脈波寬度調整控制器, 降壓轉換, PID 補償器。



# 拿破崙紙燈籠與虧格數

呂克明<sup>1</sup> 曹子殷<sup>2</sup>

## 摘 要

拿破崙紙積木有領結、眼淚、翅膀、巧克力條、船型、星型、山形袖章與鯉魚等 8 種。我們利用柏拉圖立體中，正六面體與正八面體的對偶性，成功地開發以拿破崙紙積木 8 個基本型模組，附著在對偶多面體的六面體或八面體兩種線框<sup>3</sup>上，建成 26 組 24 單位的籠狀模型<sup>4</sup>。每一基本型建成的籠狀模型，分成基本與中級兩等級。比較難建成的中級一型與中級二型，分別是基本一型與基本二型，互為多面體表面可逆性的模型。從歐拉－龐加萊公式<sup>5</sup>的一般式，求紙燈籠模型的歐拉特性數<sup>6</sup>之後，確證非流形模型<sup>7</sup>穿透的虧格數<sup>8</sup>與孔洞數，均為正確。

我們發現，非流形建成的拿破崙紙燈籠<sup>9</sup>模型，24 個單位複合體的面數，沒有改變，均是 768。在複合體結合的過程當中，角頂數會減少。角頂減少越少，越難建成。邊數有不改變與減少兩種。同樣地，邊數減少越少，越難建成。角頂減少數目與邊數減少數目最

<sup>1</sup> 亞洲大學資訊工程學系教授

<sup>2</sup> 亞洲大學資訊與設計學系兼任講師

<sup>3</sup> wireframe

<sup>4</sup> cage-like model

<sup>5</sup> Euler-Poincare formula

<sup>6</sup> Euler characteristic

<sup>7</sup> non-manifold model

<sup>8</sup> genus

<sup>9</sup> Napoleon origamic lanterns

多的複合體，均是山形袖章的基本一型，它是 26 組複合體當中體積最小、最緊密的。它也是四組有隱洞複合體之一。作為一個建築物來說，因為外面看不到，其用途，可以當作密室或是儲藏室。應用歐拉－龐加萊公式的一般式，預測複合體隱洞的方法，是一種創新。

在這些籠狀模型當中，我們發現圖形同構<sup>10</sup>與多面體表面可逆性<sup>11</sup>的現象。圖形同構應用廣泛，例如化學、網路理論、資訊擷取與恢復、自動化、交換理論、語言學、電腦輔助設計等領域，甚至於太空站工序的安排問題上，而多面體表面可逆性可以應用在建築的設計。我們藉多面體表面可逆性，開發幾個中級模型。

**關鍵詞：**拿破崙紙燈籠、籠狀模型、歐拉－龐加萊公式、歐拉特性數、虧格數、線框、非流形模型、容斥原理、圖形同構、多面體表面可逆性

## 1. 前 言

首屆沃爾夫<sup>12</sup>數學獎得主、俄國數學家蓋爾芳德<sup>13</sup>預言，組合數學<sup>14</sup>與幾何學將是二十一世紀數學研究的前沿領域<sup>15</sup>。由於計算機軟體的促進和需求，組合數學成為數學的主流分支。其實，早在西元前一世紀，《大戴禮》<sup>16</sup>記載，中國古代有象徵吉祥的

<sup>11</sup> reversibility for general polyhedral surface

<sup>12</sup> 沃爾夫獎（Wolf Prize）自 1978 年起，每年皆頒予五至六位當年的出色科學家及藝術家，只要在對人類及人與人之間的友好關係方面有成就。

<sup>13</sup> 蓋爾芳德（I. M. Gelfand, 1913-）是俄國數學家，一直到 80 餘歲還有很重要的貢獻。身體健康、家庭幸福、盡量避免繁重的行政工作，可能是數學長期創造力的關鍵要素。（Stein 1996）

<sup>14</sup> Combinatorics, 組合數學。

<sup>15</sup> 《信息時代的組合數學》，陳永川，南開大學組合數學研究中心，2004-11-20《數學科普園地》

<sup>16</sup> 《大戴禮記》據說傳自西漢戴德。鄭玄《六藝論》云：「戴德傳《記》八十五篇，則《大戴禮》是也；戴聖傳《禮》四十九篇，則此《禮記》是也。」（孔穎達《禮記正義》大題下引）晉人陳邵《周禮論序》云：「戴德刪古《禮》二百四篇為八十五篇，謂之《大戴禮》；戴聖刪《大戴禮》為四十九篇，是為《小戴禮》。」（陸德明《經典釋文·敘錄》引）其後《隋書·經籍志》、《初學記》卷二十一都有類似的說法。

河圖洛書縱橫圖<sup>17</sup>，即為「九宮算」，這被公認為現代「組合數學」最古老的發現。

在日常生活中，我們常常遇到組合數學的問題。我們有時還會遇到更複雜的調度和安排問題。例如，在生產原子彈的曼哈頓計劃<sup>18</sup>中，涉及到很多工序，許多人員的安排，很多元件的生產，怎樣安排各種人員的工作，以及各種工序間的銜接，從而使整個工期的時間盡可能短？或是未來太空站的建築，哪一些組件在地面上組裝，哪一些組件必須在資源短缺的太空中進行？對於城市的交通管理，交通規劃，哪些地方可能是阻塞要地？哪些地方應該設單行道？立交橋建在哪裡最合適？紅綠燈怎樣設定最合理，如此等等，全是組合數學的問題。

我們知道，用形狀相同的方型磚塊可以把一個地面鋪滿，但是如果用不同形狀，而又非方型的磚塊來鋪一個地面，能否鋪滿呢？這不僅是一個與實際相關的問題，也涉及到很深的組合數學問題。拿破崙密鋪平面<sup>19</sup>系統（Lu 2005）與饕餮密鋪平面系統（Lu 2006a），就是用運用組合數學的原理。應用密鋪平面系統於三維空間表面密鋪的紙積木模型（Lu 2007a — d），也是組合數學的一種創新。

紙燈籠，是紙積木堆疊而成，需要應用「組合數學」裡的容斥原理<sup>20</sup>、歐拉—龐加萊公式、非流形結構等理論。本研究的重點之一，是應用歐拉—龐加萊公式的一般式，求非流形結構紙燈籠的虧格數。並且，紙燈籠的圖形同構與多面體表面可逆性等特性，也有深入的討論。

## 1.1 紙燈籠

紙燈籠的英文，是「origamic lanterns」或「origami lanterns」。紙燈籠一詞源於英文紙建築結構「origamic architecture」或「origami architecture」。紙建築結構是摺紙工的一種造型。它是結合摺紙、精細地切割與精確計算突出的紙張工程。它們可以摺疊儲

<sup>17</sup> 河圖、洛書是中國神話傳說當中的一份古老文獻，最早出現於《易經》。宋代，人們把「河圖、洛書」的內容和「九宮」（縱橫圖的一種）聯繫在一起，如宋劉牧（1011-1064）的《易書鈞隱》中記載了：「河圖」就是九宮，而「洛書」是另一種十個數的排列，名為「天地生成數圖」。

<sup>18</sup> 曼哈頓計劃是第二次世界大戰期間美國陸軍自 1942 年起開發核武器計劃的代號。亦有譯作曼哈頓工程、曼哈頓項目。曼哈頓計劃的負責人為美國物理學家羅伯特·奧本海默，整個計劃的經費是二十億美金，計劃得到美國總統的批准。

<sup>19</sup> Plane tessellation, 有關密鋪平面，請參照普渡大學 Greg Frederickson 教授著作（1997）。

<sup>20</sup> inclusion-exclusion principle

藏或裝進郵局的信封袋，當展開時可以展現三維的立體結構。有如紙建築結構，紙燈籠是結合摺紙、精細地切割與精確計算突出的紙張工程。

## 2. 拿破崙紙燈籠數學定義與公式

### 2.1 歐拉－龐加萊公式之一般式

Marsuda (1993) 定義歐拉<sup>21</sup>－龐加萊<sup>22</sup>公式之一般式，給出非流形幾何模型<sup>23</sup>的角頂、面、邊、孔與洞數目的關係如下：

$$VFE(v, f, e) = v + f - e = (V - V_h + V_c) + (C - C_h + C_c) + r$$

其中歐拉－龐加萊公式的一端為歐拉特性函數  $VFE(v, f, e)$ ，有 3 個變數： $v$  = 角頂總數； $f$  = 面的總數； $e$  = 邊的總數。歐拉－龐加萊公式的另外一端，有 7 個變數： $V$  = 非連通形體數； $V_h$  = 穿過形體孔洞數； $V_c$  = 形體內隱洞數； $C$  = 複合體總數； $C_h$  = 穿過複合體孔洞數； $C_c$  = 複合體內隱洞數； $r$  = 形體面上孔環數。

歐拉－龐加萊公式在流形模型的計算時，因為所有的形體互相流通，等同於一個複合體，其總數  $V$  與  $C$  均為 1；同樣地， $V_h$  等同於  $C_h$ ，我們稱呼它們為手把或是用虧格數 $g$ <sup>24</sup>來代表；因為拿破崙基本型沒有孔，故  $V_c$ 、 $C_c$  與形體所有面上的內孔總數  $r$  均為 0；這時，流形模型的歐拉－龐加萊公式，如下：

$$VFE(v, f, e) = v + f - e = 2 \times (1 - g)$$

<sup>21</sup> Leonhard Euler (1707-1783) 生於 Basel，卒於聖彼得堡。瑞士數學家，貢獻遍及數學各領域，是數學史上最偉大的數學家之一，也是最多產的數學家。

<sup>22</sup> Henri Poincare (1854-1912)。龐加萊出身於醫生家庭。1873 年進巴黎綜合工科學校，畢業後又進國立高等礦業學校求學，1879 年得博士學位。1881 年起一直在卡昂大學任教，先後講授數學分析、光學、電學、流體平衡、電學中的數學、天文學、熱力學等課程。1887 年當選為法國科學院院士，1899 年因研究天體力學中的三體問題獲奧斯卡二世 (Oscar II) 獎金。1906 年當選為法國科學院院長，1908 年以作家身份成為法蘭西學院院士。

<sup>23</sup> Non-manifold geometric model, 非流形幾何模型。流形 (Manifold)，是局部具有歐氏空間性質的空間。整體的形態可以流動。譯名由著名數學家和數學教育學家江澤涵 (1902 - 1994) 引入。非流形幾何模型，是兩個以上的流形幾何模型之間，邊與邊或點與點接合，整體的形態無法流動。

<sup>24</sup> 虧格，是代數幾何和代數拓撲中最基本的概念之一。以實的閉曲面為例，虧格  $g$  就是曲面上洞眼的個數。

## 2.2 容斥原理<sup>25</sup>

當形體 A 與形體 B 結合時，A 與 B 結合體的歐拉特性數 $\chi(A \cup B)$ ，是 A 的歐拉特性數 $\chi(A)$ 與 B 的歐拉特性數 $\chi(B)$ 之和，減去交集的歐拉特性數 $\chi(A \cap B)$ 。容斥原理的公式如下：

$$\chi(A \cup B) = \chi(A) + \chi(B) - \chi(A \cap B)$$

## 2.3 模型之圖形同構

我們將相同拿破崙紙積木基本型，接合邊與邊或角與角，建成籠狀模型<sup>26</sup>。柏拉圖立體<sup>27</sup>的五個正多面體均有其對偶性<sup>28</sup>。我們首先將 4 個或 3 個同樣的拿破崙紙積木基本模型接合成 6 個或 8 個模組<sup>29</sup>，附著<sup>30</sup>在互為對偶的六面體或八面體兩種線框<sup>31</sup>上，開發 24 單位的籠狀模型（Lu 2007b）。我們發現，4 個山形袖章基本模型接合建成的 6 個模組，竟然和 3 個山形袖章基本模型接合建成的 8 個模組相同。這種應用六面體或八面體兩種線框建成相同的籠狀模型，在圖形理論稱圖形同構<sup>32</sup>。柏化沙那菲（Parthasarathy 1994）指出在「平面上使用不同的方法畫出同形圖案數<sup>33</sup>，即相同圖案，並不是很重要，代表特定圖案的數目才是重要。」這是忽視「不同的方法」的論點。

圖形同構的應用廣泛，例如化學、網路理論（Busacker 1965）、資訊擷取與恢復（Lynch 1968）、自動化（Booth 1978）、交換理論、語言學、電腦輔助設計（Amber 1973）等領域。甚至於，未來的建成工序之難易取捨，多一選項。

<sup>25</sup> Inclusive-exclusive principle, 請參照組合數學經典（Brualdi 2005）。

<sup>26</sup> cage-like model or cage-like complex, 籠狀模型或稱籠狀複合體。

<sup>27</sup> 正多面體，或稱柏拉圖立體，指各面都是相同的正多邊形的凸多面體。詳細內容請參照 [http://en.wikipedia.org/wiki/Platonic\\_solid](http://en.wikipedia.org/wiki/Platonic_solid)

<sup>28</sup> 在幾何學，若一種多面體的每個頂點均能對應到另一種多面體上的每個面的中心，它就是對方的對偶多面體。詳細內容請參照 [http://en.wikipedia.org/wiki/Regular\\_polyhedron](http://en.wikipedia.org/wiki/Regular_polyhedron)

<sup>29</sup> module or unit, 模組或稱單位。布施知子 (Fuse 1990) 建議使用英文的 unit。

<sup>30</sup> attach or adhere, 附著。

<sup>31</sup> wireframe or wireframe model, 線框，或稱線框模型是三維電子表示或者三維電腦圖形中的物體的可視化表示方法。

<sup>32</sup> Graph isomorphism, 請參照圖論經典（Bondy 1976）。

## 2.4 模型之可逆性

籠狀模型存在「可逆性」<sup>34</sup>的特性。什麼是可逆性？這是一種「衣服反穿」的觀念。我們將兩個籠狀模型的其中一個從對稱軸剪開，反向連結，就成為另外一個籠狀模型，這樣就可以稱這兩個籠狀模型，互為「可逆性」。這種摺紙的數學遊戲或稱 FLEX-AGONS 現象的是亞瑟·史東<sup>35</sup>在 1936 年，普林斯頓大學當研究生時發現的。可逆性的應用，在建築或實體造型的設計增多一選項。我們也藉可逆性，開發中級籠狀模型。

## 3. 拿破崙紙積木模型

布施知子 (Fuse 1990) 建議使用角頂、面與邊的數目來代表多面體。拿破崙平面密鋪菱形紙片有 25 個角頂、32 個面以及 56 個邊。我們將菱形紙片外緣的 16 個邊，分成兩組 8 個連續邊，角頂與角頂、邊與邊接合。當完成時，將會減少 7 個角頂與 8 個邊。即  $18 (= 25 - 7)$  個角頂、32 個面以及  $48 (= 56 - 8)$  個邊。拿破崙紙積木 (Lu 2006b)，包括領結、眼淚、翅膀、巧克力條、船型、星型、山形袖章與鯉魚等 8 個基本型的歐拉特性數  $VFE (v, f, e)$ ，均為  $VFE (18, 32, 48)$ 。拿破崙紙積木 8 個基本型，請參照圖一。

## 4. 拿破崙紙燈籠模型

拿破崙紙燈籠，是接合拿破崙紙積木基本型的邊與邊或角與角，所建成的非流形籠狀模型。我們建議將多個相同拿破崙紙積木基本型組成的模組，附著在均勻多面體<sup>36</sup>所包括的正多面體的線框上，建成非流形拿破崙紙燈籠模型。

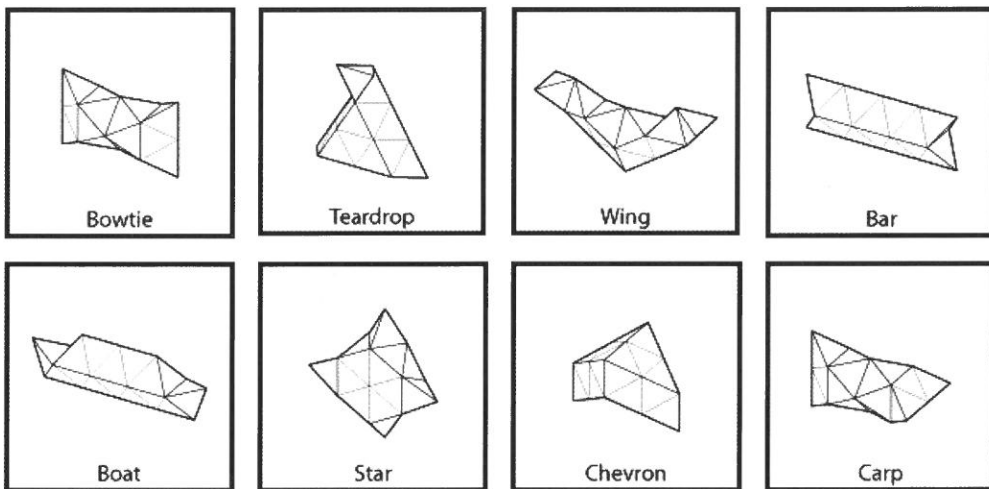
<sup>34</sup> reversibility for general polyhedral surface, 一般多面體表面之可逆性。

<sup>35</sup> Arthur Harold Stone, (1916-2000) 亞瑟·史東是英國拓樸數學專家。

<sup>36</sup> 均勻多面體 (uniform polyhedrons) 是每個頂點 (周圍的面、邊分佈) 都是全等的。它有一個外接球多面體，而球的中心就是多面體的重心 (centroid)。

#### 4.1 正多面體的特性

正多面體，或稱柏拉圖立體，指各面都是相同的正多邊形的凸多面體。因此正多面體上每條邊都連接相同數量的面，每個頂點都連接相同數量的邊。正多面體有正三角形、正正方形與正五邊形等三種正多邊形，它們的角頂均是在同一個平面上。我們可以用鋪地磚前，先將沙床鋪平來比喻。



圖一 拿破崙紙積木 8 個基本型

#### 4.2 對偶多面體

一個正多面體和以它的各面中心為頂的正多面體，叫做互為對偶的正多面體。正六面體和正八面體是互為對偶的正多面體；正十二面體和正二十面體是互為對偶的正多面體；正四面體的對偶多面體是正四面體。

### 5. 拿破崙紙燈籠模型之建成

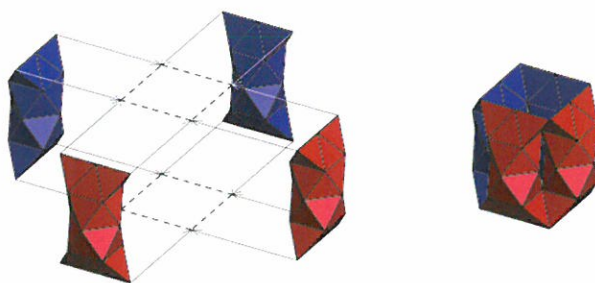
拿破崙紙積木 8 個基本型模組，附著在對偶多面體的六面體或八面體兩種線框上，

建成 26 組 24 單位的籠狀模型。每一基本型建成的籠狀模型，分成基本與中級兩等級。比較難建成的中級一型與中級二型，分別是基本一型與基本二型，互為「衣服反穿」的模型。

## 5.1 領結模型

### 5.1.1 領結基本一型

領結基本一型，是由六組四個單位的領結模型組成<sup>37</sup>。四個領結模型，肩並肩、腳並腳接合<sup>38</sup>，損失角頂 16 ( $= 1 \times 4 \times 4$ ) 與邊 8 ( $= 2 \times 4$ )。請參看圖二。



圖二 四個領結模型肩並肩、腳並腳接合

依容斥原理，歐拉特性數計算如下：

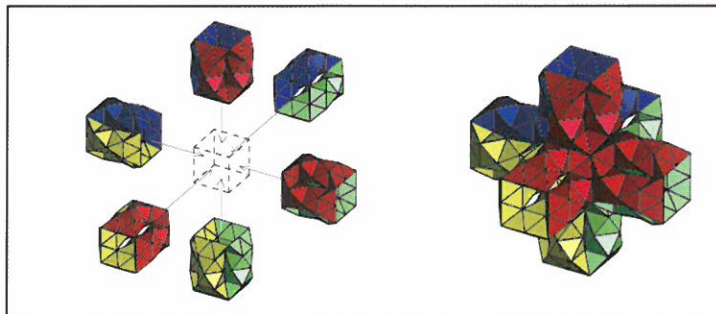
$$\begin{aligned} 4 \times \text{VFE}(18, 32, 48) - \text{VFE}(1 \times 4 \times 4, 0, 2 \times 4) &= \text{VFE}(72 - 16, 128, 192 - 8) \\ &= 56 + 128 - 184 = 0 \end{aligned}$$

因為  $V + C - Ch = 4 + 1 - Ch = 0$ ，故，可得四個單位的領結模型的虧格數  $Ch = 5$ 。同樣地，六組四個單位的領結模型，附著在六面體線框上。角頂損失，可分兩個部分，

<sup>37</sup> 這裡指的是組成 (unification)，並未說明是否為面與面的流形建成 (manifold construction) 的結合 (consolidation) 或它們必須是角頂與角頂、邊與邊、非流形建成 (non-manifold construction) 的接合 (articulation)。

<sup>38</sup> 因為紙燈籠模型，是非流形複合體 (non-manifold complex)，它們必須是角頂與角頂、邊與邊的接合 (articulate)。我們取代結合 (consolidate) 而使用接合這個字。

三組領結模型聚集結合，座落在六面體的 8 個角上，角頂損失  $16 (= 2 \times 8)$ ，同時六面體的 12 個邊，角頂損失  $12 (= 1 \times 4 \times 3)$ ；六面體 12 個邊各損失 2 個邊，邊損失  $24 (= 2 \times 4 \times 3)$ 。請參看圖三。



圖三 六組四個單位的領結模型附著在六面體線框上

依容斥原理，歐拉特性數計算如下：

$$\begin{aligned} & 6 \times \text{VFE}(56, 128, 184) - \text{VFE}(2 \times 8 + 1 \times 4 \times 3, 0, 2 \times 4 \times 3) \\ &= \text{VFE}(336 - 28, 768, 1104 - 24) \\ &= 308 + 768 - 1080 = -4 \end{aligned}$$

因為  $V + C - Ch = 24 + 1 - Ch = -4$ ，故可得領結基本一型的虧格數  $Ch = 29$ 。驗證：因為四個單位的領結模型的虧格數是 5，六組的虧格數就是 30。因為這 30 個洞是連通的，已經重複算過，必須要扣除 1 個，故，總的虧格數是 29。請參看圖四。

### 5.1.2 領結基本二型

領結基本二型，是由六組四個領結模型組成。四個領結模型，側身接合，角頂損失  $14 (= 3 \times 2 + 2 \times 4)$  與邊損失  $8 (= 2 \times 4)$ 。依容斥原理，歐拉特性數計算如下：

$$\begin{aligned} & 4 \times \text{VFE}(18, 32, 48) - \text{VFE}(3 \times 2 + 2 \times 4, 0, 2 \times 4) = \text{VFE}(72 - 14, 128, 192 - 8) \\ &= 58 + 128 - 184 = 2 \end{aligned}$$

因為  $V + C - Ch = 4 + 1 - Ch = 2$ ，故可得四個單位的領結模型的虧格數  $Ch = 3$ 。同樣地，六組四個領結模型，附著在六面體線框上。依容斥原理，歐拉特性數計算

如下：

$$\begin{aligned} 6 \times \text{VFE}(58, 128, 184) - \text{VFE}(2 \times 8, 0, 0) &= \text{VFE}(348 - 16, 768, 1104) \\ &= 332 + 768 - 1104 = -4 \end{aligned}$$

因為  $V + C - Ch = 24 + 1 - Ch = -4$ ，故可得領結基本二型的虧格數  $Ch = 29$ 。驗證：因為四個單位的領結模型的虧格數是 3，六組的虧格數就是 18；六面體線框 12 個邊的連接處，分別有虧格數為 1，加起來是 30。因為這 30 個洞是連通的要扣除 1 個，故，總的虧格數是 29。請參看圖四。

### 5.1.3 領結中級一型

領結中級一型，像中國古代的燈籠，是領結基本一型的「衣服反穿」模型。它是六組四個領結模型，頭尾連接組成，會有四個連接處。每個連接處，會失去三個角頂和二個邊，共會失去角頂  $12 (= 3 \times 4)$  與邊  $8 (= 2 \times 4)$ 。依容斥原理，歐拉特性數計算如下：

$$\begin{aligned} 4 \times \text{VFE}(18, 32, 48) - \text{VFE}(3 \times 4, 0, 2 \times 4) &= \text{VFE}(72 - 12, 128, 192 - 8) \\ &= 60 + 128 - 184 = 4 \end{aligned}$$

因為  $V + C - Ch = 4 + 1 - Ch = 4$ ，故可得四個單位的領結模型的虧格數  $Ch = 1$ 。同樣地，六組四個領結模型接合，附著在六面體線框上。角的損失，分成兩部分，六面體的 8 個角各損失 2 個，另外六面體的 12 個邊，各損失 2 個，共損失角頂  $40 (= 2 \times 8 + 2 \times 12)$ ；邊的損失，六面體的 12 個邊，各損失 2 個，共損失邊  $24 (= 2 \times 12)$ 。依容斥原理，歐拉特性數計算如下：

$$\begin{aligned} 6 \times \text{VFE}(60, 128, 184) - \text{VFE}(2 \times 8 + 2 \times 12, 0, 2 \times 12) \\ &= \text{VFE}(360 - 40, 768, 1104 - 24) \\ &= 320 + 768 - 1080 = 8 \end{aligned}$$

因為  $V + C - Ch = 24 + 1 - Ch = 8$ ，故可得領結中級一型的虧格數  $Ch = 17$ 。驗證：因為四個單位的領結模型的虧格數是 1，六組的虧格數就是 6；12 個連接處的虧格數有 12 個，加起來有 18 個。因為這 18 個洞是連通的要扣除 1 個，故，總的虧格數是 17。請參看圖四。

### 5.1.4 領結中級二型

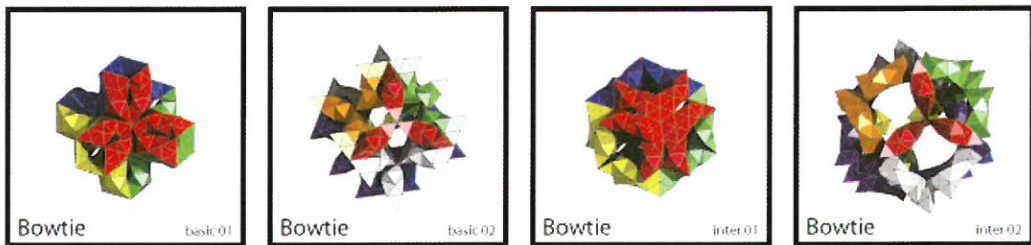
領結中級二型，是領結基本二型的「衣服反穿」模型。它是八組三個領結模型組成。三個領結模型的 3 個端點接合，角頂損失 2。依容斥原理，歐拉特性數計算如下：

$$\begin{aligned} 3 \times \text{VFE}(18, 32, 48) - \text{VFE}(2 \times 1, 0, 0) &= \text{VFE}(54 - 2, 96, 144) \\ &= 52 + 96 - 144 = 4 \end{aligned}$$

因為  $V + C - Ch = 3 + 1 - Ch = 4$ ，故可得三個單位的領結模型的虧格數  $Ch = 0$ 。同樣地，八組三個領結模型，附著在八面體線框上。八面體的 6 個角，4 個領結模型，分別損失 3 個角頂，共損失角頂 18 ( $= 3 \times 6$ )。依容斥原理，歐拉特性數計算如下：

$$\begin{aligned} 8 \times \text{VFE}(52, 96, 144) - \text{VFE}(3 \times 6, 0, 0) &= \text{VFE}(416 - 18, 768, 1152) \\ &= 398 + 768 - 1152 = 14 \end{aligned}$$

因為  $V + C - Ch = 24 + 1 - Ch = 14$ ，故可得領結中級二型的虧格數  $Ch = 11$ 。驗證：因為八面體線框的 12 個邊，各有 1 個洞，得虧格數 12。因為這 12 個洞是連通的要扣除 1 個，故，總的虧格數是 11。請參看圖四。



圖四 領結基本一型、基本二型、中級一型與中級二型

## 5.2 眼淚模型

### 5.2.1 眼淚基本一型

眼淚基本一型，是由六組四個單位的眼淚模型組成。四個眼淚模型，面朝內、肩並肩接合，兩個模型接合上下各損失 2 個角頂，損失角頂 8 ( $= 2 \times 4$ )。依容斥原理，

歐拉特性數，計算如下：

$$\begin{aligned} 4 \times \text{VFE}(18, 32, 48) - \text{VFE}(2 \times 4, 0, 0) &= \text{VFE}(72 - 8, 128, 192) \\ &= 64 + 128 - 192 = 0 \end{aligned}$$

因為  $V + C - Ch = 4 + 1 - Ch = 0$ ，故可得四個單位眼淚模型的虧格數  $Ch = 5$ 。

同樣地，六組四個單位的眼淚模型，附著在六面體線框上。六面體的 12 個邊，每個邊損失 4 個角頂，共損失角頂 48 ( $= 4 \times 12$ )；六面體的每個邊各損失 3 個邊，共損失邊 36 ( $= 3 \times 12$ )。依容斥原理，歐拉特性數計算如下：

$$\begin{aligned} 6 \times \text{VFE}(64, 128, 192) - \text{VFE}(4 \times 12, 0, 3 \times 12) &= \text{VFE}(384 - 48, 768, 1152 - 36) \\ &= 336 + 768 - 1116 = -12 \end{aligned}$$

因為  $V + C - Ch = 24 + 1 - Ch = -12$ ，故可得眼淚基本一型的虧格數  $Ch = 37$ 。驗證：因為四個單位的眼淚模型的虧格數是 5，六組的虧格數還是 30；六面體線框有八個角頂，每個角頂有一個空洞，因此虧格數有 8 個，加起來有 38 個。因為這 38 個洞是連通的要扣除 1 個，故，總的虧格數是 37。請參看圖五。

### 5.2.2 眼淚基本二型

眼淚基本二型，是由六組四個單位的眼淚模型組成。四個眼淚模型，面朝外、肩並肩接合而成。兩個模型接合上下各損失 5 個角頂與 4 個邊，共損失角頂 20 ( $= 5 \times 4$ ) 與邊 16 ( $= 4 \times 4$ )。依容斥原理，歐拉特性數計算如下：

$$\begin{aligned} 4 \times \text{VFE}(18, 32, 48) - \text{VFE}(5 \times 4, 0, 4 \times 4) &= \text{VFE}(72 - 20, 128, 192 - 16) \\ &= 52 + 128 - 176 = 4 \end{aligned}$$

因為  $V + C - Ch = 4 + 1 - Ch = 4$ ，故可得四個單位眼淚模型的虧格數  $Ch = 1$ 。

同樣地，六組四個單位的眼淚模型，附著在六面體線框上。每組底部分別與另外 4 組底部的一邊接合，接合部分分別座落在六面體的 12 個邊上，每個邊損失 1 個角頂，共損失角頂 12 ( $= 1 \times 12$ )。依容斥原理，歐拉特性數計算如下：

$$\begin{aligned} 6 \times \text{VFE}(52, 128, 176) - \text{VFE}(1 \times 12, 0, 0) &= \text{VFE}(312 - 12, 768, 1056) \\ &= 300 + 768 - 1056 = 12 \end{aligned}$$

因為  $V + C - Ch = 24 + 1 - Ch = 12$ ，故可得眼淚基本二型的虧格數  $Ch = 13$ 。驗證：

因爲四個單位的眼淚模型的虧格數是 1，六組的虧格數還是 6；八面體線框每個面各有 1 個空洞，因此虧格數有 8 個，加起來，總共有 14 個。因爲這 14 個洞是連通的要扣除 1 個，故，總的虧格數是 13。請參看圖五。

### 5.2.3 眼淚中級一型

眼淚中級一型，是眼淚基本一型的「衣服反穿」模型。它是由四組六個單位的眼淚模型組成。取六個眼淚模型，兩個一組，分成三組。將兩個模型底部三個單位的邊接合。然後，將兩組的頭部與測身對應的角頂分別接合。頭部與側身接合分別損失 3 個角頂，三組底部接合各損失 4 個角頂和 3 個邊，共損失角頂  $18 (= 4 \times 3 + 3 + 3)$  與損失邊  $9 (= 3 \times 3)$ 。依容斥原理，歐拉特性數，計算如下：

$$\begin{aligned} 6 \times \text{VFE}(18, 32, 48) - \text{VFE}(4 \times 3 + 3 + 3, 0, 3 \times 3) &= \text{VFE}(108 - 18, 192, 288 - 9) \\ &= 90 + 192 - 279 = 3 \end{aligned}$$

因爲  $V + C - Ch = 6 + 1 - Ch = 3$ ，故可得六個單位眼淚模型的虧格數  $Ch = 4$ 。

同樣地，四組六個單位的眼淚模型，附著在四面體線框上。四組 6 個頭接合處分別座落在四面體線框的四個角的位置。角頂損失僅頭部損失  $12 (= 3 \times 4)$ 。依容斥原理，歐拉特性數計算如下：

$$\begin{aligned} 4 \times \text{VFE}(90, 192, 279) - \text{VFE}(3 \times 4, 0, 0) &= \text{VFE}(360 - 12, 768, 1116) \\ &= 348 + 768 - 1116 = 0 \end{aligned}$$

因爲  $V + C - Ch = 24 + 1 - Ch = 0$ ，故可得眼淚中級一型的虧格數  $Ch = 25$ 。驗證：因爲六個單位的眼淚模型的虧格數是 4，四組的虧格數還是 16；四面體的 4 個角各有 1 個空洞，6 個邊也各有 1 個空洞，因此虧格數有 10 個，加起來有 26 個。因爲這 26 個洞是連通的要扣除 1 個，故，總的虧格數是 25。請參看圖五。

### 5.2.4 眼淚中級二型

眼淚中級二型，是眼淚基本二型的「衣服反穿」模型。它是六組四個單位的眼淚模型組成。四個眼淚模型，面朝內，頭部角頂相接合，角頂損失  $4 (= 1 \times 4)$ 。依容斥原理，歐拉特性數計算如下：

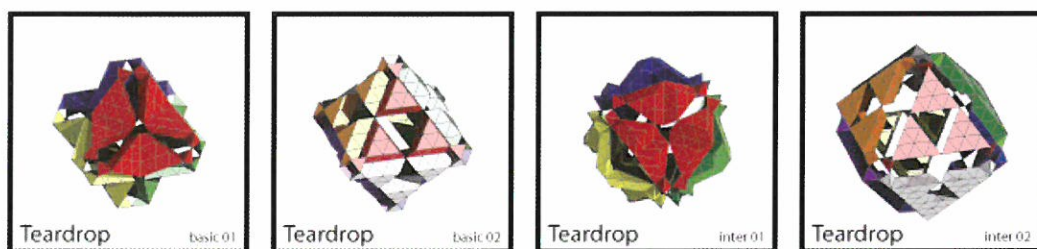
$$\begin{aligned} 4 \times \text{VFE}(18, 32, 48) - \text{VFE}(1 \times 4, 0, 0) &= \text{VFE}(72 - 4, 128, 192) \\ &= 68 + 128 - 192 = 4 \end{aligned}$$

因為  $V + C - Ch = 4 + 1 - Ch = 4$ ，故可得四個單位眼淚模型的虧格數  $Ch = 1$ 。

同樣地，六組四個單位的眼淚模型，附著在八面體線框上。每組的頭部位置在六個角頂上，底部與另外兩組的底部，分別接合在 8 個面上，每個面損失角頂 3 個，共損失角頂 24 ( $= 3 \times 8$ )。依容斥原理，歐拉特性數計算如下：

$$\begin{aligned} 6 \times VFE(68, 128, 192) - VFE(3 \times 8, 0, 0) &= VFE(408 - 24, 768, 1152) \\ &= 384 + 768 - 1152 = 0 \end{aligned}$$

因為  $V + C - Ch = 24 + 1 - Ch = 0$ ，故可得眼淚中級二型的虧格數  $Ch = 25$ 。驗證：因為四個單位的眼淚模型的虧格數是 1，六組的虧格數是 6；八面體線框，每個面有一個空洞，共有 8 個；12 個邊，各有 1 個洞，共有 12 個；加起來有 26 個。因為這 26 個洞是連通的要扣除 1 個，故，總的虧格數是 25。請參看圖五。



圖五 眼淚基本一型、基本二型、中級一型與中級二型

## 5.3 翅膀模型

### 5.3.1 翅膀基本一型

翅膀基本一型，是由八組三個單位的翅膀模型組成。三個翅膀模型的翅膀前沿接合在一起，角頂損失可分兩部分，頂部角頂損失 2 ( $= 2 \times 1$ )，翅膀部分角頂損失 9 ( $= 3 \times 3$ )；邊損失 9 ( $= 3 \times 3$ )。依容斥原理，歐拉特性數計算如下：

$$\begin{aligned} 3 \times VFE(18, 32, 48) - VFE(2 \times 1 + 3 \times 3, 0, 3 \times 3) &= VFE(54 - 11, 96, 144 - 9) \\ &= 43 + 96 - 135 = 4 \end{aligned}$$

因為  $V + C - Ch = 3 + 1 - Ch = 4$ ，故可得三個單位翅膀模型的虧格數  $Ch = 0$ 。

同樣地，八個三個單位的翅膀模型，附著在八面體線框上。八面體的六個角頂，各損失角頂 4，共損失角頂 24（ $= 4 \times 6$ ）。依容斥原理，歐拉特性數計算如下：

$$\begin{aligned} 8 \times VFE(43, 96, 135) - VFE(4 \times 6, 0, 0) &= VFE(344 - 24, 768, 1080) \\ &= 320 + 768 - 1080 = 8 \end{aligned}$$

因為  $V + C - Ch = 24 + 1 - Ch = 8$ ，故可得翅膀基本一型的虧格數  $Ch = 17$ 。驗證：因為八面體線框的六個角頂各有一個洞，共有 6 個，虧格數是 6；八面體線框的 12 邊，各有一個洞，虧格數是 12，加起來是 18。因為這 18 個洞是連通的，因此要扣除 1，故，最後總的虧格數是 17。請參看圖六。

### 5.3.2 翅膀中級一型

翅膀中級一型，是翅膀基本一型的「衣服反穿」模型。三個翅膀模型的翅膀前沿接合在一起，角頂損失可分兩部分，頂部角頂損失 2（ $= 2 \times 1$ ），翅膀部分角頂損失 9（ $= 3 \times 3$ ）；邊損失 9（ $= 3 \times 3$ ）。依容斥原理，歐拉特性數計算如下：

$$\begin{aligned} 3 \times VFE(18, 32, 48) - VFE(2 \times 1 + 3 \times 3, 0, 3 \times 3) &= VFE(54 - 11, 96, 144 - 9) \\ &= 43 + 96 - 135 = 4 \end{aligned}$$

因為  $V + C - Ch = 3 + 1 - Ch = 4$ ，故可得三個單位翅膀模型的虧格數  $Ch = 0$ 。

同樣地，八組三個單位的翅膀模型，附著在八面體線框上。八面體的六個角頂，各損失角頂 4，共損失角頂 24（ $= 4 \times 6$ ）。依容斥原理，歐拉特性數計算如下：

$$\begin{aligned} 8 \times VFE(43, 96, 135) - VFE(4 \times 6, 0, 0) &= VFE(344 - 24, 768, 1080) \\ &= 320 + 768 - 1080 = 8 \end{aligned}$$

因為  $V + C - Ch = 24 + 1 - Ch = 8$ ，故可得翅膀中級一型的虧格數  $Ch = 17$ 。驗證：因為八面體線框的六個角頂各有一個洞，共有 6 個，虧格數是 6；八面體線框的 12 邊，各有一個洞，虧格數是 12，加起來是 18。因為這 18 個洞是連通的，因此要扣除 1，故，最後總的虧格數是 17。請參看圖六。



圖六 翅膀基本一型與中級一型

## 5.4 巧克力條模型

### 5.4.1 巧克力條基本一型

巧克力條基本一型，是由六組四個單位的巧克力條模型組成。四個巧克力條模型，背對背接合，每個背脊有 5 個頂點，角頂損失  $15 (= 5 \times 3)$  與每個背脊有 4 個邊，邊損失  $12 (= 4 \times 3)$ 。依容斥原理，歐拉特性數計算如下：

$$\begin{aligned} 4 \times \text{VFE}(18, 32, 48) - \text{VFE}(5 \times 3, 0, 4 \times 3) &= \text{VFE}(72 - 15, 128, 192 - 12) \\ &= 57 + 128 - 180 = 5 \end{aligned}$$

因為  $V + C - Ch = 4 + 1 - Ch = 5$ ，故可得四個單位巧克力條模型虧格數  $Ch = 0$ 。同樣地，六組四個單位的巧克力條模型，附著在六面體線框上。三組四個單位接合點，座落在六面體的八個角上，角頂損失  $8 (= 2 \times 4)$ 。依容斥原理，歐拉特性數計算如下：

$$\begin{aligned} 6 \times \text{VFE}(57, 128, 180) - \text{VFE}(2 \times 8, 0, 0) &= \text{VFE}(342 - 16, 768, 1080) \\ &= 326 + 768 - 1080 = 14 \end{aligned}$$

因為  $V + C - Ch = 24 + 1 - Ch = 14$ ，故可得巧克力條基本一型虧格數  $Ch = 11$ 。驗證：因為六面體線框的 12 個邊各有 1 個洞，共有 12 個。因為這 12 個洞是連通的，要扣除 1 個，故，總的虧格數是 11。請參看圖七。

### 5.4.2 巧克力條基本二型

巧克力條基本二型，是由六個四個單位的巧克力條模型組成。四個巧克力條模型，側面接鄰，角頂損失 20 ( $= 5 \times 4$ )；每個側面有 4 個邊，邊損失 16 ( $= 4 \times 4$ )。依容斥原理，歐拉特性數計算如下：

$$\begin{aligned} 4 \times \text{VFE}(18, 32, 48) - \text{VFE}(5 \times 4, 0, 4 \times 4) &= \text{VFE}(72 - 20, 128, 192 - 16) \\ &= 52 + 128 - 176 = 4 \end{aligned}$$

因為  $V + C - Ch = 4 + 1 - Ch = 4$ ，故可得四個單位巧克力條模型虧格數  $Ch = 1$ 。同樣地，六組四個單位的巧克力條模型，附著在六面體線框。角頂損失分兩部分，兩組接合角頂損失 12 ( $= 3 \times 4$ )，三組接合角頂損失 16 ( $= 2 \times 8$ )；邊損失 16 ( $= 2 \times 8$ )。依容斥原理，歐拉特性數計算如下：

$$\begin{aligned} 6 \times \text{VFE}(52, 128, 176) - \text{VFE}(3 \times 4 + 2 \times 8, 0, 2 \times 8) \\ &= \text{VFE}(312 - 28, 768, 1056 - 24) \\ &= 284 + 768 - 1032 = 20 \end{aligned}$$

因為  $V + C - Ch = 24 + 1 - Ch = 20$ ，故可得巧克力條基本二型虧格數  $Ch = 5$ 。驗證：因為四個單位的巧克力條模型的虧格數是 1，六組的虧格數是 6。因為這 6 個洞是連通的要扣除 1 個，故，總的虧格數是 5。請參看圖七。

### 5.4.3 巧克力條中級一型

巧克力條中級一型，是巧克力條基本一型的「衣服反穿」模型。它是八組三個單位的巧克力條模型組成。三個巧克力條模型，聚集接合，損失角頂 2。依容斥原理，歐拉特性數計算如下：

$$\begin{aligned} 3 \times \text{VFE}(18, 32, 48) - \text{VFE}(2 \times 1, 0, 0) &= \text{VFE}(54 - 2, 96, 144) \\ &= 52 + 96 - 144 = 4 \end{aligned}$$

因為  $V + C - Ch = 3 + 1 - Ch = 4$ ，故可得三個單位巧克力條模型虧格數  $Ch = 0$ 。同樣地，八組三個單位的巧克力條模型，附著在八面體線框的八個正三角形的面上。四組巧克力條模型的角頂接合處，分別座落在八面體的 6 個角上。角頂損失 18 ( $= 3 \times 6$ )。依容斥原理，歐拉特性數計算如下：

$$\begin{aligned} 8 \times \text{VFE}(52, 96, 144) - \text{VFE}(3 \times 6, 0, 0) &= \text{VFE}(416 - 18, 768, 1152) \\ &= 398 + 768 - 1152 = 14 \end{aligned}$$

因為  $V + C - Ch = 24 + 1 - Ch = 14$ ，故可得巧克力條中級一型虧格數  $Ch = 11$ 。驗證：八面體的 12 個邊各有一個洞，共有 12 個。因為這 12 個洞是連通的要扣除 1 個，故，總的虧格數是 11。請參看圖七。

#### 5.4.4 巧克力條中級二型

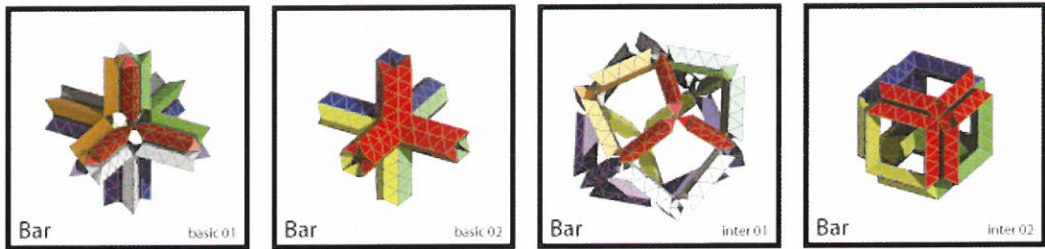
巧克力條中級二型，像中國古代的燈籠，是巧克力條基本二型的「衣服反穿」模型。它是六個四個單位的巧克力條模型組成。四個巧克力條模型，頭尾接合。角頂損失  $12 (= 3 \times 4)$ ，邊損失  $8 (= 2 \times 4)$ 。依容斥原理，歐拉特性數計算如下：

$$\begin{aligned} 4 \times \text{VFE}(18, 32, 48) - \text{VFE}(3 \times 4, 0, 2 \times 4) &= \text{VFE}(72 - 12, 128, 192 - 8) \\ &= 60 + 128 - 184 = 4 \end{aligned}$$

因為  $V + C - Ch = 4 + 1 - Ch = 4$ ，故可得四個單位巧克力條模型虧格數  $Ch = 1$ 。同樣地，六個四個單位的巧克力條模型，附著在六面體的線框上。角頂的損失分為兩部分，六面體的 12 個邊，角頂損失  $36 (= 3 \times 12)$ ；六面體的 8 個角，3 組的巧克力條模型接合在這個地方，角頂損失  $16 (= 2 \times 8)$ ；六面體的 12 個邊，損失邊  $48 (= 4 \times 12)$ 。依容斥原理，歐拉特性數計算如下：

$$\begin{aligned} 6 \times \text{VFE}(60, 128, 184) - \text{VFE}(3 \times 12 + 2 \times 8, 0, 4 \times 12) \\ &= \text{VFE}(360 - 52, 768, 1104 - 48) \\ &= 308 + 768 - 1056 = 20 \end{aligned}$$

因為  $V + C - Ch = 24 + 1 - Ch = 20$ ，故可得巧克力條中級二型虧格數  $Ch = 5$ 。驗證：因為六面體的每個面有一個洞，共有 6 個。因為這 6 個洞是連通的要扣除 1 個，故，總的虧格數是 5。請參看圖七。



圖七 巧克力條基本一型、基本二型、中級一型與中級二型

## 5.5 船型模型

### 5.5.1 船型基本一型

船型基本一型，是由六組四個單位的船型模型組成。四個船型模型，船頭聚集接合，角頂損失分為兩個部份，上下共同角頂損失  $6 (= 3 \times 2)$ ，腰部角頂  $4 (= 1 \times 4)$ ，邊損失  $8 (= 2 \times 4)$ 。依容斥原理，歐拉特性數計算如下：

$$4 \times \text{VFE}(18, 32, 48) - \text{VFE}(3 \times 2 + 1 \times 4, 0, 2 \times 4) = \text{VFE}(72 - 10, 128, 192 - 8) \\ = 62 + 128 - 184 = 6$$

因為  $V + C - Ch + Cc = 4 + 1 - Ch + Cc = 6$ ，故可得四個單位船型模型虧格數  $Ch = 0$  和隱洞數  $Cc = 1$ 。

同樣地，六個四個單位的船型模型，附著在六面體線框上。三組角頂接合在六面體線框的 8 個角，每個角損失 2 個角頂。依容斥原理，歐拉特性數計算如下：

$$6 \times \text{VFE}(62, 128, 184) - \text{VFE}(2 \times 8, 0, 0) = \text{VFE}(372 - 16, 768, 1104) \\ = 356 + 768 - 1104 = 20$$

因為  $V + C - Ch = 24 + 1 - Ch + Cc = 20$ ，故可得船型基本一型虧格數  $Ch = 11$  和隱洞數  $Cc = 6$ 。驗證：因為六面體線框有 12 個邊，每個邊有一個洞，共有 12 個。因為這 12 個洞是連通的要扣除 1 個，故，總的虧格數是 11。請參看圖八。

### 5.5.2 船型基本二型

船型基本二型，是由六組四個單位的船型模型組成。四個船型模型，船尾聚集接合，角頂損失分為兩個部份，上下共同角頂損失  $6 (= 3 \times 2)$ ，腰角頂  $8 (= 2 \times 4)$ ，邊損失  $8 (= 2 \times 4)$ 。依容斥原理，歐拉特性數計算如下：

$$\begin{aligned} 4 \times \text{VFE}(18, 32, 48) - \text{VFE}(3 \times 2 + 1 \times 4, 0, 2 \times 4) &= \text{VFE}(72 - 10, 128, 192 - 8) \\ &= 62 + 128 - 184 = 6 \end{aligned}$$

因為  $V + C - Ch + Cc = 4 + 1 - Ch + Cc = 6$ ，故可得四個單位船型模型虧格數  $Ch = 0$  和隱洞數  $Cc = 1$ 。

同樣地，六個四個單位的船型模型，附著在六面體線框上。依容斥原理，歐拉特性數計算如下：

$$\begin{aligned} 6 \times \text{VFE}(62, 128, 184) - \text{VFE}(2 \times 8, 0, 0) &= \text{VFE}(372 - 16, 768, 1104) \\ &= 356 + 768 - 1104 = 20 \end{aligned}$$

因為  $V + C - Ch = 24 + 1 - Ch = 20$ ，故可得船型基本二型虧格數  $Ch = 11$  和隱洞數  $Cc = 6$ 。驗證：因為六面體有 12 個邊每個邊有一個洞，共有 12 個。因為這 12 個洞是連通的要扣除 1 個，故，總的虧格數是 11。請參看圖八。

### 5.5.3 船型中級一型

船型中級一型，是船型基本一型的「衣服反穿」模型。它是八組三個單位的船型模型組成。三個船型模型，3 個船頭的各一個邊接合在一起，損失角頂  $4 (= 2 \times 2)$  和邊  $2 (= 2 \times 1)$ 。依容斥原理，歐拉特性數計算如下：

$$\begin{aligned} 3 \times \text{VFE}(18, 32, 48) - \text{VFE}(2 \times 2, 0, 2 \times 1) &= \text{VFE}(54 - 4, 96, 144 - 2) \\ &= 50 + 96 - 142 = 4 \end{aligned}$$

因為  $V + C - Ch = 3 + 1 - Ch = 4$ ，故可得三個單位船型模型虧格數  $Ch = 0$ 。

同樣地，八組三個單位的船型模型，附著在八面體線框上。四組船型模型船尾角頂聚集接合，座落在八面體的 6 個角頂，角頂損失  $18 (= 3 \times 6)$ 。依容斥原理，歐拉特性數計算如下：

$$8 \times \text{VFE}(50, 96, 142) - \text{VFE}(3 \times 6, 0, 0) = \text{VFE}(400 - 18, 768, 1136) \\ = 382 + 768 - 1136 = 14$$

因為  $V + C - Ch = 24 + 1 - Ch = 14$ ，故可得船型中級一型虧格數  $Ch = 11$ 。驗證：因為八面體有 12 個邊，每個邊有一個洞，共有 12 個。因為這 12 個洞是連通的要扣除 1 個，故，總的虧格數是 11。請參看圖八。

#### 5.5.4 船型中級二型

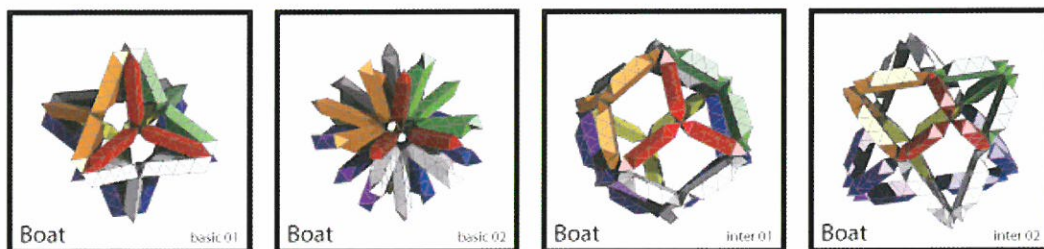
船型中級二型，是船型基本二型的「衣服反穿」模型。它是八組三個單位的船型模型組成。三個船型模型的船頭聚集接合，損失角頂 2（ $= 2 \times 1$ ）。依容斥原理，歐拉特性數計算如下：

$$3 \times \text{VFE}(18, 32, 48) - \text{VFE}(2, 0, 0) = \text{VFE}(54 - 2, 96, 144) \\ = 52 + 96 - 144 = 4$$

因為  $V + C - Ch = 3 + 1 - Ch = 4$ ，故可得三個單位船型模型虧格數  $Ch = 0$ 。同樣地，八組三個單位的船型模型，附著在八面體線框上。四組船型模型船尾接合處，座落在八面體的 6 個角，損失角頂 18（ $= 3 \times 6$ ）。依容斥原理，歐拉特性數計算如下：

$$8 \times \text{VFE}(52, 96, 144) - \text{VFE}(3 \times 6, 0, 0) = \text{VFE}(416 - 18, 768, 1152) \\ = 398 + 768 - 1152 = 14$$

因為  $V + C - Ch = 24 + 1 - Ch = 14$ ，故可得船型中級二型虧格數  $Ch = 11$ 。驗證：因為六面體有 12 個邊每個邊有一個洞，共有 12 個。因為這 12 個洞是連通的要扣除 1 個，故，總的虧格數是 11。請參看圖八。



圖八 船型基本一型、基本二型、中級一型與中級二型

## 5.6 星型模型

### 5.6.1 星型基本一型

星型基本一型，是由六組四個單位的模型組成。四個星型模型，頭碰頭，手牽手接合；頭碰頭角頂損失 3（ $= 3 \times 1$ ），手牽手角頂損失 4（ $= 4 \times 1$ ）。依容斥原理，歐拉特性數計算如下：

$$\begin{aligned} 4 \times \text{VFE}(18, 32, 48) - \text{VFE}(3 \times 1 + 1 \times 4, 0, 0) &= \text{VFE}(72 - 7, 128, 192) \\ &= 65 + 128 - 192 = 1 \end{aligned}$$

因為  $V + C - Ch = 4 + 1 - Ch = 1$ ，故可得四個單位星型模型的虧格數  $Ch = 4$ 。

同樣地，六組四個單位的星型模型，附著在六面體線框上。三組模型的底部角頂聚集接合，座落在六面體 8 個角上，角頂損失 16（ $= 2 \times 8$ ）。依容斥原理，歐拉特性數計算如下：

$$\begin{aligned} 6 \times \text{VFE}(65, 128, 192) - \text{VFE}(2 \times 8, 0, 0) &= \text{VFE}(390 - 16, 768, 1152) \\ &= 374 + 768 - 1152 = -10 \end{aligned}$$

因為  $V + C - Ch = 24 + 1 - Ch = -10$ ，故可得星型基本一型的虧格數  $Ch = 35$ 。驗證：因為四個單位的星型模型的虧格數是 4，六組的虧格數是 24；六面體有 12 個邊，每個邊有一個空洞，共有 12 個，加起來有 36 個。因為這 36 個洞是連通的要扣除 1 個，故，總的虧格數是 35。請參看圖九。

### 5.6.2 星型中級一型

星型中級一型，是星型基本一型的「衣服反穿」模型。它是由六個四個單位的模型組成。四個星型模型，手牽手接合，角頂損失 4（ $= 1 \times 4$ ）。依容斥原理，歐拉特性數計算如下：

$$\begin{aligned} 4 \times \text{VFE}(18, 32, 48) - \text{VFE}(1 \times 4, 0, 0) &= \text{VFE}(72 - 4, 128, 192) \\ &= 68 + 128 - 192 = 4 \end{aligned}$$

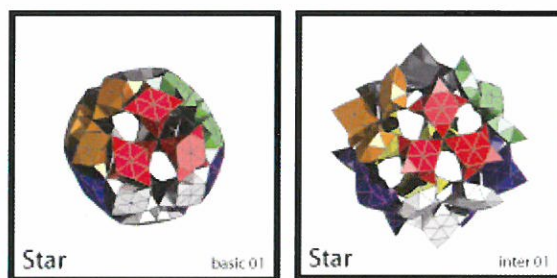
因為  $V + C - Ch = 4 + 1 - Ch = 4$ ，故可得四個單位星型模型的虧格數  $Ch = 1$ 。

同樣地，六組四個單位的星型模型，附著在六面體線框上。三組模型角頂聚集接合，座

落在六面體的 8 個角上，角頂損失  $16 (= 2 \times 8)$ 。依容斥原理，歐拉特性數計算如下：

$$\begin{aligned} 6 \times \text{VFE}(68, 128, 192) - \text{VFE}(2 \times 8, 0, 0) &= \text{VFE}(408 - 16, 768, 1152) \\ &= 392 + 768 - 1152 = 8 \end{aligned}$$

因為  $V + C - Ch = 24 + 1 - Ch = 8$ ，故可得星型中級一型的虧格數  $Ch = 17$ 。驗證：因為四個單位的星型模型的虧格數是 1，六組的虧格數是 6；六面體有 12 個邊，每個邊有一個洞，共有 12 個，加起來有 18 個。因為這 18 個洞是連通的要扣除 1 個，故，總的虧格數是 17。請參看圖九。



圖九 星型基本一型與中級一型

## 5.7 山形袖章模型

### 5.7.1 山形袖章基本一型

山形袖章基本一型，是由六組四個單位的山形袖章模型組成。四個山形袖章模型，分別聚集接合，角頂損失分兩部分，上下角頂損失  $6 (= 3 \times 2)$ ，相鄰角頂損失  $12 (= 3 \times 4)$ ；邊損失  $16 (= 4 \times 4)$ 。依容斥原理，歐拉特性數計算如下：

$$\begin{aligned} 4 \times \text{VFE}(18, 32, 48) - \text{VFE}(3 \times 2 + 3 \times 4, 0, 4 \times 4) &= \text{VFE}(72 - 18, 128, 192 - 16) \\ &= 54 + 128 - 176 = 6 \end{aligned}$$

因為  $V + C - Ch + Cc = 4 + 1 - Ch + Cc = 6$ ，故可得四個單位山形袖章模型的洞數與虧格數之差，即  $Cc - Ch = 1$ 。合理的解答是隱洞數  $Cc = 1$  與虧格數  $Ch = 0$ 。這就是

說，這個四個單位山形袖章模型的複合體的內部，有一個隱洞。

同樣地，六個四個單位的山形袖章模型，附著在六面體線框上。角頂的損失分為兩個部分，三組模型的角頂聚集接合，分別座落在六面體的 8 個角上，角頂損失 16 ( $= 2 \times 8$ )，另外角頂損失在六面體的 12 個邊上，共損失角頂 48 ( $= 2 \times 2 \times 12$ )；邊損失在六面體的 12 個邊上，邊損失 48 ( $= 2 \times 2 \times 12$ )。依容斥原理，歐拉特性數計算如下：

$$\begin{aligned} 6 \times \text{VFE}(54, 128, 176) - \text{VFE}(2 \times 8 + 2 \times 2 \times 12, 0, 2 \times 2 \times 12) \\ = \text{VFE}(324 - 64, 768, 1056 - 48) \\ = 260 + 768 - 1008 = 20 \end{aligned}$$

因為  $V + C - \text{Ch} + \text{Cc} = 24 + 1 - \text{Ch} + \text{Cc} = 20$ ，故可得山形袖章基本一型的虧格數  $\text{Ch} = 11$ ，複合體的隱洞數  $\text{Cc} = 6$ 。驗證：因為四個單位的山形袖章模型的虧格數是 0，隱洞數是 1，因此，六組的虧格數是 0，隱洞數是 6；六面體有 12 個邊，每個邊有一個洞，共有虧格數 12，隱洞數是 6 個。因為這 12 個洞是連通的要扣除 1 個，故，總的虧格數是 11；隱洞互不連通，隱洞數仍然是 6。請參看圖十。

### 5.7.2 山形袖章中級一型

山形袖章中級一型，是山形袖章基本一型的「衣服反穿」模型。它是八組三個單位的山形袖章模型組成。三個山形袖章模型，角頂損失分兩部分，頂部聚集接合損失 2 ( $= 2 \times 1$ )，底部相鄰接合損失 6 ( $= 2 \times 3$ )；邊損失 6 ( $= 2 \times 3$ )。依容斥原理，歐拉特性數計算如下：

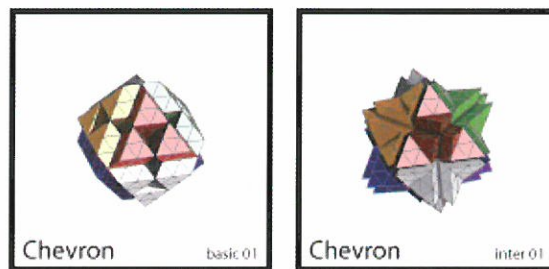
$$\begin{aligned} 3 \times \text{VFE}(18, 32, 48) - \text{VFE}(2 \times 1 + 2 \times 3, 0, 2 \times 3) = \text{VFE}(54 - 8, 96, 144 - 6) \\ = 46 + 96 - 138 = 4 \end{aligned}$$

因為  $V + C - \text{Ch} + \text{Cc} = 3 + 1 - \text{Ch} + \text{Cc} = 4$ ，故可得三個單位山形袖章模型的虧格數  $\text{Ch} = 0$ ，複合體的隱洞數  $\text{Cc} = 0$ 。

同樣地，八組三個單位的山形袖章模型，附著在八面體線框上。角頂損失分兩大部分，四組底部的一個角頂聚集損失 18 ( $= 3 \times 6$ )，八面體的 12 個邊各損失 3 個角頂，損失角頂 36 ( $= 3 \times 12$ )；12 個邊各損失 4，損失邊 48 ( $= 2 \times 2 \times 12$ )。依容斥原理，歐拉特性數計算如下：

$$\begin{aligned}
 & 8 \times \text{VFE}(46, 96, 138) - \text{VFE}(3 \times 6 + 3 \times 12, 0, 4 \times 12) \\
 & = \text{VFE}(368 - 54, 768, 1104 - 48) \\
 & = 314 + 768 - 1056 = 26
 \end{aligned}$$

因為  $V + C - Ch + Cc = 24 + 1 - Ch + Cc = 26$ ，故可得山形袖章模型中級一型的虧格數  $Ch = 0$ ，複合體的隱洞數  $Cc = 1$ 。驗證：複合體的虧格數 0，有隱洞數 1。請參看圖十。



圖十 山形袖章基本一型與山形袖章中級一型

## 5.8 鯉魚模型

### 5.8.1 鯉魚基本一型

鯉魚基本一型，是由六組四個單位的鯉魚模型組成。四個鯉魚模型，相鄰眼睛接合，角頂損失  $8 (= 2 \times 4)$ ，邊損失  $4 (= 1 \times 4)$ ；尾部一端聚集接合，角頂損失  $7 (= 3 \times 1 + 1 \times 4)$ ，邊損失  $4 (= 1 \times 4)$ 。依容斥原理，歐拉特性數計算如下：

$$\begin{aligned}
 & 4 \times \text{VFE}(18, 32, 48) - \text{VFE}(2 \times 4 + 3 \times 1 + 1 \times 4, 0, 1 \times 4 + 1 \times 4) \\
 & = \text{VFE}(72 - 15, 128, 192 - 8) \\
 & = 57 + 128 - 184 = 1
 \end{aligned}$$

因為  $V + C - Ch = 4 + 1 - Ch = 1$ ，故可得四個單位鯉魚模型的虧格數  $Ch = 4$ 。

同樣地，六組四個單位的鯉魚模型，附著在六面體線框上。三組尾部一端聚集接合，座落在六面體的 8 個角上，角頂損失  $16 (= 2 \times 8)$ 。依容斥原理，歐拉特性數計算如下：

$$\begin{aligned} 6 \times \text{VFE}(57, 128, 184) - \text{VFE}(2 \times 8, 0, 0) &= \text{VFE}(342 - 16, 768, 1104) \\ &= 326 + 768 - 1104 = -10 \end{aligned}$$

因為  $V + C - Ch = 24 + 1 - Ch = -10$ ，故可得鯉魚基本一型的虧格數  $Ch = 35$ 。驗證：因為四個單位的鯉魚模型的虧格數是 4，六組的虧格數就是 24；六面體 12 邊各有 1 個洞，加起來還是 36 個。因為這 36 個洞是連通的要扣除 1 個，故，總的虧格數是 35。請參看圖十一。

### 5.8.2 鯉魚基本二型

鯉魚基本二型，是由六個四個單位的鯉魚模型組成。四個鯉魚模型，其中 4 隻眼睛聚集接合，角頂損失  $7 (= 3 \times 1 + 1 \times 4)$ ，邊損失  $4 (= 1 \times 4)$ ；尾部相鄰接合，角頂損失  $8 (= 2 \times 4)$ ，邊損失  $4 (= 1 \times 4)$ 。依容斥原理，歐拉特性數計算如下：

$$\begin{aligned} 4 \times \text{VFE}(18, 32, 48) - \text{VFE}(3 \times 1 + 1 \times 4 + 2 \times 4, 0, 1 \times 4 + 1 \times 4) \\ &= \text{VFE}(72 - 15, 128, 192 - 8) \\ &= 57 + 128 - 184 = 1 \end{aligned}$$

因為  $V + C - Ch = 4 + 1 - Ch = 1$ ，故可得四個單位鯉魚模型的虧格數  $Ch = 4$ 。同樣地，六組四個單位的鯉魚模型，附著在六面體線框上。角頂損失分兩部分，三組鯉魚模型的尾部聚集座落在六面體 8 個角，角頂損失  $16 (= 2 \times 8)$ ，另外 12 個邊，角頂損失  $12 (= 1 \times 12)$ ；六面體的 12 邊各損失 2 個邊，邊損失  $24 (= 2 \times 12)$ 。依容斥原理，歐拉特性數計算如下：

$$\begin{aligned} 6 \times \text{VFE}(57, 128, 184) - \text{VFE}(2 \times 8 + 1 \times 12, 0, 2 \times 12) \\ &= \text{VFE}(342 - 28, 768, 1104 - 24) \\ &= 314 + 768 - 1080 = 2 \end{aligned}$$

因為  $V + C - Ch = 24 + 1 - Ch = 2$ ，故可得鯉魚基本二型的虧格數  $Ch = 23$ 。驗證：因為四個單位的鯉魚模型的虧格數是 4，六組的虧格數就是 24。因為這 24 個洞是連通的要扣除 1 個，故，總的虧格數是 23。請參看圖十一。

### 5.8.3 鯉魚中級一型

鯉魚中級一型，是鯉魚基本一型的「衣服反穿」模型。它是八組三個鯉魚模型組成。三個鯉魚模型，尾部與尾部 3 角頂接合，損失角頂 2 ( $= 2 \times 1$ )。依容斥原理，歐拉特性數計算如下：

$$\begin{aligned} 3 \times \text{VFE}(18, 32, 48) - \text{VFE}(2 \times 1, 0, 0) &= \text{VFE}(54 - 2, 96, 144) \\ &= 52 + 96 - 144 = 4 \end{aligned}$$

因為  $V + C - Ch = 3 + 1 - Ch = 4$ ，故可得三個單位鯉魚模型的虧格數  $Ch = 0$ 。

同樣地，八組三個單位的鯉魚模型，附著在八面體線框的正三角形面上。四組鯉魚模型的眼睛結合處，座落在八面體的 6 個角上，角頂損失 24 ( $= 4 \times 6$ )。依容斥原理，歐拉特性數計算如下：

$$\begin{aligned} 8 \times \text{VFE}(52, 96, 144) - \text{VFE}(4 \times 6, 0, 0) &= \text{VFE}(416 - 24, 768, 1152) \\ &= 392 + 768 - 1152 = 8 \end{aligned}$$

因為  $V + C - Ch = 24 + 1 - Ch = 8$ ，故可得鯉魚中級一型的虧格數  $Ch = 17$ 。驗證：因為八面體線框的 6 個角上各有一個洞，共有 6 個洞。八面體的 12 個邊，每一個邊有 1 個洞，共有 12 個洞，加起來有 18 個洞。因為這 18 個洞是連通的要扣除 1 個，故，總的虧格數是 17。請參看圖十一。

### 5.8.4 鯉魚中級二型

鯉魚中級二型，是鯉魚基本二型的「衣服反穿」模型。它是四組六個單位的鯉魚模型組成。六個鯉魚模型，眼睛與眼睛接合在一起，角頂損失有 3 個部分，六組共 6 隻眼睛接合，角頂損失 5；六組另外的眼睛相鄰接合，角頂損失 6 ( $= 3 + 3$ )；翻過來，三對眼睛的底部接合，角頂損失 6 ( $= 2 \times 3$ )；邊的損失有兩部分，正面損失 6 ( $= 3 + 3$ )；翻過來，反面損失 3 ( $= 1 \times 3$ )。依容斥原理，歐拉特性數計算如下：

$$\begin{aligned} 6 \times \text{VFE}(18, 32, 48) - \text{VFE}(5 + 2 \times 3 + 6, 0, 6 + 3) &= \text{VFE}(108 - 17, 192, 288 - 9) \\ &= 91 + 192 - 279 = 4 \end{aligned}$$

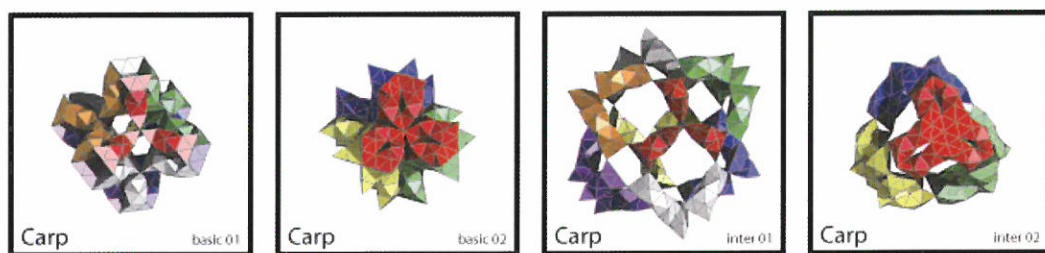
因為  $V + C - Ch = 6 + 1 - Ch = 4$ ，故可得六個單位鯉魚模型的虧格數  $Ch = 3$ 。

同樣地，四組六個單位的鯉魚模型，附著在四面體正三角形的面上，四組鯉魚模型的尾

部接合，角頂損失  $12 (= 3 \times 4)$ 。依容斥原理，歐拉特性數計算如下：

$$\begin{aligned} 4 \times \text{VFE}(91, 192, 279) - \text{VFE}(3 \times 4, 0, 0) &= \text{VFE}(364 - 12, 768, 1116) \\ &= 352 + 768 - 1116 = 4 \end{aligned}$$

因為  $V + C - Ch = 24 + 1 - Ch = 4$ ，故可得鯉魚中級二型的虧格數  $Ch = 21$ 。驗證：因為六個單位的鯉魚模型的虧格數是 3，四組的虧格數就是 12。四面體線框 6 個邊各有 1 個洞，共有 6 個洞；四面體 4 個頂點各有一個洞，共有 4 個洞，加起來有 10 個洞，加上 12 個洞，共有 22 個。因為，這 22 個洞是連通的，要扣除 1 個，故，虧格數是 21。請參看圖十一。



圖十一 鯉魚基本一型、基本一型、中級一型與中級二型

## 6. 討論與結論

我們利用柏拉圖立體中，正六面體與正八面體的對偶性，成功地開發以拿破崙紙積木 8 個基本型模組，附著在對偶多面體的六面體或八面體兩種線框上，建成 26 組 24 單位的籠狀模型。每一基本型建成的籠狀模型，分成基本與中級兩等級。比較難建成的中級一型與中級二型，分別是基本一型與基本二型，互為「衣服反穿」的模型。從歐拉－龐加萊公式的一般式，求紙燈籠模型的歐拉特性數之後，驗證非流形模型的虧格數與空洞數，均為正確。

因為拿破崙紙燈籠模型是非流形建成，故 24 個單位的模型面數不減，均是 768 (= 單位面數  $32 \times 24$ )。複合體角頂減少的數目，等於 24 個單位模型的角頂數 432 (= 單位角頂數  $18 \times 24$ ) 減去複合體角頂數  $v$ 。複合體當中，角頂減少最多的是山形袖章的基本

一型 172 ( $= 432 - 260$ )，角頂減少最少的是 34 ( $= 432 - 398$ )。角頂減少越少，越難建成。

表一 拿破崙紙燈籠之拓樸與所屬特性

基本模型	基本/中級	v 角頂數	f 面數	e 邊數	VFE 特性數	Ch 虧格	Cc 隱洞數	圖形同構		可逆性衣服反穿
領結	基本一型	308	768	1080	- 4	29	0	4x6	6x4	中級一型
	基本二型	332		1104	- 4	29	0	4x6	3x8	中級二型
	中級一型	320		1080	8	17	0	4x6	6x4	基本一型
	中級二型	398		1152	14	11	0	3x8	4x6	基本二型
眼淚	基本一型	336		1116	- 12	37	0	4x6	6x4	中級一型
	基本二型	300		1056	12	13	0	4x6	3x8	中級二型
	中級一型	348		1116	0	25	0	4x6	6x4	基本一型
	中級二型	384		1152	0	25	0	3x8	4x6	基本二型
翅膀	基本一型	320		1080	8	17	0	3x8	6x4	中級一型
	中級一型	320		1080	8	17	0	3x8	6x4	基本一型
巧克 力條	基本一型	326		1080	14	11	0	4x6	3x8	中級一型
	基本二型	284		1032	20	5	0	4x6	6x4	中級二型
	中級一型	398		1152	14	11	0	3x8	4x6	基本一型
	中級二型	308		1056	20	5	0	4x6	6x4	基本二型
船型	基本一型	356		1104	20	11	6	4x6	3x8	中級一型
	基本二型	356		1104	20	11	6	4x6	3x8	中級二型
	中級一型	382		1136	14	11	0	3x8	4x6	基本一型
	中級二型	398		1152	14	11	0	3x8	4x6	基本二型
星型	基本一型	374		1152	- 10	35	0	4x6	3x8	中級一型
	中級一型	392		1152	8	17	0	4x6	3x8	基本一型
山形	基本一型	260		1008	20	11	6	4x6	3x8	中級一型
	中級一型	314		1056	26	0	1	3x8	4x6	基本一型
鯉魚	基本一型	326		1104	- 10	35	0	4x6	3x8	中級一型
	基本二型	314		1080	2	23	0	4x6	6x4	中級二型
	中級一型	392		1152	8	17	0	3x8	4x6	基本一型
	中級二型	352		1116	4	21	0	6x4	4x6	基本二型

同樣地，複合體邊減少的數目，等於 24 個單位的邊數 1052（＝單位邊數  $48 \times 24$ ）減去複合體邊數  $e$ 。複合體當中，邊數減少最多的也是山形袖章的基本一型 144（＝ $1152 - 1008$ ），邊數減少最少的是 0（＝ $1152 - 1152$ ）。邊數減少越少，越難建成。值得一提的是，角頂減少數目與邊數減少數目最多的複合體，均是山形袖章的基本一型，它是複合體當中體積最小、最緊密的。

最高虧格數是眼淚基本一型有 37 個，最少的是山形袖章中級一型虧格數為 0。虧格數越多，即空洞數越多，在建築物來說是窗戶越多，採光越好。山形袖章基本一型、船型基本一型與船型基本二型各有 6 個隱洞，而山形袖章中級一型則有 1 個隱洞。在建築物來說，因為外面看不到，其用途，可以當作密室或是儲藏室。

在這些籠狀模型當中，我們發現圖形同構與衣服反穿可逆性現象。圖形同構應用廣泛，例如化學、網路理論、資訊擷取與恢復、自動化、交換理論、語言學、電腦輔助設計等領域，甚至於太空站工序的安排問題上，而「衣服反穿」可以應用在建築的設計。我們也藉可逆性，開發中級複合體模型。拿破崙紙燈籠之拓樸與所屬特性，請參照表一。

## 7. 誌謝與未來研究工作

非流形複合體虧格數的計算，沒有實體模型，一定會發生錯誤的。我們要感謝亞洲大學資訊工程學系四年級的林依婷、李玟穎、鍾鎮澤、林秋慧、汪育庭、陳蔚仁等六位專題研究生，沒有他們努力地趕製紙籠狀模型，就不會有正確的歐拉特性數的計算。這裡特別感謝，負責船型製作的林秋慧同學，她的提醒：四個船型模型的船頭聚集接合，就會產生一個隱洞。自從研究非流形複合體虧格數以來，應用歐拉－龐加萊公式一般式預測隱洞，這是我們再一次的重要發現。

我們未來的研究工作，將放在非流形複合體附著的線框選擇上，繼續做完柏拉圖立體當中的 4 面體、12 面體與 20 面體等三種。然後，阿基米德立體<sup>39</sup>13 種與強生立體<sup>40</sup>92 種，期望會有更多新特性的發現。最後，我們希望致力於流形複合體非流形接合的研究。

<sup>39</sup> Archimedean solid, 阿基米德立體。

<sup>40</sup> Johnson solids, 強生立體。

## 參考文獻

- [1] Amber, J. A. P., Barrow, H. G., Brown, C. M. Burstall, R. M. Popplestone, R. J. (1973), "A versatile computer — controlled assembly system", Proc. of Third International Joint Conf. on Artificial Intelligence, pp. 298 — 307, 1973.
- [2] Bondy, J. A. and Murty, U. S. R. (1976), "Graph Theory with Applications", Elsevier
- [3] Booth, K. S. (1978), "Isomorphism testing for graph, semigroups, and finite automata are polynomial equivalent problems", SIAM J. Comput. 7:273 — 279, 1978
- [4] Brualdi, Richard A., (2005), Introductory Combinatorics, Fourth Edition, Prentice Hall, Inc., 2005
- [5] Busacker, R. and Saaty, T. (1965), "Finite Graphs and Networks — An Introduction with Applications", McGraw Hill, New York: 196 — 199, 1965
- [6] Frederickson, Greg (1997), Dissections: Plane and Fancy, Cambridge University Press, 1997
- [7] Fuse, Tomoko, (1990), Unit Origami — Multidimensional Transformations, Tokyo and New York: Japan Publication, Inc. p.228.
- [8] Lu, Keh — Ming, Tsaur, Alan S & Chen, Mei — Fan (2007a), Napoleon paper building blocks [Abstract]. Journal of Vision, 7(9):847, 847a, <http://journalofvision.org/7/9/847/>, doi:10.1167/7.9.847
- [9] 呂克明，曹子殷，陳美汎（2007b），摺紙積木，亞洲大學，九十五學年度吾愛（5I）吾校教學卓越計畫，獎勵創新紙本教材，2007 年 6 月。第六章。
- [10] 呂克明，曹子殷，陳美汎（2007c），拿破崙紙積木動態玩具，2007 創意、創新、創業國際研討會，INSPIRE 2007，5 月 30 日至 6 月 1 日，亞洲大學，pp.125 — 134。
- [11] 陳美汎，曹子殷，呂克明（2007d），饕餮紙積木與動態玩具，2007 創意、創新、創業國際研討會，INSPIRE 2007，5 月 30 日至 6 月 1 日，亞洲大學，pp.209 — 216。
- [12] 呂克明，曹子殷，白嘉祥（2006a），饕餮密舖，CGW2006（2006 年電腦圖學研討會），東吳大學。Lu, Keh — Ming, Tsaur, Alan S and Bai, Jia — Xiang, (2006a), Taotie Tessellation, CGW2006（Computer Graphics Workshop）, Soochow University
- [13] Lu, Keh — Ming, Tsaur, Alan S and Chen, Mei — Fan, (2006b), A Study of Napoleon Paper Building Blocks, Fu Ren Studies (Science and Engineering), Taipei: Fu Ren Catholic

- University, College of Science and Engineering, Vol. 40, pp. 39 — 70.
- [14] Lu, Keh — Ming, (2005), A Study of Innovative Plane Tessellation Patterns Systems, Fu Ren Studies (Science and Engineering), Taipei: Fu Ren Catholic University, College of Science and Engineering, Vol. 39, pp. 111 — 140.
- [15] Lynch, M. F. (1968), "Storage and retrieval of information on chemical structures by computer", Endeavour 27:68 — 71, 1968
- [16] Masuda, H., (1993), Topological operators and Boolean operations for complex — based nonmanifold geometric models, Computer — Aided Design, Vol. 25, No. 2, 1993, pp. 119 — 129.
- [17] Parthasarathy, K.R., (1994), Basic Graph Theory, India: Tata McGraw — Hill Publishing Company Limited, pp. 3 — 5
- [18] Stein, S. K., (1996), Strength in Numbers: Discovering the Joy and Power of Mathematics in Everyday Life, John Wiley & Sons, Inc., 1996, p. 37

*Received October 25, 2007*

*Revised December 12, 2007*

*Accepted December 19, 2007*

# Napoleon Origamic Lanterns and Genus

Keh-Ming Lu Alan S Tsaur

## Abstract

Napoleon paper building blocks consist of Bowtie, Teardrop, Wing, Bar, Boat, Star, Chevron, and Carp models. Having attached the modules built by 24 units of the same models of building blocks onto the duality wireframe of hexahedron and octahedron of Platonic solids, we developed 26 cage-like models. These cage-like models are divided into Basic and Intermediate groups. Intermediate I and II models are the mutually reversible models of Basic I and II, respectively. Based on numbers of vertices, faces, and edges of a complex, we can calculate its Euler characteristic by using generalized Euler-Poincare formula. We then verify their genus and cavity number of complexes.

We found the total face numbers of 24 units of Napoleon paper building blocks is 768 in the non-manifold construction process. The more reduction of vertex numbers, the tougher the construction process is. The same observation holds true also on the edge number. Chevron Basic I model has the most reduction of numbers of vertex and edges. It is not only the smallest and most compact one among these complexes but also the one of four complexes with cavity. From architecture viewpoints, since we can not see the cavity from outside, the application can be used as compartment or storage room. Method using generalized Euler-Poincare formula to predict the cavities is innovative.

Among these cage-like models, we found graph isomorphism and reversibility for general polyhedral surface. Applications of graph isomorphism can be found in the fields of chemistry, network theory, data re-

trieve, automation, switch theory, languish, computer aided design. It may also be applied on the optimization of processes in aerospace issues. Applications of reversibility for general polyhedral surface can also be found in the architectural design and development of intermediate models.

**Key Words :** Napoleon origamic lanterns, cage-like model, Euler-Poincare formula, Euler characteristic, genus, wireframe, non-manifold model, inclusion-exclusion principle, graph isomorphism, reversibility for general polyhedral surface

# 使用 BSCR 方法計算 Ca 原子在 4p-5s 間的 共振態能量和寬度

陳昭宏

親民技術學院通識中心

## 摘 要

在本文中，我們利用 BSCR(B-Spline based Complex Rotation)方法計算出 Ca 原子在 4p – 5s 之間的共振態的能量位置和寬度。在這計算過程中，首先求得  $S(\theta = -0.32)$  和  $d(\theta = -0.32)$  這兩個開放通道的最佳  $\beta$  值分別是 0.32 和 0.28，再利用這最佳  $\beta$  值，我們成功的計算出 Ca 原子在 4p – 5s 之間的共振態位置和寬度並給定各共振態的名稱。

**關鍵詞：**BSCR 方法，光游離，鈣原子

## I. INTRODUCTION

T. K. Fang.等人[1]首先利用 BSCR 方法計算鎂原子光譜，再將這個方法加入自旋軌道交互作用[2]，有很不錯的結果。接著，我們利用這種加入自旋軌道交互作用的 BSCR (B-Spline based Complex Rotation)方法計算鈣原子的光游離截面，發現和實驗值相當吻合[3-4]。而在我們的另外幾項研究中也詳細的計算出在 4s – 3d 間之最佳  $\beta$  值並找出這個區間之共振態位置和寬度[5]，而在 3d – 4p 之間之最佳  $\beta$  值和共振態位置和寬度也已經成功的計算出來並命名之[6]。

接著，在這項研究中我們將利用 BSCR 方法求得 4p — 5s 之間的共振態位置和寬度，因為這一區間需要考慮五個開放通道，而且在這個區間  $\beta$  值的選擇會影響共振態位置和光譜的外觀。因此，在做這項計算之前，我們先針對每一項開放通道分別求得其最佳  $\beta$  值，然後再對應每一個  $\beta$  值畫出共振態能量的對應位置，並排除非共振態的本徵值以便命名。

在本文中，仍然將簡單的提及本計算所採用的理論，並介紹本計算所使用之參數，在最後將展示各共振態的位置和寬度大小及最後命名的結果。

## II. THEORETICAL PROCEDURE

在這個方法中和 BSCI、BSK 相同，是利用 B-splines 為基底，並利用下式找出單電子的波函數[7][8]。

$$h_i^{eff}(r)\chi_{vi}(r) = \varepsilon_{vi}\chi_{vi}(r) \dots\dots\dots (1)$$

其中  $h_i^{eff}$  是等效的單電子的哈特—弗克漢米頓，也就是單一電子的漢米頓  $h_i^{HF}$  之總和。

$$\text{其中 } h_i^{HF} = \left(-\frac{1}{2} \frac{d^2}{dr^2} - \frac{Z}{r} + \frac{1}{2} \frac{l(l+1)}{r^2}\right) + V_i^{FCHF}(r) + V_p(r) \dots\dots\dots (2)$$

而  $V_i^{FCHF}$  是凍結核的哈特—弗克電位。在此可以參考[9]中 P.218 的第(14)式。同時，在這裡也須先調整長範圍的電偶極極性的大小（也就是模型電位  $V_p$ ）

$$\text{其中 } V_p = -\frac{\alpha}{r^4} (1 - \exp(-(\frac{r}{r_0})^6)) \dots\dots\dots (3)$$

其中  $\alpha$  是靜電偶極極化率和  $r_0$  是半徑趨近於零時的截止參數。

接著使用正弦節點序列當作 B-splines 之控制點以取得我們需要的基底，有了 B-splines 基底之後，再由(4)式形成單電子的波函數。

$$\chi(r) = \sum_{i=1}^N C_i B_i(r) \dots\dots\dots (4)$$

在(4)式中  $B_i(r)$  的就是選用的 B-Splines 基底含數 ( $i = 1 \sim 200$ )。這 200 個基底函數可以經由下列(5)式找到（但是在兩個端點時，除了  $B_1(r=0)=1$ ； $B_n(r=R)=1$  外其餘的 B-splines 均為 0。）

$$B_{i,k}(r) = \frac{r-t_i}{t_{i+k-1}-t_i} B_{i,k-1}(r) + \frac{t_{i+k}-r}{t_{i+k}-t_{i+1}} B_{i+1,k-1}(r) \dots\dots\dots (5)$$

$\chi(r)$  確定之後，接著再利用  $r \rightarrow re^{-i\theta}$  建造出複數的基底函數和波函數[5]，也就是開放通道。

$$\chi(re^{-i\theta}) = \sum_{i=1}^N C_i B_i(re^{-i\theta}) \dots\dots\dots (6)$$

因為當  $r \rightarrow re^{-i\theta}$  時，波函數將發散，故必須引入衰減因子  $e^{-\beta r}$  來修正，因此如(6)式可以改寫成(7)式

$$\tilde{\chi}(re^{-i\theta}) = \sum_{i=1}^N C_i \tilde{B}_i(re^{-i\theta}) \dots\dots\dots (7)$$

其中  $\tilde{B} = B_i(r) e^{-\beta r}$ ， $\beta$  是可變的參數。其中  $\beta$  可經由變分的方法求出最佳值，

$$\text{也就是利用 } \left[ \frac{\partial |E_{\text{res}}(\theta)|}{\partial \beta} \right] = 0 \dots\dots\dots (8)$$

求出極小值，這個極小值就是最佳的  $\beta$  值。一旦  $\beta$  值決定之後，就可以求出最佳的共振態之位置寬度和光譜。這個  $\beta$  值對共振能量之影響是隨著能量增加越高越明顯，故  $\beta$  值的尋找可說是 BSCR 計算中最重要的一項工作。

矩陣元素的求法，可利用 Rescigno et. al. [10] 所提的內積投影技術的方法，其中  $\langle n(\theta) | \hat{H} | n'(\theta) \rangle$  可用下式求解 ( $n, n' = 1, 2, 3$ )。

$$\begin{aligned} & \langle n_0 l_0 \varepsilon_v l_v(\theta) | H | n'_0 l'_0 \varepsilon_{v'} l_{v'}(\theta) \rangle \\ &= \sum_{\mu\mu'} \langle n_0 l_0 \varepsilon_v l_v(\theta) | n_0 l_0 \varepsilon_\mu l_\mu \rangle \langle n_0 l_0 \varepsilon_\mu l_\mu | H | n'_0 l'_0 \varepsilon_{\mu'} l_{\mu'} \rangle \\ & \quad \langle n'_0 l'_0 \varepsilon_{\mu'} l_{\mu'} | n'_0 l'_0 \varepsilon_{v'} l_{v'}(\theta) \rangle \dots\dots\dots (8) \end{aligned}$$

而  $\langle i | \hat{H} | n(\theta) \rangle$  和  $\langle n(\theta) | \hat{H} | j \rangle$  則可令一邊的  $\beta = 0, \theta = 0$ ，以便求出矩陣元素。而  $\langle i | \hat{H} | j \rangle$  和  $\langle j | \hat{H} | i \rangle$  均為實數，故很容易求得我們所需的矩陣元素。有了這些矩陣元素之後，再將這個矩陣對角化，就可以得到複數的本徵值。其中實數部分就是共振能量( $E_{\text{res}}$ )，而虛數部分就是寬度( $-\Gamma/2$ )。

### III. RESULTS AND DISCUSSION

#### 1. 計算過程：

在我們的這項計算中，先選定最大半徑  $200 a_B$ （波爾半徑），並建造出單電子的波函數。在這裡 B-splines 的階數  $k = 13$ ，基底數  $N = 80$ ，其他各項所採用之參數如下列表一所示。

表一 在這項計算中所採用的參數

Radius	200a <sub>B</sub>				
nuclear charge	20				
Alpha	3.5				
Effective charge for electron in the	19.5(1s)	17.5(2s)	10.5(3s)		
the core	15.5(2p)	3.0(3p)			
parameter related to orbit polar	1.75	1.81	1.9728	1.089	1.089
B-spline number	80				
B-spline order	13				
number of states for s, p, d, f, g, h	75(s)	75(p)	75(d)	75(f)	75(g)
Z <sub>eff</sub>	19.2(p)	7.9(d)	18.9(f)	19.1(g)	

當我們經由  $r \rightarrow re^{i\theta}$  求得開放通道之後，就可以計算漢米頓之每一個元素。由我們先前的研究[3]中，曾經對  $\theta$  可用的範圍作一調查，發現  $\theta$  可用的範圍約在  $-0.2$  到  $-0.5$  之間，隨著  $\theta$  的不同，最佳的  $\beta$  值也會有些微的不同。在這次的計算程序中，我們對  $\theta$  取  $-0.2$  和  $-0.5$  之中間值約為  $-0.32$  以固定這項變數。而我們在計算矩陣元素時所使用的組態如表二中所示，其中當計算  $s(\theta)$  時，採用  $|4(\theta)\rangle$  其餘  $|1(\theta)\rangle$ 、 $|2(\theta)\rangle$ 、 $|3(\theta)\rangle$  和  $|5(\theta)\rangle$  暫時不用。而計算  $d(\theta)$  時，採用  $|5(\theta)\rangle$  其餘  $|1(\theta)\rangle$ 、 $|2(\theta)\rangle$ 、 $|3(\theta)\rangle$  和  $|4(\theta)\rangle$  暫時不用。求出  $s(\theta)$  和  $d(\theta)$  這兩個 open channel 之最佳  $\beta$  值。

表二 在計算  $^1P$  時，所選取的組態，其中  $|4s4p(\theta) > \sim |4s13p(\theta) > \sim |3d4p(\theta) > \sim |3d13p(\theta) > \sim |3d4f(\theta) > \sim |3d15f(\theta) > \sim |4p5s(\theta) > \sim |4p12(\theta) > \sim |4p4d(\theta) > \sim |4p14d(\theta) >$  是開放通道其餘的是封閉通道，而在最後一欄中則是利用 **Rescigno et. al.** 所提的計算矩陣元素之所採用之完全集。

Symbol	Configuration	Number of the configuration	Complete set for open channel
$ 1(\theta) >$	$ 4s4p(\theta) > \sim  4s13p(\theta) >$	10	$ 4s4p > \sim  4s51p >$
$ 2(\theta) >$	$ 3d4p(\theta) > \sim  3d13p(\theta) >$	10	$ 3d4p > \sim  3d51p >$
$ 3(\theta) >$	$ 3d4f(\theta) > \sim  3d15f(\theta) >$	12	$ 3d4f > \sim  3d53f >$
$ 4(\theta) >$	$ 4p5s(\theta) > \sim  4p12s(\theta) >$	13	$ 4p5s > \sim  4p12s >$
$ 5(\theta) >$	$ 4p4d(\theta) > \sim  4p14d(\theta) >$	11	$ 4p4d > \sim  4p14d >$
$ 6 >$	$ 5s5p > \sim  5s21p >$	17	
$ 7 >$	$ 4d5p > \sim  4d21p >$	17	
$ 8 >$	$ 4d4f > \sim  4d23f >$	20	
$ 9 >$	$ 4f5d > \sim  4f22d >$	18	
$ 10 >$	$ 4f5g > \sim  4f24g >$	20	

本計算之矩陣架構可參考圖一所示。

## 2. 計算結果

### (1) $s(\theta = -0.32)$

在計算  $s(\theta)$  時，開放通道只採用  $|4(\theta) >$  其餘  $|1(\theta) > \sim |2(\theta) > \sim |3(\theta) >$  和  $|5(\theta) >$  暫時不用。在這個計算中，我們將  $\beta$  由 0 到 1 之間分別取 100 個點，再取前面 10 個本徵值並用變分方法分別求其極小值。結果我們發現：在這十個共振態中有些未出現極小值，其關係圖和結果如圖二和其下方的表格所示。

再將每個  $\beta$  對應的本徵值的實數部分的關係作一圖，如圖三所示，發現除了第一個本徵值呈現不穩定之外其他均相當穩定。

在這個計算中，雖然有許多共振態未出現最佳化值，但是每一個共振態之最大值和最小值的差異約只有十萬分一甚至百萬分一，故相當穩定（也就是說： $\beta$  取 0.2 到 0.9

之間均相當理想)。而對於這些共振態的最佳 $\beta$ 值選擇，我們取有出現極值的三個共振態  $E_{\text{res}3}$  ( $\beta = 0.28$ )， $E_{\text{res}4}$  ( $\beta = 0.36$ )， $E_{\text{res}6}$  ( $\beta = 0.32$ ) 的平均值 0.32 做為這個系列之最佳  $\beta$  值。

	$ 1(\theta)\rangle$	$ 2(\theta)\rangle$	$ 3(\theta)\rangle$	$ 4(\theta)\rangle$	$ 5(\theta)\rangle$	$ 6\rangle$	$ 7\rangle$	$ 8\rangle$	$ 9\rangle$	$ 10\rangle$
$\langle 1(\theta) $										
$\langle 2(\theta) $										
$\langle 3(\theta) $			$\langle n(\theta) H n'(\theta)\rangle$					$\langle n H n'(\theta)\rangle$		
$\langle 4(\theta) $										
$\langle 5(\theta) $										
$\langle 6 $										
$\langle 7 $										
$\langle 8 $			$\langle n(\theta) H n'\rangle$					$\langle n H n'\rangle$		
$\langle 9 $										
$\langle 10 $										

圖一 本計算之矩陣示意圖

圖二 Ca 在 5s 到 4d 間旋轉  $S(\theta, \theta = -0.32)$  並取十個共振態，再分別將每一個共振態的  $\beta$  每間隔 0.01 由 0.18 改變到 0.99，由圖形來觀察其極小值的位置。在比對計算的結果發現在(b)(c)(d)(f)圖中出現極值，其中(b)出現極大值  $\beta_{\text{max}} = 0.46$ ，(c)出現極小值  $\beta_{\text{min}} = 0.28$ ，(d)出現極小值  $\beta_{\text{min}} = 0.36$ ，(f)出現極小值  $\beta_{\text{min}} = 0.32$ 。而其他幾個共振態中並沒有出現極值。

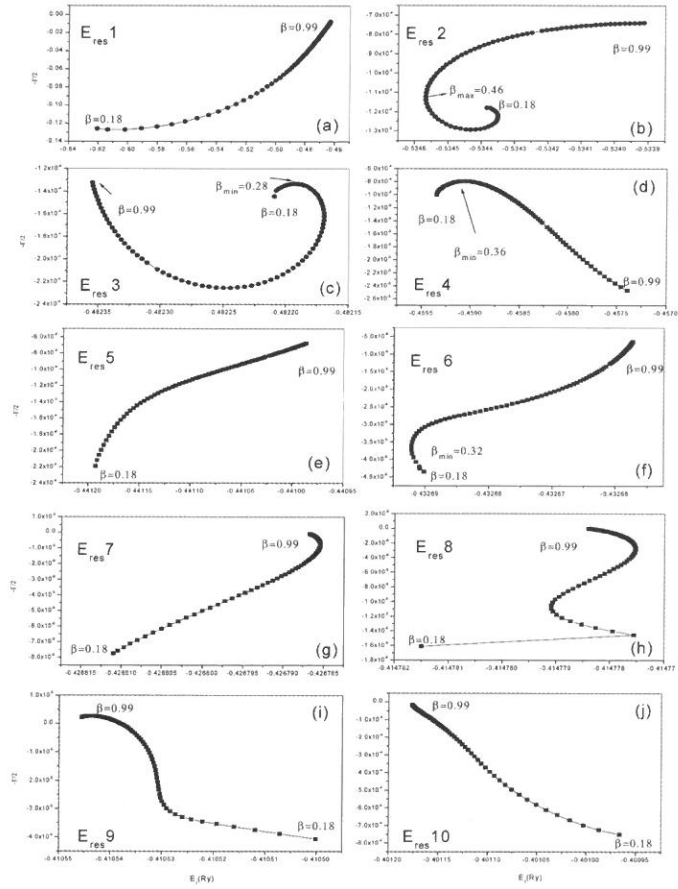
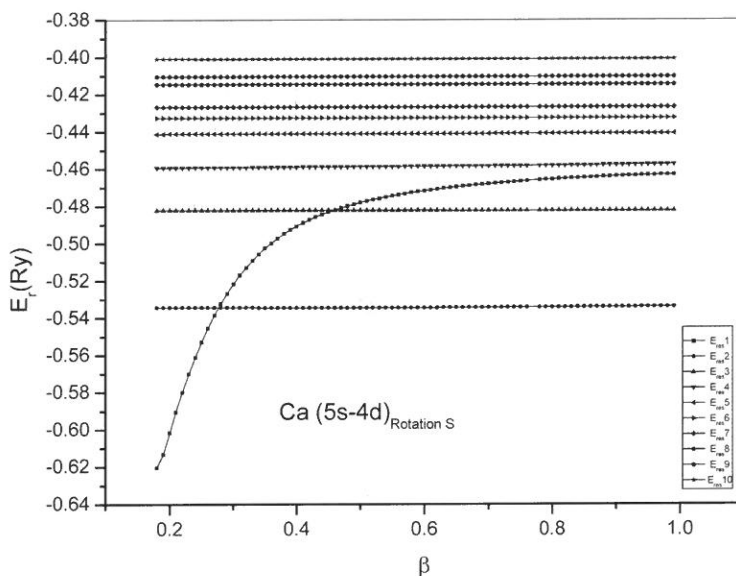


圖 10

	$E_{\text{res } 1}$	$E_{\text{res } 2}$	$E_{\text{res } 3}$	$E_{\text{res } 4}$	$E_{\text{res } 5}$	$E_{\text{res } 6}$	$E_{\text{res } 7}$	$E_{\text{res } 8}$	$E_{\text{res } 9}$	$E_{\text{res } 10}$	$\beta_{\text{op}}$
$\beta_{\min}$	no	0.46 (max)	0.28	0.36	no	0.32	no	no	no	no	0.32

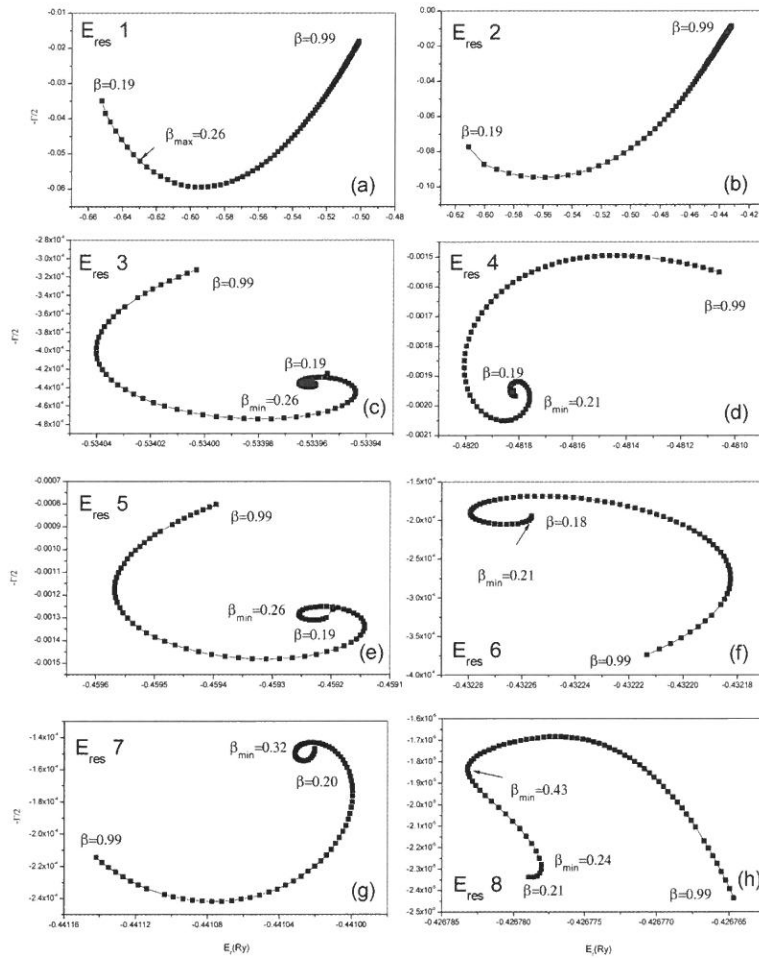


圖三

圖三 Ca 在 5s 到 4d 間旋轉  $S(\theta, \theta = -0.32)$  並取十個共振態，再分別將每一個共振態的  $\beta$  每間隔 0.01 由 0.18 改變到 0.99，分別畫出每一個  $\beta$  所對應的  $E_r$  值。在這裡可以明顯的看到  $E_{res\ 1}$  隨著  $\beta$  改變而呈現劇烈之變化，故這個值應該是對角化計算過程時出現之開放通道的能量，在命名的過程時應該將其捨去。

## (2) $d(\theta = -0.32)$

當計算  $d(\theta)$  時，採用  $|5(\theta)\rangle$  其餘  $|1(\theta)\rangle, |2(\theta)\rangle, |3(\theta)\rangle$  和  $|4(\theta)\rangle$  暫時不用。將這矩陣對角化之後，取前面 8 個本徵值分別求其  $\beta$  之極小值，其結果如圖四所示。在這計算結果中發現：除了  $E_{res\ 1}$  和  $E_{res\ 2}$  沒有出現極小值外，其餘本徵值均出現極小值，其結果整理如圖四下方之表格所示。

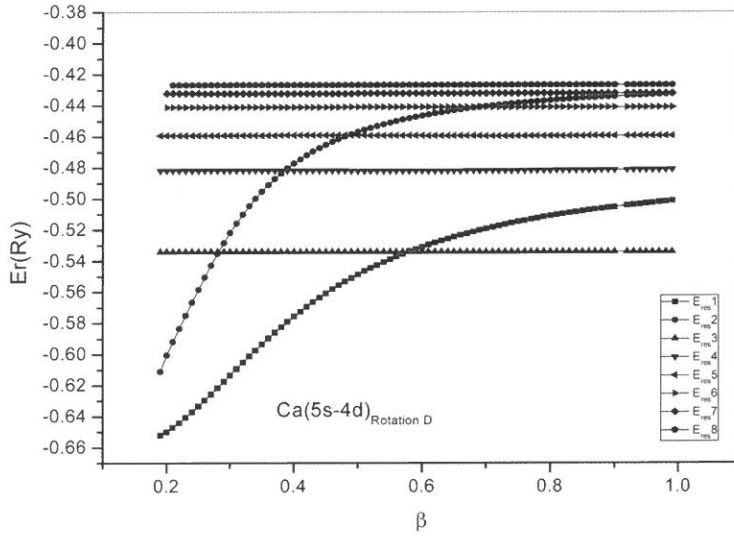


圖四

	E <sub>res</sub> 1	E <sub>res</sub> 2	E <sub>res</sub> 3	E <sub>res</sub> 4	E <sub>res</sub> 5	E <sub>res</sub> 6	E <sub>res</sub> 7	E <sub>res</sub> 8	E <sub>res</sub> 9	E <sub>res</sub> 10	$\beta_{op}$
$\beta_{min}$	0.26 (max)	no	0.26	0.21	0.26	0.21	0.32	0.43	0.28	no	0.32

接著將本徵值實數的部分和  $\beta$  的對應關係做一圖，如圖五所示。在這個圖中可以發現 E<sub>res</sub> 1 和 E<sub>res</sub> 2 隨著  $\beta$  的改變而呈現較不穩定的現象，其餘各共振態都相當穩定。

圖四 Ca 在 5s 到 4d 間旋轉  $d(\theta, \theta = -0.32)$  並取八個共振態，再分別將每一個共振態的  $\beta$  每間隔 0.01 由 0.18 改變到 0.99，由圖形來觀察其極小值的位置。在比對計算的結果發現只有(b)圖沒有出現極值，其餘(a)出現極大值  $\beta_{\max} = 0.26$ ，(c)出現極小值  $\beta_{\min} = 0.26$ ，(d)出現極小值  $\beta_{\min} = 0.21$ ，(e)出現極小值  $\beta_{\min} = 0.26$ ，(f)出現極小值  $\beta_{\min} = 0.21$ ，(g)出現極小值  $\beta_{\min} = 0.32$ ，(h)出現兩個極小值  $\beta_{\min} = 0.24$  和 0.43。



圖五

圖五 Ca 在 5s 到 4d 間旋轉  $d(\theta, \theta = -0.32)$  並取八個共振態，再分別將每一個共振態的  $\beta$  每間隔 0.01 由 0.18 改變到 0.99，分別畫出每一個  $\beta$  所對應的  $E_r$  值。在這裡可以明顯的看到  $E_{\text{res } 1}$  和  $E_{\text{res } 2}$  隨著  $\beta$  改變而呈現劇烈之變化，故這個值跟圖三中相同應該是對角化計算過程時出現之開放通道，在命名的過程中也應該將其捨去。

在這個部份，除了前面兩個共振態隨著  $\beta$  值而呈現大幅度的變化以外，其餘幾個共振態也是相當的穩定。因此對於這個系列的共振態的最佳  $\beta$  值選擇，我們取有出現極值的三個共振態  $E_{\text{res } 3} (\beta = 0.26)$ ， $E_{\text{res } 4} (\beta = 0.21)$ ， $E_{\text{res } 5} (\beta = 0.26)$ ， $E_{\text{res } 6} (\beta = 0.21)$ ， $E_{\text{res } 7} (\beta = 0.32)$ ， $E_{\text{res } 8} (\beta = 0.43)$  的平均值約為 0.28 做為這個系列之最佳  $\beta$  值。

### (3) 計算共振態能量位置和寬度

將前面幾項研究中所得到的各開放通道之最佳  $\beta$  值整理如表三所示，在將這些值代

入圖一之矩陣架構圖中經過對角化計算，可以得到各共振態之位置和寬度。其結果如表四所示。

表三 Ca 原子各能量區間之各 open channel 之最佳  $\beta$  值

The range of resonance energy	Open channel	Optimized $\beta$ value
4s ~ 3d (Ref.[5])	4s $\epsilon$ p ( $\theta = -0.32$ )	0.21
3d ~ 4p (Ref.[6])	3d $\epsilon$ p ( $\theta = -0.32$ )	0.21
	3d $\epsilon$ f ( $\theta = -0.32$ )	0.24
4p ~ 5s	4p $\epsilon$ s ( $\theta = -0.32$ )	0.32
	4p $\epsilon$ d ( $\theta = -0.32$ )	0.28

表四 這是在 4p ~ 5s  $^1P$  系列的共振態名稱和位置 ( $1\text{Ry} = 13.6\text{ev}$ )，其中  $N_{\text{eff}}$  是有效量子數。

State	Closed Channel			Closed Channel+Open channel			
	Er(Ry)	$N_{\text{eff}}(5s)$	$N_{\text{eff}}(4d)$	Er(Ry)	$N_{\text{eff}}(5s)$	$N_{\text{eff}}(4d)$	$-\Gamma/2$
5s5p $^1P$	- 0.53555	2.68	2.33	- 0.52436	2.80	2.40	- 0.00417
4d5p $^1P$	- 0.48291	3.40	2.75	- 0.47609	3.55	2.82	- 0.00322
5s6p $^1P$	- 0.45930	3.99	3.03	- 0.45849	4.02	3.04	- 0.00177
5s7p $^1P$	- 0.44130	4.73	3.32	- 0.43798	4.91	3.38	- 0.00061
4d6p $^1P$	- 0.43376	5.19	3.47	- 0.42558	5.87	3.65	- 0.00037
5s8p $^1P$	- 0.42691	5.74	3.62	- 0.42094	6.41	3.77	- 0.00095

## IV. CONCLUSION

使用 BSCR 方法計算 Ca 原子共振態位置和寬度的確相當快速穩定。但是，在矩陣對角化之後會出現一些非共振態的本徵值，經由詳細的計算每一個  $\beta$  值對應之共振態位置之後，發現：刪除這些不穩定的本徵值之後，將可順利的找到這個區間之各共振態名稱。除此之外，在這個研究中我們也找到最佳  $\beta$  值，並用這些值，找到更精確的共振態位置和寬度。

## REFERENCES

- (1) T. K. Fang, Y. K. Ho and Y.C.Lin, Proceedings of International Seiminar on photoionization in Atom, Kyoto, Japan, pp.12-17.
- (2) T. K. Fang, T. N. Chang, Phys. Rev. A76, 012721, (2007)
- (3) J. H. Chen, T. K. Fang, T. N. Chang, "Ca ground-state photoionization to spin-mixed continua", Physics Bimonthly, vol.28, no.1, p335, 2006 Annual Meeting of the Chinese Physical Society
- (4) J. H. Chen, T. K. Fang, T. N. Chang, "B-spline-based Complex-rotation Method with Spin-dependent Interaction for Ca Ground-state Photoionization", Physics Bimonthly, vol.29, no.1, p401, 2007 Annual Meeting of the Chinese Physical Society
- (5) J. H. Chen, "The optimized  $\beta$  value of  $^1P$  and  $^3P$  for Calcium photoionization in BSCR method" *Journal of St. John's University*, (2007)
- (6) J. H. Chen, *Journal of Chin-Min College* Vol. 14, (to be published)
- (7) Y. K. Ho, Phys. Rep.99, 1 (1993).
- (8) T. K. Fang, T. N. Chang, Phys. Rev. A61, 062704, (2000)
- (9) T. N. Chang, Many-body Theory of Atomic Structure and Photoionization, edited by T.N. Chang (World Scientific, Singapore, 1993), p. 213
- (10) T. N. Rescigno, C. W. McCurdy, Jr. and A. E. Orel, Phys. Rev. A17, 1931(1978).

*Received October 26, 2007*

*Revised December 13, 2007*

*Accepted December 20, 2007*

## Calculating Resonance Energies and widths of Ca between 4p and 5s by BSCR method

J. H. Chen

*Center for General Education, Chin Ming Institute of Technology*

### Abstract

We utilized BSCR (B-Spline based Complex Rotation) method to calculate the position and width of the Ca resonances energy between 4p-5s. In the course of this calculation, we obtained the optimized  $\beta$  value of these two open channels, s ( $\theta = -0.32$ ) and d ( $\theta = -0.32$ ), is 0.32 and 0.28 respectively. By using these optimized  $\beta$  values, we calculated out the position and width of the Ca resonances energy between 4p-5s and gave its name successfully.

**Keywords:** BSCR method, photoionization, Calcium



# 利用聲部結構於多音音樂之比對與排序<sup>1</sup>

袁欣華 徐嘉連<sup>2</sup>

輔仁大學資訊工程系

## 摘 要

關於內涵式音樂資訊查詢 (content-based music information retrieval) 的研究領域已從過去的單音音樂資料庫發展至多音音樂資料庫。在現存的多音音樂資訊檢索 (polyphonic music information retrieval) 中，大部分都是以計算音高與音長之絕對位置，與所欲查詢之旋律比對的方式來做音樂搜尋，此種方法雖能夠尋找出包含使用者所查詢旋律的答案，卻忽略了多音音樂結構的重要性，也就是聲部 (voice) 的概念。根據樂理，當多音音樂旋律在進行時，曲子是由數個單音音樂旋律所組成，每個旋律即是聲部。因此若經由演算法，所比對出的結果分佈於不同的聲部中，其相似度應該要相對較低。本篇論文主要針對多音音樂資料庫，以單音音樂去做查詢。首先，將音樂物件之音符以線段表示，接著經由本篇論文所提出的方法判斷每個線段所位在的聲部，最後經過改良的動態規劃 (dynamic programming) 演算法計算其相似度，將查詢結果做更為符合樂理的排序。最後，本論文並根據所提之演算法實作系統。

**關鍵詞：**多音音樂資訊檢索 (polyphonic music information retrieval)、聲部切割演算法 (voice segment algorithm)、音樂不相似度 (music dissimilarity)、音樂排序 (music ranking)

<sup>1</sup> 本論文研究為輔仁大學補助研究、計畫編號：409531040123

<sup>2</sup> Corresponding author. E-mail: alien@csie.fju.edu.tw

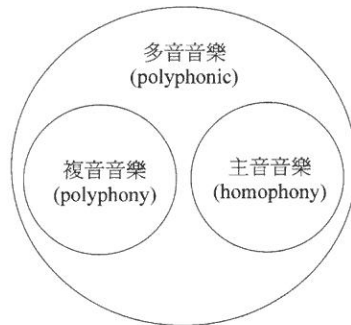
## 1. 序 論

內涵式音樂資訊查詢 (content-based music information retrieval) 在近年已經成爲一個越來越重要的研究領域。在典型的內涵式音樂資訊查詢系統中，將音樂物件中的音高 (pitch) 或音頻 (frequency) 轉換爲數值或符號，並以序列 (series) 的方法表示，進一步以字串比對 (string matching) [Korn98][Uitd98][Uitd99]、動態規劃 (dynamic programming) [Dove01][Pard05]或馬可夫鏈[Pick02]等方法進行查詢。

音樂可分爲單音音樂 (monophonic) 與多音音樂 (polyphonic)。同時只有一個聲音進行的音樂，謂之單音音樂；相對的，多音音樂乃是指同一時間有兩個或兩個以上的聲音。其中多音音樂包含兩部份：主音音樂 (homophony) 與複音音樂 (polyphony) (圖一)。主音音樂 (homophony) 作品以其中某一個聲部 (多數情況是高音部) 的「旋律」爲主，其餘聲部以「和聲」或「節奏」等手法陪襯和伴奏。所謂的複音音樂 (polyphony) 是一種「多聲部音樂」，作品中含有兩條以上 (含) 獨立旋律，利用對位法的技巧，和諧地結合在一起，這樣的音樂就叫做複音音樂 (表一)。

近年來，音樂資訊查詢研究已從單音音樂資料庫的查詢進而發展爲針對多音音樂資料庫的查詢。在現存的多音音樂資訊檢索 (polyphonic music information retrieval) 演算法中，大部分都是以計算音高與音長之位置，與所欲查詢之旋律比對的方式來做音樂搜尋，此種方法雖能尋找出相似答案，但是卻忽略了音樂的結構性，也就是聲部 (voice) 的概念。

圖二(a)爲巴哈三聲部創意曲第七首之第三、四小節之樂譜，此首曲子爲 e 小調、3/4 拍的作品，我們將此小節以座標表示 (圖二(c))。其中橫軸爲拍子 (meter)，縱軸爲音高 (pitch)，每條線段 (segment) 分別代表一音符。由於擷取起始於第三小節，因此拍子由第七拍起算。此首作品分爲三個聲部，我們以黃線標示連結。圖二(b)爲使用者所下之查詢，查詢結果如圖二(c)中之斜線方框，其分散於第一聲部與第二聲部之間。在比對上雖完全出現，然則以音樂結構的角度來說，此查詢卻結果分散於第一與第二聲部中；因此這樣的查詢結果，我們認爲不能當做「精確比對」 (exact matching) 的查詢答案。



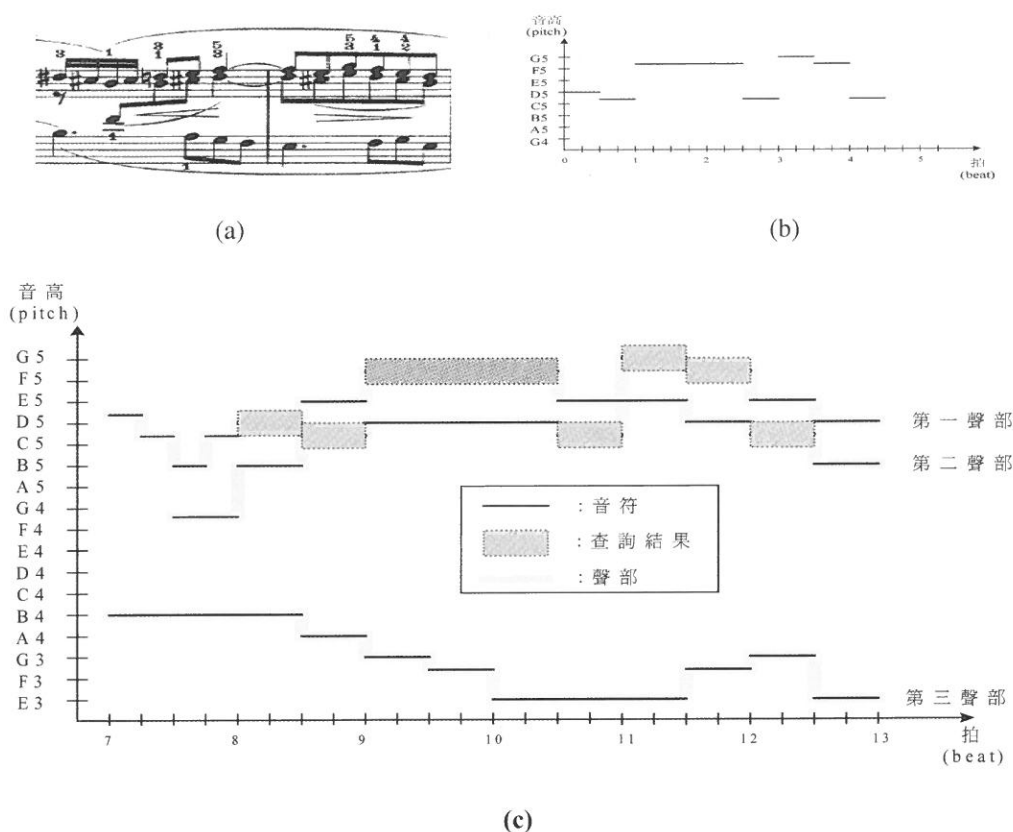
圖一 多音音樂、複音音樂與主音音樂之關係圖

表一 多音音樂的分類〔劉 06〕

	主音音樂 (homophony)	複音音樂 (polyphony)
定義	以其中某一個聲部（多數情況是高音部）的「旋律」為主，其餘聲部以「和聲」或「節奏」等手法陪襯和伴奏	一種「多聲部音樂」，作品中含有兩條以上（含）獨立旋律，通過技術性處理，和諧地結合在一起
技巧	和聲學	對位法

本篇論文針對多音音樂資料庫，採 MusicXML 的音樂格式，提供相似性音樂查詢，考慮多音音樂的聲部，使查詢結果更加符合音樂的結構。其中，從多音音樂中判定個別聲部的演算法、相似度（similarity）的公式和查詢比對的演算法是本篇論文的關鍵。使用者經由介面下單音旋律的查詢，系統與多音音樂資料庫做比對，搜尋出相似的結果，並依照其相似度與音樂結構的符合性做排序。

本篇論文架構如下：第二章針對近年來的相關議題作綜合性的討論，第三章介紹我們所使用的音樂資料形式 MusicXML 與 MusicXML Tag，第四章針對音樂表示法和音樂的不相似度與排序有詳細的介紹與定義，第五章包含系統架構與兩個演算法：聲部切割演算法（Voice Segment Algorithm）和音樂不相似度（Music Dissimilarity），第六章則是系統實作成果，最後第七章是本篇論文的結論與未來工作。



圖二 (a) 巴哈三聲部創意曲第七首之第三、四小節樂譜  
 (b) 使用者查詢  
 (c) 圖(a)聲部與查詢結果

## 2. 文獻探討

針對多音音樂內涵式音樂資訊查詢 (Polyphonic content-based music information retrieval)，過去學者提出許多相關的研究，主要方法分為三類。第一種是將多音音樂擷取出一單音音樂的旋律，然後利用查詢單音音樂的技巧進行查詢。Themefinder[Korn98] 將每筆多音音樂資料擷取出單音音樂型態的主旋律，當使用者下查詢後，則以字串比對的演算法 (string matching algorithm) 找出相似的旋律。Uitdenbogerd 和 Zobel[Uitd98]

[Uitd99]利用擷取最高音高的方法將多音音樂資料轉換成單音音樂。這些方法普遍的缺點就是假設多音音樂資料能夠以單音音樂的形式表達。然而在[Pick01]中研究發現，這並不正確。

第二類是先將多音音樂水平切割成數個單音音樂，再接著以單音音樂查詢的技巧進行查詢的動作。[Kili02]基於隨機的區域搜尋方法提出了新的聲部切割演算法（voice separation algorithm），有別於過去的研究，此演算法允許在個別的聲部中有和弦（chord）的存在；並且能夠依據調整不同的係數產生不同要求的音樂風格。Stream Segregation Algorithm [Szet03]將音樂以一個個的事件（event）的形式呈現，以人類聽覺心理學的角度計算出各事件與各叢集之間的相似度後，無須輸入群組的個數，即可依照相似程度的大小將叢集與叢集之間連結，形成數個單音旋律的叢集。[Chew04]將生物資訊中的 Conting Mapping Approach 技術使用在多音音樂的聲部切割（voice separating），根據聲部的數量（voice count）將樂曲切割成數個 contings，接著經由最短距離的計算再將其接合。[Kirl05]提出和實作了一個系統— VoiSe，可將多音音樂中的聲部（voice）脫離出來，此系統設計使用在符號式（symbolic）的音樂表達和弦上。[Pard05]針對多音音樂資料庫，提出 homophonic alignment 的演算法，進而推廣至 polyphonic alignment 上，將多音音樂視為複音音樂的形式做 string alignment。

第三種方法是設計專門的演算法直接針對多音音樂進行查詢。SEMEX [Lems00]延用[Wu92]所提出的 shift-or algorithm，以字串比對的方式找出多音音樂資料中所有的相似單音音樂片段，此系統最大的特色乃是能夠找出所查詢單音旋律移調之後相似的答案。更進一步，PROMS [Clau00] 採用反轉檔案式的方法（inverted-file based method）記錄每一筆多音音樂資料中每一個音符的資訊，包含音高、小節線、起始時間，使系統能夠進行多音音樂的查詢。然則，它的查詢結果僅能呈現出在音高與起始時間是絕對相同的音樂片斷。由於每個音符的起始時間必須與查詢的音符相同，因此這個系統優點在於可以查詢出精確的結果，相對的，缺點則是無法進行相似的查詢。另一方面，Dovey [Dove01]在多音音樂查詢上提出了動態規劃（dynamic programming）方法，除了精確的比對外，進一步的考慮了相似的查詢。然而由於動態規劃的限制因素，其效能會由於過長的音樂資料或資料量過大的資料庫而不佳。Pickens [Pick02]使用 HMM（Hidden Markov Model）以類似機率矩陣（probability matrices）的方式，分別描述多音音樂資料與多音音樂查詢的和弦分佈機率（probability distributions）；在這個方法中，依照兩者機率矩陣的不同進行查詢與資料相似度的計算。這樣的方法適用於變奏的音樂，然而字串的機率分佈卻與子字串的機率分佈十分的不同，因此，HMM的方法僅適用於當查詢與

資料具有相同的長度時。

我們將具有相同起始時間的音符視為一個事件 (event) [Dove01]，因此一首曲子就可視為一事件串列 (string of events)。為了解決各種的事件的複雜情況，傳統的索引方法，例如 suffix tree [McCr76] [Park00] 或 n-gram [Down00]，隨之被研究者帶入多音音樂查詢的領域中。在 [Dora01] [Dora04] 的研究中，Doraisamy 和 Ruger 提出 musical word 的概念，利用 n-gram 的技巧和 text retrieval method，對音樂物件，提供內涵式查詢的功能。[Uitd02] 利用 local alignment 擷取多音音樂的旋律特徵，以四種不同的方法：All-mono、Entropy-channel、Entropy-part 與 Top-channel 從多音音樂中擷取單音旋律，並於實驗中比較 n-gram 與 local alignment 的效能，發現 n-gram 只有在較短的查詢與手動式查詢時具有較佳的效能，而 local alignment 在自動查詢的效能上比 n-gram 要好。

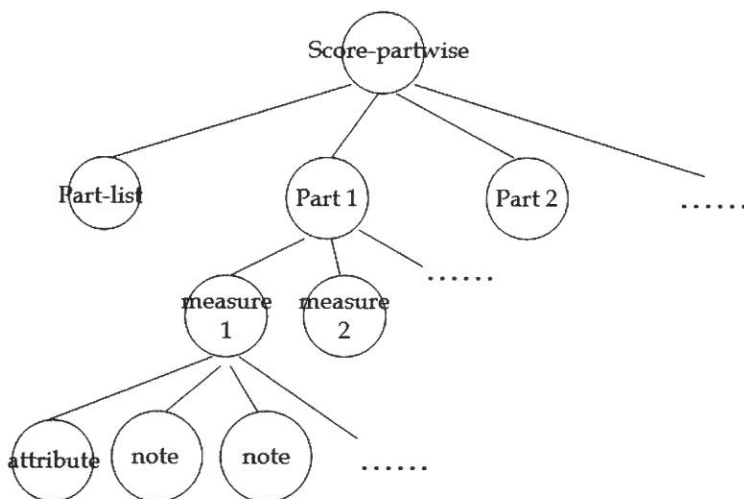
事實上，各種的記分函數 (scoring functions) 都能夠計算出任兩串字串的相似程度。當使用者給予一查詢字串與記分函數，有兩種方法均是挑選出最適當的答案，換言之就是刪除不適當的答案。第一種是刪去相似度低於門檻值的資料，然而對於不同的查詢訂定適當的門檻值是較困難的。另一種是僅挑選出所指定前 K 個相似的答案 [Liu03]，此種方法適合當使用者已決定欲查詢的數量時進行音樂檢索。

### 3. MusicXML

#### 3.1 MusicXML

XML 是在資訊交換上，目前廣泛被使用的一種資料格式。在這樣的趨勢下，以 XML 的技術為基礎，發展出一種新的音樂資料格式稱之為 MusicXML。基於 XML 的架構，因此 MusicXML 能夠廣泛的被應用。在網路或是資料交換與傳輸上都是很常用的格式。MusicXML 目前廣泛用於古典音樂表示，並且完整的呈現樂譜原貌。MusicXML 的設計目的是：為了音樂資訊的分析與擷取。MusicXML 是一種儲存樂譜 (score-like) 的資料格式，包含了符號式 (symbolic) 的音樂資料，以及許多的 metadata。如：作者 (creator)、譜號 (clef)、調性 (key)、節拍 (beat)、小節 (measure)、音高 (pitch)、音長 (duration)、旋律 (melody)、節奏 (rhythm)、和弦 (chord)、圓滑線 (slur)、音符類型 (type)、裝飾記號 (grace)、歌詞 (lyrics) ... 等的音樂相關資訊。

對於 MusicXML documents 來說，大部分的 MusicXML document 都有相似的階層與高度。如圖三所示，score-partwise 包含 part-list、part，part 包含 measure number，measure 包含 note，note 包含 pitch、duration、voice、type、stem...等樹狀的結構。



圖三 MusicXML 樹狀資料結構

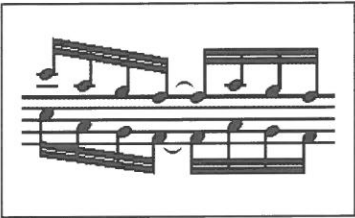
### 3.2 MusicXML Tag

voice 的切割是爲了讓我們增加多音音樂查詢的品質。在查詢之前，先針對我們資料庫內的音樂作前處理，使多音音樂切割成數個單音音樂旋律(voice)，進而當使用者進行查詢時，能夠查詢出更加符合音樂結構與旋律的結果。

我們採用 MusicXML 的音樂資料結構來做 voice 的切割。在 MusicXML 中有下列的特殊標籤：

#### (1) <backup>

backup 標籤主要是在標明當多音音樂進行時，若在同一個時間點上，此音符與其他音符並不是同一個和絃，則由於 MusicXML 的規定，此音符的順序將排在較後面，而爲符合樂譜的形式，我們必須註明此音符將回溯多少時間。舉例如下：



(a)

```

<beam number="1">end</beam>
<beam number="2">end</beam>
</note>
<backup>
<duration>8</duration>
</backup>
<note default-x="111">

```

(b)

圖四 backup tag 範例

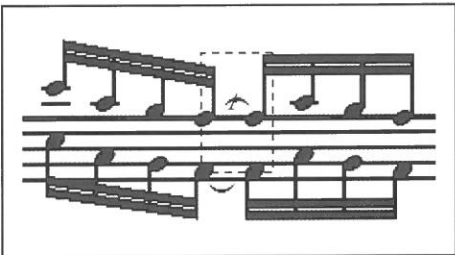
圖四(a)中，在 MusicXML 的紀錄順序為，上排八個音由左而右，接著紀錄下排由左而右，因此當紀錄完畢上排的最後一個音後，我們必須知道下一個音，也就是下排第一個音必須回溯多少時間，因此在 MusicXML 的程式碼中，利用 **backup** 這個標籤，如圖(b)虛線方框的部分，告知必須回溯 8 個單位時間，如此方可正確的紀錄音符的位置。

也就是，當有 **backup** 這個標籤的出現時，同一個小節內的旋律可視為不同的 voice。因此當每遇到 **backup** 標籤，我們就必定將其切割為不同的 voice。並且經由 **backup** 標籤我們能夠準確的計算每個音符的起始時間。

## (2) <tie>

**tie** 標籤是在紀錄樂譜中的連結線。所謂連結線記號為一弧線，記在兩個或兩個以上高度相同的音符上，表示弧線內各音結合為一音，如圖五的 A。

舉例如下：



(a)

```

<notations>
<tie orientation="over" type="start" />
</notations>
</note>
.....
.....
<beam number="1">begin</beam>
<beam number="2">begin</beam>
<notations>
<tie type="stop" />
</notations>
</note>

```

(b)

圖五 tied tag 範例

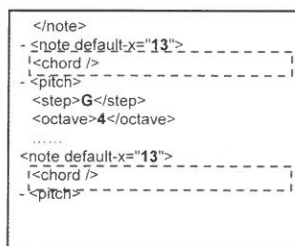
圖五(b)是圖五(a)中上排音符第四與第五個音的程式片段，虛線方框乃是紀錄第四與第五的音之間的連結線的起始與結束。在音樂的樂句中，當連結線出現就代表其為一連續的樂句，不可分割。因此當有 **tied** 這個標籤出現，我們將其所連結的音符視為在同一個 **voice** 中。

### (3) <chord>

**chord** 標籤是在紀錄樂譜中的和絃。在音樂的定義中，若將音符以同一個音桿連接，那麼其為一個和絃。圖六(a)虛線方框中即為一和弦，在同一時間此三個音同時出現，三個音分別落在不同的聲部中。



(a)



(b)

圖六 chord tag 範例

### (4) <rest>

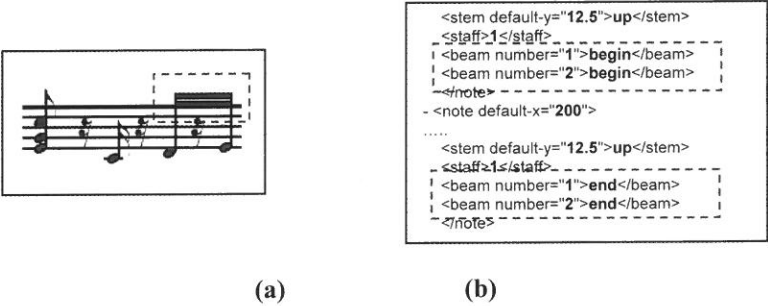
**rest** 標籤代表休止符。

### (5) <beam>

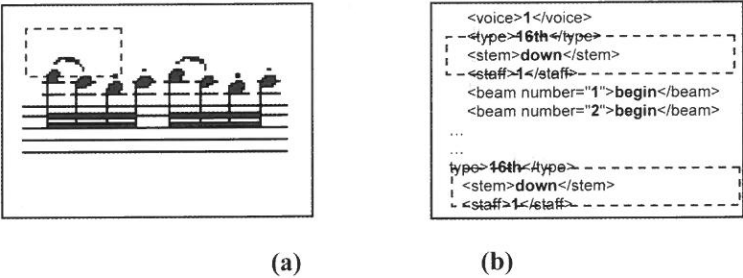
**beam** 標籤紀錄樂譜中連音的符號，如圖七(a)中虛線方框。連音代表前後音符要連續出現，也就是會在同一個聲部中。

### (6) <slur>

圓滑線記號為一弧線，它有兩種作用：如果它是記在兩個高度不同的音符上，表示第一音突強，第二音輕而短；如果記在兩個以上高度不同的音符上，表示弧線內的音符，需演奏得非常圓滑，也就是前後必定是連續的兩個音符。圖八(a)中的虛線方框就是圓滑線。



圖七 beam tag 範例



圖八 slur tag 範例

以上所述 MusicXML 的特殊標籤，能夠幫助我們在切割 voice 上更為正確。我們考慮進音樂上譜曲的相關規定與技巧，使 voice 的切割能夠更加符合音樂結構上的特性，也使結果更加正確。更進一步 voice 切割的演算法請參考 5.1 節。

### 4. 音樂表示法和不相相似度

在本章中，4.1 節我們首先將音樂物件中的旋律表達為線段，便於之後計算不相相似度。接著於 4.2 節說明不相相似度的定義。

## 4.1 音樂表示法

### 定義 4.1：音高 (pitch)

音樂物件中音高的紀錄包含兩個部份：音階 (step) 與八度音程 (octave)。例如，C4 中的 C 為音階 (step)，4 為八度音程 (octave)。休止符則以符號 r 代表。

### 定義 4.2：音長 (duration)

一個音樂物件的音長為其終止時間減去起始時間，且音長的長度是相對的量。

### 定義 4.3：線段 (segment)

我們將音符以線段 (segment) 表示，每條線段視為一四個維度 ( $p, s, e, v$ ) 的向量，其中  $p$  代表音高， $s$  代表起始時間， $e$  代表終止時間， $v$  代表聲部值。假設給予兩個線段  $S_1 = (p_1, s_1, e_1, v_1)$  和  $S_2 = (p_2, s_2, e_2, v_2)$ 。如果  $e_1 \leq s_2$ ，則  $S_1 < S_2$ ；如果，則  $e_2 \leq s_1$ ，則  $S_1 > S_2$ 。

### 範例 4.1：

以圖九(a)中片段多音曲子為例，我們將其以線段 (segment) 表示如下(C5, 1, 6, 1) (C4, 9, 16, 3) (E4, 9, 16, 2) (C5, 9, 16, 1) (F4, 1, 4, 3) (A5, 1, 4, 2) (E4, 5, 6, 3) (G4, 5, 6, 2) (D4, 7, 8, 3) (F4, 7, 8, 2)。

### 定義 4.4：重疊 (overlape)

$$\text{overlape}(S_1, S_2) = \begin{cases} 0, & \text{if } S_1 < S_2 \text{ or } S_2 < S_1. \\ 1, & \text{otherwise.} \end{cases}$$

若以起始時間為基準，將相同起始時間的音符置於同一個集合裡，則可形成一集合的序列  $S = C_1 C_2 C_3 \dots C_m$ ，其中  $m$  為集合的個數，定義如下：

### 定義 4.5：音群 (pitch cluster)

一個音群 (pitch cluster)  $C_i = n_{i1} n_{i2} n_{i3} \dots n_{il}$  代表一群同步的音樂物件，也就是每一個在同一音群中的音樂物件都具有相同的起始時間，其中  $l$  代表此音群中音樂物件之個數，並以  $S(C_i)$  表示音群  $C_i$  的起始時間。

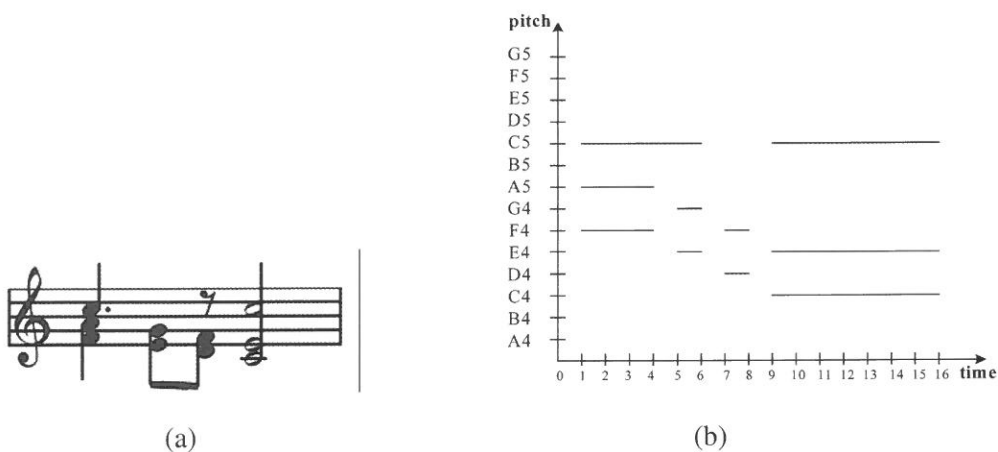
#### 定義 4.6：音群序列（sequence of pitch cluster）

我們將多音音樂以音群序列（sequence of pitch cluster）來表示： $SP = C_1 C_2 C_3 \dots C_m$ ，其中  $m$  代表此音群序列中音群之個數。若  $S(C_i) < S(C_j)$ ，則  $C_i < C_j$ ，其中  $i < j$ 。

#### 範例 4.2：

下表我們將圖九之片段音樂依照音群（pitch cluster）定義，結果如下：

$$\begin{aligned} C_1 &= \{(C5, 1, 6, 1), (A4, 1, 4, 2), (F4, 1, 4, 3)\}, \\ C_2 &= \{(G4, 5, 6, 2), (E4, 5, 6, 3)\}, \\ C_3 &= \{(F4, 7, 8, 2), (D4, 7, 8, 3)\}, \\ C_4 &= \{(C5, 9, 16, 1), (E4, 9, 16, 2), (C4, 9, 16, 3)\}, \\ S(C_1) &= 1, S(C_2) = 5, S(C_3) = 7, S(C_4) = 9. \end{aligned}$$



圖九 (a)旋律片段 (b)圖(a)以線段（segment）表示（橫軸為時間，縱軸為音高）。

音高我們採MIDI檔案的規定模式，將其量化為可計算之數值，以C5為基準採60，每增高半度增1，相對每減低半度減1。

#### 範例 4.3：

將範例 4.2 的音高量化表示如下：

$$C_1 = \{(60, 1, 6, 1), (57, 1, 4, 2), (53, 1, 4, 3)\}$$

$$C_2 = \{(55, 5, 6, 2), (52, 5, 6, 3)\}$$

$$C_3 = \{(53, 7, 8, 2), (50, 7, 8, 3)\}$$

$$C_4 = \{(60, 9, 16, 1), (52, 9, 16, 2), (48, 9, 16, 3)\}.$$

## 4.2 音樂不相似度與排序

不相似度的計算是在於比較兩段音樂或是兩首曲子之不相似度。我們考慮其絕對音高與音長，公式如下：

**定義 4.7：線段距離 (segment distance)**

若有兩個線段  $S_1 = (p_1, s_1, e_1, v_1)$  和  $S_2 = (p_2, s_2, e_2, v_2)$ ，則此兩線段距離 (segment distance) SDIST 為

$$SDIST(S_1, S_2) = \begin{cases} \sqrt{(\alpha d)^2 + (\beta(p_1 - p_2))^2} & \text{if } \text{overlape}(S_1, S_2) = 0 \\ \infty & \text{if } \text{overlape}(S_1, S_2) = 1 \end{cases}$$

其中  $\alpha$  代表時間參數， $\beta$  代表音高參數。並且

$$d = \begin{cases} e_1 - s_2, & \text{if } S_1 \prec S_2 \\ e_2 - s_1, & \text{if } S_1 \succ S_2 \end{cases}.$$

參數的設定乃是在於正規化兩個不同單位之數值，以上述公式為例，時間與音高之單位不同，所表達出之意義也相異，因此採用此參數之設計。

**定義 4.8：片斷 (fragment)**

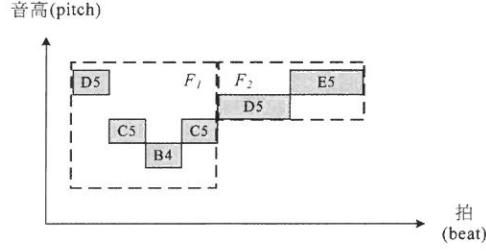
片斷 (fragment) 是一連續音符的序列，且片斷中的音符屬於同一個聲部。如圖十所示，將此旋律分為兩個片斷  $F_1$  與  $F_2$ 。

**定義 4.9 片斷距離 (fragments distance)**

任兩個片斷的距離 (FDIST) 即為前片斷之最後一個音符與後片斷之第一個音符之距離。假設有兩個片斷  $F_1 = \{n_{11}, n_{12}, \dots, n_{1k}\}$  和  $F_2 = \{n_{21}, n_{22}, \dots, n_{2k}\}$ ，如

果  $e_{n_{1k}} \leq s_{n_{21}}$ ，則  $F_1 < F_2$ ；如果  $e_{n_{21}} \leq s_{n_{11}}$ ，則  $F_1 > F_2$ 。若  $F_1 < F_2$ ，則兩片斷距離  $FDIST$  爲：

$$FDIST(F_1, F_2) = SDIST(n_{1k}, n_{21}).$$



圖十 片斷範例

**定義 4.10：**和弦與音符之不相似度（**dissimilarity between chord and note**）

假設  $C_i = n_{i1} n_{i2} n_{i3} \dots n_{ik}$  爲一和弦包含  $k$  個音符， $q$  則爲一音符。則  $C_i$  與  $q$  的不相似度爲：

$$Dsim(C_i, q) = \min_{i \leq j \leq k} \{FDIST(n_{ij}, q)\}$$

**定義 4.11：**不相似度遞迴函數（**dissimilarity recursion function**）

假設  $S = C_1 C_2 C_3 \dots C_m$  爲一多音音樂旋律片段， $Q = q_1 q_2 q_3 \dots q_k$  是一單音音樂旋律片段，則此兩者之不相似度遞迴函數（**dissimilarity function**） $D(S, Q)$  如下：

$$D(S, Q) = Dsim(C_i, q_j) + \min \begin{cases} D(C_i, q_{j-1}) \\ D(C_{i-1}, q_{j-1}) \\ D(C_{i-1}, q_j) \end{cases}$$

，其中  $1 \leq i \leq m, 1 \leq j \leq k$   $D(i, 0) = 0, D(0, j) = \infty$ 。

**定義 4.12：不相似度比對函數 (dissimilarity match function)**

根據不相似度遞迴函數的公式，我們可以得到以  $Q = q_1 q_2 q_3 \dots q_k$  單音音樂旋律片段去查詢  $S = C_1 C_2 C_3 \dots C_m$  多音音樂旋律片段之相似度比對函數 (dissimilarity match function)  $DM(S, Q)$  爲：

$$DM(S, Q) = \min_{i \leq j \leq k} D(C_m, j)$$

**定義 4.13：聲部分佈 (Voice distribution)**

假設  $S = C_1 C_2 C_3 \dots C_m$  爲一多音音樂旋律片段， $Q = q_1 q_2 q_3 \dots q_k$ ， $A = n_1 n_2 n_3 \dots n_k$  是  $Q$  一旋律序列之聲部值數列。則其聲部分佈 (voice distribution)  $VD(A)$  爲：

$$VD(S, Q) = \frac{\sum W(v_{ni}) \times N(v_{ni})^2}{k^2}$$

，其中  $W(v_{ni})$  代表  $v_i$  在  $A$  中所佔之比例， $N(v_{ni})$  代表此聲部值數列中連續爲  $v_i$  值個數。

**範例 4.14：**

若  $(57, 0, 3, 1)$   $(55, 4, 5, 1)$   $(53, 6, 7, 2)$   $(52, 8, 15, 1)$  爲一查詢後之結果，則其聲部分佈

$$VD(S, Q) = \frac{\frac{4}{3} \times 2^2 + \frac{1}{4} \times 1^2 + \frac{3}{4} \times 1^2}{4^2} = \frac{1}{4} = 0.25.$$

**定義 4.15：排序函數 (Ranking function)**

假設  $A$  爲從多音音樂中所查詢出相似於單音音樂  $Q$  之單音音樂序列。則  $A$  之排序函數 (ranking function) 爲：

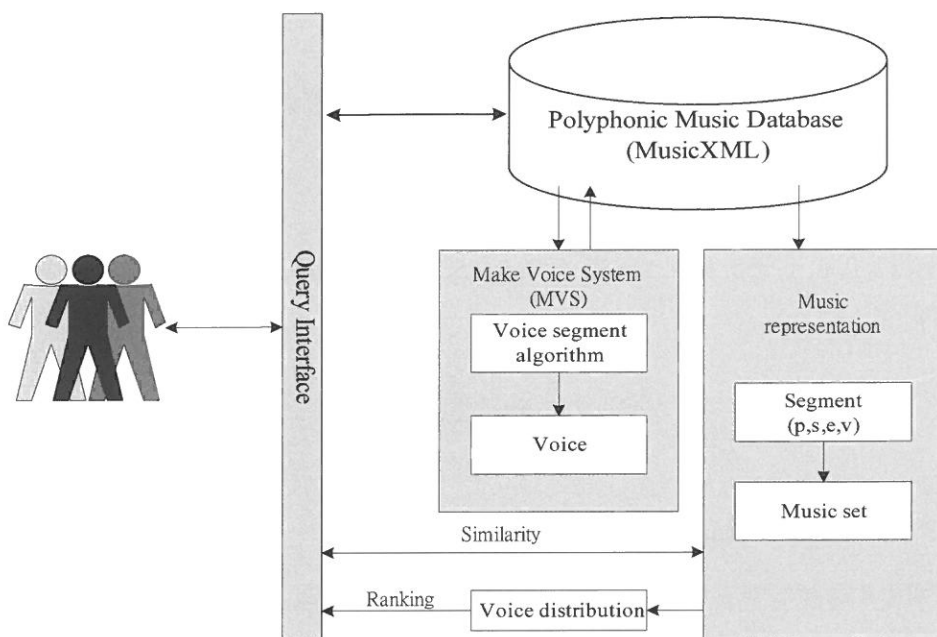
$$R(A) = \gamma DM(A, Q) + \delta \frac{1}{VD(A)}.$$

，其中  $\gamma$  和  $\delta$  爲  $D(A, Q)$  和  $VD(A)$  倒數之參數，並且  $\gamma + \delta = 1$ 。若排序函數計算出之值越小，代表其排序之優先順序越前面。

## 5. 系統架構與演算法

### 5.1 系統架構

系統架構（圖十一）主要分為兩個的部份，第一部分是將以 MusicXML 格式儲存之多音音樂資料庫中的音樂，計算出其聲部（voice）值，亦即判斷音樂物件位於哪個聲部當中。第二部份是與使用者查詢比對，計算其相似度值，並將結果排序回傳給使用者。排序越前面的代表與查詢的相似度越高。計算相似度時，不僅是比對旋律之絕對位置，並考慮其聲部的分佈情形，因此相似度高者不僅是旋律之絕對位置較接近，其聲部分佈也較為集中。

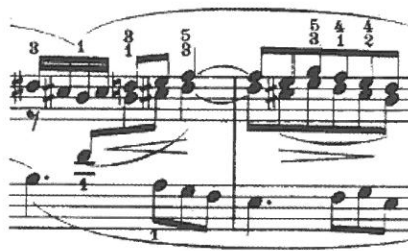


圖十一 系統架構圖

## 5.2 聲部切割演算法 (voice segment algorithm)

根據音樂的結構特性，我們能夠計算多音音樂中每個音符的聲部 (voice) 值，其計算的基準除了 MusicXML 所紀錄的特殊標籤，還有音樂結構的變化，以及其相對的距離。因此在本節中我們綜合上述各觀點，完成聲部 (voice) 的切割演算法。

以圖十二巴哈三聲部創意曲第七首之第三、四小節為例，我們將之前線段的表示法換為方塊圖 (圖十三) 表示，每個方塊即代表一音符。起始的最高前四個音符 D5、C5、B5、C5 以連音符號連結，因此此四音符即為一片斷 (fragment)，如圖十三虛線方框所示。相同的，若音符間以圓滑線或連結線連接，也將其視為同一片斷 (fragment)。因此我們能夠將其劃分出九個片斷 (fragment)。



圖十二 巴哈三聲部創意曲第七首之第三、四小節

### 範例 5.1

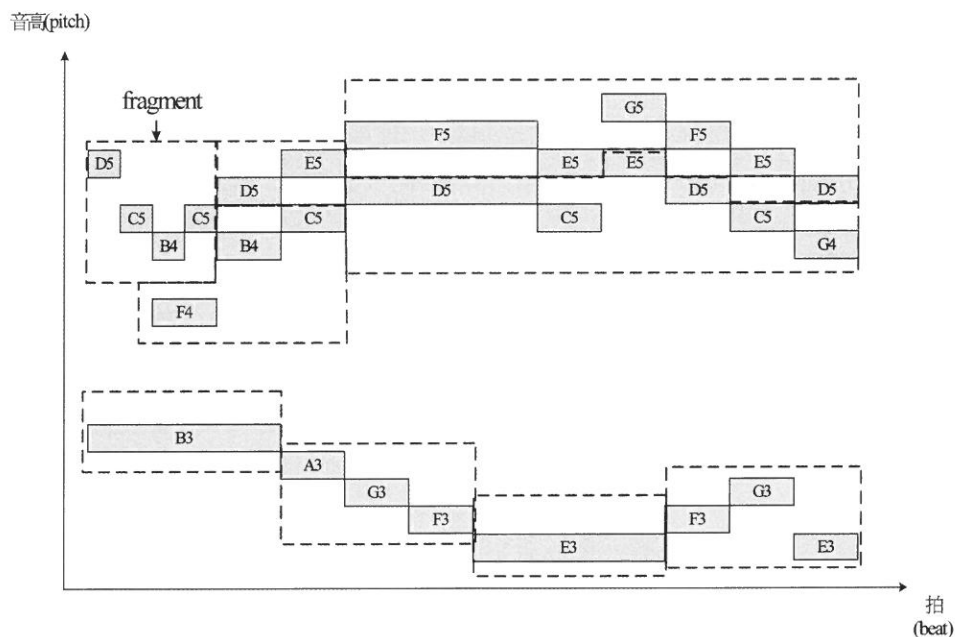
以下圖十四為例，計算此二片斷距離 (fragments distance)：

$$FDIST(F_1, F_2) = SDIST(C_5, C_5) = \sqrt{(\alpha(62 - 60))^2 + (\beta(5 - 5))^2}$$

設  $\alpha = \beta = 0.5$ ，則  $FDIST(F_1, F_2) = \sqrt{2} \approx 1.414$

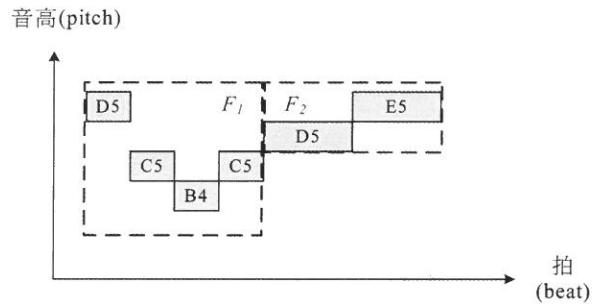
### 定義 5.2 [contig]

contig 是一個重疊片斷的集合，並且在任何時間點，重疊片段的深度 (即重疊片斷個數) 為定值。

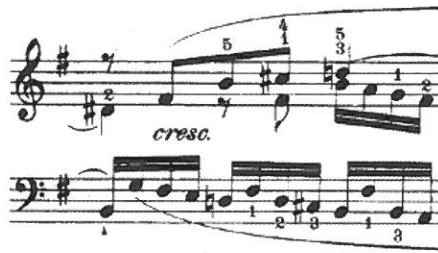


圖十三 片斷 (fragment) — 巴哈三聲部創意曲第七首之第三、四小節

圖十五為巴哈三聲部創意曲第七首的第十六小節，我們依照上面的定義將這一小節分割如圖十六。contig 的切割是依照音符 (note) 或者片斷 (fragment) 的個數有所變化，以及當前後聲部 (voice) 的地位不同時。所謂的聲部 (voice) 的地位不同乃是指前後兩個 contig 具有相同的聲部 (voice) 個數，但是 contig 內的音符 (note) 或者片斷 (fragment) 位於不同的聲部 (voice) 中，這樣的情況時常發生於某一個不同。圖十六例子中，(b)圖之 a、b、c 線段的切割是由於前後聲部 (voice) 個數有所改變。a 線段中之 D4# 為依連續之音符，因此可以判斷 a 線段前之 D4# 為第二聲部。線段 b、c 間之 B4 由於與前後之 F4、C5# 在同一片斷 (fragment) 中，因此可判斷位於同一聲部，如圖十六(c)。



圖十四 片斷距離 (fragments distance) 計算範例



圖十五 巴哈三聲部創意曲第七首的第十六小節

若無法依據上述性質判斷聲部 (voice) 的分佈，則採用定義 4.9 所述之片斷 (fragment) 距離計算公式，距離越近之片斷 (fragment) 則位於同一聲部 (voice) 中。下述兩演算法即為聲部 (voice) 分割之演算法：

#### 演算法 5.1 [contig 切割]

輸入：MusicXML 文件

輸出：contig

{

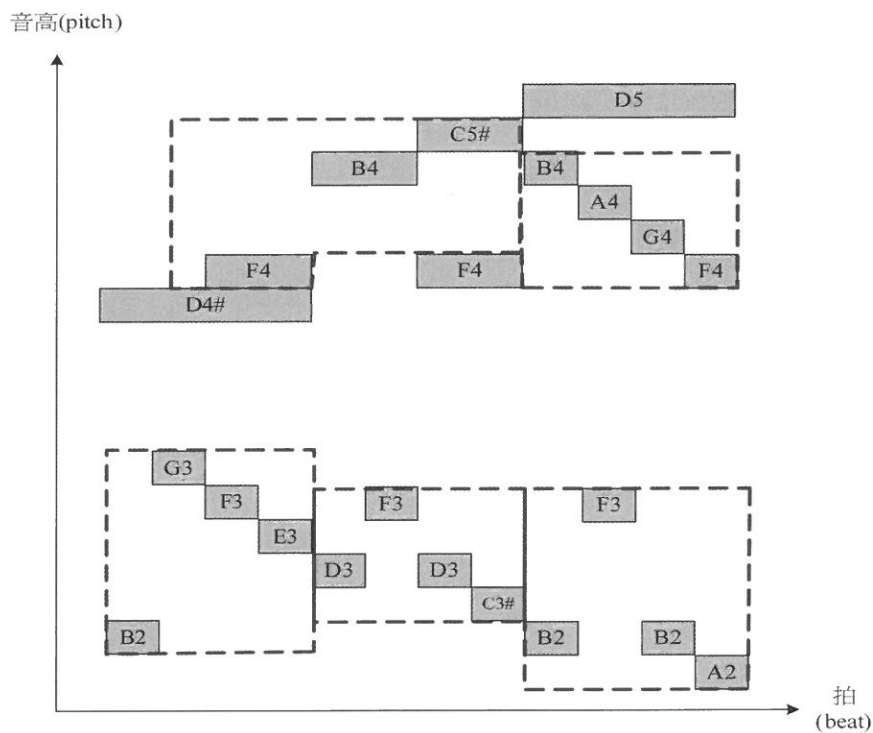
將音樂物件中之音符表示為  $m_1, m_2, m_3, \dots, m_i$

若  $v_t$  代表一時間片段邊界  $t$  時間點之聲部個數，

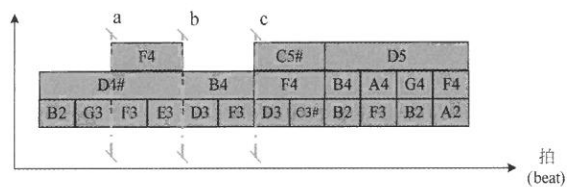
若發生以下之一情況，則  $t - 1$  至  $t$  即為一片斷範圍：

- $v_t \neq v_{t-1}$ ；
- 或  $v_t = v_{t-1}$  但聲部的狀態發生改變

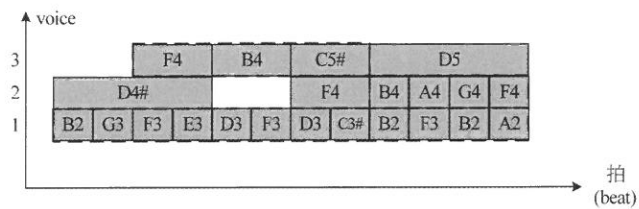
}



(a)fragment



(b)contig



(c)contig consider the fragment

圖十六 座標表示巴哈三聲部創意曲第七首的第十六小節

## 演算法 5.2 [連結]

輸入：兩個相鄰的 contigs, X 和 Y

輸出：聲部

{

    假設  $q_X$  為 contig X 中最後一個音符， $p_Y$  為另一 contig Y 中第一個音符

$c(q_X, p_Y)$  代表相鄰之  $q_X$  至  $p_Y$  的距離，其計算規則如下：

- 若兩音符代表一相同更長音符之切割，則  $c(q_X, p_Y) = k$ ;
- 若兩者之一或兩者皆為無效， $c(q_X, p_Y) = -k$ ;
- 若兩者為相異之兩音符，則  $c(q_X, p_Y)$  遵循下列絕對優先規則

    絕對優先規則：

        若兩音符由 <backup> tag 連接，則下一個音符位於相異之聲部中

        若兩音符由 <tied type>, <beam>, <slur> tag 連接，則兩者位於相同聲部

        若兩音符由 <chord> tag 連接，則所連接之音符必位於不同聲部

}

## 5.3 音樂不相似度

範例 5.2：

以圖十七(a)之多音音樂為例，計算與單音音樂(57,0,3,1) (55,4,5,1) (53,6,7,1) (52,8,15,1)之不相似度。圖十七(b)將圖十七一(a)分為四個音群。圖十七(c)根據定義 4.11 之不相似度函數計算兩者之不相似度。實線箭頭表示其計算之途徑，虛線箭頭代表計算完畢後回尋最短路徑，也就是回尋最小值。因此計算之值越小代表其不相似度越小，也就是相似度越大。

計算出不相似度之後，我們將所查詢的結果進行排序，排序的準則除了相似度較近之外，還必須考慮所在聲部的位置，若在同一個聲部的比例越大且越連續，那麼其排序越前面。



(a)

$$\begin{aligned}
 C_1 &= \{(60,1,6,1), (57,1,4,2), (53,1,4,3)\} \\
 C_2 &= \{(55,5,6,2), (52,5,6,3)\} \\
 C_3 &= \{(53,7,8,2), (50,7,8,3)\} \\
 C_4 &= \{(60,9,16,1), (52,9,16,2), (48,9,16,3)\}.
 \end{aligned}$$

(b)

$C_4$	17	11	7	0
$C_3$	10	2	0	7
$C_2$	4	0	1	7
$C_1$	0	4	6	11
	(57,0,3,1)	(55,4,5,1)	(53,6,7,1)	(52,8,15,1)

(c)

圖十七 DTW 計算範例，(a)旋律段落 (b) 音群 (pitch cluster) (c)DTW 計算

## 6. 系統實作

本章節描述我們實作的部份。所用電腦配備是 Intel CPU，Pentium 4，3.0GHz，作業系統為 Windows XP sp2，撰寫使用軟體是 Borland C++ Builder 6.0，音樂資料的格式為 MusicXML document。系統主要分為兩個部份：聲部值計算系統與查詢排序系統。前者於 6.1 節介紹，後者於 6.2 節中介紹。

## 6.1 聲部值計算系統（Make Voice System，MVS）

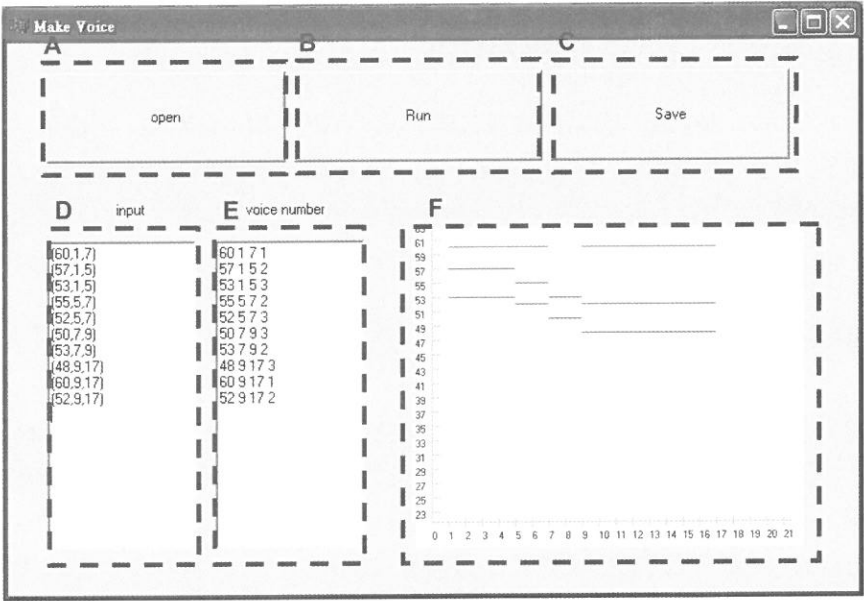
如圖十八所示，A 按鈕可以手動方式開啓資料庫中 MusicXML 之檔案，擷取所需之資訊，並於 D 視窗中顯示。B 按鈕執行聲部值計算，並將結果顯示於 E 視窗中，並且 F 視窗將會將結果以座標圖表示，以便使用者解讀。執行完畢後，C 按鈕能夠將結果加以儲存，建立與原始 MusicXML 相對應的文字檔，以利往後計算相似度時之使用。

## 6.2 查詢與排序系統（Query and Ranking System，QRS）

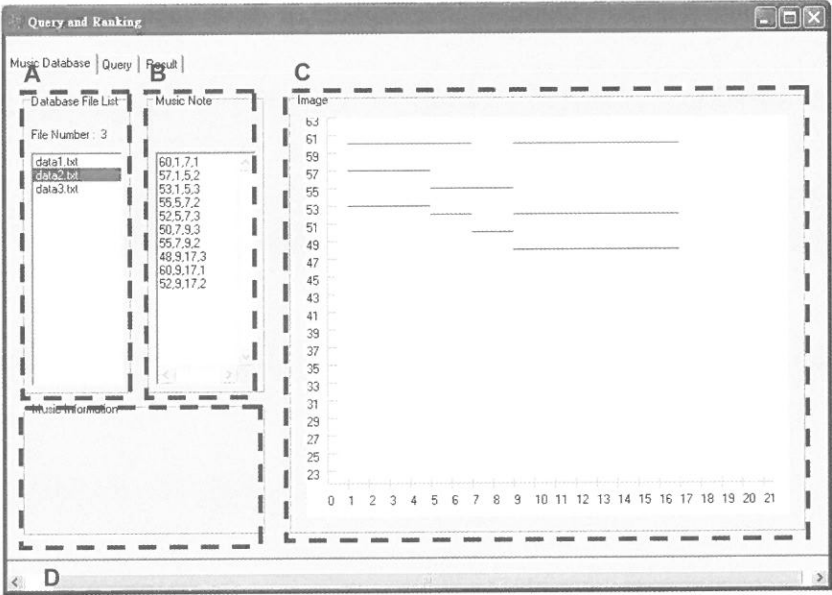
查詢與排序系統分爲三個子介面，第一個爲音樂資料庫（Music Database）介面，如圖十九。視窗 A 會展現音樂資料庫中，所有的音樂資料，使用者可隨意點選欲觀看之音樂檔案，視窗 B 會展現所選擇檔案之音符資訊，包含音高、起始時間、終止時間與聲部值。視窗 C 將其以座標圖表示。視窗 C 則會顯現出此首音樂之相關資訊，如作者、曲名等。

第二個部份爲查詢介面，如圖二十。A 部分提供使用者輸入查詢，可直接開啓以建立之文字檔，或者也可直接於視窗中輸入。若選擇直接開啓文字檔，則開啓檔案資訊會顯示於 A 部份下面的視窗中，使用者可依需求直接於視窗中修改。B 部分則以座標圖顯示查詢資訊。

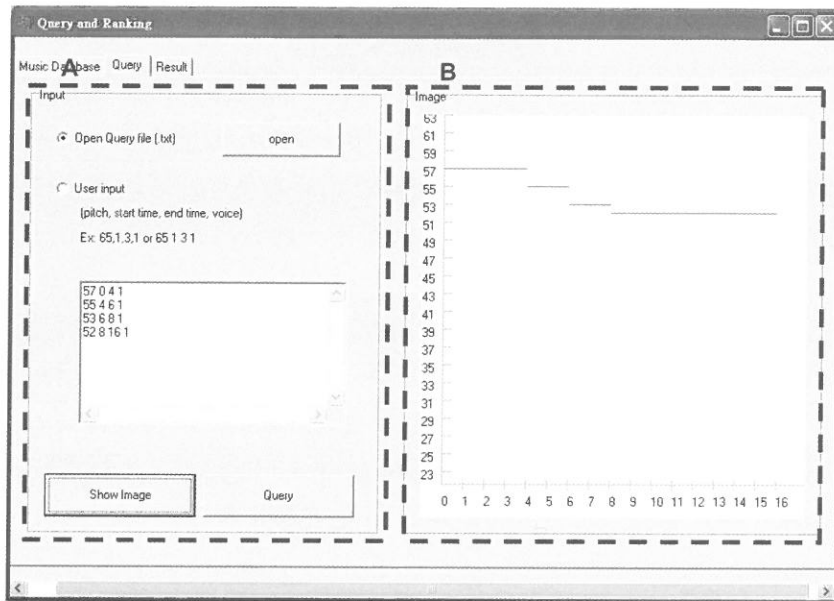
第三部份爲結果展示之排序介面，如圖二十一。A 部分展示依照相似度之大小排序之結果，排序越前面代表越相似。B 部分爲其相似度值。C 部分爲其回溯路徑。D 部分爲查詢之結果資訊。E 部分將結果以座標圖表示，並將查詢結果以紅色之線段標示。使用者可隨意點選 A 部份之各音樂檔案，其相關資訊均會展現於其他視窗中。



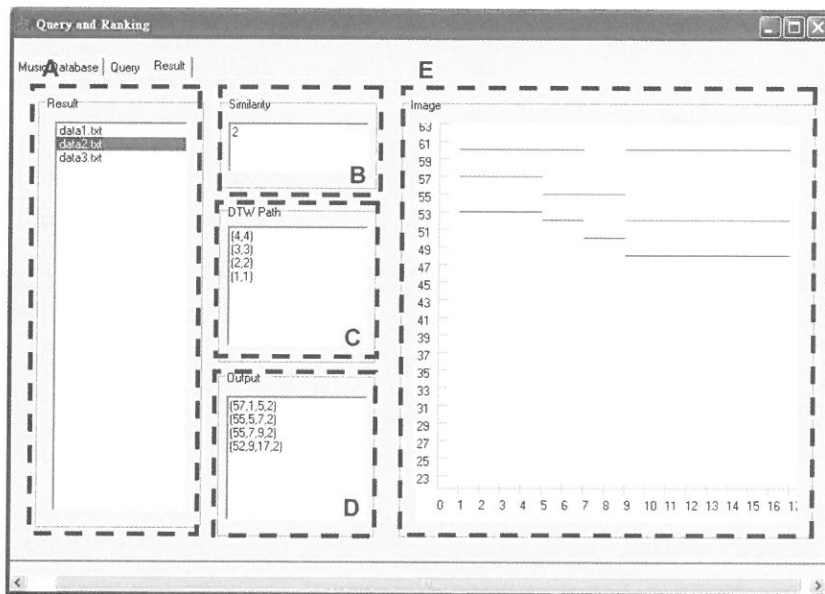
圖十八 聲部值計算系統系統介面圖



圖十九 查詢與排序系統（QRS）－音樂資料庫介面



圖二十 查詢與排序系統 (QRS) – 查詢介面



圖二十一 查詢與排序系統 (QRS) – 排序介面

## 7. 結論與未來工作

本篇論文針對多音音樂資料庫，提供單音音樂旋律的相似度查詢。首先計算音樂物件的聲部，當使用者下單音旋律的查詢，系統與多音音樂資料庫做比對，搜尋出相似的結果，並依照其相似度與音樂結構的符合性做排序，此查詢結果將更加符合音樂的結構。

在未來工作上面，期使能夠更進一步的分析本篇之效能與結果，並與其他方法相互比較。關於相似度的計算上，本篇論文是以 DTW 之演算法來計算，期能夠增進演算法之效能。在聲部值的計算上，我們主要是考慮樂譜的音樂結構特徵與音高，希望能更進一步考慮古典音樂在作曲上之技巧，增加聲部值計算上的準確性。系統實作方面計劃能夠提供線上系統，使用者能夠透過網路直接查詢音樂資料庫。

## 參考文獻

- [Chew04] E. Chew and X. Wu, "Separating voices in polyphonic music : A contig mapping approach," in *Proceedings of Computer Music Modeling and Retrieval : Second International Symposium*, pages 1-20, 2004.
- [Clau00] M. Clausen, R. Engelbrecht, D. Meyer and J. Schmitz, "Proms : A Web-Based Tool for Searching in Polyphonic Music," in *Proceedings of International Symposium on Music Information Retrieval (ISMIR)*, 2000.
- [Clau04] M. Clausen and F. Kurth, "A Unified Approach to Content-Based and Fault-Tolerant Music Recognition," *IEEE Transactions on Multimedia*, Vol. 6, No.5, October 2004.
- [Dora01] S. Doraisamy and S. M. Ruger, "An Approach toward a Polyphonic Music Retrieval System," in *Proceedings of International Symposium on Music Information Retrieval (ISMIR)*, 2001.
- [Dora04] S. Doraisamy and S. Ruger, "A Polyphonic Music Retrieval System Using N-Grams," in *Proceedings of International Symposium on Music Information Retrieval (ISMIR)*, 2004

- [Dora04] S. oraisamy and S.M. Ruger, "A Polyphonic Music Retrieval System Using N-Grams," in *Proceedings of International Symposium on Music Information Retrieval (ISMIR)*, 2004.
- [Dove01] M. J. Dovey, "A technique for "regular expression" style searching in polyphonic music," in *Proceedings of International Symposium on Music Information Retrieval (ISMIR)*, 2001.
- [Dove01] M. J. Dovey, "A technique for "Regular Expression" Style Searching in Polyphonic Music," in *Proceedings of International Symposium on Music Information Retrieval (ISMIR)*, 2001.
- [Down00] S. Downie and M. Nelson, "Evaluation of A Simple and Effective Music Information Retrieval Method," in *Proceedings of ACM Special Interest Group on Information Retrieval (SIGIR)*, 2000.
- [Kili02] J. Kilian and H. H. Hoos, "Voice separation—a local optimisation approach," in *Proceedings of the Third Annual International Symposium on Music Information Retrieval (ISMIR)*, 2002.
- [Kirl05] P. B. Kirlin and P. E. Utgoff, "Voise : Learning to Segregate Voices in Explicit and Implicit Polyphony," in *Proceedings of International Symposium on Music Information Retrieval (ISMIR)*, 2005.
- [Korn98] A. Kornstadt, "Themefinder : A Web-Based Melodic Search Tool," *Computing in Musicology*, MIT Press, 1998.
- [Lems00] K. Lemstrom and J. Tarhio, "Searching monophonic patterns within polyphonic sources," in *Proceedings of Content-Based Multimedia Information Access (RIAO)*, 2000.
- [Lems00] K. Lemström and S. Perttu, "SEMEX—An Efficient Music Retrieval Prototype," in *Proceedings of International Symposium on Music Information Retrieval (ISMIR)*, 2000.
- [Liu03] N. H. Liu, Y. H. Wu and A.L.P. Chen, "Efficient K-NN Search in Polyphonic Music Databases Using a Lower Bounding Mechanism," in *Proceedings of ACM MM'03 Workshop on Multimedia Information Retrieval (MIR)*, 2003.
- [MacN97] R. J. MacNab, L. A. Smith, D. Bainbridge and I. H. Witten, "The New Zealand Digital Library MELodyinDEX," *Digital Library Magazine*, May 1997.

- [McCr76] E. M. McCreight, "A Space-Economical Suffix Tree Construction Algorithm," *Journal of the ACM*, 23(2) : 262-272, 1976.
- [Pard05] B. Pardo and M. Sanghi, "Polyphonic Musical Sequence Alignment For Database Search," in *Proceedings of International Symposium on Music Information Retrieval (ISMIR)*, 2005.
- [Park00] S. Park, W. W. Chu, J. Yoon and C. Hsu, "Efficient Searches for Similar Subsequences of Different Lengths in Sequence Databases," in *Proceedings of the International Conference on Data Engineering (ICDE)*, 2000.
- [Pick01] J. Pickens, "A Survey of Feature Selection Techniques for Music Information Retrieval," in *Proceedings of International Symposium on Music Information Retrieval (ISMIR)*, 2001.
- [Pick02] J. Pickens and T. Crawford, "Harmonic Models for Polyphonic Music Retrieval," in *Proceedings of ACM International Conference on Information and Knowledge Management (CIKM)*, 2002.
- [Szet03] W. M. Szeto and M. H. Wong, "A Stream Segregation Music Databases," in *Proceedings of International Database Engineering and Applications Symposium (IDEAS)*, 2003.
- [Uitd02] A.L. Uitdenboger and J. Zobel, "Music Ranking Techniques Evaluated," in *Proceedings of the Australasian Computer Science Conference (ACSC)*, 2002.
- [Uitd98] A. L. Uitdenboger and J. Zobel, "Manipulation of Music for Melody Matching," in *Proceedings of ACM International Multimedia Conference*, 1998.
- [Uitd99] A.L. Uitdenboger and J. Zobel, "Melodic Matching Techniques for Large Music Databases," in *Proceedings of ACM International Multimedia Conference*, 1999.
- [Wu92] S. Wu and U. Manber, "Fast Text Searching Allowing Errors," *Communications of the ACM*, 35(10) : 83-91, October 1992.
- [王 99] 王沛綸, 《音樂字典》, 台北: 大陸書局, 1999。
- [劉 06] 劉岷渭、江玉玲《音樂圖驥》, 台北: 小雅出版, 2006。

*Received October 31, 2007*

*Revised December 17, 2007*

*Accepted December 24, 2007*

# Pattern Matching and Ranking with Voice Structure in Polyphonic Music Databases<sup>3</sup>

Hsin-Hua Yuan and Jia-Lien Hsu<sup>4</sup>

*Department of Computer Science and Information Engineering  
Fu Jen Catholic University  
Taipei, Taiwan 242, R.O.C.*

## Abstract

Researches in the field of content-based music information retrieval have been continued on handling polyphonic music data, rather than monophonic data. To represent melodies of polyphonic music objects, melody, *i.e.*, pitch and/or duration of notes, are considered as one of most important features. When resolving a user query, those music objects, in the database, which *matches* features of the query, will be considered as candidates and reported as query results. Therefore, various query processing algorithms and similarity functions are proposed. However, concepts of musicology, especially the voice, are rarely considered when designing those methods. According to musicology, a polyphonic music object consists of one or more monophonic melodies. With respect to a monophonic query, the similarity of candidate which belongs to various and separate voices will not be equal to the similarity of candidate which belongs to a single voice. In this paper, we develop an approach to search polyphonic music database with respect to monophonic queries. We design a voice segmen-

---

<sup>3</sup> This research was supported by Fu Jen Catholic University, Project no. 409531040123.

<sup>4</sup> Corresponding author. E-mail : alien@csie.fju.edu.tw

tation algorithm to determine voices of polyphonic music objects. By applying the techniques of local alignment, those candidates will be identified and ranked according to our similarity function. We also implement a prototype to demonstrate our approach.

**Keyword :** polyphonic music information retrieval, voice segment algorithm, music dissimilarity, music ranking

# Scalable and Efficient Interconnection of DHT-Based Peer-to-Peer Systems<sup>1</sup>

Chun-Hsien Lu and Cheng-Fu Kuo

*Dept. of Computer Science and Information Engineering  
Fu Jen Catholic University*

## ABSTRACT

Today peer-to-peer networks have been wildly used due to the massive popularity of the Internet, and many types of peer-to-peer networks have been created. Most of the research work had focused on enhancing the performance and improving the shortcomings of a single system, without paying much attention on resource sharing across different systems. Users in different systems have difficulty in accessing the resources from each other. In this paper, we design an interconnection architecture based on extended distributed hash tables (DHTs) to allow different peer-to-peer systems to link to each other. We also propose an efficient search process that allows fast search across systems. The simulation results show that search hit rate can be increased from 58% to 99% when isolated systems are interconnected to form an extend system. The cost of the interconnection approach is lower than that of merging all the systems directly into a large one.

**Keywords:** Peer-to-peer systems, Distributed hash table, Interconnection of systems.

---

<sup>1</sup> 本篇論文感謝輔仁大學研發處研究計畫 409531040420 之補助。

\* jonlu@csie.fju.edu.tw

## 1. Introduction

Due to the massive popularity and improvement of the Internet, peer-to-peer (P2P) networks have become an important application for information sharing. On P2P networks, resources are distributed on numerous peers instead of being provided on a limited number of servers. A peer can access the resources by directly contacting other peers. Due to the distributed properties of P2P networks, users could search and exchange large amount of information rapidly. There have been three models of P2P system architecture: centralized, decentralized unstructured, and decentralized structured. The centralized model contains an index server which collects the contents lists from all the peers to create a search index. A well-known example built on the centralized model is Napster [1]. This model suffers from the problems of poor scalability and single point of failure at the index server. In the decentralized unstructured model, peers in the system connect to each other in a random manner and a peer searches for a content by flooding the query to all the other peers. Both Gnutella [2] and Freenet [3] belong to this model. However, the flooding of messages in this model consumes a significant amount of bandwidth. The decentralized structured model uses distributed hash tables (DHTs) to manage and record the index information. Every peer first hashes each of its contents to a corresponding key value, and then registers the index information to the index peer responsible for holding the index information for that key value. When a peer wants to search for a specific content, it first computes its key value using the same hash function, then consults the corresponding index peer to find the content. Chord [4], Pastry [5], Tapestry [6], CAN [7], Koorde [8], and Viceroy [9] are all examples of P2P networks of the decentralized structured model. The main advantages of this model are good load balancing and efficient content searching. With a careful design of the interconnection between the peers, the search complexity could be limited to  $O(\log N)$  hops where  $N$  is the number of peers in the system.

Since there exist different types of structured peer-to-peer systems, a peer must join all those systems one by one before it can access the resources on all the systems. If two peers in different systems have established a connection via a separate means, neither of them would be able to communicate with the remaining peers in each other's system. In a decentralized structured system, peers are interconnected to each other following specific rules, which are differ-

ent from system to system. When many different systems are operating at the same time, having to ask a peer to join all of them results in unnecessary resource consumption. Therefore, it has become an important task to develop a mechanism to interconnect different P2P systems such that content search across the systems can be done in an efficient and scalable manner. In this work, we focus on the interconnection of the decentralized structured systems. We assume that all the systems use the same hash function such that a single key value always matches to a specific content. Our goal is to interconnect multiple systems together with good scalability and efficiency.

The rest of this paper is organized as follows: Section two presents the related work. In section three, we describe how to interconnect the decentralized structured systems to facilitate content search across systems. Section four displays the simulation results, and section five gives the conclusion.

## 2. Related Work

Several approaches have been proposed to address this issue in the past. Canon in G Major [10] proposed the concept of linking DHT-based P2P systems by constructing a hierarchical structure. Peers in the same domain would form a DHT-based P2P system and every system in the hierarchical structure has its own domain information. The P2P systems search each other by the domain information, which is similar to locating a computer by its domain name. A system searches another system by expanding the search domain to include the target system. However, it may not be easy to obtain the domain information of each peer. Even in the case where domain information is readily available, the total number of levels of the hierarchical structure could grow to a large value and the cost of constructing this kind of domain-based hierarchical structure between P2P systems could be very high. Jelly [11] proposed to link P2P systems into a two-level hierarchical structure. The bottom level consists of the usual DHT-based P2P systems, where a designated super peer in each system maintains the content index of the system. The top level is constructed by those super peers forming another P2P system. A peer in the bottom level performs search by sending the query to its super peer, which then conducts a search at the top level. The super peer that is in charge of the requested content would transmit the content to the initiating peer. Since each of the contents must be registered at both

levels, the cost of a system joining or leaving could be very large. Furthermore, the loading at super peers can be quite heavy. Cyclone [12] used the peer identifiers to cluster the peers into various levels of systems. The scheme divides the peer identifier into two parts: prefix and suffix bits. The suffix part serves as the cluster identifier for those peers that have the same suffix bits, while the prefix part is the identifier of each peer in the cluster. Cyclone clusters peers into a hierarchical structure based on the suffix and each cluster forms a DHT-based P2P system. When searching for a document, a peer searches its cluster first. If it can not find the document, it would remove the leftmost bit from its suffix and search the expanded cluster again. The process continues to expand the suffix until the document is found or the whole system has been searched. This interconnection scheme lacks flexibility because the identities of the P2P systems at each level are fixed and cannot be modified.

### 3. Extended DHT-based P2P Systems

#### 3.1 Architecture Overview

Each DHT system has an ID, which is created by the first peer of the system using the following function:  $\text{DHT ID} = \text{Hash}(\text{IP address of first peer} + \text{current time at first peer})$ . After the DHT ID has been generated, other peers who join this system later will share this DHT ID. There are two tables used for storing routing information in our systems: the interconnection table and the DHT table. A DHT-based P2P system can communicate with the other systems by using these tables. The purpose of the interconnection table is for peers to reach the other systems. The first peer (called *registrar peer*) of each system is designated to be responsible for maintaining the interconnection table, whose format is shown in Table 1. It contains the DHT ID, the level of the system, and the IDs of the two peers at the endpoints of the link between two systems. A peer can contact a different system by first looking up the link information to that system in the interconnection table. It then sends a request to the local peer, which will be forwarded to the remote peer in the target system. In other words, the interconnection table plays the role of providing gateway information.

Every peer maintains a DHT table that records the list of the systems it can forward a query

to. The DHT table consists of the DHT ID, the level of the system, priority, and the shortcut to that system. Table 2 shows its format. The priority of each system is initialized to 50 and can vary from 0 to 100 according to the success or failure of the query replies. A higher priority value means that the system offered a higher query hit rate in the past. A peer always forwards a query to the system with the highest priority first. When a reply message from a remote peer in a different system arrives, a peer can store the remote peer ID as a shortcut to that system.

**Table 1. Interconnection Table.**

DHT ID	Level	Link	
		Local Peer	Remote Peer

**Table 2. DHT Table.**

DHT ID	Level	Priority	Shortcuts

### 3.2 Hierarchical Model

Figure 1 shows the hierarchical model of our architecture, where each ring in the figure represents a DHT-based P2P system marked with its DHT ID and Level. The dash lines represent logical links between the systems. There could be multiple systems at each level. The level of a system is determined based on the number of peers in that system because a larger system usually contains more contents leading to a higher query hit probability. A system with more peers will be assigned to a higher level. A system is said to belong to level  $K$  if the number of peers it has is between  $P^{K-1}$  and  $P^K$ , where  $P$  is a parameter for controlling the number of levels. To estimate the number of peers in its own system, a peer periodically sends a simple probe query to a random destination in its system. The probe contains a hop counter initialized to 0,

and each intermediate peer increments it by one. When the destination receives the probe message, it returns it back to the sender. Since a query usually travels at most  $\log N$  hops in a DHT-based system with  $N$  peers, a peer can estimate the number of peers in its system by the number of hops recorded in the probe reply message. Once the estimate is obtained, a peer can then determine the level of its system belongs to. The level of a system can change as its number of peers varies. In our model, we assume that a system will try to connect to as many other systems at the same level as possible. Each system will also connect to at least one system one level higher and lower each.

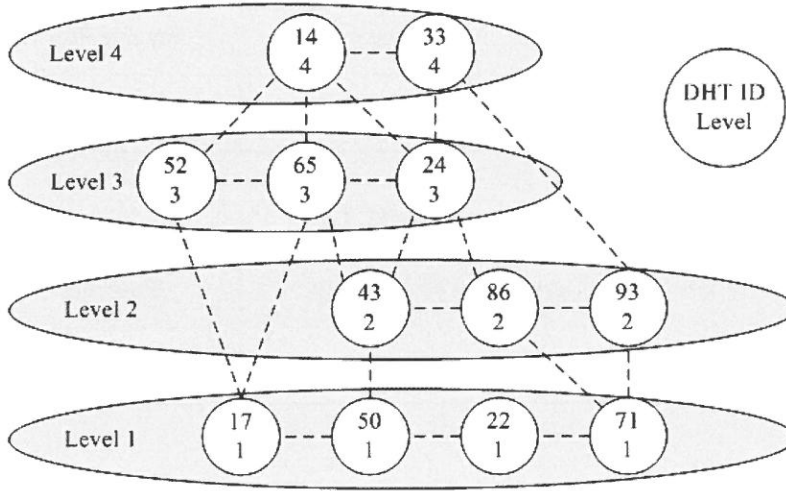


Figure 1. Hierarchical DHTs.

### 3.3 Registration

A system needs a way to find the existence of the other systems as well as the paths to them. If a peer  $P_1$  in system  $S_1$  has a connection with peer  $P_2$  in system  $S_2$ ,  $P_1$  then sends this link information to the registrar peer  $RP_1$  in  $S_1$  to be recorded in its interconnection table. The information shows the existence of a link from  $S_1$  to  $S_2$  by going from  $P_1$  to  $P_2$ . The same registration process also takes place at  $RP_2$  in  $S_2$ . After that,  $P_1$  and  $P_2$  would exchange their DHT

tables to acquire information about more systems. Figure 2 shows an example of the registration process: Suppose peer 28 in system 9 establishes connection with peer 12 in system 47. Peer 28 registers the link to registrar peer 49, which then records the DHT ID, the level, and the link between peer 28 in system 9 and peer 12 in system 47 as the local peer and remote peer into its interconnection table. Any peer in system 9 who tries to forward queries to system 47 would first consult peer 49 and then forward queries via the link. After the registrar peer records the link information in its interconnection table, it then broadcasts an announcement to all the other peers in its system. Upon receiving the announcement each peer updates its DHT table by adding an entry for the new connected DHT ID and its level. As Figure 2 shows, peer 49 announces the existence of system 47 to all the other peers in system 9, and each peer would add an entry for system 47 in its DHT table. Shortcuts will be filled in if a successful query reply is later returned from system 47. Through the broadcast from the registrar peer, peers learn about more DHTs to search in the future.

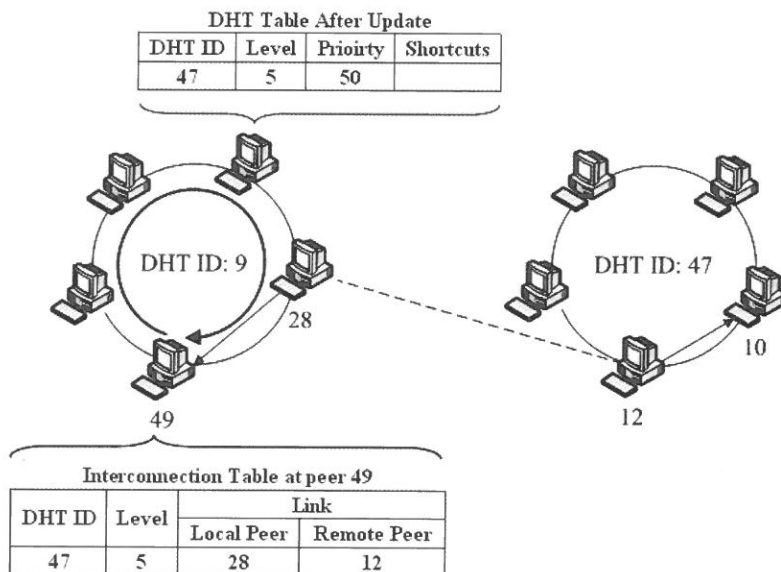


Figure 2. Registration of a link at the registrar.

Two peers in different systems will exchange their DHT tables when they establish a con-

nection. From this, peers can find out about systems that are not currently in its DHT table. Suppose a peer  $P_1$  in system A at level  $L_A$  exchanges its DHT table with another peer  $P_2$  in system B. Let  $(C, L_C, X, S_C)$  denote an entry in the DHT table that  $P_1$  receives from  $P_2$ . For  $P_1$  to process this entry, four cases may occur: (i)  $L_C = L_A$ .  $P_1$  will notify the  $RP$  in system A to connect to  $S_C$  in order to connect to more systems at the same level. (ii)  $|L_C - L_A| = 1$ . In this case,  $P_1$  adds the entry to its DHT table unless there are already too many such type of entries. (iii)  $|L_C - L_A| > 1$ . To reduce maintenance cost of the interconnection, the peer discards the entry except when system C is closer (in terms of number of levels) to A than any other system listed in  $P_1$ 's DHT table. In this case  $P_1$  retains the entry. (iv)  $P_1$  will connect to C if  $L_C$  equals the highest level. Figure 3 illustrates this process. A registrar peer maintains the correctness of the interconnection table by testing each link periodically. It sends a keepalive request to the remote peer of each link in its interconnection table and waits for the reply. If the reply fails to arrive, the corresponding link will be removed from the table. If the links to the same system all fail, that system is removed from its interconnection table. The registrar peer will also send a copy of its interconnection table to its successor peer periodically for fault tolerance.

### 3.4 Search Process

The search process consists of two phases: search in the local system and search in the remote systems. When a peer requests for a content, it would search the local system first by forwarding the query to the index peer who holds the index information for the requested content. Since there can be different types of DHT design, the forwarding path could be varying from one system to another. For example, peers in Chord use the finger table, while peers in Pastry use the NodeId table to speed up routing queries to the index peer. However, even under different searching approaches, the maximum number of hops required is still limited to  $\log N$ . In our approach, the index peer would not reply immediately if the queried content does not exist in its index list. It would try to search the remote systems instead. If searching the remote systems fails also, the index peer then replies a query miss message to the initiator of the query. Next we explain how searching of the remote systems can be done. The index peer chooses a system from its DHT table with the highest level and priority attributes and forwards the query to that remote system. When a peer of the remote system receives the query, it does a local search first.

If the search fails, it then search the other systems at the same level one by one in the order of decreasing priority values until there is a query hit. If none of the systems at the same level has the content, the query is forwarded to a system one level lower and the search process repeats from there. That is, the search is done level by level from top to bottom and stops as soon as there is a query hit. Figure 4 shows the pseudo code for the search algorithm.

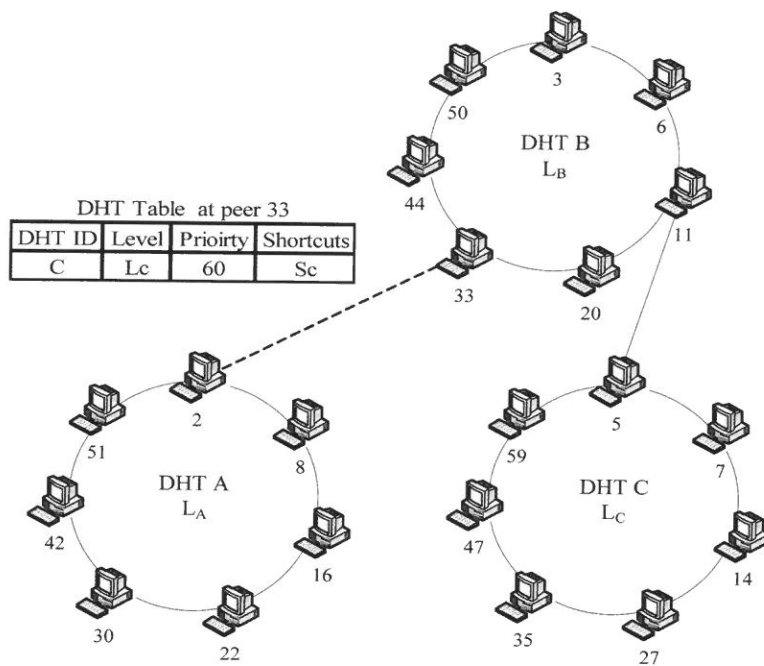


Figure 3. Example of exchanging DHT tables.

**Search algorithm (query  $q$ )**

*/\* Assume that peer  $p$  in system  $R$  receives a query  $q$  from system  $S^*$  \*/*

**If**  $S$  and  $R$  are at the same level **then** {

    Search system  $R$

**If** query hit **then**

        Reply query hit to initiator through reverse path

**}** **else** */\*  $S$  is higher than  $R$  \*/*

**While** (query miss **and** there are still same-level systems in  $p$ 's DHT table that have not been searched) {

        Forward the query to the system with the highest priority

**If** search at the same level misses **then**

**If** there exists a lower-level system in  $p$ 's DHT table **then**

                Forward the query to that lower-level system

**else**

            Reply query miss to sender in system  $S$

**}**

**Figure 4. Pseudo code for the search algorithm.**

Figure 5 shows an example of searching between two systems at the same level. Suppose peer 9 in system 9 queries for content 14. Since the index peer 15 does not have content 14 in its index list, it selects system 47, which has the highest priority, from its DHT table and forwards the query to the registrar peer (peer 49 in this example) that records the gateway information to system 47. Peer 49 forwards the query to system 47 through the link between peer 28 and peer 12 according to its interconnection table. Remote peer 12 searches system 47 and finds a query hit for content 14 at peer 18. Peer 18 sends back a query hit message to peer 9 of system 9 through the reverse path. Index peer 15 then records peer 18 as a shortcut to system 47 in its DHT table. If later another peer, say peer 11, queries for content 14 also, peer 15 could use the shortcut to forward the query to peer 18 in system 47 directly without consulting the registrar peer again. We use priority to help us improve searching the same-level systems. When a reply

comes back from a same-level system, the peer increases its priority for a query hit and decreases its priority for a query miss. As mentioned, a peer searches the other systems at the same level one by one in the order of decreasing priority values. The reply from a remote system can be used to establish shortcuts such that queries can be forwarded much faster to the peers that are likely in charge of the requested content in the remote systems.

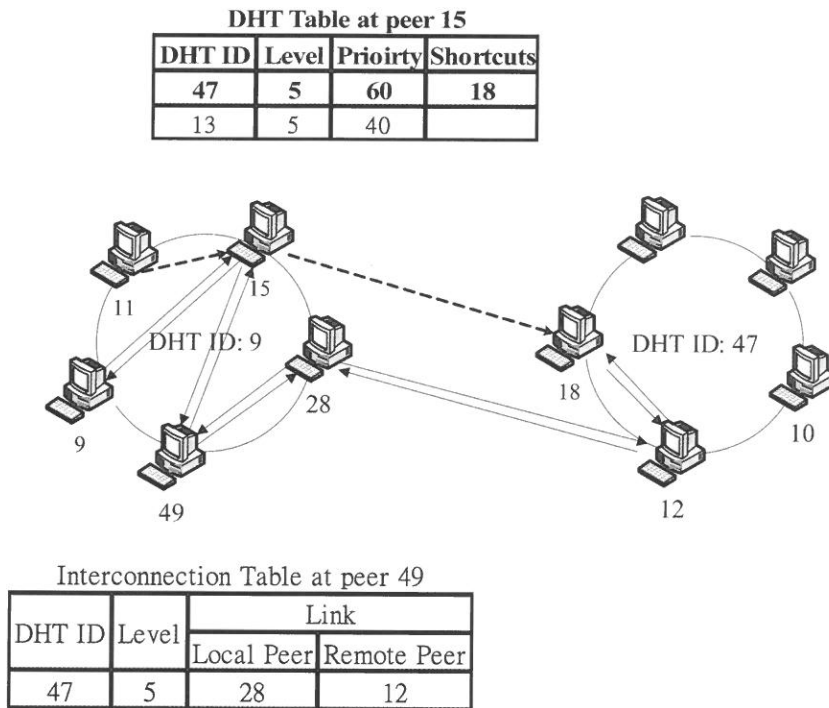


Figure 5. Example of file searching across systems.

## 4. Performance Evaluation

### 4.1 Cost of Interconnection and Merging

To make the resources in two DHT-based systems shareable to each other, we can either

merge them into one large system, or simply create interconnection links between them and transmit queries back and forth. Merging is more straightforward but the cost can be larger. Here we compare the cost of merging versus interconnection. For example, suppose two separate Chord systems with  $N_1$  and  $N_2$  peers, respectively, are to be merged. To do this, we need to designate one peer from each system to collect the list of the IDs of all the peers in its own system and exchanges the list to each other. Once a designated peer knows the IDs of all the peers in both systems, it can easily determine the necessary information (which includes the responsible key space, successor node, and predecessor node) for every peer in the final system and passes the information to that peer. Table 3 compares the cost of merging and interconnection. To merge two systems it is necessary to collect information from all the peers in both systems and redistributed the results back to the peers, and the amount of messages required is in the order of  $O(N_1 + N_2)$ . On the other end, it requires the establishment of one link only between two systems to interconnect them, which requires  $O(1)$  messages. However, the number of hops a query may traverse when searching over the interconnected systems can be as large as  $\log N_1 + \log N_2 = \log(N_1 N_2)$ , which is higher than  $\log(N_1 + N_2)$  for the case of merging. Although merging of systems results in a lower cost for query search, there are cases when it is not feasible to merge different DHT-based  $P_2P$  systems and we have to resort to the interconnection mechanism. For example, a Chord system and a CAN system could not be easily merged, because they work on two different infrastructures.

**Table 3. Cost of merging vs. interconnection.**

	Messages required to link two systems	Messages required for content search
Merging	$O(N_1 + N_2)$	$\log(N_1 + N_2)$
Interconnection	$O(1)$	$\log N_1 + \log N_2 = \log(N_1 N_2)$

## 4.2 Simulation Results

We developed a simulation program to evaluate the performance of our design. We gen-

erated 64,960 peers, which collectively from 340 Chord ring systems distributed in four levels. Each peer was identified by a 16-bit ID. The top level consisted of four systems of 10 000 peers each. The second level had 16 systems of 1000 peers each. The third level had 64 systems of 100 peers, while the fourth level had 256 systems of 10 peers. Figure 10 shows the structure of our hierarchical systems in the simulation. No cache storage was provided for a peer. Each peer contained twenty contents whose key values were randomly drawn from between 0 to 64 960. Every peer issued twenty queries requesting contents in the other systems randomly. Table 4 shows the query hit rates and the average number of hops traveled per query for both the case when all the systems were isolated and the case when the systems were interconnected. When those Chord systems were isolated from each other, the hit rate was only 58% because peers could not access the contents in different systems. The hit rate increased to 99% when the systems were interconnected with our approach, but the average number of hops traveled per query increased from 16.35 to 27.65 hops as well. In the case when all the systems were merged into a single large Chord ring, each query took only 7.99 hops on the average.

**Table 4. Hit rates and average number of hops.**

DHT ID	Hit Rates	Average Number of Hops per query
Original Chord systems	58%	16.35
Extended Chord systems	99%	27.65
One Chord Systems	99%	7.99

We next studied the case where the contents held by the peers in the same system shared a high similarity. Two contents were said to be similar if their key values were close to each other. For the peers in each single system, we assumed that a fraction of the queries issued would be requesting documents of key values within a given interval (i.e. those documents are similar). The rest of the queries were searching for documents randomly outside the interval. We computed the average number of hops traveled per query by increasing the similarity fraction of queries for both the cases of using and not using shortcuts. Figure 6 shows that with the

help of shortcuts, the average number of hops could be lowered by 34%.

Next we investigated the effects of the differences in size between the parent and child systems. Let  $M$  be the ratio of the number of peers in a parent system over that in a child system and we assumed that  $M$  remained the same for all the levels. Given a value of  $M$ , we distributed 64 960 peers into a number of systems that form a topology of a complete binary tree where the number of peers in a parent system was always  $M$  times that of its child system. No shortcuts were used. Figure 7 shows the number of levels of the resultant binary tree and the average number of hops traveled per query under different value of  $M$ . As  $M$  increased, both the number of levels and the number of hops decreased. Figure 8 displays the average number of queries that a peer at the top level had to process, which also became smaller as  $M$  got larger. When  $M$  became large, the systems at the top levels contained a large number of peers where most of the queries could be satisfied. The results show that the best performance can be achieved by organizing all the peers into a single large system. However, in case this is not possible and interconnection of systems is still necessary, our results suggest that a topology of four or five levels can provide very good performance.

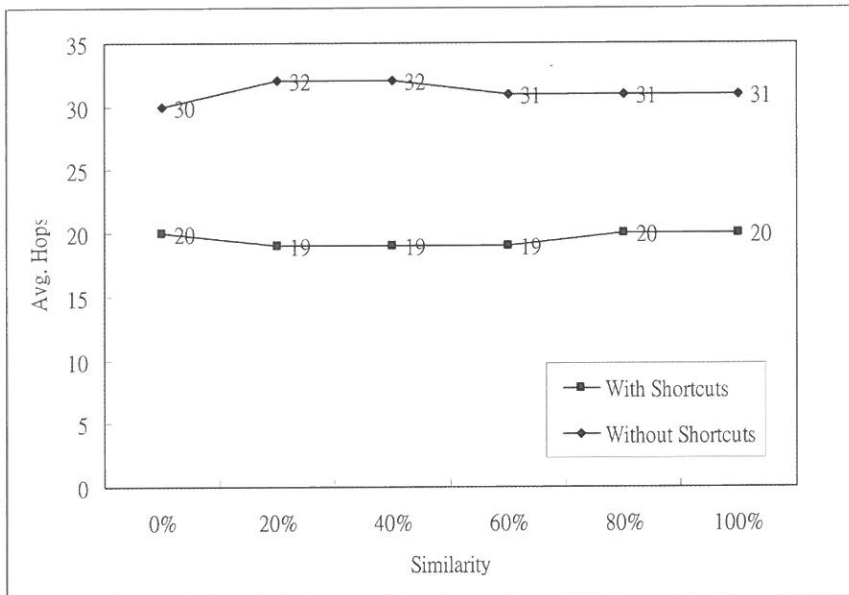


**Figure 6.** Average number of hops with and without shortcuts.

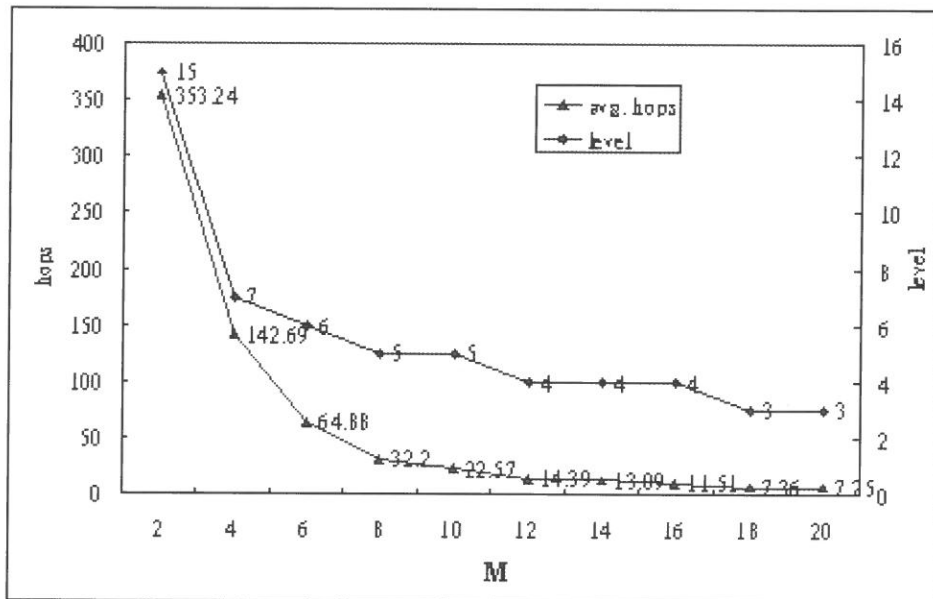


Figure 7. Number of hops and levels for different M.

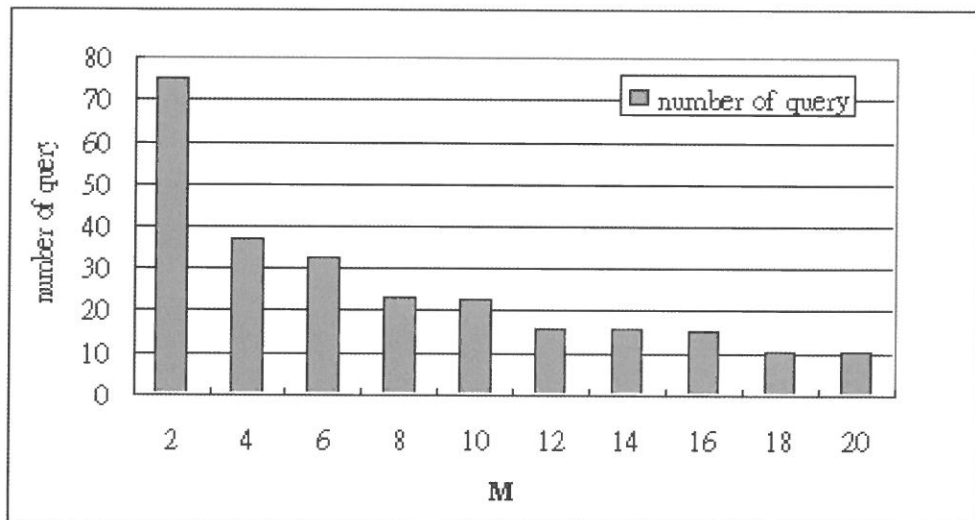


Figure 8. Average number of queries processed by a peer at the toplevel.

## 5. Conclusion

Powerful peer-to-peer networks are becoming the trend for resources sharing between users on the Internet. In order to access the resources in the other decentralized structured P2P systems, we came up with an interconnection approach to provide efficient search across different systems. We designed a mechanism of interconnecting multiple systems hierarchically to form an extended DHT-based system and to distribute the search load. We also proposed a search process that could seek contents between systems efficiently. The simulation results indicated that the cost of interconnection is much lower than the cost of merging systems. The number of hops traversed by a query could be decreased by using shortcuts. The result also suggested that the number of levels of the interconnected system should not be more than five. Our work can be easily integrated into the existing systems such as Chord, CAN, Pastry, and allow them forward search queries to each other.

## References

- [1] Napster, "<http://www.napster.com>"
- [2] R. Matei, A. Iamnitchi, and P. Foster, "Mapping the Gnutella network", *IEEE Internet Computing*, Volume 6, Issue 1, pp.50-57, Jan/Feb, 2002.
- [3] I. Clarke, O. Sandberg, B. Wiley, and T. W. Hong, "Freenet: A distributed anonymous information storage and retrieval system", *Workshop on Design Issues in Anonymity and Unobservability*, pp.46-66, Berkeley, Jul. 2000.
- [4] I. Stoica, R. Morris, D. Karger, M. Kaashoek, and H. Balakrishnan, "Chord: A Scalable Peer-to-Peer Lookup Protocol for Internet Applications", *IEEE/ACM Transactions on Networking*, Feb 2003
- [5] A. Rowstron and P. Druschel, "Pastry: Scalable, decentralized object location, and routing for large-scale peer-to-peer systems," *18th IFIP/ACM International Conference on Distributed Systems Platforms*, November 2001.
- [6] B. Zhao, J. Kubiawicz, and A. Joseph, "Tapestry: An infrastructure for fault-tolerant

widearea location and routing", Technical Report UCB/CSD-01-1141, U.C. Berkeley, April 2001.

- [7] S. Ratnasamy, P. Francis, M. Handley, R. Karp, and S. Shenker, "A scalable content addressable network", *Proceedings of SIGCOMM '01*, Volume 31 Issue 4, August 2001.
- [8] K. Frans, R. David and Karger, "Koorde: A simple degree-optimal distributed hash table", *Proceedings of the 2nd International Workshop on Peer-to-Peer Systems (IPTPS '03)*, February 2003.
- [9] M. Dahlia, N. Moni, and R. David, "Viceroy: A Scalable and Dynamic Emulation of the Butterfly", *Proceedings of the 21st annual ACM Symposium on Principles of Distributed Computing*, July 2002.
- [10] P. Ganesan, K. Gummadi, H. Garcia-Molina, "Canon in G Major: Designing DHTs with Hierarchical Structure" *24th IEEE International Conference on Distributed Computing Systems (ICDCS'04)*, pp. 534-540, March 2004.
- [11] R. Hsiao, W. Sheng-De, "Jelly: a dynamic hierarchical P2P overlay network with load balance and locality" *24th IEEE International Conference on Distributed Computing Systems (ICDCS'04)*, pp.23-24, March 2004.
- [12] S. Marc, G. Pedro, P. Jordi, S. Antonio, "Cyclone: a Novel Design Schema for Hierarchical DHTs" *the Fifth IEEE International Conference on Peer-to-Peer Computing*, September 2005.
- [13] H. Shen, C. Xu, and C. Guihai, "Cycloid: a constant-degree and lookup-efficient P2P overlay network" *18<sup>th</sup> International Parallel and Distributed Processing Symposium*, 2004.
- [14] J. Risson, S.Qazi, T. Moors, and A. Harwood, "A Dependable Global Location Service using Rendezvous on Hierarchic Distributed Hash Tables" *ICN/ICONS/MCL*, pp.23-29, April 2006.

*Received October 31, 2007*

*Accepted December 28, 2007*

## 有效率及擴充性的連結分散式雜湊表為基礎之點對點網路

呂俊賢 郭正夫

輔仁大學資訊工程系

### 摘 要

由於網際網路的普及化，使得越來越多的同儕網路技術廣泛被使用在檔案傳輸、分散式計算與語音通訊等方面，各式各樣的同儕網路也因此而誕生。過去大部分的研究都著重於如何提升單一同儕網路系統的效率和改善其缺點，使得各個同儕網路系統的運作都有良好的效能，但卻忽略了不同的同儕網路系統間，不能使用彼此的資源也不能相互溝通的問題。如果我們能將不同的同儕網路系統有效地連結起來，並提供一套搜尋方法，讓使用者能在這些系統間搜尋檔案，如此便能提高搜尋到檔案的機會，也使得不同的同儕網路間，能互相使用彼此的資源。在本篇論文之中，我們設計了一個延伸的同儕網路系統架構，將同儕網路系統使用者數目多寡形成層級式架構，各個同儕網路系統之間一旦建立連線，便能互相登記註冊並記錄該連線，並利用連線來做互相的溝通。我們並提出一個有效率的搜尋演算法，讓使用者能在不同的系統間一層層的搜尋，以有效率方式的搜尋到檔案。模擬的結果顯示所提出的階層互連架構將原本隔離的系統互連在一起時，搜尋成功率能從 58% 提升到 99%，而且互連的代價也遠較直接將系統合併成單一系統的花費來的少。

**關鍵詞：**點對點系統、分散式雜湊表、系統互連

# Estimation for Exponentiated Weibull under Type-I Censoring

Sy-Mien Chen\* and Hsin-Hsin Lee

*Department of Mathematics, Fu-Jen University,*

*Department of Applied Mathematics, Chung-Yuan University, Taiwan, R. O. C.*

## Abstract

In this paper, we discuss point estimators of two shape parameters for an Exponentiated Weibull distribution under type-I censoring. The maximum likelihood method and some Bayes estimators are considered.

**Key words:** MLE; GMLE; squared-error loss function; Linex loss function.

## 1. Introduction

Let  $X$  be a random variable with probability density function

$$f_X(x) = \frac{\alpha\theta}{\sigma} \left(\frac{x}{\sigma}\right)^{\alpha-1} e^{-\left(\frac{x}{\sigma}\right)^\alpha} (1 - e^{-\left(\frac{x}{\sigma}\right)^\alpha})^{\theta-1}, 0 \leq x \leq \infty; \alpha > 0, \theta > 0, \sigma > 0,$$

where  $\alpha, \theta$  are the shape parameters, and  $\sigma$  is the scale parameter, then we say  $X$  follows an Exponentiated Weibull distribution  $EW(\alpha, \theta, \sigma)$ . This distribution was first introduced by Mudholkar, G. S. and Srivastava, D. K. [5]. As was pointed out by Singh *et al.* [12] that different hazard function shapes of the model occur because of the shape parameter but not because of the scale parameter, hence for simplicity, we assume that  $\sigma = 1$  throughout. In this case the

---

\*smchen@math.fju.edu.tw

probability density function of the two-parameter Exponentiated Weibull distribution  $EW(\alpha, \theta)$  becomes

$$f_X(x) = \alpha\theta x^{\alpha-1} e^{-x^\alpha} (1 - e^{-x^\alpha})^{\theta-1}, \quad 0 \leq x \leq \infty; \alpha > 0, \theta > 0.$$

The hazard function is given by

$$h(x) = \frac{\alpha\theta x^{\alpha-1} e^{-x^\alpha} (1 - e^{-x^\alpha})^{\theta-1}}{1 - (1 - e^{-x^\alpha})^\theta}, \quad x > 0.$$

Under different combinations of the two shape parameters, there are several different shapes of the hazard function which contains bathtub, unimodal and monotone. See Fig 1 and Table 1.

Statistical properties of this distribution were discussed by many authors. Among others are Mudholkar, G. S. and Srivastava, D. K. [6], Mudholkar, G. S. and Hutson, A. D. [7], Nassar, M. M. and Eissa, F. H. [8], Choudhury, A. [1], Nadarajah, S. and Gupta, A. K. [10]

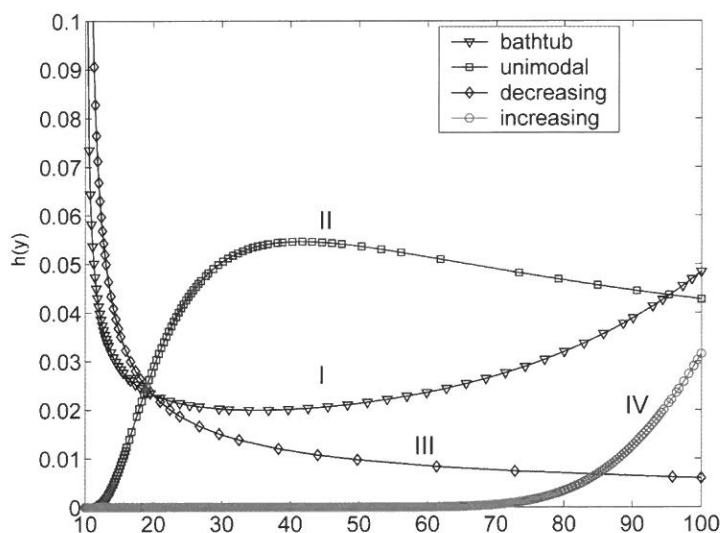


Figure 1: the hazard function of  $EW(\alpha, \theta)$

$\alpha$	$\theta$	hazard shape
1	1	constant (exponential)
	1	monotonic (Weibull)
<1	<1	decreasing(IV)
>1	>1	increasing(III)
>1	<1	bathtub(I) or increasing
<1	>1	unimodal(II) or decreasing

**Table1: shapes of the hazard function**

There are some occasions that the complete data can not be obtained in certain period of time. For example, in life testing, there may be some expected or unexpected situation, or to reduce cost and time. Therefore the so-called censored data has emerged. Nassar, M. M. and Eissa, F. H. [9] and Singh, U., Gupta, P. K. and Upadhyay, S. K. [13] discussed the estimating problems for Exponentiated Weibull under complete and type-II censoring scheme. In this paper, we will discuss similar estimating problems but under type-I censoring.

In section 2, maximum likelihood method (MLE) is considered. In section 3, from Bayesian point of view, we consider the following estimators: the generalized maximum likelihood estimator (GMLE), the Bayes estimators under squared-error loss function (BS), and the Bayes estimators under the Linex loss function (BL).

## 2. Maximum Likelihood Method

Ler  $X_1, X_2, \dots, X_n$  be the real lifetime of a sample with sample size  $n$  from an Exponentiated Weibull distribution  $EW(\alpha, \theta)$ , and let  $\underline{Y} = (Y_1, Y_2, \dots, Y_n)$  be the corresponding observed type-

I censored data, such that  $Y_i = \begin{cases} X_i & \text{if } X_i < t \\ t & \text{if } X_i \geq t. \end{cases}$  Let  $\delta_i = I(Y_i < t)$ , then the likelihood function of  $(\alpha, \theta)$  based on the observed  $\underline{Y}$  is given by

$$L(\alpha, \theta | \underline{Y} = \underline{y}) = (\alpha\theta)^{\sum_{i=1}^n \delta_i} [1 - (1 - e^{-t^\alpha})^\theta]^{n - \sum_{i=1}^n \delta_i} \prod_{i=1}^n [y_i^{\alpha-1} e^{-y_i^\alpha} (1 - e^{-y_i^\alpha})^{\theta-1}]^{\delta_i}.$$

## 2.1 When $\alpha$ is known

Assume that  $\alpha = \alpha_0 > 0$  is given, then the logarithm of the likelihood function can be expressed as

$$\begin{aligned} l(\theta | \underline{y}) = & \left( \sum_{i=1}^n \delta_i \right) \ln(\alpha_0 \theta) + (\alpha_0 - 1) \sum_{i=1}^n \delta_i \ln y_i - \sum_{i=1}^n \delta_i y_i^{\alpha_0} \\ & + (\theta - 1) \sum_{i=1}^n \delta_i \ln(1 - e^{-y_i^{\alpha_0}}) + (n - \sum_{i=1}^n \delta_i) \ln[1 - (1 - e^{-t^{\alpha_0}})^\theta]. \end{aligned}$$

Then

$$\frac{dl}{d\theta} = \frac{r}{\theta} + \sum_{i=1}^n \delta_i \ln(1 - e^{-y_i^{\alpha_0}}) - (n - r) \frac{(1 - e^{-t^{\alpha_0}})^\theta \ln(1 - e^{-t^{\alpha_0}})}{1 - (1 - e^{-t^{\alpha_0}})^\theta},$$

and

$$\frac{d^2 l}{d\theta^2} = -\frac{r}{\theta^2} - (n - r) v_t (\ln e_t)^2 (1 + v_t),$$

where

$$r = \sum_{i=1}^n \delta_i, \quad e_t = 1 - e^{-t^{\alpha_0}}, \quad v_t = \frac{e_t^\theta}{1 - e_t^\theta}.$$

Since  $\frac{d^2l}{d\theta^2} < 0$ , the MLE  $\hat{\theta}_M$  of  $\theta$  can be obtained by solving the estimating equation:

$$\frac{dl}{d\theta} = 0.$$

## 2.2 When $\alpha$ and $\theta$ are both unknown

When both parameters  $\alpha, \theta$  are unknown, the logarithm of the likelihood function can be expressed as

$$\begin{aligned} l(\alpha, \theta | \underline{y}) = & \left( \sum_{i=1}^n \delta_i \right) \ln(\alpha\theta) + (\alpha - 1) \sum_{i=1}^n \delta_i \ln y_i - \sum_{i=1}^n \delta_i y_i^\alpha \\ & + (\theta - 1) \sum_{i=1}^n \delta_i \ln(1 - e^{-y_i^\alpha}) + (n - \sum_{i=1}^n \delta_i) \ln[1 - (1 - e^{-t^\alpha})^\theta]. \end{aligned}$$

Then

$$\begin{aligned} \frac{\partial l}{\partial \alpha} = & \frac{r}{\alpha} + \sum_{i=1}^n \delta_i \ln y_i - \sum_{i=1}^n \delta_i y_i^\alpha \ln y_i + (\theta - 1) \sum_{i=1}^n \frac{\delta_i y_i^\alpha e^{-y_i^\alpha} \ln y_i}{1 - e^{-y_i^\alpha}} \\ & - (n - r) \frac{\theta t^\alpha e^{-t^\alpha} (1 - e^{-t^\alpha})^{\theta-1} \ln t}{1 - (1 - e^{-t^\alpha})^\theta}, \\ \frac{\partial l}{\partial \theta} = & \frac{r}{\theta} + \sum_{i=1}^n \delta_i \ln(1 - e^{-y_i^\alpha}) - (n - r) \frac{(1 - e^{-t^\alpha})^\theta \ln(1 - e^{-t^\alpha})}{1 - (1 - e^{-t^\alpha})^\theta}. \end{aligned}$$

The possible MLEs  $\hat{\alpha}_M$  and  $\hat{\theta}_M$  of  $\alpha$  and  $\theta$  can be obtained by solving the estimating equations:

$$\frac{\partial l}{\partial \alpha} = 0 \text{ and } \frac{\partial l}{\partial \theta} = 0.$$

### 3. Bayesian Approach

Some statisticians have assumed that there is no information available about the true value of the parameter beyond that provided by the data. However, in Bayesian inference, parameters are treated as random variables with known prior distributions. This subjective prior distribution is based upon past experiences.

An estimator  $\hat{\eta}$  which maximizes the posterior distribution of a parameter  $\eta$  is called a generalized maximum likelihood estimator of  $\eta$ . See Harry, F. M. and Ray, A. W. [2] for more detail.

If one considers the seriousness that an overestimate and an underestimate create are equivalent, then he can choose the squared-error loss function, and the Bayes estimator  $\hat{\eta}_{BS}$  of  $\eta$  based on a sample  $\underline{x}$  is

$$\hat{\eta}_{BS} = E_{\eta}(\eta|\underline{x}), \quad (1)$$

provided that it exists. (See Hogg, R. V. *et. al* [3].)

However, in some situations, use of symmetric loss functions may be inappropriate. For example, when a pharmacist judges the dosage taking in adults or children, the result of overestimation is more serious than that of underestimation. On the contrary, the result of underestimation is quite serious under the residuum of agricultural pesticides on vegetables. To overcome this problem, Varian [14] proposed the Llinex loss function which is defined by

$$\mathcal{L}_{\infty}(\Delta) = be^{a\Delta} - c \Delta - b, \text{ where } a \neq 0, b > 0, c \in \mathbb{R}.$$

The Llinex loss function provides a variety of asymmetric effects when the parameters  $a$ ,  $b$  and  $c$  are varied. Zellner [15] considered the case when  $c = ab$  such that

$$\mathcal{L}(\Delta) = b[e^{a\Delta} - a \Delta - 1], \quad a \neq 0, b > 0.$$

For small values of  $|a|$ , the function is almost symmetry and not far from a squared-error loss function. For the choice of negative (positive) value of  $a$ , it gives more weight to overestimation

(underestimation). By assuming that  $b = 1$ , the Bayes estimator  $\hat{\eta}_{BL}$  under the Linex loss function  $\mathcal{L}(\Delta)$  is

$$\hat{\eta}_{BL} = -\frac{1}{a} \ln E_{\eta}(e^{-a\eta}|\underline{x}), \quad (2)$$

provided that  $E_{\eta}(e^{-a\eta}|\underline{x})$  exists and is finite. See Robert, C. P. [11].

### 3.1 When $\alpha$ is known

By assuming that the parameter  $\alpha$  known, say  $\alpha = \alpha_0$ , and the shape parameter  $\theta \sim \text{Gamma}(\tau, \frac{1}{\beta})$ , the posterior distribution of  $\theta$  based on an observed sample  $\underline{y}$  from  $EW(\alpha_0, \theta)$  is

$$\Pi(\theta|\underline{y}) = \frac{(\beta + q)^{r+\tau}}{S\Gamma(r+\tau)} \theta^{r+\tau-1} e^{-(\beta+q)\theta} [1 - (1 - e^{-t^{\alpha_0}})^{\theta}]^{n-r},$$

where

$$\begin{aligned} q &= -\ln \left[ \prod_{i=1}^n (1 - e^{-y_i^{\alpha_0}})^{\delta_i} \right], \\ S &= \sum_{j=0}^{n-r} (-1)^j \binom{n-r}{j} \left(1 - \frac{\rho j}{\beta + q}\right)^{-(r+\tau)}, \\ \rho &= \ln(1 - e^{-t^{\alpha_0}}). \end{aligned}$$

- (i) It is clear that the generalized maximum likelihood estimator  $\hat{\theta}_{GM}$  of  $\theta$  exists if  $\tau > 1$  and can be obtained by solving the following estimating equation:

$$\begin{aligned} 0 &= \frac{\partial \ln \Pi(\theta|\underline{y})}{\partial \theta} \\ &= \frac{r + \tau - 1}{\theta} - (\beta + q) - (n - r) \frac{(1 - e^{-t^{\alpha_0}})^{\theta} \ln(1 - e^{-t^{\alpha_0}})}{1 - (1 - e^{-t^{\alpha_0}})^{\theta}}. \end{aligned}$$

- (ii) By formula (1), the Bayes estimator of the shape parameter  $\theta$  under squared-error loss function is

$$\hat{\theta}_{BS} = \frac{r + \tau}{S(\beta + q)} \sum_{j=0}^{n-r} (-1)^j \binom{n-r}{j} \left(1 - \frac{\rho j}{\beta + q}\right)^{-(r+\tau+1)}; \quad (3)$$

(iii) By formula (2), the Bayes estimator of the shape parameter  $\theta$  under Linex loss function is

$$\hat{\theta}_{BL} = -\frac{1}{a} \ln \left[ \frac{1}{S} \sum_{j=0}^{n-r} (-1)^j \binom{n-r}{j} \left(1 + \frac{a - \rho j}{\beta + q}\right)^{-(r+\tau)} \right]. \quad (4)$$

### 3.2 When $\alpha$ and $\theta$ are independent random variables

Assume that the parameters  $\alpha$  and  $\theta$  are independent, and are from a non-informative prior  $g_1(\alpha) = 1$ ,  $0 < \alpha$  and an improper prior  $g_2(\theta) = \frac{1}{\theta}$ ,  $0 < \theta$ , respectively. Then the joint posterior distribution of  $\alpha$ ,  $\theta$  based on an observed sample  $\underline{y}$  from  $EW(\alpha, \theta)$  is given by

$$\Pi(\alpha, \theta | \underline{y}) = \frac{\alpha^r \theta^{r-1} [1 - (1 - e^{-\alpha})^\theta]^{n-r} \prod_{i=1}^n [y_i^{\alpha-1} e^{-y_i^\alpha} (1 - e^{-y_i^\alpha})^{\theta-1}]^{\delta_i}}{\int_0^\infty \int_0^\infty \alpha^r \theta^{r-1} [1 - (1 - e^{-\alpha})^\theta]^{n-r} \prod_{i=1}^n [y_i^{\alpha-1} e^{-y_i^\alpha} (1 - e^{-y_i^\alpha})^{\theta-1}]^{\delta_i} d\theta d\alpha}.$$

#### 3.2.1 Generalized Maximum Likelihood Estimator

The marginal posterior distributions of  $\alpha$  and  $\theta$  are

$$\Pi(\alpha | \underline{y}) = \frac{\alpha^r \prod_{i=1}^n (y_i^{\alpha-1} e^{-y_i^\alpha})^{\delta_i} J_2(\alpha)}{J_1},$$

$$\Pi(\theta | \underline{y}) = \frac{\theta^{r-1} J_3(\theta)}{J_1},$$

respectively, where

$$\begin{aligned}
 J_1 &= \int_0^\infty \int_0^\infty \alpha^r \theta^{r-1} [1 - (1 - e^{-t^\alpha})^\theta]^{n-r} \prod_{i=1}^n [y_i^{\alpha-1} e^{-y_i^\alpha} (1 - e^{-y_i^\alpha})^{\theta-1}]^{\delta_i} d\theta d\alpha, \\
 J_2(\alpha) &= \int_0^\infty \theta^{r-1} [1 - (1 - e^{-t^\alpha})^\theta]^{n-r} \prod_{i=1}^n (1 - e^{-y_i^\alpha})^{\delta_i(\theta-1)} d\theta, \\
 J_3(\theta) &= \int_0^\infty \alpha^r [1 - (1 - e^{-t^\alpha})^\theta]^{n-r} \prod_{i=1}^n [y_i^{\alpha-1} e^{-y_i^\alpha} (1 - e^{-y_i^\alpha})^{\theta-1}]^{\delta_i} d\alpha.
 \end{aligned}$$

The the possible GMLEs  $\hat{\alpha}_{GM}$  and  $\hat{\theta}_{GM}$  of  $\alpha$  and  $\theta$  can be obtained by solving the following estimating equations:

$$\begin{aligned}
 0 &= \frac{\partial \ln \Pi(\alpha|\underline{y})}{\partial \alpha} = \frac{r}{\alpha} + \sum_{i=1}^n \delta_i (\ln y_i - y_i^\alpha \ln y_i) + \frac{1}{J_2(\alpha)} \times \frac{\partial J_2(\alpha)}{\partial \alpha}, \\
 0 &= \frac{\partial \ln \Pi(\theta|\underline{y})}{\partial \theta} = \frac{r-1}{\theta} + \frac{1}{J_3(\theta)} \times \frac{\partial J_3(\theta)}{\partial \theta},
 \end{aligned}$$

provided that they exist.

### 3.2.2 Bayes Estimator Under Squared-Error Loss Function

Notice that the Bayes estimator of a parameter  $w(\alpha, \theta)$  under the squared-error loss function is

$$\hat{w} = E(w(\alpha, \theta)|\underline{y}) = \frac{\int_\alpha \int_\theta w(\alpha, \theta) g(\alpha, \theta) e^{l(\alpha, \theta|\underline{y})} d\theta d\alpha}{\int_\alpha \int_\theta g(\alpha, \theta) e^{l(\alpha, \theta|\underline{y})} d\theta d\alpha},$$

which involves a ratio of two complex integrals that are analytically intractable. One way to handle such problem is to apply the Lindley's approximation procedure [4].

In the two-parameter case, Lindley's approximation form reduces to the following form:

$$\hat{w} \approx w(\alpha, \theta) + \Phi_1 w_1 + \Phi_2 w_2 + \Psi,$$

where

$$\begin{aligned}\Psi &= \frac{1}{2D}(Aw_{11} + Cw_{12} + Cw_{21} + Bw_{22}), \\ \Phi_1 &= \frac{1}{D}(Ap_1 + Cp_2) + \frac{1}{2D^2}[A^2m_{30} + BCm_{03} + 3ACm_{21} + (AB + 2C^2)m_{12}], \\ \Phi_2 &= \frac{1}{D}(Cp_1 + Bp_2) + \frac{1}{2D^2}[ACm_{30} + B^2m_{03} + (AB + 2C^2)m_{21} + 3BCm_{12}]\end{aligned}\quad (5)$$

$$\begin{aligned}A &= -\frac{\partial^2 l}{\partial \theta^2} = \frac{r}{\theta^2} + (n-r)v_t(\ln e_t)^2(1+v_t) \\ B &= -\frac{\partial^2 l}{\partial \alpha^2} = \frac{r}{\alpha^2} + \sum_{i=1}^n \delta_i y_i^\alpha (\ln y_i)^2 - (\theta-1) \sum_{i=1}^n \delta_i u_i (\ln y_i - y_i^\alpha \ln y_i - u_i) \\ &\quad + (n-r)\theta v_t u_t (\ln t - t^\alpha \ln t - u_t + \theta u_t + \theta v_t u_t) \\ C &= \frac{\partial^2 l}{\partial \alpha \partial \theta} = \sum_{i=1}^n \delta_i u_i - (n-r)v_t u_t (1 + \theta \ln e_t + \theta v_t \ln e_t) \\ D &= AB - C^2\end{aligned}$$

and

$$\begin{aligned}p &= \ln g(\alpha, \theta) = \ln \frac{1}{\theta}, \quad p_1 = \frac{\partial p}{\partial \alpha} = 0, \quad p_2 = \frac{\partial p}{\partial \theta} = -\frac{1}{\theta}, \\ \sigma_{11} &= \frac{A}{D}, \quad \sigma_{22} = \frac{B}{D}, \quad \sigma_{12} = \sigma_{21} = \frac{C}{D}\end{aligned}$$

$$\begin{aligned}
m_{30} &= \frac{\partial^3 l}{\partial \alpha^3} = \frac{2r}{\alpha^3} - \sum_{i=1}^n \delta_i y_i^\alpha (\ln y_i)^3 + (\theta - 1) \left[ \sum_{i=1}^n \delta_i u_i (\ln y_i)^2 (1 - 3y_i^\alpha + y_i^{2\alpha}) \right. \\
&\quad + 3 \sum_{i=1}^n \delta_i u_i^2 \ln y_i (-1 + y_i^\alpha) + 2 \sum_{i=1}^n \delta_i u_i^3 \left. \right] \\
&\quad + 3(n-r)\theta v_t u_t^2 \ln t (-1 + t^\alpha) (-1 + \theta + \theta v_t) \\
&\quad + (n-r)\theta v_t u_t (\ln t)^2 (-1 + 3t^\alpha - t^{2\alpha}) \\
&\quad + (n-r)\theta v_t u_t^3 (-2 + 3\theta - \theta^2 + 3\theta v_t - 3\theta^2 v_t - 2\theta^2 v_t^2)
\end{aligned}$$

$$m_{03} = \frac{\partial^3 l}{\partial \theta^3} = \frac{2r}{\theta^3} - (n-r)v_t (\ln e_t)^3 (1 + 3v_t + 2v_t^2)$$

$$\begin{aligned}
m_{21} &= \frac{\partial^3 l}{\partial \theta \partial \alpha^2} = (n-r)\theta v_t u_t^2 \ln e_t (1 - \theta + v_t - 3\theta v_t - 2\theta v_t^2) \\
&\quad + \sum_{i=1}^n \delta_i u_i (\ln y_i - y_i^\alpha \ln y_i - u_i) + (n-r)\theta v_t u_t \ln t \ln e_t (-1 + t^\alpha) (1 + v_t)
\end{aligned}$$

$$\begin{aligned}
&\quad + (n-r)v_t u_t (-\ln t + t^\alpha \ln t + u_t - 2\theta u_t - 2\theta v_t u_t) \\
m_{12} &= \frac{\partial^3 l}{\partial \theta^2 \partial \alpha} = -2(n-r)v_t u_t \ln e_t (1 + v_t) - (n-r)\theta v_t u_t (\ln e_t)^2 (1 + 3v_t + 2v_t^2)
\end{aligned}$$

and

$$\begin{aligned}
e_i &= 1 - e^{-y_i^\alpha}, \quad v_i = \frac{e_i^\theta}{1 - e_i^\theta}, \quad u_i = \frac{y_i^\alpha e^{-y_i^\alpha} \ln y_i}{e_i}, \\
e_t &= 1 - e^{-t^\alpha}, \quad v_t = \frac{e_t^\theta}{1 - e_t^\theta}, \quad u_t = \frac{t^\alpha e^{-t^\alpha} \ln t}{e_t}.
\end{aligned}$$

All functions on the right-hand side of above equations are to be evaluated at  $\hat{\alpha}_M, \hat{\theta}_M$ , the MLE of  $\alpha, \theta$  respectively.

Apply Lindley's approximation to our case, i.e.

(i) When  $w(\alpha, \theta) = \alpha$ ,

$$w_1 = \frac{\partial w}{\partial \alpha} = 1, \quad w_2 = \frac{\partial w}{\partial \theta} = 0,$$

$$w_{11} = \frac{\partial^2 w}{\partial \alpha^2} = 0, \quad w_{12} = \frac{\partial^2 w}{\partial \alpha \partial \theta} = 0, \quad w_{21} = \frac{\partial^2 w}{\partial \theta \partial \alpha} = 0, \quad w_{22} = \frac{\partial^2 w}{\partial \theta^2} = 0.$$

Then,

$$\hat{\alpha}_{BS} = E(\alpha|y) \approx \hat{\alpha}_M + \Phi_1. \quad (6)$$

(ii) When  $w(\alpha, \theta) = \theta$ ,

$$w_1 = 0, w_2 = 1, \\ w_{11} = w_{12} = w_{21} = w_{22} = 0.$$

Then

$$\hat{\theta}_{BS} = E(\theta|y) \approx \hat{\theta}_M + \Phi_2. \quad (7)$$

### 3.2.3 Bayes Estimator Under Linex Loss Function

Recall that the Bayes estimator of a function  $w(\alpha, \theta)$  relative to the Linex loss function is

$$\hat{w}_{BL} = -\frac{1}{a} \ln[E(w(\alpha, \theta)|\underline{y})],$$

which involves a ratio of two integrals too. Apply the Lindley's approximation procedure again with

(i)  $w(\alpha, \theta) = e^{-a\alpha}$ ,

$$w_1 = \frac{\partial w}{\partial \alpha} = -ae^{-a\alpha}, \quad w_2 = \frac{\partial w}{\partial \theta} = 0,$$

$$w_{11} = \frac{\partial^2 w}{\partial \alpha^2} = a^2 e^{-a\alpha}, w_{12} = w_{21} = 0, w_{22} = \frac{\partial^2 w}{\partial \theta^2} = 0,$$

then the Bayes estimator of  $\alpha$  under Linex loss function is

$$\hat{\alpha}_{BL} \approx \hat{\alpha}_M - \frac{1}{a} \ln(1 - a\Phi_1 + \frac{a^2 A}{2D}) \quad (8)$$

$$(ii) w(\alpha, \theta) = e^{-a\theta},$$

$$w_1 = 0, w_2 = -ae^{-a\theta},$$

$$w_{11} = w_{12} = w_{21} = 0, w_{22} = a^2 e^{-a\theta},$$

then the Bayes estimator of  $\theta$  under Linex loss function is

$$\hat{\theta}_{BL} \approx \hat{\theta}_M - \frac{1}{a} \ln(1 - a\Phi_2 + \frac{a^2 B}{2D}). \quad (9)$$

### 3.3 When $\alpha$ and $\theta$ are dependent random variables

It happened that parameters are not independent. Assume that the conditional prior distribution of  $\theta$  given  $\alpha$  is

$$g_1(\theta|\alpha) = \frac{\alpha^{-\tau}}{\Gamma(\tau)} \theta^{\tau-1} e^{-\frac{\theta}{\alpha}}, \theta > 0, \tau > 0,$$

and the prior distribution for  $\alpha$  is

$$g_2(\alpha) = \frac{1}{k} e^{-\frac{\alpha}{k}}, \alpha > 0, k > 0,$$

then the joint prior distribution of  $\alpha$  and  $\theta$  is

$$g(\alpha, \theta) = \frac{\alpha^{-\tau} \theta^{\tau-1}}{k\Gamma(\tau)} e^{-\frac{\alpha^2 + \theta k}{\alpha k}}, \alpha > 0, \theta > 0.$$

Therefore, the joint posterior distribution of  $\alpha$  and  $\theta$  based on the sample  $\underline{y}$  from  $EW(\alpha, \theta)$  becomes

$$\begin{aligned} & \Pi(\alpha, \theta | \underline{y}) \\ &= \frac{g(\alpha, \theta) L(\alpha, \theta | \underline{y})}{\int_0^c \int_0^\infty g(\alpha, \theta) L(\alpha, \theta | \underline{y}) d\theta d\alpha} \\ &= \frac{\alpha^{r-\tau} \theta^{r+\tau-1} e^{-\frac{\alpha^2 + \theta k}{\alpha k}} [1 - (1 - e^{-t^\alpha})^\theta]^{n-r} \prod_{i=1}^n [y_i^{\alpha-1} e^{-y_i^\alpha} (1 - e^{-y_i^\alpha})^{\theta-1}]^{\delta_i}}{\int_0^\infty \int_0^\infty \alpha^{r-\tau} \theta^{r+\tau-1} e^{-\frac{\alpha^2 + \theta k}{\alpha k}} [1 - (1 - e^{-t^\alpha})^\theta]^{n-r} \prod_{i=1}^n [y_i^{\alpha-1} e^{-y_i^\alpha} (1 - e^{-y_i^\alpha})^{\theta-1}]^{\delta_i} d\theta d\alpha}. \end{aligned}$$

### 3.3.1 Generalized Maximum Likelihood Estimator

Let  $\Pi_1(\alpha, \theta | \underline{y})$  be the logarithm of the joint posterior distribution of  $\alpha$  and  $\theta$ , then

$$\begin{aligned} \Pi_1(\alpha, \theta | \underline{y}) &= (r - \tau) \ln \alpha + (r + \tau - 1) \ln \theta - \frac{\alpha}{k} - \frac{\theta}{\alpha} + (\alpha - 1) \sum_{i=1}^n \delta_i \ln y_i \\ &\quad + (\theta - 1) \sum_{i=1}^n \delta_i \ln(1 - e^{-y_i^\alpha}) + (n - r) \ln[1 - (1 - e^{-t^\alpha})^\theta] \\ &\quad - \sum_{i=1}^n \delta_i y_i^\alpha - \ln J_4 \end{aligned}$$

where  $J_4$  is a constant. Then

$$\begin{aligned} \frac{\partial \Pi_1}{\partial \alpha} &= \frac{r - \tau}{\alpha} - \frac{1}{k} + \frac{\theta}{\alpha^2} + \sum_{i=1}^n \delta_i \ln y_i - \sum_{i=1}^n \delta_i y_i^\alpha \ln y_i \\ &\quad + (\theta - 1) \sum_{i=1}^n \frac{\delta_i y_i^\alpha e^{-y_i^\alpha} \ln y_i}{1 - e^{-y_i^\alpha}} - (n - r) \frac{\theta t^\alpha e^{-t^\alpha} (1 - e^{-t^\alpha})^{\theta-1} \ln t}{1 - (1 - e^{-t^\alpha})^\theta}, \end{aligned}$$

$$\frac{\partial \Pi_1}{\partial \theta} = \frac{r + \tau - 1}{\theta} - \frac{1}{\alpha} + \sum_{i=1}^n \delta_i \ln(1 - e^{-\gamma_i^\alpha}) - (n - r) \frac{(1 - e^{-t^\alpha})^\theta \ln(1 - e^{-t^\alpha})}{1 - (1 - e^{-t^\alpha})^\theta}.$$

The possible GMLE  $\hat{\alpha}_{GM}$  and  $\hat{\theta}_{GM}$  of  $\alpha$  and  $\theta$  can be obtained by solving the following estimating equations:  $0 = \frac{\partial \Pi_1}{\partial \alpha}$ , and  $0 = \frac{\partial \Pi_2}{\partial \theta}$ .

### 3.3.2 Bayes Estimator Under the Squared-Error Loss Function

Apply the Lindley's procedure again with

(i)  $w(\alpha, \theta) = \alpha$ , then the Bayes estimator under the Squared-Error Loss Function of  $\alpha$  is

$$\hat{\alpha}_{BS} = E(\alpha|\underline{y}) \approx \hat{\alpha}_M + \Phi_1, \quad (11)$$

(ii)  $w(\alpha, \theta) = \theta$ , then the Bayes estimator under the Squared-Error Loss Function of  $\theta$  is

$$\hat{\theta}_{BS} = E(\theta|\underline{y}) \approx \hat{\theta}_M + \Phi_2, \quad (12)$$

where  $\Phi_1$  and  $\Phi_2$  are defined as in (5), with

$$\begin{aligned} p = \ln g(\alpha, \theta) &= (-\tau) \ln \alpha + (\tau - 1) \ln \theta - \frac{\alpha}{k} - \frac{\theta}{\alpha} - \ln k \Gamma(\tau). \\ p_1 &= \frac{\partial p}{\partial \alpha} = \frac{\theta}{\alpha^2} - \frac{\tau}{\alpha} - \frac{1}{k}, \\ p_2 &= \frac{\partial p}{\partial \theta} = \frac{\tau - 1}{\theta} - \frac{1}{\alpha}. \end{aligned}$$

### 3.3.3 Bayes Estimator Under Linex Loss Function

The Bayes estimator of  $\alpha$  and  $\theta$  based on the Linex loss function are

$$\hat{\alpha}_{BL} \approx \hat{\alpha}_M - \frac{1}{a} \ln(1 - a\Phi_1 + \frac{a^2 A}{2D}). \quad (13)$$

$$\hat{\theta}_{BL} \approx \hat{\theta}_M - \frac{1}{a} \ln(1 - a\Phi_2 + \frac{a^2 B}{2D}), \quad (14)$$

respectively.

## 4. Example

From the previous discussion, it shows that most of the estimators do not have explicit forms. In this section, we use computer simulation and Monte Carlo methods to study the problem. We study the performance of MLE, GMLE, BS and BL based on two types of risks. One of them is the expectation of the squared-error loss function and the other is the expectation of Linex loss function with  $a = -3, -1, 1, 3$  and  $b = 1$ .

Notice that when the parameters  $\alpha$  or  $\theta$  tends to either 0 or  $\infty$ , the hazard function becomes 0 or  $\infty$ , which are not the cases we are interested in. In this simulation study, We consider samples from the Exponentiated Weibull distributions  $EW(1.8, 1.5)$ ,  $EW(1.5, 0.8)$ ,  $EW(0.8, 1.5)$  with sample sizes  $n = 30, 50, 100, 200, 300$  and five uncensored rate, namely 100%, 90%, 80%, 70% and 60%.

In the case when the shape parameter  $\alpha$  is known, we assume the prior distribution of  $\theta$  to be *Gamma* (3, 1/3). For the case when both shape parameters  $\alpha$  and  $\theta$  are unknown, consider the following two cases: (1) Assume  $\alpha$  and  $\theta$  are independent random variables with the improper priors  $g_1(\alpha) = 1$ , if  $\alpha > 0$  and  $g_2(\theta) = \frac{1}{\theta}$ , if  $\theta > 0$ . (2) For the case when  $\alpha$  and  $\theta$  are dependent, we assume the conditional distribution of  $\theta$  given  $\alpha$ , i.e.  $\theta|\alpha \sim \text{Gamma}(3, \alpha)$  and  $\alpha \sim \text{Exp}(4)$ .

Systems of equations are involved when solving for the MLE and GMLE, which is impossible to solve them analytically. We use the routine DUV MID and DNEQNJ in IMSL to handle the problem. The accuracy is up to the fifth decimal point. There are some integrations involved in the expression of estimators for the Bayes estimators under squared-error loss function (BS) and under Linex loss function (BL). When  $\alpha$  is known, we use the importance sampling technique to get the approximations. The number of iteration of this approximation is 100000. When both  $\alpha$  and  $\theta$  are unknown, ratio of two complex integrals were involved, for this part we apply the Lindley's approximation. For each different combination of parameters, the

simulations are repeated 10000 times.

To save the space, except the case when  $\alpha$  is known, we only list the graphs for the case when  $n = 300$  and uncensored rate 70% because the patterns are all similar. Method 1, 2, 3, 4, 5, 6, 7 on the x-axis of Figure 2 correspond to estimators MLE, GMLE, BS, BL(-3), BL(-1), BL(1), BL(3). Method 1, 2, 3, 4, 5, 6, 7, 8, 9, 10, 11 on the x-axis of Fig 3 ~ Fig 5 correspond to the estimators MLE, GMLE, BS, BL(-25), BL(-10), BL(-3), BL(-1), BL(1), BL(3), BL(10), BL(25).

Risk1 ~ Risk4 in each figure denote the regular risk when the Linex loss function is applied with  $a = -3, -1, 1$  and  $3$ , respectively. Risk 5 means the risk with the squared-error loss function. As we can see from the figures that except Risk1 and Risk4, the curves for the other risks are too smooth and are hard to tell the differences within estimators. Theoretically speaking, if the prior is used, then the Bayes estimator is the best within all estimators under the given loss function. Hence for each curve (risk method), the minimum of the Bayes risk should occur at the corresponding estimator. i.e. when  $\alpha$  is known, the best estimator under each risk should be as the following:

Risk	1	2	3	4	5
Best Method	4	5	6	7	3
Best Estimator	BL(-3)	BL(-1)	BL(1)	BL(3)	BS

From Fig 2, we observe the following when the sample is from  $EW(1.8, 1.5)$  and  $\alpha$  is known:

- (1) Under risk 1, the curve is quite smooth, and the risk of GMLE is quite close to the risk of BL(-3), especially when the sample size is large;
- (2) Under risk 4, the risk induced from GMLE is closer to the risk from BL(3) ;
- (3) As the sample size increases, the curves for risk 1 and risk 4 are smoother and are closer to each other;
- (4) The risks of all estimators decrease rapidly when the sample size increases;
- (5) The curves of risk 2 and risk 3 are almost overlapped. On the other hand, the curve for risk 5 is also close to the curves of risk2 and risk3, which is reasonable, because as the value of  $|a|$  is small, the Linex loss function is close to the squared error loss function;
- (6) As  $n \rightarrow \infty$ , all the estimators are asymptotically unbiased.

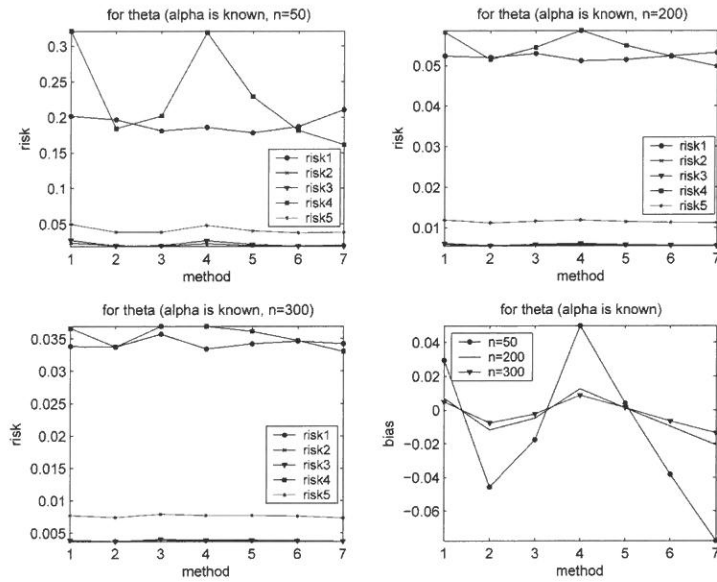


Figure 2: Risk and bias of different estimators for  $\theta$  as  $(\alpha, \theta) = (1.8, 1.5)$  ( $\alpha$  is known)

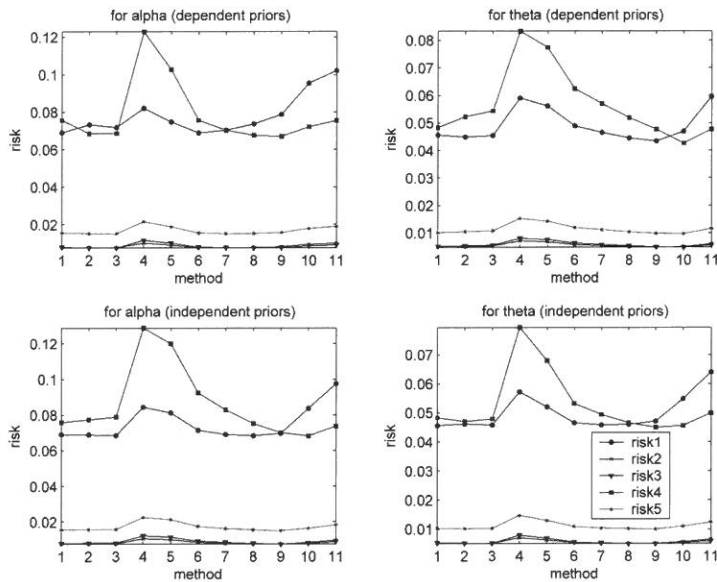


Figure 3: Risk of different estimators for  $\alpha$  and  $\theta$  as  $(\alpha, \theta) = (1.8, 1.5)$  ( $n = 300$ )

For the case when  $\alpha$  and  $\theta$  are both unknown, the best estimator under each risk should be as the following:

Risk	1	2	3	4	5
Best Method	6	7	8	9	3
BEst Estimator	BL(-3)	BL(-1)	BL(1)	BL(3)	BS

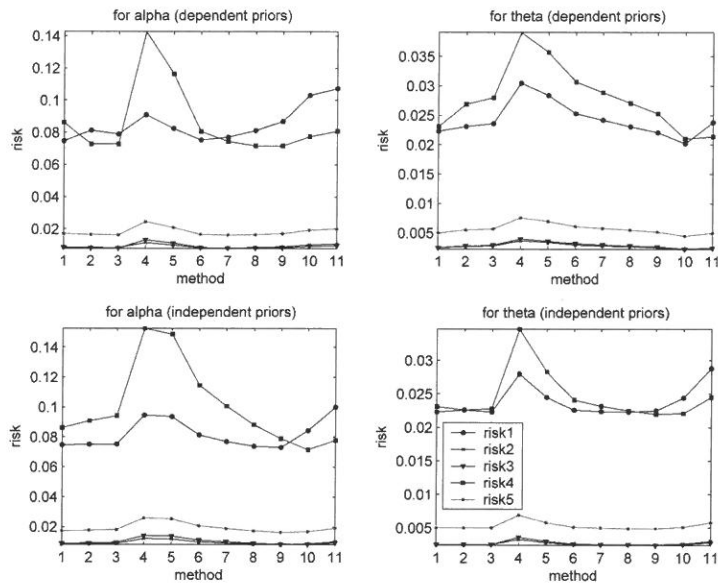


Figure 4: risk of different estimators for  $\alpha$  and  $\theta$  as  $(\alpha, \theta) = (1.5, 0.8)$  ( $n = 300$ )

From Fig 3 ~ Fig 5, for distributions  $EW(1.8, 1.5)$ ,  $EW(1.5, 0.8)$ ,  $EW(0.8, 1.5)$ , we observe that:

1. For the estimators of  $\alpha$ ,

- (a) with dependent prior, under risk 1, the MLE and BS perform equally well as BL(-3). But for  $EW(0.8, 1.5)$ , the risk 1 for GMLE, BL(-1), BL(1), BL(3) are also close to the risk for BL(-3). For risk 4, GMLE, BS, BL(1) perform equally well as BL(3). But for  $EW(0.8, 1.5)$ , the risk4 for BL(10) is also close to the risk4 for BL(-3);
- (b) with independent prior, under risk 1, the MLE, GMLE, BS, BL(-1), BL(1) and BL(3)

perform equally well as BL(-3); For risk 4, MLE, GMLE, BL(10) performs equally well as BL(3);

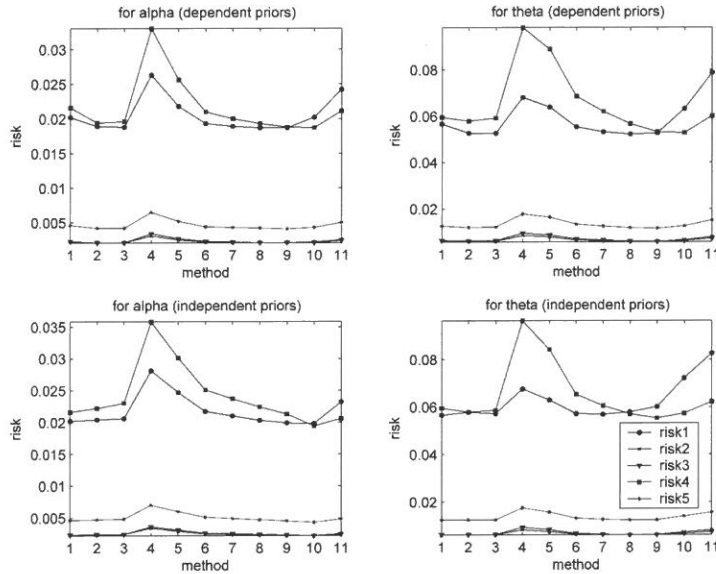


**Figure 5: risk of different estimators for  $\alpha$  and  $\theta$  as  $(\alpha, \theta) = (0.8, 1.5)$  ( $n = 300$ )**

2. For the estimators of  $\theta$ .

- (a) with dependent prior, under risk 1, the GMLE, BS, BL(-1), BL(1), and BL(3) perform equally well as BL(-3); For risk 4, MLE, BL(10) perform equally well as BL(3) for  $EW(1.8, 1.5)$  and  $EW(1.5, 0.8)$ . For  $EW(0.8, 1.5)$ , the risk of BL(10) is close to the risk of BL(3);
- (b) with independent prior, under risk 1, the MLE, GMLE, BS, BL(-1), BL(1) and BL(3) perform equally well as BL(-3); For risk 4, BL(10) performs equally well as BL(3);
3. Under Risk 2, 3, 5, except BL(-25), BL(-10), BL(10), BL(25), the risks of all the other estimators in all figures are almost the same;
4. For a fixed estimator, the risk derived by Linex loss function with larger  $a$  is much larger than those risks with smaller value of  $a$ ;
5. From Fig 3~Fig 4, under a fixed risk rule, the risks for estimators of  $\alpha$  based on  $EW(1.8, 1.5)$

and  $EW(1.5, 0.8)$  are larger than the risks of estimators for  $\theta$ , especially when the value of  $|a|$  is large. However, for the distribution  $EW(0.8, 1.5)$ , the results are reversed.

Over all speaking, the effect of sample size is quite significant. The pattern of the curves under different censoring rate, e.g. 100%, 90%, 80%, 70% and 60% are all similar. Here we only list the results for 70% to save the space.

## 5. Conclusions and Suggestions

From the results listed in the previous section, overall speaking, we know that all the estimators behave equally well when the sample size is large enough. If large sample is not attainable, then a decision maker has to decide if a parametric type estimator or a Bayesian type estimator is proper based on the information one has on hand, and then use the idea we have in this report as reference.

One may wonder that what will happen if the priors of the parameters are different from what we have here, indeed, we have done some cases and looked like the results are similar to the current situation. However, it is hard to make the conclusion that all the priors will give the same results. We will leave more general cases as further study.

## References

- [1] Choudhury, A., (2005). A simple derivation of moments of the exponentiated Weibull distribution. *Metrika* 62(1), pp. 17-22.
- [2] Harry, F.M. and Ray, A.W., (1982). Bayesian Reliability Analysis; John Wiley and Sons: New York.
- [3] Hogg, R. V., McKean, J.W. and Craig, A.T., (2005). Introduction to Mathematical Statistics, 6th Ed; Pearson Prentice Hall.
- [4] Lindley, D.V., (1980). Approximate Bayesian method. *Trabajos Estadística* 31, pp. 223-237.
- [5] Mudholkar, G.S. and Srivastava, D.K., (1993). Exponentiated-Weibull family for analyzing bathtub failure data. *IEEE Transactions on Reliability* 42(2) pp. 299-302.

- [6] Mudholkar, G.S., Srivastava, D.K. and Marshall, F., (1995). The Exponentiated Weibull Family: A Reanalysis of the Bus-Motor-Failure Data. *Technometrics* 37(4), pp. 436-445.
- [7] Mudholkar, G.S. and Hutson, A.D., (1996). Exponentiated-Weibull family: some properties and flood data application. *Communications in Statistics: Theory and Methods* 25(12), pp. 3050-3083.
- [8] Nassar, M.M. and Eissa, F.H., (2003). On the Exponentiated Weibull distribution. *Communications in Statistics: Theory and Methods* 32(7), pp. 1317-1336.
- [9] Nassar, M.M. and Eissa, F.H., (2004). Bayesian estimation for the exponentiated Weibull model. *Communications in Statistics: Theory and Methods* 33(10), pp. 2343-2362.
- [10] Nadarajah, S. and Gupta, A.K., (2005). On the moments of the exponentiated Weibull distribution. *Communications in Statistics: Theory and Methods* 34(2), pp. 253-256.
- [11] Robert, C. P. and Casella, G. (2004). Monte Carlo Statistical Methods, 2nd Ed; Springer.
- [12] Singh, U., Gupta, P.K. and Upadhyay, S.K., (2002). Estimation of exponentiated-Weibull shape parameters under linex loss function. *Communications in Statistics: Simulation and Computation Methods* 31(4), pp. 523-537.
- [13] Singh, U., Gupta, P.K., Upadhyay, S.K., (2005). Estimation of parameters for exponentiated-Weibull family under type-II censoring scheme. *Computational in Statistics & Data Analysis* 48(3), pp. 509-523.
- [14] Varian, H.R., (1975). A Bayesian approach to real estate assessment. *Studies in Bayesian Econometrics and Statistics in Honoer of Leonard J. Savage*, pp. 195-208.
- [15] Zellner, A., (1986). Bayesian estimation and prediction using asymmetric loss function. *Journal of the American Statistical Association* 81(394), pp. 446-451.

*Received October 31, 2007*

*Revised December 21, 2007*

*Accepted December 31, 2007*

## 指數韋伯分佈在型 I 設限資料之估計

陳思勉<sup>1</sup> 李欣馨<sup>2</sup>

<sup>1</sup> 輔仁大學數學系

<sup>2</sup> 中原大學應用數學系

### 摘 要

本文討論指數偉伯分佈之型 I 設限資料之參數估計，其中包括最大概似估計式及三類貝式估計式。



# The influence of thermal loading in a diode-pumped Nd:GdVO<sub>4</sub> laser on its beam propagation ratio( $M^2$ )

Lien-Bee Chang\*, Cheng-Ping Huang, and Yu-Yun Chen

*Department of Physics, Fu Jen Catholic University, Taipei 242, Taiwan, ROC*

## Abstract

The detrimental effect of thermal loading within a diode-pumped Nd:GdVO<sub>4</sub> laser on its beam propagation ratio ( $M^2$ ) is investigated. When the pump power was increased from 2 to 12 W, the  $M^2$  factor was raised from a value of 1.02, reasonably close to the theoretical value of 1.0 for a TEM<sub>00</sub> Gaussian beam, to 1.86, and the equivalent focal length was greatly reduced from 2700 mm to about a tenth of the initial length in both the x- and y-direction.

**Keyword** , Diode-pumped, Nd:GdVO<sub>4</sub>, thermal lensing,  $M^2$

## Introduction

In recent years, compact diode-end-pumped neodymium-doped all-solid-state lasers operating in the near infrared and visible spectral regime have been attracting much attention by their high efficiency, compact and beam quality and by urgent needs for a wide range of applications such as reprographics, holography, ophthalmology, medical diagnostics, optical data storage, entertainment and laser displays. Frequency doubling of diode-pumped near-infrared las-

---

\* Corresponding author, Tel., +886-2-29052018; fax, +886-2-29021038

E-mail address: [lbchang@mail.fju.edu.tw](mailto:lbchang@mail.fju.edu.tw)

ers by inserting a proper nonlinear crystal in the cavity is an attractive and promising approach to generate compact all-solid-state red, green, and blue visible lasers because the intensities within the cavity are so high that efficient conversion could be realized. Nevertheless, the nonlinear optical conversion efficiency is significantly influenced by the beam quality of the fundamental radiation within the cavity.

The beam quality of a laser can be characterized by a crucial parameter, the beam propagation ratio  $M^2$  [1-4]. It is the ability of a beam to be tightly focused. For a perfect Gaussian beam, often referred to as a diffraction-limited beam,  $M^2$  is equal to unity. Values of  $M^2$  greater than unity connote that the laser beam has higher-order transverse modes as well as the fundamental TEM<sub>00</sub> Gaussian mode. However, the accumulation or deposition of heat generating within the laser crystal leads to a spatial variation in temperature. The gain medium is hotter on the beam axis, compared with the outer regions, causing transverse temperature gradient of the refractive index and hence forming an effective lens. Because of the highly aberrated nature of thermal lens, the deleterious thermal loading results in degradation in laser beam quality [5-6].

As a result, more thermally stable laser crystals are required. Nd:GdVO<sub>4</sub> crystals are promising 1- $\mu$ m laser media for realizing efficient lasers with sufficient thermal stability because of its large emission cross section [7-8] and high thermal conductivity [9-10].

In this paper we put forward a model and an approach to indirectly determine the thermal loading by measuring the equivalent focal lengths of thermal lens, and report on the dependence of the propagation ratio  $M^2$  on thermal loading in a diode-end-pumped Nd:GdVO<sub>4</sub> laser.

### Description of the Model

It was shown in reference 2 that the ray matrix (ABCD matrix) approach and the formalism that has been developed to utilize the complex beam parameter,  $q$ , apply to real beams as well as Gaussian beams. The spot size of a real beam is *everywhere* larger than that of the *imbedded* Gaussian beam for TEM<sub>00</sub> mode by  $M=\sqrt{M^2}$ . Therefore, to explore the TEM<sub>00</sub> cavity modes by using a flat-flat cavity, with an equivalent thermal lens located at the place of the laser crystal, we exploit the ABCD law, the stability criteria and the complex beam parameter  $q$ , as defined by

$$\frac{1}{q(z)} = \frac{1}{R(z)} - j \frac{\lambda_0}{\pi W^2(z)} \quad (1)$$

where  $q(z)$ ,  $R(z)$ ,  $W(z)$ , and  $\lambda_0$  are the complex beam parameter, the radius of curvature of the beam, the spot size, and the wavelength in vacuum, respectively [11].

The equivalent laser cavity and the equivalent-lens waveguide are shown in figs. 1 and 2, respectively. After some algebra the ABCD matrix is given by

$$\begin{bmatrix} A & B \\ C & D \end{bmatrix} = \begin{bmatrix} 1 - \frac{2}{f_{th}}(L - \frac{d_1 d_2}{f_{th}}) & 2(1 - \frac{d_1}{f_{th}})(L - \frac{d_1 d_2}{f_{th}}) \\ -\frac{2}{f_{th}}(1 - \frac{d_2}{f_{th}}) & 1 - \frac{2}{f_{th}}(L - \frac{d_1 d_2}{f_{th}}) \end{bmatrix} \quad (2)$$

Furthermore, the value of  $q$  at the plane  $z_1$  can be determined by forcing the  $q$  to transform into itself after around trip, thus resulting in

$$q(z_1) = \frac{Aq(z_1) + B}{Cq(z_1) + D} \quad (3)$$

This yields the radius of curvature of the beam and the spot size at the plane  $z_1$ , as given by

$$R(z_1) = -\frac{2B}{A-D} \quad (4)$$

$$\frac{\pi W^2(z_1)}{\lambda_0} = \frac{B}{\sqrt{1 - (\frac{A+D}{2})^2}} \quad (5)$$

It should be noted that the spot size at  $z_1$  is reduced to the value of the minimum spot size or the beam waist radius  $W_0$ . If the total cavity length  $L$ , the distances  $d_1$  and  $d_2$  as defined in the figures, and the minimum spot size  $W_0$  are given, the solution for the desired equivalent thermal focal length  $f_{th}$  can be completely solved.

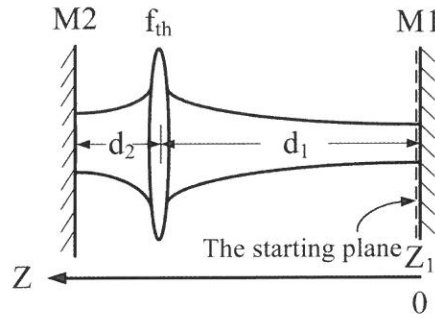


**Fig. 1** The equivalent laser cavity. Where the laser crystal has been replaced by a thermal lens

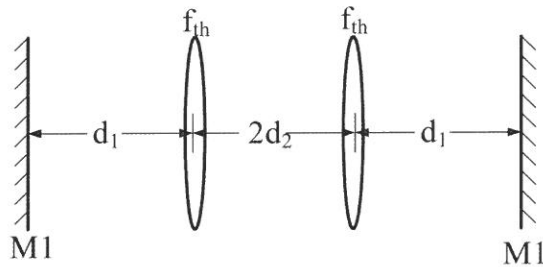


**Fig. 2** The equivalent-lens waveguide (a unit cell)

## Experimental arrangement

The schematic of the experimental arrangement is shown in Fig. 3 for the measurement of the equivalent thermal focal lengths and the values of the beam propagation ratio  $M^2$ . A commercial 808-nm fiber-coupled diode-laser-array of 12 W (Coherent Semiconductor) was used as the pump source. The pump laser was focused into a Nd:GdVO<sub>4</sub> crystal by a 1:1 coupling lenses. The laser crystal had a dimension of 3×3 mm<sup>2</sup> in cross-section and 5 mm in length, and the Nd-doping concentration was 0.5 at. %. In addition, the first face of the crystal was AR coated at 1064 nm and 808 nm, and the other was AR coated at 1064 nm. It was wrapped with

indium foil and mounted in a water-cooled copper block, and a thermal probe was inserted into the block to monitor the temperature of the wrapped crystal surfaces. The temperature of the surfaces was maintained near  $17^{\circ}\text{C}$  and can be controlled within  $0.1^{\circ}\text{C}$  with a feedback loop controlled by a PC, via a program written in LabView graphical language to obtain a stable output.

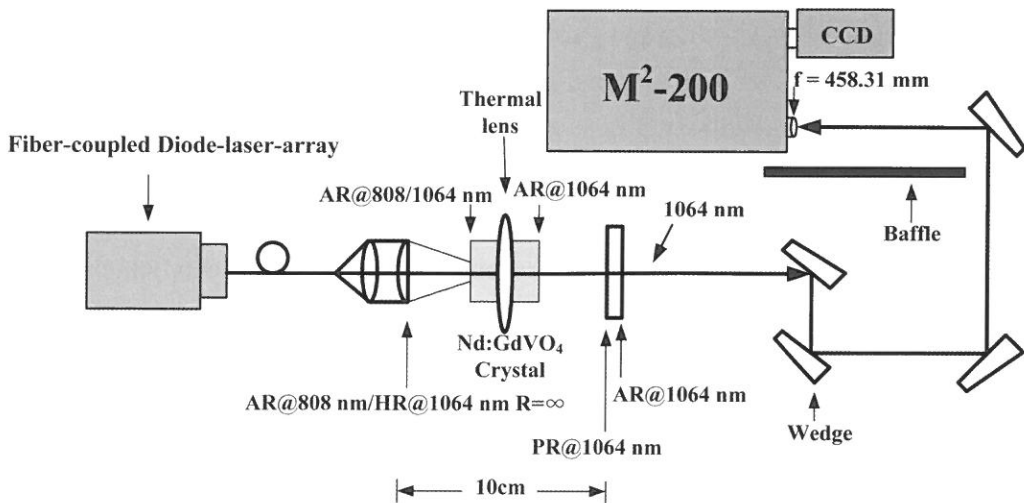


Fig. 3. Schematic of experimental setup for the measurement of beam propagation ratio  $M^2$ .

We employed a linear flat-flat cavity as shown in the Fig. 1 to explore the thermal loading effect in the diode end-pumped Nd:GdVO<sub>4</sub> laser system. Two flat mirrors were used as the input and output couplers (M1 and M2). The input coupler M2 was HR coated at 1064 nm and HT coated at 808 nm, and the other mirror (M1) with 90% reflectivity at 1064 nm was used as the output coupler. Moreover, the total resonator cavity length was set to about 100 mm. The laser beam propagation ratio  $M^2$  and its beam waist radius were measured by an automatic  $M^2$  beam propagation analyzer (Spiricon,  $M^2$ -200). Both the values of  $M^2$  and the real beam waist radii can be measured by the instrument at the same time. The ideal beam waist  $W_0$  is just the ratio of the measured radius to the square root of the measured  $M^2$ . Then the ratio and the wavelength of 1064 nm are substituted into equation (5) to find the equivalent thermal focal length. In addition, four high quality windows with a large wedge of  $3^{\circ}$  and a zero-order half-wave

plate were used in the experiment to smoothly and continuously attenuate the laser intensity to obtain high quality beam profile images taken by a CCD. Finally, the radii and beam propagation ratios can be computed correctly by the  $M^2$ -200 software.

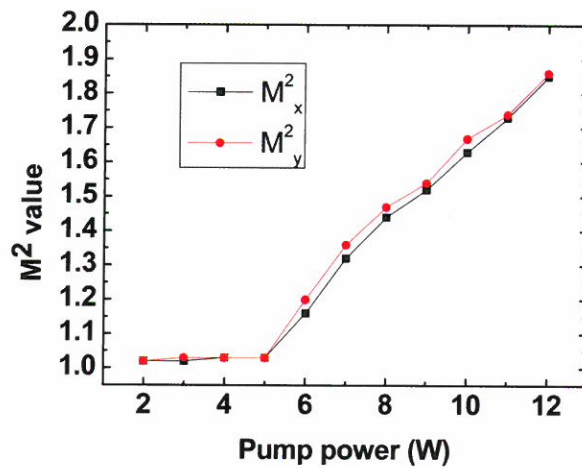
## Results and discussion

The experimental results are shown in Table 1. Both the equivalent thermal focal lengths and the propagation ratios in both x- and y-direction are almost the same when the pump power was raised from 2 to 12 W. It is interesting to note that a significant increase in  $M^2$  occurred as the pump power was increased from 5 W to 6 W, and the rising slope reached to approximately 0.12, as shown in figure 4. This implies that the rate of heat deposition begins to exceed that of heat dissipation within the laser crystal, and the gain medium on the beam axis becomes hotter despite the fact that the temperature of the wrapped crystal surfaces stays approximately constant. This is because the thermal conductivity of Nd:GdVO<sub>4</sub> crystals are approximately 11 W/mK [12] and is much smaller than that of copper, which is 397 W/mK [13]. By using the data about Nd:GdVO<sub>4</sub> crystals, a simple estimation of the temperature difference between the center and the surface of the crystal can be made and is about 50 K if the power of heat generation in the crystal is 4W.

Therefore, the gradient of temperature in the gain medium steepens. This leads to a reduction in the equivalent thermal focal length. The figures 5 and 6 indicate that the beam waist diameter and the thermal focal length were fairly reduced as the pump power was increased further. The highly aberrated nature of the thermal lensing also results in an increase in  $M^2$ . In addition, figure 7 shows the optical-optical conversion efficiency slope was close to 50%. When the pump power is lower than 6 W, the values of  $M^2$  are reasonably close to the theoretical value of 1.0 for the perfect Gaussian beam, and the beam profile is fairly circular and symmetric, as shown in figure 8. Obviously, as the pump is increased to 12 W, the thermal problem deteriorates rapidly, and the beam profile is seriously distorted, as shown in Fig. 9.

**Table. 1. The thermal focal length and the propagation ratio  $M^2$  versus the pump power.**

Pump power (w)	Thermal focal length (x) (mm)	$M_x^2$	Thermal focal length (y) (mm)	$M_y^2$
2	2635.8	1.02	2722.9	1.02
3	1567.7	1.03	1554.7	1.03
4	1047	1.03	1022.6	1.03
5	763.5	1.03	727.3	1.03
6	622.1	1.16	574.8	1.20
7	526.2	1.32	476.1	1.36
8	433.7	1.44	399.4	1.47
9	367.8	1.52	334.6	1.54
10	343.9	1.63	304.5	1.67
11	299.7	1.73	275	1.74
12	281.5	1.85	267.8	1.86

**Fig. 4. The propagation ratio  $M^2$  versus the pump power.**

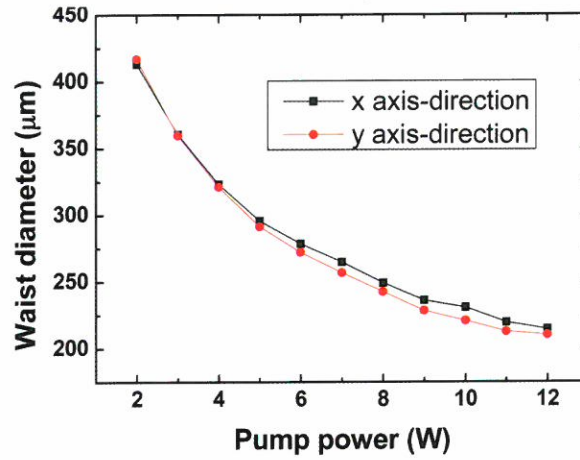


Fig. 5. The beam waist size versus the pump power.

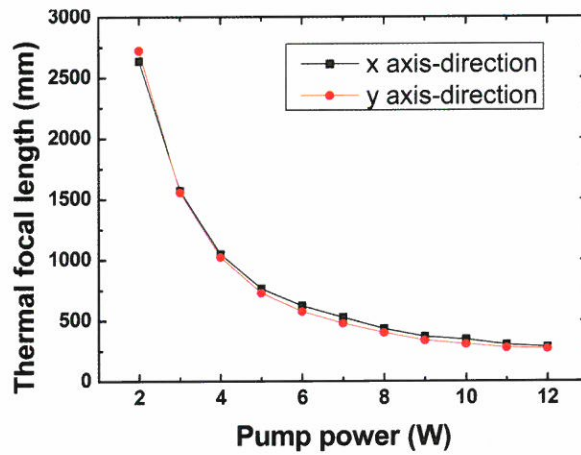


Fig. 6. The thermal focal length versus the pump power

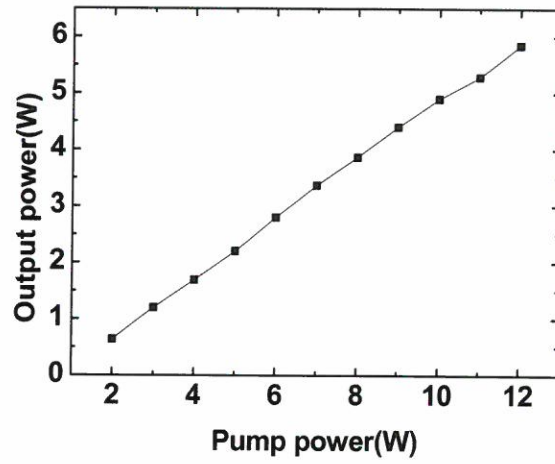


Fig. 7. The output power versus the pump power

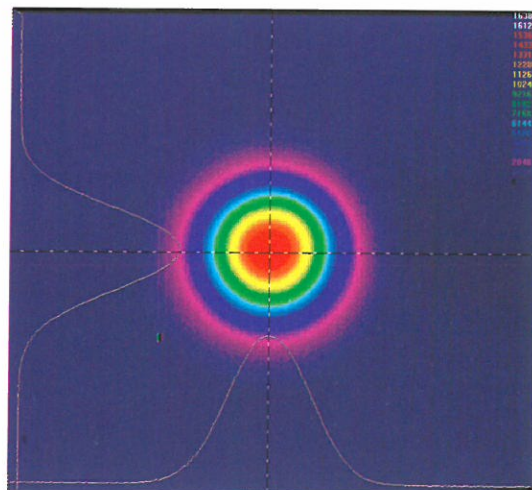
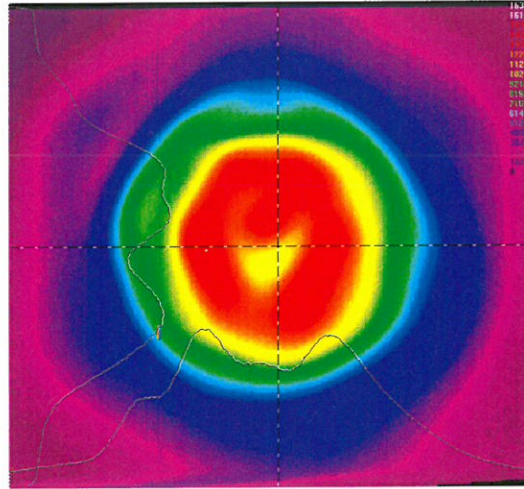


Fig. 8. The beam profile measured at an input pump power of 2W.



**Fig. 9. The beam profile measured at an input pump power of 12W**

## Conclusion

This paper has described the influence of thermal loading in laser crystals on laser beam quality. The study has demonstrated that the thermal conductivity is a key point to generate an excellent TEM<sub>00</sub> laser beam. As a result, thermal lensing effect can be reduced by using a gain medium with good thermal conductivity and small thermo-optical coefficients and by choosing pump and laser wavelengths in order to obtain a small quantum effect to reduce heat generation in laser crystals. The further research is in progress using several different Nd-doped crystals with a diverse range of doping concentration as gain media.

## References

- [1] M. W. Sasnett, *The physics and Technology of Laser Resonators*, (D. R. Hall and P. E. Jackson, eds.), Chap. 9, p.132, Hilger, New York, 1989.
- [2] M. W. Sasnett and T. F. Johnston, Jr., *Proc. SPIE*, vol. 1414, p. 21, 1991.
- [3] A. E. Siegman, *Proc. SPIE*, vol. 1868, p. 2, 1993.
- [4] ISO 11146-1, 2005 and ISO/TR 11146-3, 2004.
- [5] W. A. Clarkson, *J. Phys. D: Appl. Phys.*, vol. 34, p.2381, 2001.

- [6] J. L. Blows, T. Omatsu, J. Dawes *et al.*, IEEE Photo. Technol. Lett., vol. 10, p. 1727, 1998.
- [7] A. Agnesi, G.C. Reali and P.G. Gobbi, IEEE J. Quantum Electron., vol. 34, p. 1297, 1998.
- [8] T. Jensen, V.G. Ostroumov, J.P. Meyn *et al.*, Appl. Phys. B, vol. 58, p. 373, 1994.
- [9] Y.D. Zavartsev, A.I. Zagumennyi, F. Zerrouk *et al.*, Quantum Electron., vol. 33. p. 651, 2003.
- [10] C. Czeranowsky, M. Schmidt, E. Heumann *et al.*, Opt. Commun., vol. 205, p. 361, 2002.
- [11] Joseph T. Verdeyen: *Laser Electronics*, Prentice Hall, Inc., Upper Saddle River, 3rd edition, 1995.
- [12] L.J. Qin, X.L. Meng, H.Y. Shen *et al.*, Cryst. Res. Technol., vol. 38, p. 793, 2003.
- [13] R.A. Serway and J.S. Faughn, *College Physics*, Thomson, Brook/Cole, Pacific Grove, 6<sup>th</sup> edition, p. 343, 2003.

*Received October 31, 2007*

*Revised December 24, 2007*

*Accepted December 31, 2007*

## 半導體雷射泵浦之 Nd:GdVO<sub>4</sub> 雷射 其熱負載對光束品質之影響

張連壁 黃承平 陳譽云

輔仁大學物理系

### 摘 要

我們利用由兩面平面鏡所構成之雷射共振腔，研究由半導體雷射泵浦之 Nd:GdVO<sub>4</sub> 固態雷射其熱負載對雷射光束品質之影響。研究發現當泵浦雷射功率超過 5 瓦時，雷射品質發生顯著的變化，其雷射強度輪廓之扭曲程度會隨著泵浦雷射功率增加而急遽惡化，同時等效之熱焦距長 (The equivalent thermal focal length) 亦隨著泵浦功率的增加而顯著縮短。

**關鍵詞：**半導體雷射泵浦、Nd:GdVO<sub>4</sub>、摻釹離子、熱透鏡、光束品質因子。